Insight into the Rules Dictating the Formation of Arene Ruthenium Metalla-Assemblies

Thèse présentée à la Faculté des Sciences par

Amine Garci

Ingénieur en Chimie Analytique de la Faculté des Sciences de Tunis, Tunisie

Pour l'obtention du grade de Docteur ès Sciences

Directeur de thèse : Prof. Bruno Therrien

Membres du jury :

Prof. B. Therrien	**Prof. G. Süss-Fink**	**Prof. M. Sallé**
Directeur de thèse, Université de Neuchâtel	Rapporteur interne, Université de Neuchâtel	Rapporteur externe, Université d'Angers

UNIVERSITÉ DE NEUCHÂTEL

Institut de Chimie, Université de Neuchâtel

Mai 2015

UNIVERSITÉ DE NEUCHÂTEL

Faculté des sciences
Secrétariat-décanat de Faculté
Rue Emile-Argand 11
2000 Neuchâtel - Suisse
Tél: + 41 (0)32 718 2100
E-mail: secretariat.sciences@unine.ch

IMPRIMATUR POUR THESE DE DOCTORAT

La Faculté des sciences de l'Université de Neuchâtel autorise l'impression de la présente thèse soutenue par

Monsieur Amine GARCI

Titre:

"Insight into the rules dictating the formation of arene ruthenium metalla-assemblies"

sur le rapport des membres du jury composé comme suit:

- Prof. ass. Bruno Therrien, directeur de thèse, Université de Neuchâtel
- Prof. Georg Süss-Fink, Université de Neuchâtel
- Prof. Marc Sallé, Université d'Angers, France

Neuchâtel, le 8 juin 2015

Le Doyen, Prof. B. Colbois

B. Colbois.

Remerciements

Ce manuscrit décrit les résultats de mon travail de thèse effectué au sein du Laboratoire de Chimie Organométallique et de Catalyse Moléculaire de l'Université de Neuchâtel, sous la direction du Professeur Bruno Therrien. Qu'il soit ici chaleureusement remercié pour m'avoir accueilli au sein de son groupe et fait partager son enthousiasme pour la recherche. Ses conseils et son soutien durant cette période, m'ont aidé à mener avec succès, ce projet jusqu'à son terme. Je ne saurais donc assez remercier Professeur Therrien pour cette transmission sans retenue de son expérience tant au niveau scientifique, qu'humain.

Mes remerciements vont aussi au Professeur Georg Süss-Fink, pour avoir accepté de faire partie du jury de ma thèse et de la relire attentivement. Pour ses remarques éclairées et pertinentes, j'exprime également ma gratitude au Professeur Marc Sallé.

Ma gratitude va en outre, au groupe du Professeur Paul J. Dyson de l'EPF-Lausanne pour les tests biologiques, au groupe du Professeur Vincent Sol de l'Université de Limoge, pour l'étude photodynamique, au groupe du Professeur Stefan Schürch de l'Université de Berne, pour les analyses par spectrométrie de masse, au groupe du Professeur Vladimir Arion de l'Université de Vienne, pour sa collaboration productive, ainsi qu'aux Docteurs Claudio Dalvit et Armelle Vallat, pour les analyses par spectroscopie RMN et de masse.

Je remercie mes nouveaux et anciens collègues du Laboratoire de Chimie Organométallique et de Catalyse Moléculaire, à savoir : Mona, Justin, Farooq, Julien, Gajendra, Ersin, Raja, Bing, Minghui, Wassila, Thomas, Manu et David, pour la bonne ambiance de travail et les moments passés ensemble, au laboratoire et en dehors du cadre professionnel. Merci aussi à mon apprentie Line qui a réussi à me supporter, pendant sa première année d'apprentissage, me permettant ainsi d'avancer plus rapidement et dans la bonne humeur.

Je remercie également mes chèrs amis Chaabane, Hichem, Asma, Jihane, Amine, Gary, Racem, Ezzeddine et AbdelBassit pour m'avoir soutenu durant ses quatres années.

Enfin, ces remerciements ne peuvent que se conclure par un grand merci à toute ma famille, particulièrement à ma chère mère Maaouia, sans qui je ne serai pas de ce monde, ainsi qu'à mes frères et sœurs pour leur soutien et leurs encouragements d'une importance inestimable au cours de toutes ces années.

A la mémoire de mon père Hedi GARCI

Résumé

Le processus d'auto-assemblage est un phénomène naturel capable d'organiser des systèmes biologiques. Son utilisation par les chimistes comme procédé de synthèse a permis la formation de structures esthétiques et de systèmes supramoléculaires hautement complexes, avec des fonctions biologiques avérées. Depuis 1990, la stratégie d'auto-assemblage dirigée par des métaux a largement contribué à la conception et à la synthèse d'architectures discrètes. La formation de ces architectures spécifiques nécessite un contrôle minutieux des différents facteurs dirigeant le processus d'auto-assemblage.

L'objectif de cette thèse est d'offrir un aperçu des règles dictant la formation des assemblages métalliques arène-ruthénium. Ceux-ci sont construits à l'aide de clips métalliques stables et de ligands polypyridiniques. La caractérisation des échanges dynamiques des ligands, au moyen d'une stratégie de marquage isotopique $^{1}H/^{2}D$ a démontré la stabilité et l'inertie relative de la structure rectangulaire. En outre, l'étude par résonance magnétique nucléaire, des espèces intermédiaires impliquées dans l'assemblage de cycles métalliques, a permis de mettre en exergue la nature dynamique de la liaison Ru-N en solution, avant la fermeture définitive des cycles métalliques. Cela nous a permis de décrire une voie de germination thermodynamique plausible avec une réactivité spécifique de ces assemblages métalliques.

Par ailleurs, l'activité anticancéreuse prometteuse des complexes mononucléaires arène-ruthénium, ainsi que l'accumulation préférentielle de leurs espèces macromoléculaires dans les cellules cancéreuses, confèrent un potentiel antiprolifératif très intéressant aux cages métalliques arène-ruthénium. Ainsi notre stratégie pour optimiser l'activité biologique des prismes métalliques comportait deux approches. Dans un premier temps, la fonctionnalisation des ligands pontés, a permis d'améliorer la sélectivité des composés actifs contre les cellules cancéreuses. Dans un second temps, la modification de la taille des ouvertures, de la cavité des cages métalliques, a permis de contrôler la libération d'un photosensibilisateur hydrophobe dans une lignée cellulaire humaine du cancer du côlon HT-29.

Mots Clés

Complexes arène-ruthenium, chimie supramoléculaire, auto-assemblage, cycles métalliques, Ligands N, processus dynamique, mécanismes réactionnels, complexes dinucléaires, complexes tétaranucléaires, complexes hexanucléaires, complexe hôte-invité, activité anti-cancéreuse, administration de médicaments, thérapie photodynamique.

Summary

The self-assembly process is a natural phenomenon with the ability to organize biological systems. Its development by chemists as a synthetic process allowed the formation of esthetical structures as well as highly complex supramolecular systems with remarkable biological functions. Since 1990, metal directed self-assembly strategy has largely contributed to the design and synthesis of discrete architectures. The formation of these specific architectures needs some control over the different factors ruling the coordination self-assembly process.

The aim of this thesis was to offer an insight into the rules dictating the formation of arene ruthenium metalla-assemblies built from stable dinuclear metalla-clips and polypyridyl linkers. The characterization of the dynamic ligand exchanges using the $^{1}H/^{2}D$ isotope labeling strategy showed relative stability and inertness of the final structure. In addition, the study of the intermediate species involved during the assembly of metalla-cycles by NMR experiments highlighted the dynamic nature of the Ru-N bond in solution before the final closure of the metalla-cycles. This helped us to describe a plausible thermodynamic germination pathway together with the specific reactivity of such metalla-assemblies.

The promising anticancer-activities of the mononuclear arene ruthenium complexes along with the preferential accumulation of macromolecular species in the cancer cells led to more interest in the anti-proliferative potential of arene ruthenium metalla-cages. Our strategies in order to optimize the biological activity of arene ruthenium metalla-prisms were: Functionalization of the bridging linkers resulted in selectivity improvements of the active compounds towards target cancer cells; and the modification of the portal's size of metalla-cages to control the release of a hydrophobic photosensitizer on the human colon cancer cell line HT-29.

Keywords

Arene ruthenium complexes, supramolecular chemistry, self-assembly, metalla-cycles, N ligands, dynamic processes, reaction mechanisms, dinuclear complexes, tetranuclear complexes, hexanuclear complexes, host-guest complex, anticancer activity, drug delivery, photodynamic therapy.

Table of Contents

1 Introduction

1.1 Supramolecular Chemistry

Supramolecular chemistry or "chemistry of molecular assemblies and intermolecular bonding" as described by Lehn,[1] is a branch of chemistry "beyond the molecules".[2] This concept is opposed to molecular chemistry by the type of chemical bonds involved, the preparation process and also in terms of the size and dimension of the formed molecule.[3] While molecular chemistry focuses more on the synthesis of a single molecule constructed via covalent bonds, supramolecular chemistry deals, however, with macromolecules assembled spontaneously from finite number of individual molecules. These molecules are hold together via a variety of intermolecular interaction of different strength.[4] In nature, weak forces such as hydrogen bonds, Van der Waals and electrostatic interactions are responsible for the spatial organization of the majority of bio-macromolecules (DNA, RNA, Proteins…).[5, 6] In chemistry, an ever-increasing number of elegant systems and discrete architectures with unique properties have been synthesized via metal-ligand coordination bond, strictly covalent bonds, weak interactions where sometimes two or both are gathered. This flexibility leads to unusual application in biology, physics and material science, allowing this new area of chemistry to be a highly interdisciplinary field.[7, 8]

Historically the concept of supramolecular chemistry was based on three principles.[4] The first one was proposed in 1893 by the Nobel laureate Alfred Werner (1913) who introduced the notion of coordination chemistry: electronically saturated molecules can still bind if they have "mutual affinity" to form "complexes".[9, 10] The second principle concerns the molecular recognition, which was established in 1894 by the Nobel laureate Emil Fisher (1902) for introducing the "lock-and-key" concept.[11] For the enzyme-substrate interactions, "binding must be selective", and the recognition requires size and shape complementarity.[11, 10] The third principle was proposed by the Nobel laureate Paul Ehrlich (1908) in 1906, who introduced the concept of receptor: molecules do not react if they do not bind.[12, 10] All these three fundamental principles have certainly been developed over the years, but they remain the foundation of supramolecular chemistry. And noticeably, 1987 is a headlight date in this field, when three pioneers, Donald J. Cram, Jean-Marie Lehn, and Charles J. Pedersen, were awarded the Nobel Prize for Chemistry in recognition of their contribution to rationalize the general concept of supramolecular chemistry. The development of a series of rigid hosts like spheroids,[13] cryptands[2] and crown ethers[14] able to recognize selectively a guest was highlighted as a major contribution to chemistry (Fig. 1). The breadth of supramolecular chemistry has progressively increased since then, and today is a mature field of science which gathers chemistry, physics and biology.[8]

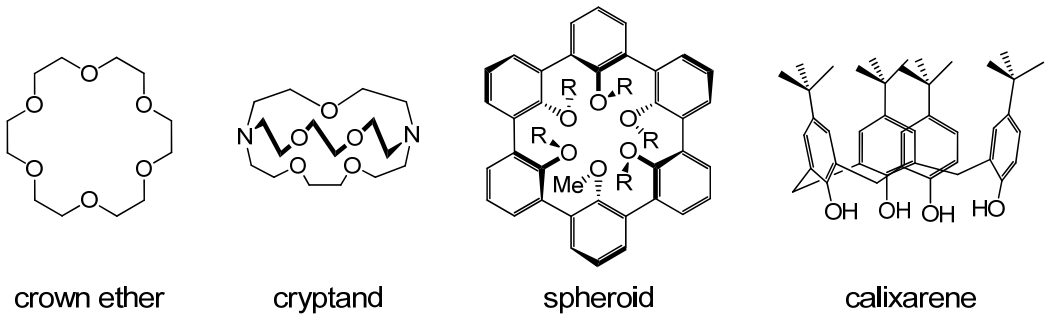

Figure 1. Some examples of supramolecular host molecules.

1.1.1 General Concept in Supramolecular Chemistry

As we described above, the germination process of supramolecular assemblies and the recognition "catch and release" of a guest by a receptor, constitutes the main pillar of supramolecular chemistry.[4, 8, 15, 16] In addition, supramolecular species assembled spontaneously from a number of different building blocks by recognition of each other

through thermodynamic preferences.[17] This process called "self-assembly" is a successful synthetic tool which gives rise to the complex targeted structure in high yield as compared to conventional organic synthetic strategies.[17, 18]

Molecular recognition, the "key-lock" concept described in the early 1894 by Emil Fisher, is a fundamental facet in the "host-guest" chemistry.[11] A substrate or a "guest" molecule binds (interacts) selectively to a molecular receptor (host) to form a host-guest complex.[19] The manner in which the molecules are able to identify each other is a form of self-assembling process. The chemical and the thermodynamic properties of the final complex should be unique and have different physicochemical properties as compared to the single starting units.[8]

1.1.2 Molecular Self-Assembly

George M. Whitesides fixed the major elements leading to a successful self-assembly strategy. He summarized five characteristics related to supramolecular assemblies (components, interactions, reversibility or adjustability, environment, transport and agitation).[17]

Components: The self-assembling supramolecular architecture results from the organization of a finite number of molecules or segment of macromolecules via an interaction, occurring through unfavorable entropy.[17, 20] The shape complementarity of the molecules to recognize each other via a specific interaction is a crucial factor.[21]

Interactions: The forces responsible for the spatial arrangement of the different blocks vary from weak and noncovalent interaction (hydrogen bonds, Van der Waals forces, hydrophobic effects…) to relatively weak (coordination) bonds.[4] The strength, the stability and the lability of the interaction presents the key-factor to predict the architecture and to determine the physicochemical properties of the final system.[22, 23, 24] If George M. Whitesides described this intermolecular linkage as "balances of attractive and repulsive" interactions,[17] Lehn and Stang put forward the notion of the "interactional algorithms".[8, 25]

Reversibility (or adjustability): The self-assembly is a kinetically reversible process. Before reaching the final closure, the reaction intermediates may pass through numerous correction and reorganization steps. The final system is thermodynamically stable.[26, 27]

Environment: Solvent,[28] species and external stimuli such as light,[16] pH,[29] are able to direct the synthetic process pathway affecting the final geometries of the targeted molecule. For example, using a template synthesis to favor the formation of a specific shape and architecture was well investigated.[30]

Transport and Agitation: During the process, the reaction intermediates gain advantages in mass and size. In fact, their mobility is becoming increasingly difficult and the risk of their precipitation before reaching the target compound increases as well. Therefore, assuring the motion required to maintain the mobility of the compound in solution is a challenge for chemists.[17]

Another classification, proposed by Stang, is based on the nature of the interactions used in the self-assembling process. He suggested three main classes of supramolecular compounds depending on the nature of the interaction: (i) supramolecular architectures via hydrogen boding; (ii) supramolecular structures designed by using non-covalent interactions such as ion-ion, ion-dipole, π-stacking, van der Waals forces and hydrophobic interactions, and (iii) those employing a strong and directional metal-ligand links for assembly process.[8]

1.1.3 Molecular Self-Assemblies via Hydrogen Bonds

It is evident that the most visible example highlighting the potential of the non-covalent interaction in making extremely complex macro-molecules in our life comes from Nature.[31] For example, in protein folding, hydrogen bonds are responsible to maintain the stability. The self-assembling of the phospholipids through the hydrophobic effect gives a bilayer supramolecular structure.[32] Similarly, the double helical structure of DNA is another example of Nature's supramolecular chemistry, where different nucleotides carried by each DNA strands interact via hydrogen bonding.[31] Inspiration for chemists from these aforementioned structures is not limited in mimicking the biomolecules but giving rise to a highly fertile ground of creativity.[8, 33] The breadth of these interactions as synthetic tools has progressively increased due to their unique advantages. Mirkin gathered two major points: i) the flexibility of the self-assembling system allows free spatial conformational switches (changes) to the structure. ii) the specificity in the synthetic process in which the final compound occurs in the lowest state of energy leading to the most thermodynamically favorable structure.[6]

The Rebek group developed a number of supramolecular capsules by assembling two cavitands and four glycoluril derivatives holding via hydrogen bonding,[34, 35] to overcome the problems of the polymerization during the process which present the main challenges in this area of chemistry (Scheme 1).[15b, 36]

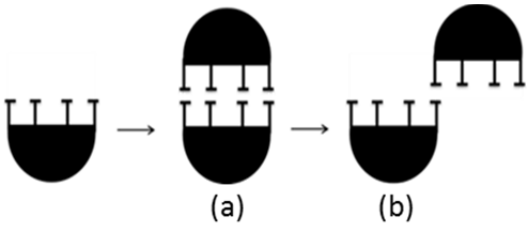

Scheme 1. Potential structures formed by assembling cavitands via non covalent bonds (a) discrete capsule and (b) polymeric species.[15b]

Aekeroy *et al.* designed a new kind of cavitands and functionalized it with tetra-acetamido groups (like a chelating group) generating a N-H···O hydrogen bonds, "a self-complementary hydrogen-bond interaction" leading to the formation of a discrete supramolecular capsule **C1** (Fig. 2).[15b]

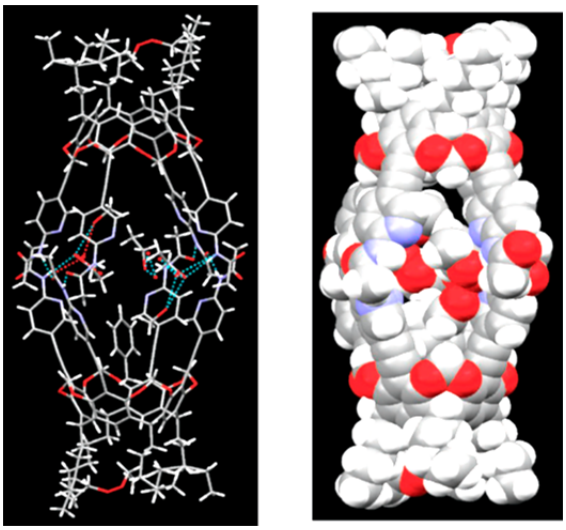

*Figure 2. Molecular structure and space filling diagram of the discrete supramolecular capsule (**C1**).*[15b]

A new class of synthetic bio-nanoassembly using biomolecules like segment of protein or DNA precursor as main building blocks has become a challenging area.[37, 38, 39] An elegant example of macrocycle constructed through a hydrogen bonding, using DNA precursor has been described by H. Sleiman *et al.* in the presence of ruthenium (II) complex as a template.

The mixture of the subunits leads spontaneously to the formation of a square structure. Without addition of the template (assistance), a number of systems with different shape and size are formed in the final mixture (Fig. 3).[40]

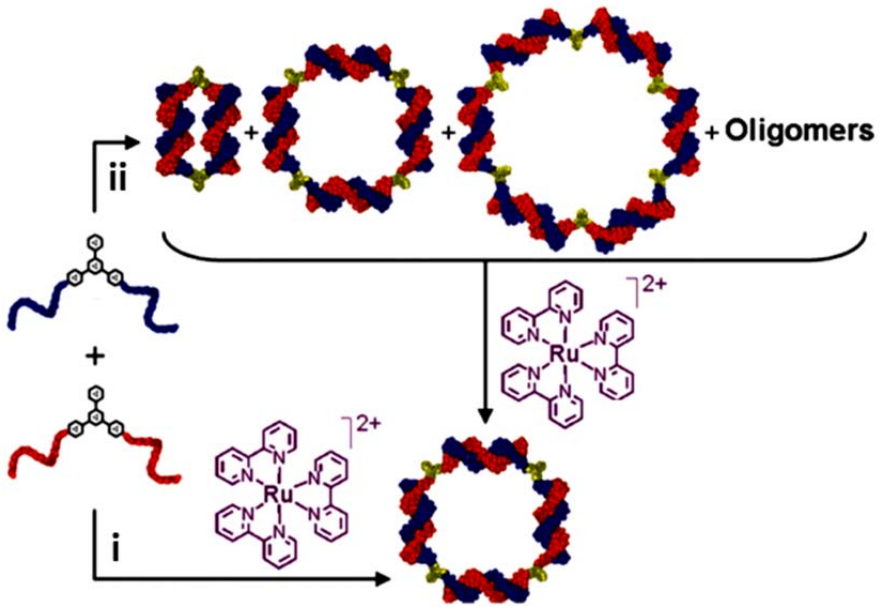

Figure 3. Selective formation of self-assembling cycles using DNA precursors in the presence of the template synthesis (ruthenium (II) complex) (ii) A mixtures of oligomers and self-assembling cycles with different geometries. (Adapted from ref.[40])

Interesting developments have been made by chemists in the last decades to increase the efficiency of these kinds of interactions by using a new synthetic strategy like template synthesis and controlling the complementarity in the shape (chelate effect).[15b,40] Despite of this, during the germination process of the desired structure, the scale and the degree of complexity increases. However the ability to control the geometry of the structure becomes more and more difficult, due to the lack of the directionality.[38] Coordination-driven self-assembly, which defines the third approach, is an interesting subset of self-assembly. The highly directional and relatively strong metal-ligand coordination bonds affords the possibility to design and synthetize a numerous of 2D and 3D supramolecular assemblies with well-defined shapes, sizes and geometries.[41, 42, 43]

1.2 Coordination-Driven Self-Assembly

The effectiveness of the metal directed self-assembly strategy to design and synthesize discrete architectures has been widely demonstrated. Based on the "bottom-up" synthetic strategy, a plethora of two and three dimensional structures have been produced in recent years.[8, 44] Starting with simple structure like squares,[45] polyhedrals[46] and triangles,[47] chemists have created well-defined structure such as grids[48], double squares[49] and helicates[48, 50] with high precision, great efficiency and different functionalities.[51]

In addition to the basic concepts of coordination chemistry, nowadays supramolecular chemists are establishing the fundamental concepts of this new area of chemistry. These new developments can be classified into three major elements. The first focuses more on the characteristics of the metal-ligand bond (strength, lability and stability), which provides precious information about the rigidity, thermodynamic and kinetic stability of the final structure. The second concerns the geometrical algorithms: the prearrangement of the coordination angles, availability of the coordination sites together with the complementarity in shapes between the starting building blocks is crucial to perform the directionality to the target supramolecular architecture. The third is based on the thermodynamic and the kinetic driven formation of the final system. Based on these concepts, three major synthetic strategies have been established "Weak-Link", "Symmetry Interaction" and "Directional Bonding" approaches.[6, 8]

1.2.1 Metal-Ligand Linkage

To gain further insights about the structure, reactivity and stability of supramolecular assemblies produced via a coordination-driven self-assembly strategy, knowing the thermodynamic, kinetic and geometric aspects of the metal coordination precursors are essential. While the stability and the inertness are the main characteristics of organic or inorganic molecules produced via classical chemical covalent bonds, the lability and the relative stability are however crucial in the case of coordination metal compounds. These differences come from many factors such as bonding mode, bond strength and electronic structure of the final molecules.[52] The covalent bonds are formed by two non-metal atoms sharing two electrons from both elements. The linkage generated by this electronic interaction

is quite robust. It varies from 250-500 kJ·mol^{-1} for a single bond (C−H, C−C, O−H and N−H), up to 500 kJ·mol^{-1} for a double bond (C=O, C=N) and 800 kJ·mol-1 for a triple bond (C≡C). The coordination bond is on the other hand formed when a ligand (Lewis base) provides an electron pair to a charged or neutral metal (Lewis acid). The force connecting the metal center with ligands depends on the energy of the atomic orbitals interacting between the two elements. The metal-ligand bond is a part of the large family of the weak interactions. Their strength (50-150 kJ·mol^{-1}) is intermediate between the intermolecular interactions (eg. hydrogen bond, Van der Waals forces (<60 kJ·mol^{-1})) and the covalent bonds (Table 1).[52, 53]

Table 1. Strength of some covalent and non-covalent forces

Type of interaction or bonding	**Strength (kJ·mol^{-1})**
Van der Waals forces	<5
π-π	10-40
Hydrophobic effects	<50
Cation-π	5-80
Dipole-dipole	5-50
Hydrogen bond	20-60
Metal-ligand	50-150
Covalent bond	250-800

The bond strength is an energetic parameter. Even though it's merely indicative of an order of magnitude, it leads to a clear classification of the chemical interactions (weak and strong). It clearly shows that the energetic barrier for such bond, which is usually easily formed and broken, is more favorable compared to the covalent bond. Despite this facility of the dynamic exchange, the efficiency of the weak interactions to generate systems with good thermodynamic stability has been well demonstrated.[52]

For the coordination metal compounds, the thermodynamic stability is crucial to rationalize our knowledge about the behavior of metal complexes in solution. It deals with the stability constant (K) and the Gibbs free energy (ΔG°) in the reaction equilibrium. If the association constant K is very high, the energy is negative (ΔG° < 0) and the final complex is stable. This thermodynamic factor is directly related to the reaction environment (solvent, temperature, ligand and metal ion). The charge, the electronic and the geometric structure of the metal ion and the sterical (geometrical factor) and the chelating effect (entropic factor

(ΔS)) related to the ligand are the major elements affecting the stability of the final complex. Another qualitative theory was developed in 1963 by Ralph G. Pearson who introduced the notion of the "hard, soft" acid and base or class (a) and class (b). "Hard acids bind strongly to hard bases and soft acids bind strongly to soft bases". This theory gives the opportunity to better predict the thermodynamic behavior of such metal complexes.[54]

The stability and the inertness of the complexes are two different types of parameters: the first one related to the thermodynamic stability and the second one to the kinetic stability. To overcome this confusion, many examples are discussed in the literature in which coordination compounds are stable and labile or inert and instable. Despite their stability, the rates of the ligand exchange in these three complexes $[Ni(CN)_6]^{3-}$, $[Mn(CN)_6]^{3-}$, $[Cr(CN)_6]^{3-}$ are different. The substitution of the CN^- ligand by their labeled $^{14}CN^-$ in the nickel system is very rapid (30s) compare the last two complexes (1h and 24d, respectively). Therefore, the Ni-CN coordination bond in the complex $[Ni(CN)_6]^{3-}$ is termed labile, whereas the Mn-CN bond in $[Mn(CN)_6]^{3-}$ and the Cr-CN bond in $[Cr(CN)_6]^{3-}$ are called inert.[55, 56]

								half life
$[Ni(CN)_6]^{2-}$	+	$4\ ^{14}CN^-$	$\rightleftharpoons$	$[Ni(^{14}CN)_4]^{2-}$	+	$6\ CN^-$		30s
$[Mn(CN)_6]^{3-}$	+	$6\ ^{14}CN^-$	$\rightleftharpoons$	$[Mn(^{14}CN)_6]^{3-}$	+	$6\ CN^-$		1h
$[Cr(CN)_6]^{3-}$	+	$6\ ^{14}CN^-$	$\rightleftharpoons$	$[Mn(^{14}CN)_6]^{3-}$	+	$6\ CN^-$		24d

In acid solution the $[Co(NH_3)_6]^{3+}$ complex with inert coordination bonds decompose following this pathway:

$$[Co(NH_3)_6]^{2-} + 6\ H_3O^+ \rightleftharpoons [Co(H_2O)_6]^{3+} + 6\ NH_4^+$$

Henry Taube (Nobel Prize in Chemistry, 1983) is a pioneer who studied the dynamic behavior and developed the kinetic parameters of several coordination compounds.[57] He classified the complexes into labile and inert groups based on the reaction time and the rate of the metal-ligand exchange on the basis of substitution reaction and isomerization. In addition, labile complexes react fast, about one minute in 0.1 M solution at room temperature (25 °C) and those that are inert, under the same conditions react slowly (more than 2 hours). The rate of the metal-ligand exchange was also rationalized by Taube with the study of the

substitutions reactions of water molecules in different complexes. He noted that even the strength of the M-OH_2 bond is merely in the same order of magnitude, the rate of exchange vary largely according to the metal ions. For example the rate of exchange for the Mg(II), Ni(II), Ca(II) and Na(I) is very fast (up to 10^9 sec^{-1}) compared to the Pt(II), Ru(II), Os(II), Ir(III), Cr(III) with a slow rate of exchange (taking hours or even days) (Fig. 4). This lability is related to the nature of the coordinated groups, the radius, the charge and the electronic configuration of the complex ion.[52, 57]

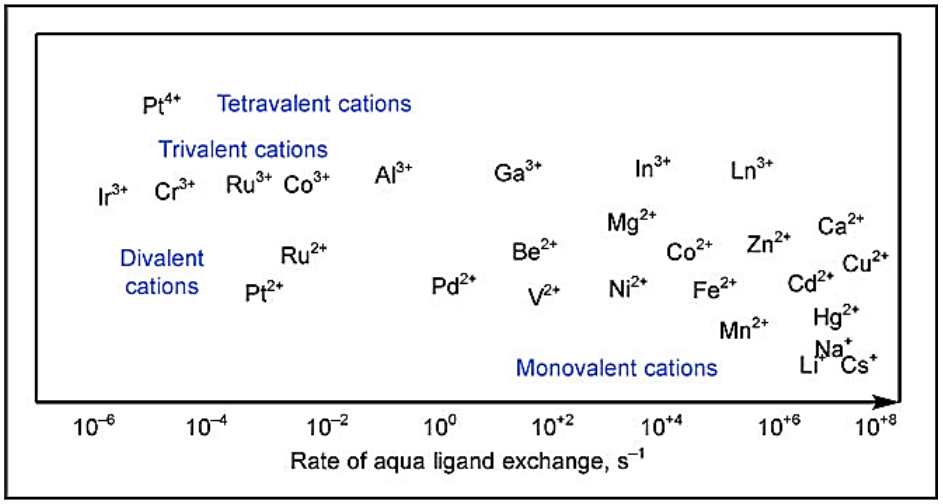

Figure 4. Schematic, logarithmic presentation of relative kinetics of aqua (H_2O) ligand exchange, for a variety of metal ions.[52]

The lability of the metal coordination bond is clearly demonstrated in the substitution reactions which proceed via two kinetic pathways, namely associative and dissociative process. The substitution can be easily followed if the incoming ligand is a water molecule (which can be labeled with the isotope oxygen-18) or by isotopic labeled molecular analogue of the substituted ligand.[56]

Associative Process: This pathway is abundant for square planar complexes, where the dissociation of the substituted ligands takes place after the coordination of an incoming group as a fifth ligand (Fig. 5). The rate of the exchange is generally enhanced by the *trans* effect of the incoming ligands that are opposite to other certain ligands.

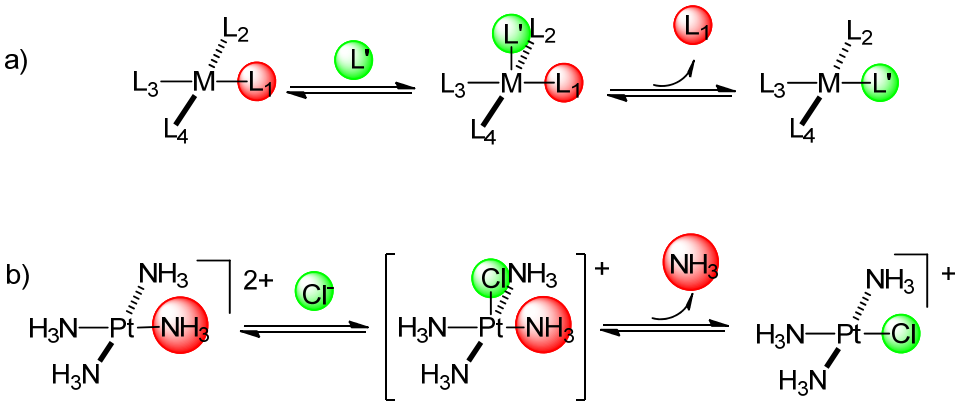

Figure 5. Metal-ligand exchange via an associative process: a) General pathway; b) Substitution of an ammonia ligand by a chloro ion in the complex $[Pt(NH_3)_4]^{2+}$.

Dissociative Process: The dissociation of the coordinated groups takes place before the association of the new ligands. For example, in octahedral coordination compounds, a five-coordinate intermediate is generated during the process before reaching the equilibrium (Fig. 6).

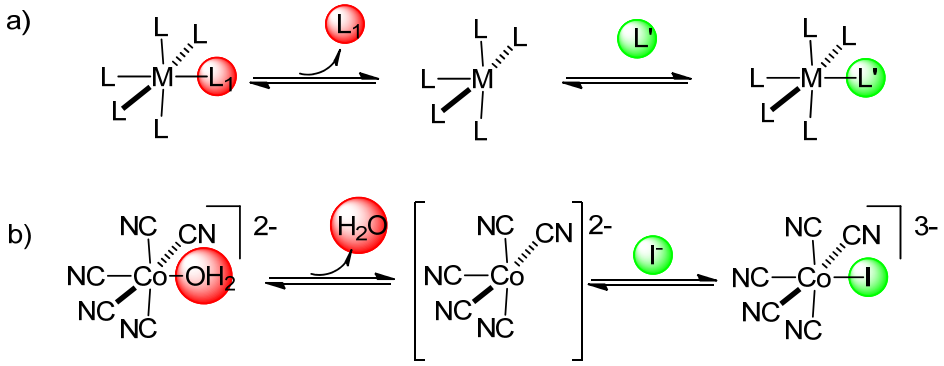

Figure 6. Metal-ligand exchange via a dissociative process: a) General pathway; b) Substitution of water molecule by an iodide ion in the complex $[Co(CN)_5(H_2O)]^{2-}$.

The versatility of the coordination bonds, in addition to the ligands exchange are two major advantages provided by the coordination compounds. This dynamic behavior has been explored in two large areas: catalysis and biology. In the field of catalysis, this behavior is used to enhance the rate of the reaction and to produce original compounds inaccessible with conventional synthetic processes. Different catalytic processes with a collection of transformations and exchange mechanisms have been reported.[58]

In biology, reactivity and activity correlations give precious information about the mechanism and mode of action of the metallo-drugs with DNA and the bio-molecules.[52, 59] Moreover, it plays a key role in explaining and predicting the dynamic behavior and the

flexibility of the different blocks forming the coordination driven metalla-assemblies and an eventual self-organizations phenomena which presents the main topic of this work.

1.2.2 Synthetic Strategies

At the molecular level, it has been proven that the dynamic behavior of a single metal complex is related to the reversibility of the interaction between the metal ion and the ligands. However, the extrapolation of the same models to predict or to have deep information about such dynamic process at the macromolecular level may lead to false interpretations.

A supramolecular system is an arrangement of a finite number of metal complexes and a collection of flexible ligands held together via a reversible and spontaneous process. In this pathway the initial precursors, the intermediates and the thermodynamic stable supramolecular assemblies are in vivacious interactions.[8] The thermodynamic and the kinetic pathway of this course depend on the chemical properties, the geometrical affinity and the assembly conditions of this species.[22, 60, 61] The design and the elaboration of the coordination driven metalla-assemblies can be understood by considering three different synthetic approaches. Each of these strategies possesses its specific and proper rules which dictate the formation of the metalla-assemblies.[6, 62]

a- Weak-Link Approach

The "Weak Link Approach" (WLA) is a simple convergent synthetic route capable of producing a number of flexible 2D and 3D metalla-rectangles, prisms and cylinders with adaptable cavity and geometry.[63] The first bimetallic Rh(I) macrocycles synthesized via this strategy was presented by Mirkin *et al.* in 1998. He reacted a 1:1 stoichiometric ratio of Rh(I) precursor with a phosphanyl alkyl ether hemilabile ligand in the presence of silver tetrafluoroborate to produce the condensed structure A1, and isolated as tetrafluoroborate salt with high yield (<95%).[64]

The phosphanyl alkyl ether ligand is an unsymmetric chelating ligand with two different connecting side (P,O). It interacts with the metal center through a strong (M-P) and weak (M-O) bonds. Addition of a small molecule such as carbone monoxide or acetonitrile (anscillary ligand) to the solution of the complex **A1** breaks the weak bonds (M-O) and forms

strong (M-CO) or (M-CH_3N) bonds. This self-rearrangement in the chemical forces generate a spontaneous spatial self-reorganization, leading to the formation of the open form structures **A2** and **A3** respectively, in which the two rings are expanded by 6 Å. In this thermodynamic stable structure, still the metal center is not inert. It possesses free coordination sites which can be used in many purposes. Mirkin *et al.* connected the two metalla-rectangles **A2** and **A3** using ditopic ligands. For example, addition of one equivalent of 4,4`-biphenyldiisocyanide or 4,4`-biphenyldicarbonitrile to **A3** results in two elegant multifunctional cylinders **C1** and **C2** respectively (Fig. 7).[64]

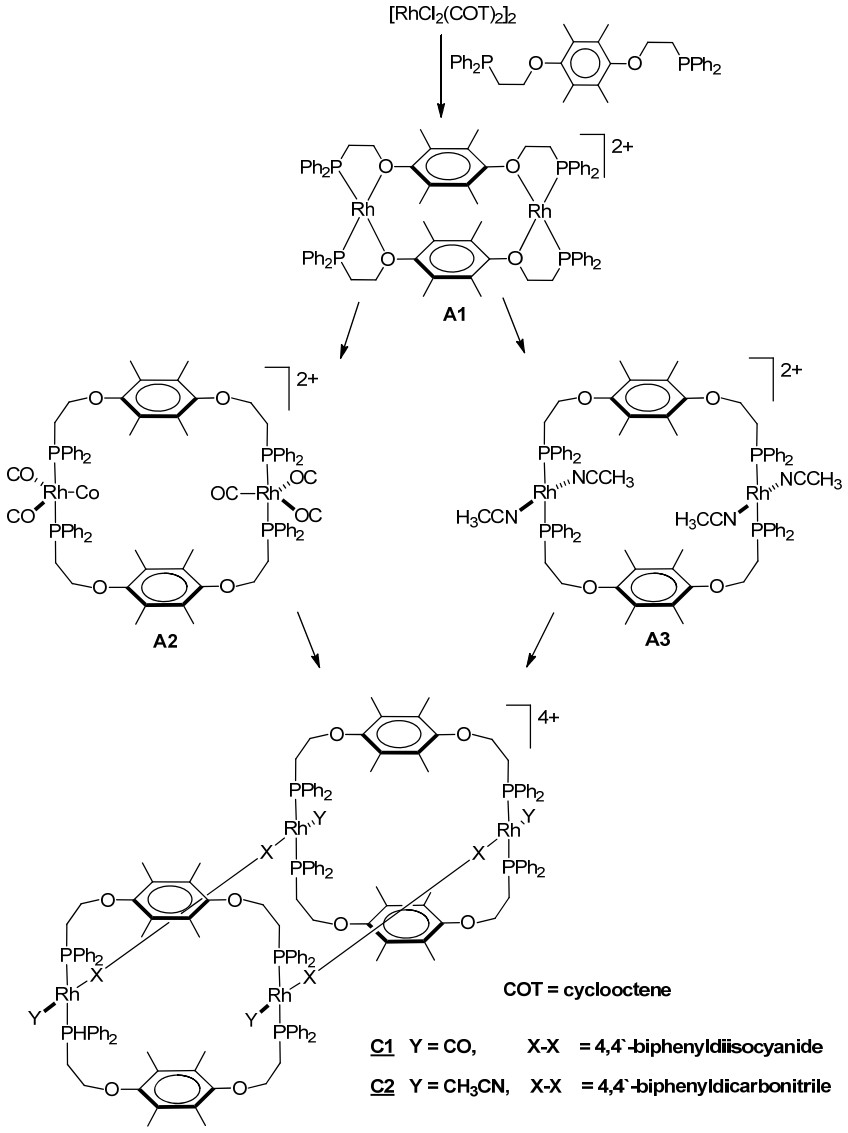

Figure 7. Generation of 2D and 3D supramolecular assemblies with tailorable geometries from a starting condensed structure. An example highlighting the dynamic stuructural behavior of the coordination metalla-assemblies synthesized via the Weak-Link Approach.[64]

Later on, this work inspired chemists to successfully design a number of homo-metallic supramolecular architectures with variable geometries and wide range of properties (Scheme 2).[65] The major concept dictating the formation of these structures still deals with three major elements: simple flexible hemilabile ligands, rigid anscillary ligands and naked transition metal precursors.[66]

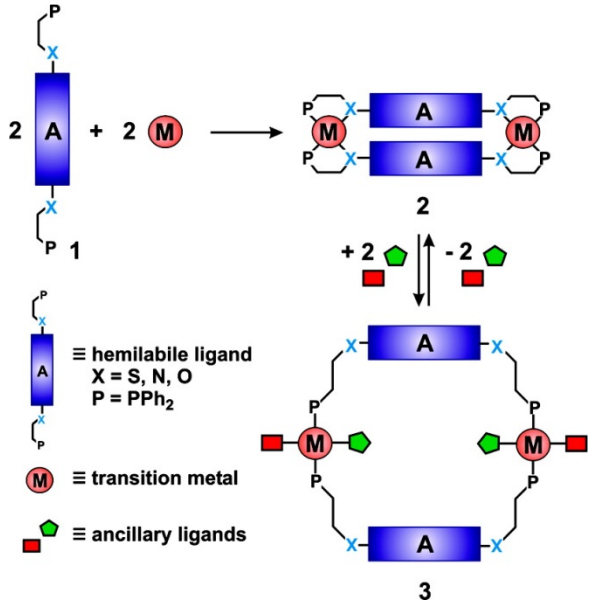

Scheme 2. Principle of the Weak-Link Approach.[67]

The spontaneous substitution of an anscillary ligand by another flexible donator group and the partial ligand dissociation of the hemilabile ligand without impacting the geometry of desired supramolecular structure are the major advantage of this approach. This trademark gives the possibility to produce a new class of supramolecular assemblies with high versatility and dynamic structures.[68]

Even though, the major drawback resides in the low thermodynamic stability of the condensed structure. In fact an increasing of the temperature leads to the decomposition of the kinetic supramolecular system (fig. 8).[6, 63a, 69]

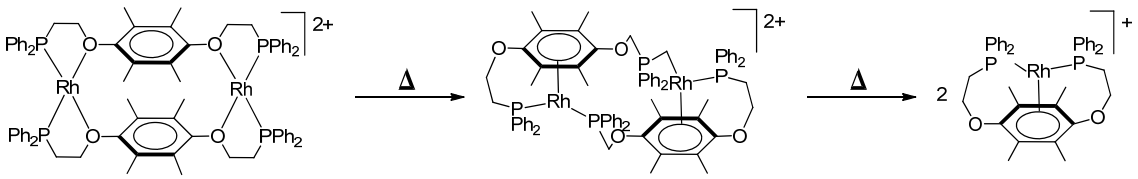

Figure 8. Decomposition of the dimer structure into the thermodynamic stable monomer under thermodynamic control.[6, 63a, 69]

b- Symmetry Interaction Approach

In this synthetic strategy, the geometry requirement to design the supramolecular structure is more important than in the other two strategies. Specific attention to the complementarity and symmetrical demands between the initial precursors is needed to overcome the wrong pathway leading to the formation of oligomeric mixtures.[8] This specificity comes from both the metal ions and the ligands. In fact the acceptor groups used are generally naked metal ions which have a collection of binding possibilities and availability in their binding sites. The donor groups are rigid multibranched chelating ligands acting as bidentate ligands which are kinetically less labiled than monodentate analogues with respect to the coordination geometry of the metal ion. These kinds of ligand provide, however, a great stability in the targeted system due to the strong binding affinity with metal ions. This design strategy has been pioneered by Maverick[70, 71] and developed later by Saalfrank[72], Lehn[73] and Raymond[74]. A plethora of highly symmetrical neutral or negatively charged supramolecular clusters based on the metal-ligands coordination bonds has been synthesized.[75] The M_4L_6 tetrahedron is one of the most common tridimensional structures developed with this strategy.[76] It consists of four metal ions at the vertices and six bis-bidentate ligands at the edges of the final structure (Fig. 9).[77]

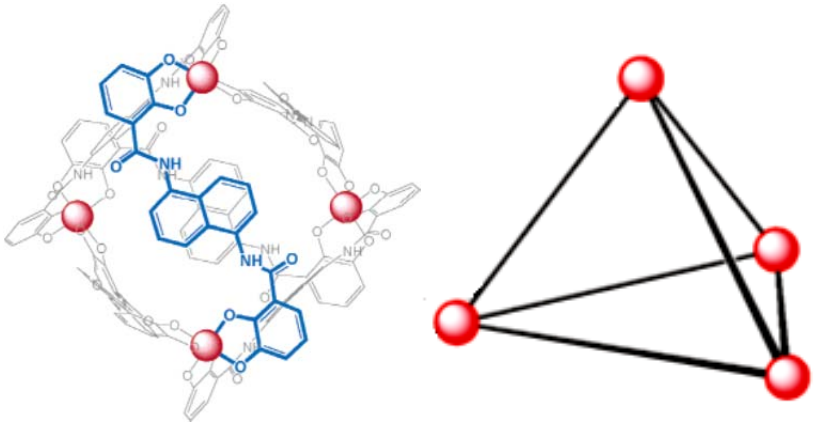

Figure 9. The tetrahedral M_4L_6 host assembled from four pseudo-octahedral metal centers and six bis-bidentate catechol-amide ligands.[77]

These tetrahedrons possess a cavity, whose ability to hide a guest molecules, especially cationic species, was intensively studied.[78] The investigation of the kinetic self-corrections and self-rearrangement phenomena under thermodynamic control has greatly progressed in recent years.[77,] The main target of these studies was to determine the main

elements and the pathway of the dynamic exchange of the guest from the M_4L_6 supramolecular tetrahedral host. In fact two mechanism of exchange have been proposed, a dissociative or a non-dissociative pathway (Fig. 10).[77]

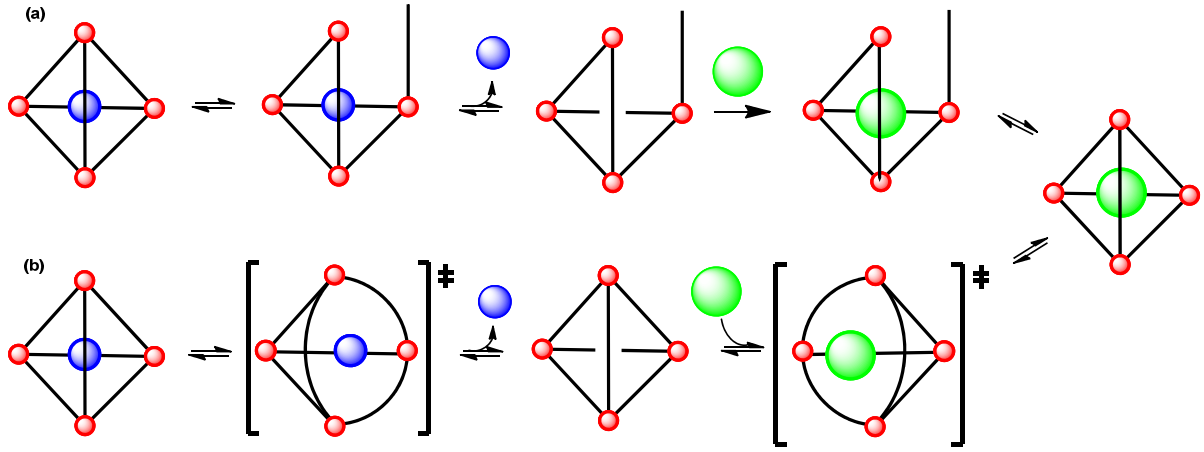

Figure 10. Guest-exchange mechanisms involving host rupture (a) or passage through an aperture (b). An example of the flexibility and the dynamic behavior of the metalla-supramolecular assemblies synthesized via the symmetry interaction approach has been empirically proved.[77]

The first mechanism consists of a partial disconnection of the ligand to the metal ion, thus opening a gate to ingress or egress the guest molecule: The tetrahedral structure being maintained. While in the second process a spatial self-rearrangement based on the elasticity of the host is needed to generate a gate for the release and catch of small molecules. In these studies, the results are in favor of mechanism (b) as the most plausible exchanging pathway. In fact, three arguments put evidences in that conclusion: i) the rapid exchange of NEt_4^+ by PEt_4^+ in both labile ($[Ga_4L_6]^{12-}$) and inert hosts($[Ti_4L_6]^{8-}$ and $[Ge_4L_6]^{8-}$) (Fig. 11); ii) the flexibility of the hosts to provide a gate for an eventual catch and release of a guest molecule through a non-dissociative pathway has been confirmed by theoretical calculations; iii) no exchange noted in the case of the $CoCp^{*2+}$, a bulky guest molecule.[77]

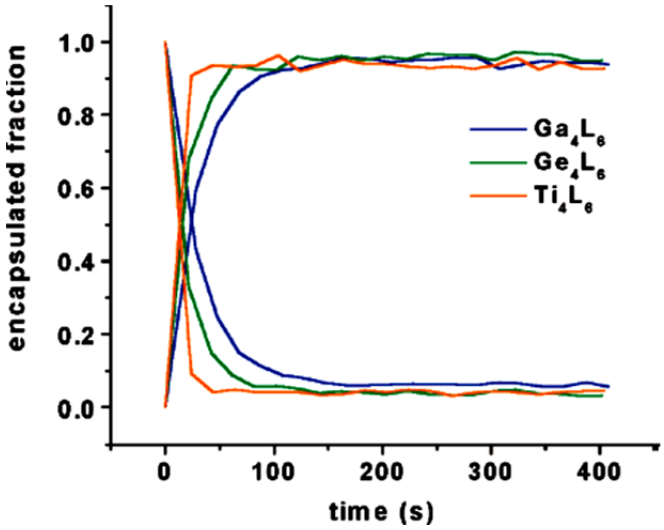

Figure 11. The dynamic guest exchange of NEt_4^+ by PEt_4^+ in the $[Ga_4L_6]^{12-}$, $[Ge_4L_6]^{8-}$, and $[Ti_4L_6]^{8-}$ hosts in DMF-d_7 at room temperature. (The ingress of PEt_4^+ within the cavity of the hosts increases with time, while encapsulated NEt_4^+ decreases).[77]

1.2.3 Directional Bonding Approach: General Concept

With a simple self-assembly synthetic pathway, a narrow geometrical design require high efficiency in the construction of metalla-assemblies structures, whether two or three-dimensional. Nowadays, the directional bonding approach has become the most commonly used strategy. It consists of combining a stoichiometric ratio of building blocks with complementarity in shapes and geometries via the most suitable low-energy pathway.[79] The form and the self-assembly properties depend on the affinity between the initial precursors (ligand and metal complex), their direction, angles and energies.[41b] The first polygon obtained via this strategy, **A4**, was developed by Fujita *et al.* in 1990. It is a square metalla-assembly, consisting of a 1:1 stoichiometric ratio of two type of building blocks, a linear ditopic ligand (4,4'-bipyridine) and an end capped (non-naked) metal complex (palladium (II) ethylene diamine, Pd (en)) (Fig. 12).[45]

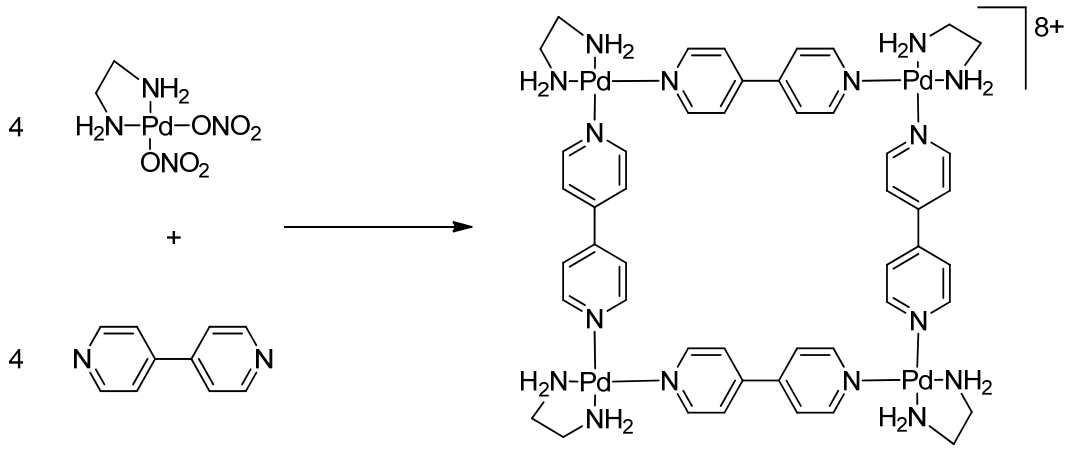

Figure 12. Synthesis of the square ***A4*** *($\{[(en)Pd(4,4'\text{-bipyridine})_4]^{8+}\}$).*[43]

The pre-arrangement of the suitable rules favoring the formation of this coordination driven metalla-assembly are crucial. It can be summarized in three different aspects: geometrical concepts, properties of the chemical interactions and thermodynamics considerations.[43]

While the major concepts dictating the formation of the structure described above are resuming the fundamental rules of the directional bonding strategy. Many pioneers in this field like Stang[80], Severin[81] and Fujita[45] groups have successfully reprogrammed these three aspects. A large number of two and three dimensional metalla-assemblies having unique geometries, properties and applications were produced.[51] The generalization and the rationalization of these rules in a general approach called (directional bonding approach) are very much reviewed.

a- Geometrical Considerations

Basically in this approach, the angles and the availability of the coordination sites of the metal complex are intentionally prearranged and designed. In fact, for A4, the 90° angle was produced and protected during the synthetic process by an inert metal-ligand bond forming a highly stable five membered metalla-cycle. Therefore, the rigidity is provided by the ethylene diamine - a chelating group occupying two available coordination sites at the metal ion. The complementarity in shape also favored square-planar geometry between Pd(II) metal complex and the bipyridine groups by replacing the two (NO_3^-) ligands and coordinating to the metal while respecting the initial molecular geometry.[43]

Even though, the use of naked metal ions (availability in the coordination sites) led to the formation of structures with miscellaneous shape, size and number of metals.[82,41a] Similarly in 2010, coordination of dipyridylthiophene with palladium (II) complex enabled the formation of spherical supramolecular structure **C3** of type $M_{24}L_{48}$ containing 72 assembly units. This giant cage was characterized by X-ray crystallographic analysis (Fig. 13).[83]

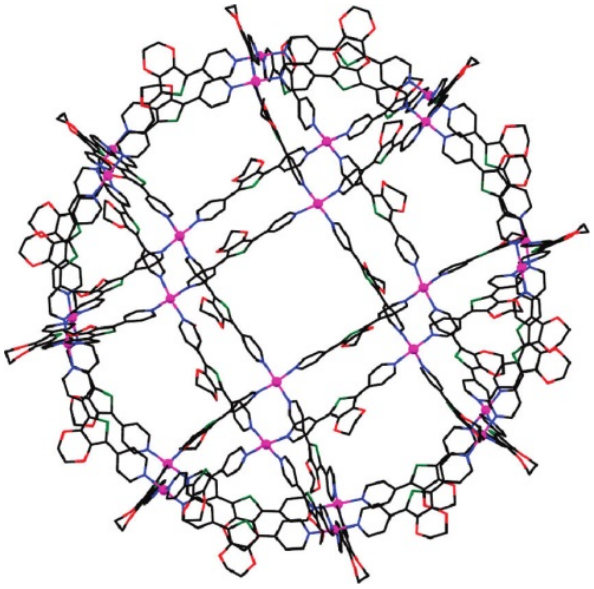

*Figure 13. Molecular structure of rhombicuboctahedron **C3** composed of dipyridylthiophene ligands and palladium (II).*[83, 84]

Stang is one of the pioneers in this field, who intensively developed this chemistry. He not only synthesized a plethora of metalla-assemblies: cubes, rectangles, squares, prisms, but also rationalizes the knowledge by coding the geometrical algorithm giving rise to the major number of the two and three dimensional structures with different shapes, size and geometries. [30, 84] For example, of a square-shaped supramolecular structure can be conceivable by various paths. One approach is to take a metal complex having coordinate angle 90 ° and mix it with the same proportion of a ditopic linear ligand. It is also possible to reverse the angles between the metal and the ligand. Finally, another alternative may be the mixing of ligand and complex (1:1) both having 90° angle of coordination. This approach results in different combinations of discrete structures as listed in (Table 2).[8]

Table 2. Library of ditopic ligands and metal complexes leading to various polygones.[8]

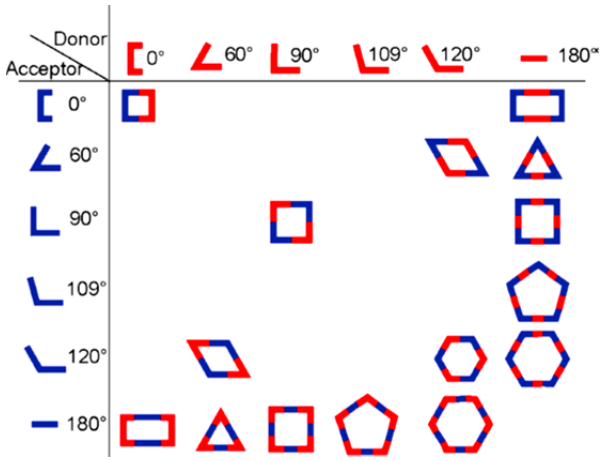

The development of three-dimensional systems (polyhedra) follows the same principle. In the case of a cube, for instance, a metal complex with tritopique angles of 90 ° is coordinated with a linear ditopic ligand. Different combinations of resulting polyhedron are listed in (Table 3).[8]

Table 3. Library of ditopic and tritopic unit leading to various polyhedrons.[8]

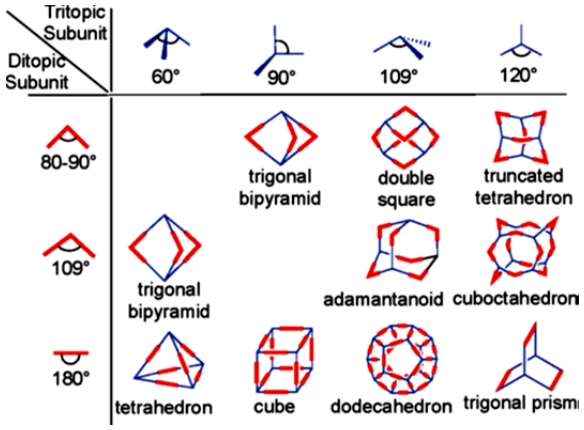

b- Metal-Ligand Coordination Bond

As described in the section (1.2.1), the strength of the bonds, kinetic and thermodynamic properties of the metal-ligand coordination precursors is highly dependent on the metal center and the ligands. Their impact on the self-assembly formation of supramolecular entities has already been demonstrated. In addition, as reviewed by Fujita, it is empirically proven that [(en)Pd(NO_3)$_2$] and 4,4- bipyridine are the most successful precursor combinations. Many others experiments using different metals ions like (Ni, Co, Fe, Mn) and

combinations with different chelating ligands was never successful, except in the case of the platinum(II) but under high temperature 100 °C and slow reaction (several weeks).[85] Examination of the synthesis of Pt and Pd squares with cyano-ligand is another example (Figure 14). Under kinetic control, the palladium precursors form the targeted square. However a mixture of oligomers was found for the platinum analogue (Fig. 14).[22, 23]

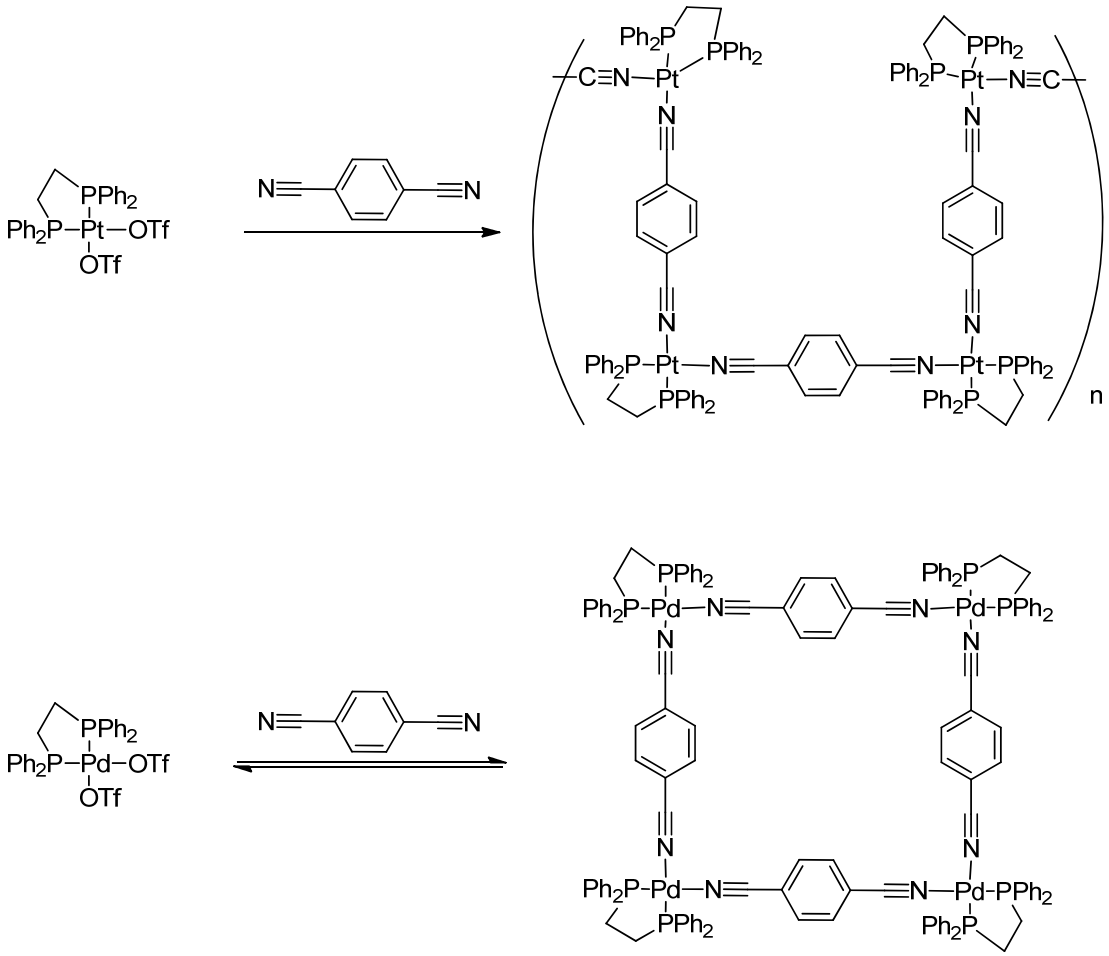

Figure 14. The formation of Pt oligomers versus thermodynamic product the Pd square. An example of the kinetic self-corrections phenomena.[22, 23]

While the Pt corners possess similar chemical properties and spatial geometry as the Pd(II) complex, the reactivity and bonding strength of two metal ions with the linear ditopic ligand are different. The rate of the exchange of the 4,4-bipyridine with the Pt(II) complex is slower than the Pd(II) counterpart. Therefore, the rapid exchange between the initial building blocks, the reaction intermediates and the final compound is crucial during the synthetic process. This dynamic behavior favor the self-rearrangement and the self-correction during the synthetic process, transforming an eventual intermediate oligomers into a stable thermodynamically system.[43]

c- Thermodynamic Aspects

It is evident that targeting a single product can only be achieved if it is energetically favored *vis a vis* other systems. Therefore, the initial precursors should correctly pass through the right thermodynamic pathway to give quantitatively high yield. Otherwise, the reaction process may pass through many level and minima of thermodynamic energy, generating some byproducts such as oligomer mixture or closing structures (Scheme 3).[43]

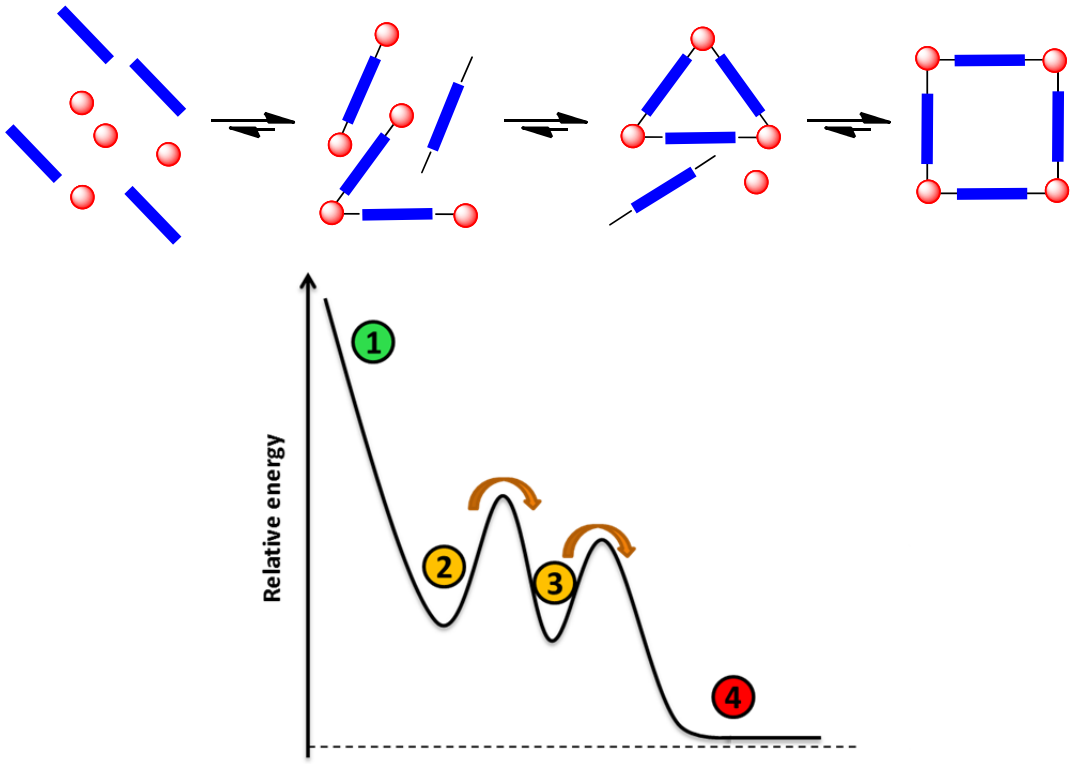

Scheme 3. A putative germination pathway of some supramolecular squares: 1) initial precursors; 2) oligomers mixture; 3) unstable closing structure; 4) thermodynamic system.

If kinetic correction phenomena are not efficient, a thermodynamic equilibrium between triangle and rectangle is commonly encountered.[86] This balance can be rationalized and interpreted from a thermodynamic point of view. Indeed, the enthalpy promotes squares to minimize the steric constraints (angle of 90° to 60°), while the entropy favors the triangle formation which involves fewer components and therefore generates more species from the same quantity of reagents.

According to Le Chatelier principle, any variation of an external element (temperature, concentration, stoichiometric ratio) in the reaction environment affects this fluctuation and

favor one structure vis a vis another. An increase in concentration leads to the species favored by enthalpy (square) and a rise in temperature (and therefore the disorder) benefits the entropic species (triangle).[20a, 84]

In the case of thermodynamic stable assemblies, exerting an external stimulus leads to novel self-organization phenomena.[87] Severin *et al.* reported an example of a kinetic self-rearrangement of an octanuclear arene ruthenium metalla-cage to a tetranuclear metalla-plate. The thermodynamic stability of these two structures is very sensitive to the solvent. In chloroform solution the system A5 is the most stable. While in the dichloromethane solution it decomposes into the complex A6 (Fig. 15).[28]

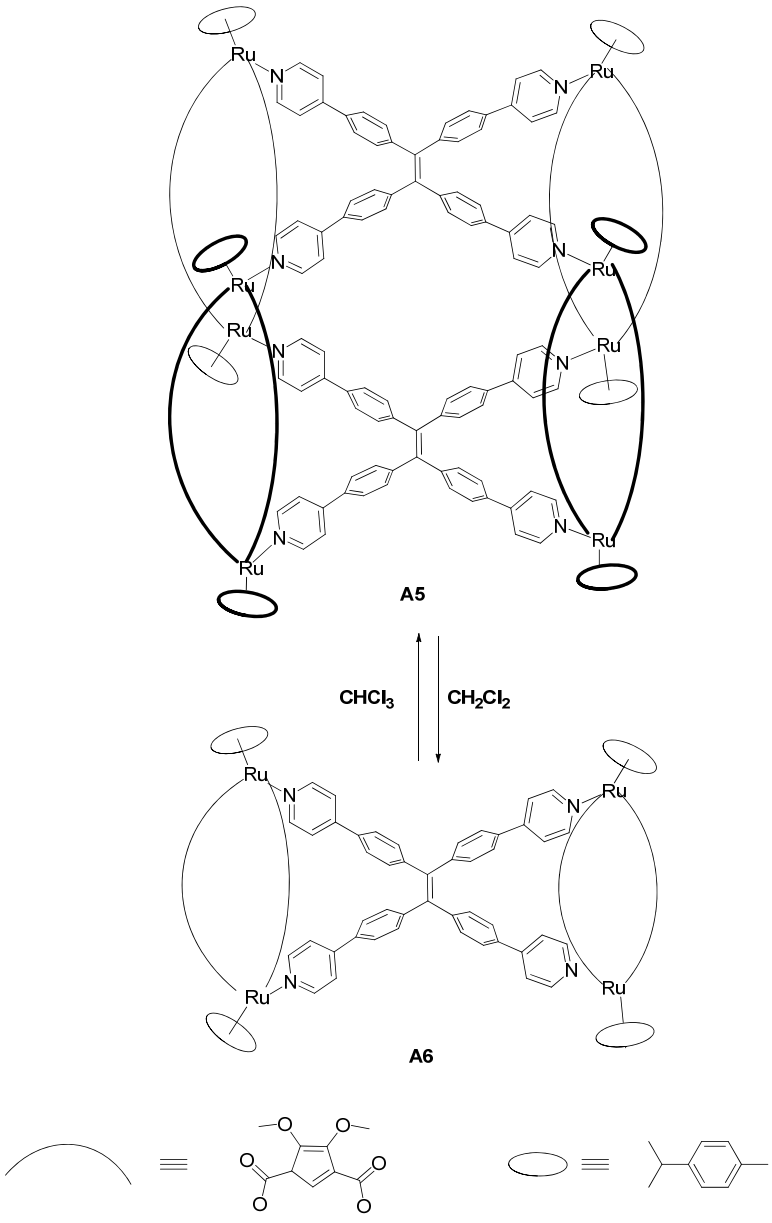

Figure 15. Dynamic structural transformations of the systems A5 vs A6 under solvent control.[28]

Changing the stoichiometric balance of reacting species has been examined by Neogi *et al.*.[88, 89] The response of defined heteroleptic metallosupramolecular racks, rectangles, and trigonal prisms through the addition of pyridine ligands has been investigated. For example, excess of 1,2-di(pyridine-4-yl)ethyne, forces the metalla-rectangle to alter into a rack architecture in the solution (Fig. 16).[89]

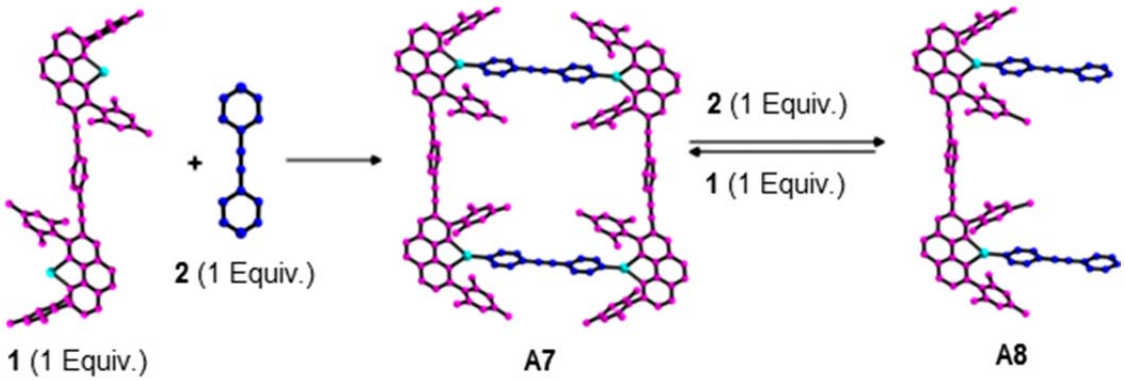

Figure 16. Dynamic interconversion of a thermodynamic stable closed system (A7) to an open structure (A8) under a stoichiometric control.[89]

The spontaneous selection of a specific product from a collection of possibilities remains the main challenge in coordination-driven self-assembly. These spontaneous selections are related to the self-repairing, self-recognition, and self-rearrangement of the different species during the synthetic process, transforming an eventual intermediate oligomers into a stable thermodynamically system.[21a] These self-organization phenomena are commonly encountered as theoretical argument to explain a successfully running algorithm. It was supported by the versatility of the coordination bonds and sometimes by such dynamic structural properties and thermodynamic fluctuations of some coordination-driven self-assemblies. Indeed, examples that directly and quantitatively evidence these dynamic behaviors remain scarce. The kinetic and thermodynamic aspects of the assembly-disassembly processes involved during the preparation of such supramolecular assemblies are the major factors of this trademark. In addition, a better understanding of these rules is essential for further chemical development.

The current work focuses on the arene-ruthenium metalla-assemblies built from stable dinuclear arene ruthenium units and polypyridyl donor via the directional bonding approach.[90] Investigations insight into the thermodynamic and kinetics rules dictating the formation of these systems in solution is the main issue of this thesis.

1.3 Arene Ruthenium Metalla-Assemblies

1.3.1 Introduction

Ruthenium is a transition metal with the electronic configuration [Kr] [$4d^7$] [$5s^1$]. It is a group VIII member together with iron (Fe) and osmium (Os) and the element number 44 of Mendeleev's periodic table. The oxidation states of ruthenium in organometallic chemistry vary from 0 to IV, the oxidation states of II and III being the most importantes.[91, 92] Most of the ruthenium complexes possess an octahedral geometry stabilized by an 18-electron configuration. Some exceptions, however, do exist. For example, the triisopropylphosphine ruthenium compound [$CpRuCl(PPr^i_3)$] is a 16-electron complex with a square-planar stereochemistry.[93]

In the past four decades, ruthenium became a potential alternative to its analogues in the family of "platinum metals" (Ru, Os; Rh, Ir; Pd, and Pt) owing to many reasons:

i) a remarkable reactivity due to the flexibility in its oxidation states, the geometries, the coordination numbers, and a relative lability in the interaction between the metal ion and the ligands;[58, 94]

ii) an important biological activity which has been interpreted as the similarity with iron in biological medium. Ruthenium is a nontoxic metal that can mimic the behavior of iron (Fe) which is from the same group VIII of Mendeleev's periodic table.[95, 96, 97]

In many examples, a facile oxidation of the ruthenium ion and the lack of stability has also been observed. Especially, the reduction of Ru(III) to Ru(II) in biological medium was noteworthy in many active ruthenium species.[98] Therefore a better control of the electronic environment of the metal center along with the ligands exchange is crucial.

The use of the arene ligand in the ruthenium complex provides many advantages:

i) robustness and protection of the metal center, therefore the stability of the complex is maintained while the three remaining ligands keep a possibility of a "slow" exchange;[52, 99]

ii) the facile functionalization of the arene ligands by biologically active compounds, resulting in the co-existence of hydrophobic character with the

hydrophilic metal center which produce an amphilic system with remarkable biological properties;[97]

iii) the arene is an L_3 ligands with hapticity (η^6). It occupies three coordination sites, providing a predictable coordination angle and directionality to the incoming ligand which is crucial in supramolecular chemistry.[99-100]

The reactivity of the arene ruthenium complexes, their impact in the final supramolecular assemblies along with the host-guest properties and the biological activities are the main issues of the current work.

1.3.2 Half-Sandwich Arene Ruthenium Complexes: Synthetic Strategies and Reactivity

a- Preparation

The dinuclear benzene ruthenium chloride was the first arene ruthenium complex discovered in 1967 by Winkhaus and Singer. The reaction of $RuCl_3 \cdot nH_2O$ with the 1,3-cyclohexadiene derivative in ethanol solvent leads to a brown product.[101] Even though, the identification of the correct formula and the dimeric structure of this new complex was confirmed only seven years later by Bennett.[102] The X-ray analysis showed chloro-bridged dimers in which the two ruthenium metal ions were in oxidation state II and were coordinated to benzene (an L_3 ligand with hapticity η^6).[103] The precise formula of this compound is $[(\eta^6\text{-}C_6H_6)Ru(\mu_2\text{-}Cl)Cl]_2$.

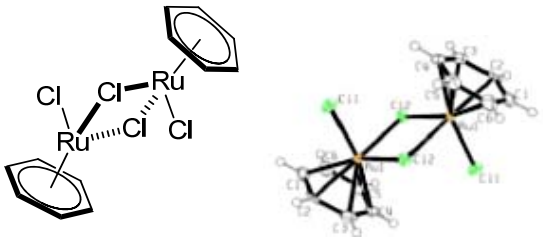

Later on, many dimeric arene ruthenium analogues have been designed. Many synthetic routes are discovered related to the arene nature.[104] The most commonly used strategy is still the one discovered early by Winkhaus and Singer employing the electronically poor dienes such as α-phellandrene or 1-methyl-1,3-cyclohexadiene.[102]

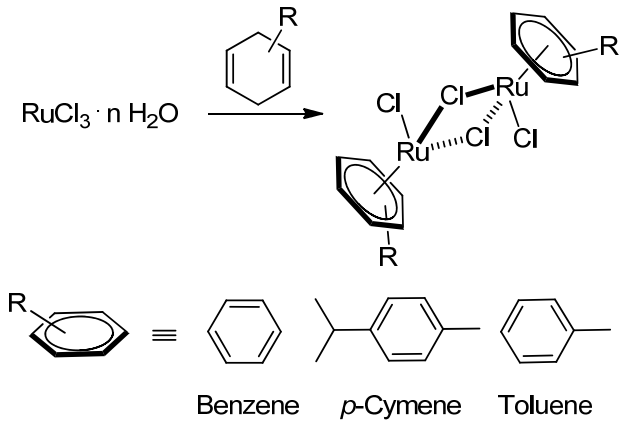

Other complexes containing electronically rich arenes, such as (C_6Me_6) or durene (1,2,4,5-$Me_4C_6H_2$) are however synthesized only through the arene exchange route. For example, the exchange of the para-cymene ligand by the hexamethylbenzene analogue at high temperature (around 200°C) leads to the desired hexamethylbenzene dimer.[105]

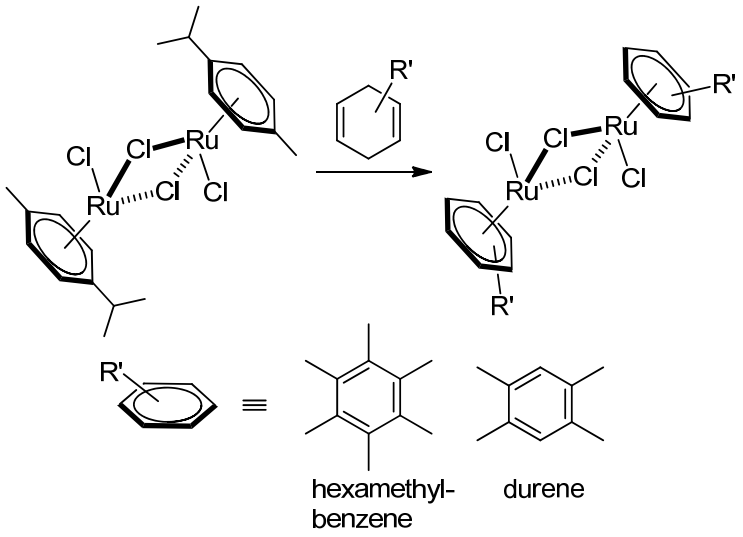

In order to improve the biological properties of the arene ruthenium complexes, different functions are grafted to the ruthenium dimers.[106] One possibility is a general and multi-steps approach, which consists of the functionalization of the arene ligand via conventional coupling reaction such as esterification reaction, followed by Birch reduction to generate the diene through the reduction of the aromatic ring.[107] Finally, the complexation reaction gives rise to the targeted compound via the Winkhaus and Singer method. The dinuclear complex [$RuCl_2\{C_6H_5(CH_2)_3OCO$-*p*-$C_6H_4$-$OC_8H_{17}\}]_2$ synthesized in 2006, in our groups is a good example of the developed form of dimeric ruthenium complexes.[108]

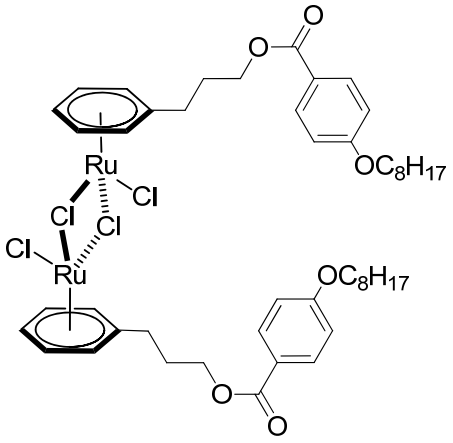

The second approach was reported at first by White in 2005, in which the formation of the functionalized complex can be formed via one pot strategy. The mixture of the ruthenium tri-chloride with 1-methoxy-1,4- cyclohexadiene (commercially available diene) in ethanol, or 1,2-ethanediol gives rise to the desired compounds. [109] The coupling reaction occurs by an alkoxy exchange via an acid catalyzed mechanism.[99]

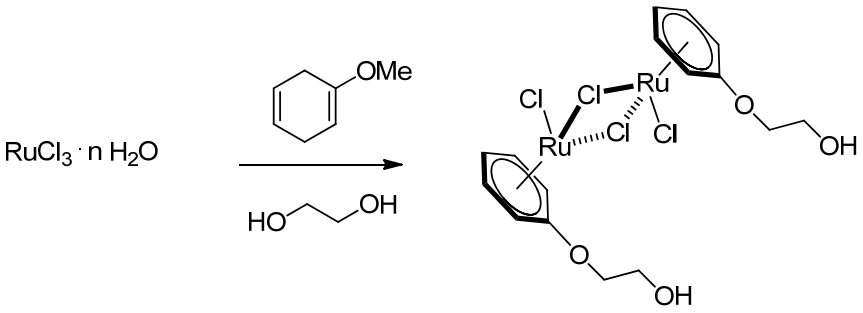

b- Reactivity

Apart from the substitution reactions of the arene ligands occurring under harsh conditions, these π ligands are inert and attributed to the protection of the oxidation state of the metal ion and the stability of the complex.[99] In general, the rich chemistry of the dimeric arene ruthenium complexes is based on their air stability and the reactions with a collection of neutral donor ligands having two electrons (phosphines, nitriles, pyridines, carbonyle and dimethylsulfoxide).[102] These reactions lead to the decomposition of the dimeric structure yielding mononuclear complexes $[(\eta^6\text{-arene})RuCl_2L]$ via cleavage of the chloro-bridge (route ***A1***). Cationic mononuclear complexes with type $[(\eta^6\text{-arene})RuClL_2]^+$ or $[(\eta^6\text{-arene})RuClL_2]^+$ usually have been obtained by the coordination of two or three ligands L. Eventually, these

cationic species are favorable in polar solvents or in the presence of a halide scavenger (route ***A2, A3***) (Scheme 4).[102]

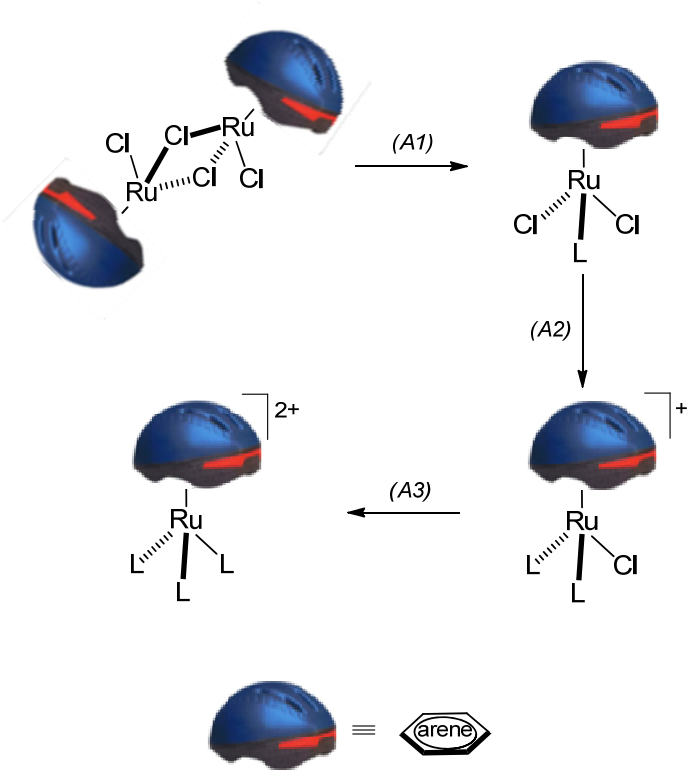

Scheme 4. Reactivity of the chloro-bridged arene ruthenium complexes.

One of the original aspects of the reactivity of the ruthenium-arene complexes is their behavior in aqueous solution. In 1972, Zelonka and Baird observed aqua complexes of ruthenium during the hydrolysis of $[(arene)RuCl_2]_2$ in D_2O.[110] Few years later, Ludi isolated and characterized the ruthenium and the osmium aqua dicationic complexes ($[(C_6H_6)Ru(OH_2)_3]^{2+}$ and its analogue $[(C_6H_6)Os(OH_2)_3]^{2+}$) as a tosylate salt.[111] The X-ray analysis of the ruthenium species shows a mononuclear tri-aqua complex in a pseudo octahedral geometry at the ruthenium (II) atom. The structure is similar to a three legged "piano stool" in which the arene ligand presents the seat and the water molecules are the legs (Scheme 5). Hence then, the term "piano stool" was assigned and nowadays this kind of complexes are an attractive systems in many field of applications.[111]

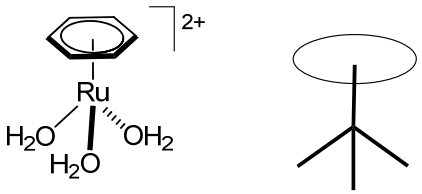

« Piano-stool » structure of the tri-aqua arene ruthenium complex

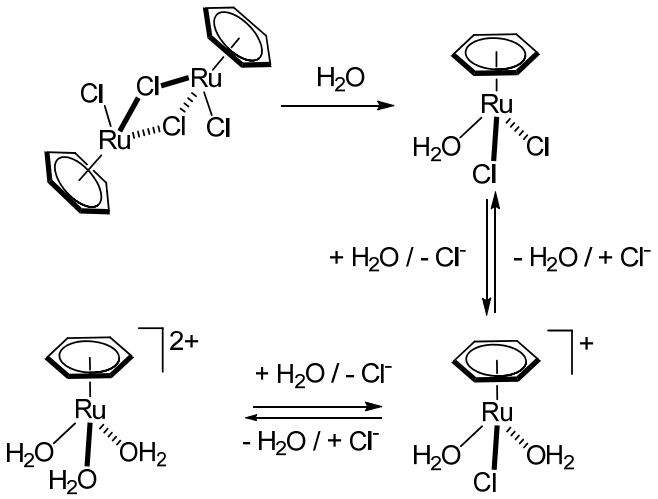

Scheme 5. Hydrolysis of the arene ruthenium chloro-bridged complexes.[112]

In the past two decades, these chloro-bridged arene-ruthenium complexes were used as initial precursors to synthesize new molecular clips with different shape, size and stability. Indeed, the chloro-bridge was substituted by a rigid multibranched chelating ligands or thiol groups, increasing in a controlled manner the distance between ruthenium atoms, along with the rigidity of the dimeric structure.[113] Some of these half-sandwich complexes showed a very high activity against cancer cells, especially the thiols compounds.[114] Their ability to oxidase the glutathione facilitate the destruction of the tumor cells has already been confirmed (Fig. 17).[115]

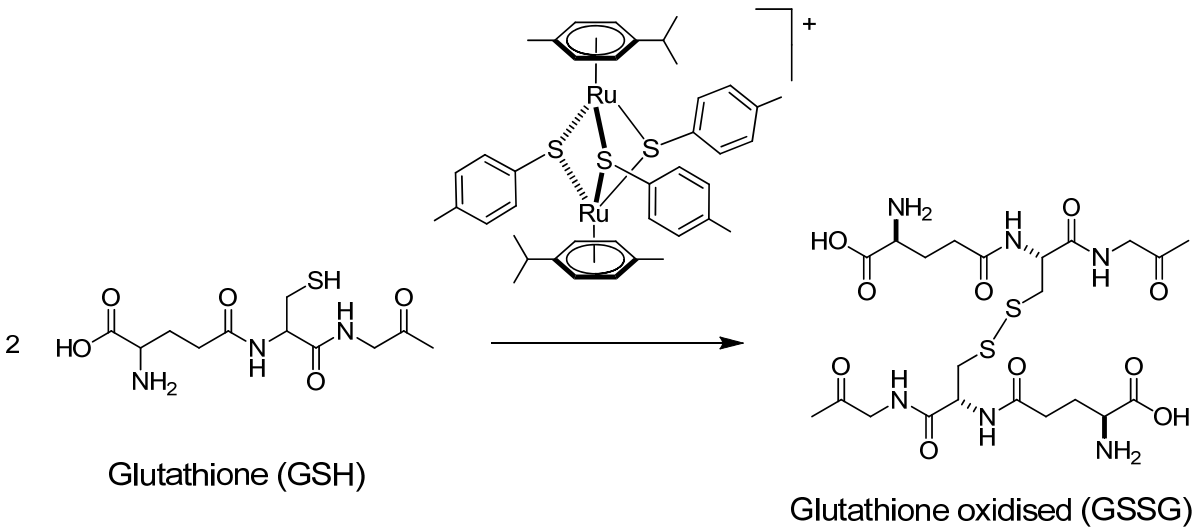

Figure 17. Oxidation of the glutathione by tri-thiolato bridged arene ruthenium complex.[115a]

Another application of these complexes is their ability to generate supramolecular assemblies. In fact, the two chloro ligands are labile and usually easily replaced by solvent molecules or others donor groups. For example, the coordination of the methanol groups in the oxalato clip in the presence of the silver triflate (Fig. 18).[116] This reactivity of the half sandwich complexes is crucial to elaborate supramolecular self-assembling systems.[100]

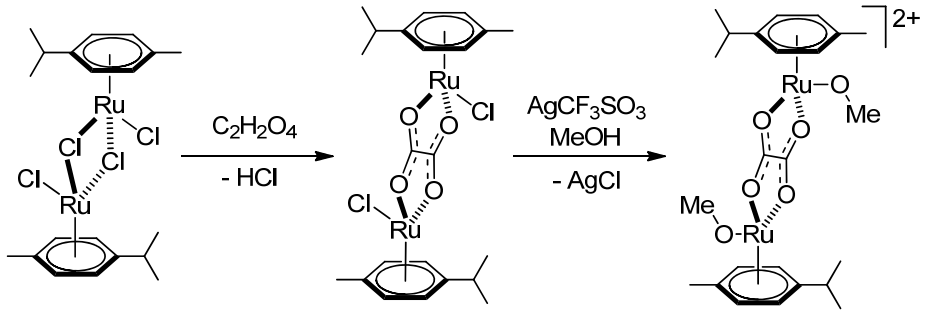

Figure 18. Synthesis and reactivity of the oxalato metalla-clips [(arene)$_2$Ru$_2$(μ-C$_2$O$_4$)Cl$_2$].[116]

1.3.3 Overview of Arene Ruthenium Metalla-Assemblies

Arene ruthenium metal-assemblies produced via directional bonding approach are remarkable examples of successful coordination driven self-assembly strategy. Many two and three dimensional metallacycles have been reported showing great efficiency in sensing,[117] catalysis[118] and drugs transportations.[119]

As building blocks of metalla-assemblies, arene ruthenium complexes offer a unique and controllable octahedral geometry. Blocking of three coordination sites of metal center allows the three remaining coordination sites to be available for self-assemblies.[90a] Two main strategies have been employed to generate metalla-assemblies from arene ruthenium building blocks (Fig. 19):

(A) by mixing tritopic ligands composed of a bidentate and a monodentate end with "naked" arene ruthenium corners,[117] (B) by forming stable dinuclear arene ruthenium clips prior to the final assembly step involving various connectors.[116] Both methods have successfully produced esthetical architectures as well as functional metalla-assemblies.

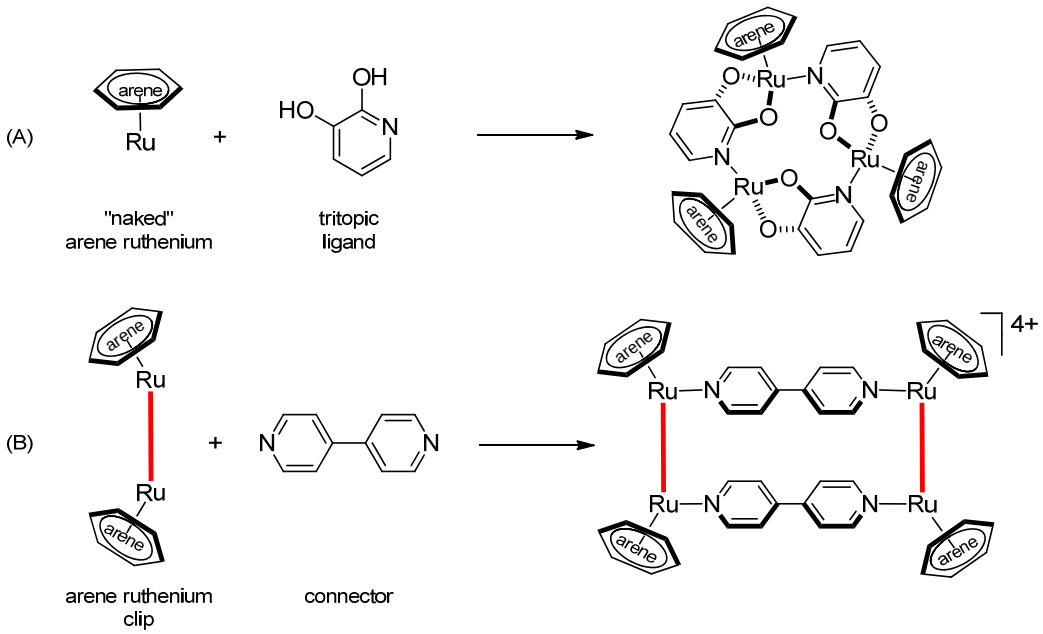

Figure 19. Schematic representation of the two main strategies to form arene ruthenium metalla-cycles.

During the past two decades Severin[120] and Fujita[121] groups produced numerous tri- and hexanuclear metalla-cycles with spherical or circular geometries. These host systems show very good ability to selectively recognize many cationic species such Li^+.[117] The first metalla-cycle was synthesized in 2001 by Severin *et al.*. The synthetic approach consists of 1:1 stoichiometric ratio of mononuclear complexes with three available coordination sites with unsymmetrical tritopic ligands. The final ruthenium metalla-cycle is a chiral and ionophore trimeric complex with great sensing ability.[122]

In the second strategy, the dinuclear metalla-clips are the main building blocks. The two ruthenium metal ions are linked by very stable bis-chelating ligands. Consequently, two remaining sites with an angle of 90° are available to coordinate to di, tri or tetradentate symmetrical ligands. Furthermore, the stereochemistry of reactional intermediates before reaching the final closure steps giving raise to the ruthenium metalla-assembly is still not clear. Indeed, the incoming ligands can take a *syn* or *anti* spatial configuration, unlike the platinum metalla-assemblies analogous, produced by Stang, who forced a cis-orientation of the ligands connected to the metal-complex precursors.[123] Investigation of the stereochemical properties of the plausible reaction intermediates involved during the preparation of arene ruthenium metalla-assemblies is the main objective of this current work.

In 1997, Süss-Fink reported the first tetracationic arene ruthenium metalla-rectangle formed from two [(arene)$_2$Ru$_2$(μ-C$_2$O$_4$)Cl$_2$] complex and two 4.4' bipyridine (bpy) units (Fig. 20).[116] This new finding offered a new possibility to overcome the thermodynamic problems encountered in the synthesis of metalla-rectangles.[124]

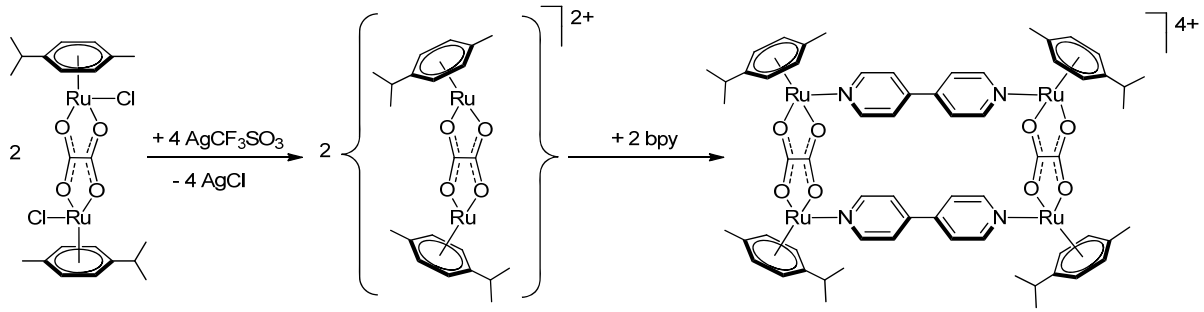

Figure 20. Synthesis of the [(p-cymene)$_4$Ru$_4$(C$_2$O$_4$)$_2$(bpy)$_2$]$^{4+}$ metalla-rectangle.

Later on, our group and some other supramolecular chemists developed this strategy further. Different metalla-clips with different functionalities and size have been synthesized.[90b] The dinuclear arene ruthenium precursors with general formula [(η^6-arene)$_2$Ru$_2$(*OO*∩*OO*)Cl$_2$] (*OO*∩*OO* = oxalato, 2,5-dioxydo-1,4-benzoquinonato (dobq), 5,8-dioxydo-1,4-naphthoquinonato (donq), 2,5-dichlorido-1,4-benzoquinonato (dClobq)) are intensively used by our groups.[100] The combination of ruthenium building blocks with bidentate, tridentate and tetradentate connectors generated metalla-rectangles, metalla-prisms and metalla-cubes with general formula [(η^6-arene)$_n$Ru$_n$(L)$_{n/2}$(*OO*∩*OO*)$_{n/2}$]$^{n+}$ {n = 4, 6, 8} (Scheme 6). These two- and three-dimensional assemblies are well defined and they have been fully characterized, and in some cases by single-crystal X-ray structure analysis.

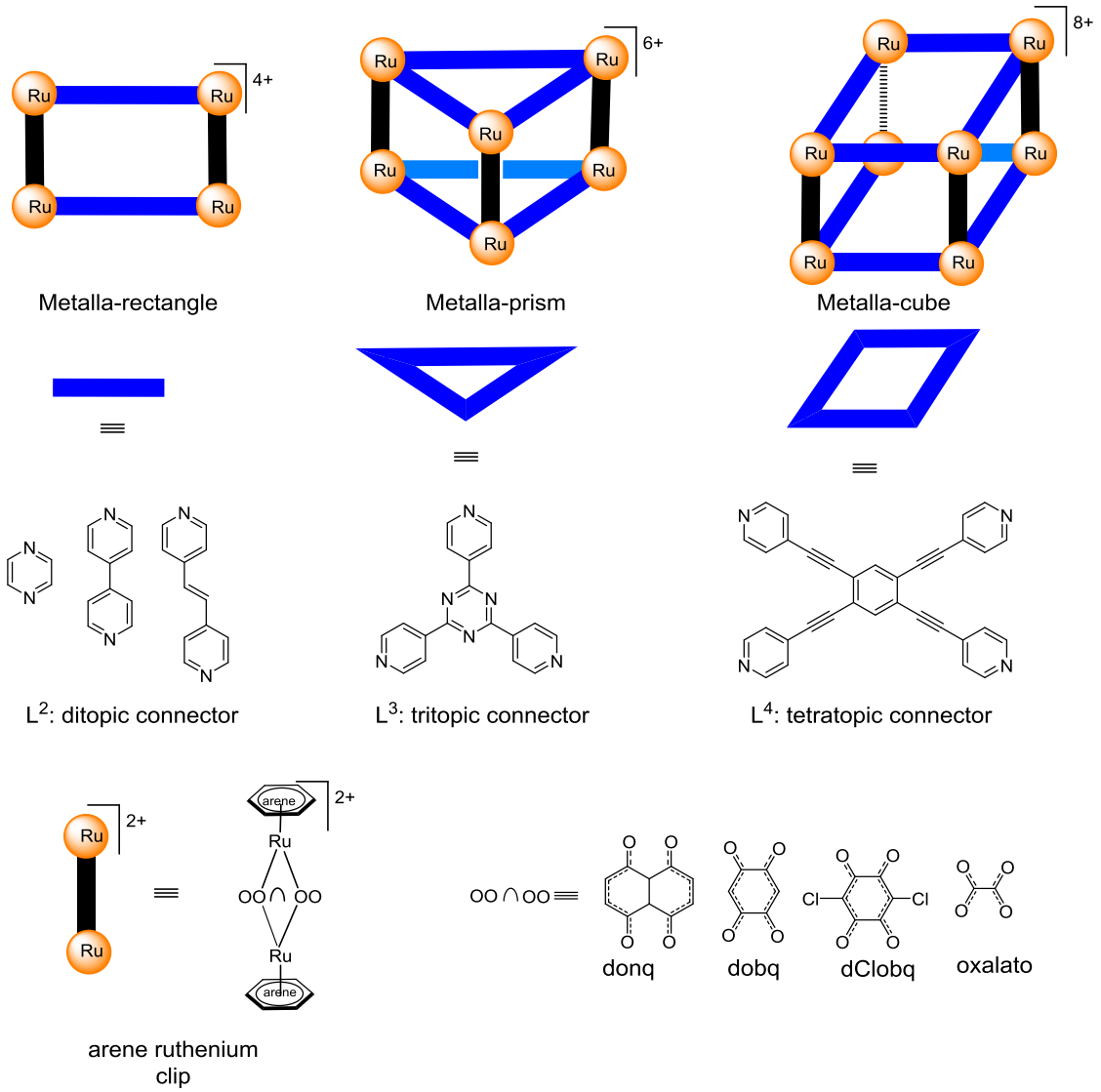

Scheme 6. Tetranuclear ,hexanuclear and octanuclear arene ruthenium metalla-assemblies held form dinuclear arene ruthenium metlla-clips and a collection of connectors.

The general synthetic approach consists of the activation of the metalla-clips by removal of two chloride ions by a halide scavenger followed by the separation of the di-cationic arene ruthenium reactional intermediate. Addition of the suitable stoichiometric ratio of the panels leads to the desired metalla-assemblies via the self-assembly process. The final compounds are usually isolated as salts such as trifluoromethane sulfonate salts.

In recent years, our groups extensively used the second strategy to prepare metalla-assemblies with biological functions. The potential of the arene-ruthenium metalla-assemblies as anticancer drugs has been well demonstrated. The *in-vitro* results of these compounds show higher cytotoxicity compared to the cis-platine the common metallo-drugs used in chemotherapy.[119a, 125]

Furthermore, the physicochemical properties of these metal-assemblies in biological medium have been reported recently. A notable example is the reactivity between ruthenium hexa-cationic prisms and biological ligands such as Arginine (Arg), Histidine (Hi), and Lysine (Ly) (Fig. 21). This study shows that some of these supramolecular hosts can maintain their stability more than 12 hours. Even after destruction of the metalla-prism structure, the construction of new active species is noteworthy, which presents the plausible pathway giving raise to the high cytotoxicity of these systems.[126]

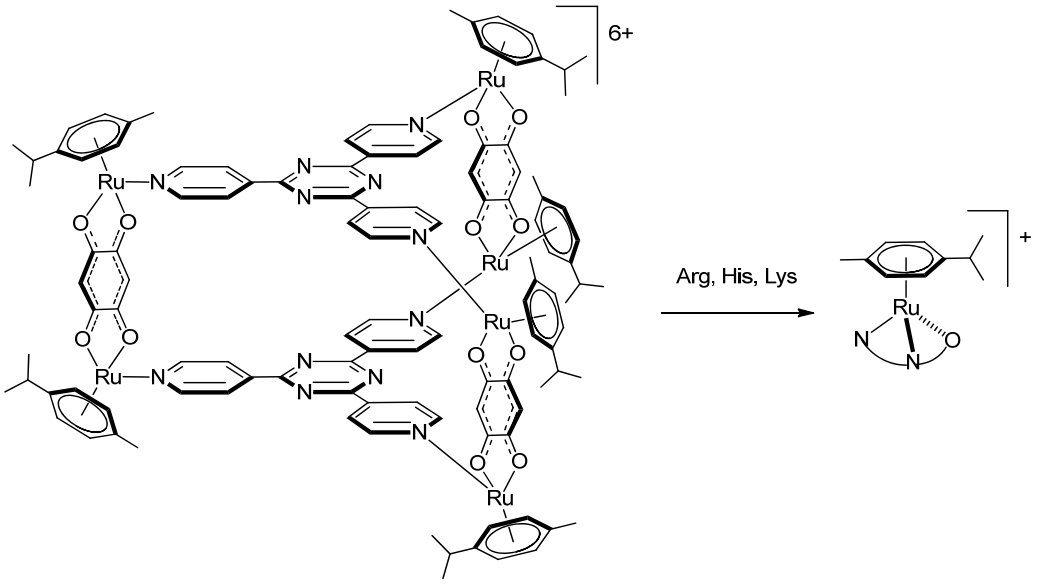

Figure 21. Formation of chelate complexes from the interaction between [(p-cymene)$_6$Ru$_6$(tpt)$_2$(dobq)$_3$]$^{6+}$ and some amino acids, (tpt: 2,4,6-tri(pyridin-4-yl)-1,3,5-triazine).[126]

The high cytotoxicity, the relative robustness, along with the existence of a hydrophobic cavity capable of recognizing a biological active guest molecule favored these systems to be an excellent drug delivery vectors.

1.3.4 Arene Ruthenium Metalla-Assemblies and Host-Guest Chemistry

After the success of the platinum and palladium metalla-assemblies as micro reactors for some catalytic reactions or an efficient drug delivery vectors,[51] a remarkable interest to the ruthenium host systems analogues has been noted. This popularity is due to the interesting host-guest features of this kind of supramolecular hosts. Their ability to recognize planar aromatic molecules or some biologically actives species inside their cavity is one of the key

elements of this success.[127] Furthermore, their host-guest properties in sensing and drug transportation have been extensively developed.[128, 119b]

Severin *et al.*, designed the first ruthenium ionophore metallacycle which selectively recognized cationic species in water.[122] Recently, several nitroaromatic compounds such as 4-nitrotoluene, nitrobenzene, 4-nitrophenol and trinitrotoluene (TNT) have been trapped inside the cavity of arene ruthenium metalla-cages, which confirms their potential ability as sensors for explosive compounds.[128]

Furthermore, the water solubility and the high cytotoxicity of arene ruthenium complexes allow these systems to provide new features in the drug design:

i) Protection of the active molecules from the harsh conditions of biological media such as in stomach and liver;
ii) Facile transportation in the blood stream and accessibility into the cell membranes and others barriers due to the amphilic and cationic properties of the host-guest system;[129]
iii) High intrinsic cytotoxicity;
iv) Enhancing the selectivity due to the enhanced permeability and retention (EPR effect) resulting from the big molecular weight of final host-guest system.[130]

The enhanced permeability and retention is a biological phenomenon which describes the preferential accumulation of the macromolecular system in tumour cells.[130] Nowadays, the extrapolation of this strategy to the host-guest chemistry targeting an efficient cancer treatment has become popular.[131] Since 2008, our group has developed this new approach by designing many active host guest compounds. This application revolves around two areas of cancer treatment, which is chemotherapy and photodynamic therapy (PDT).

Many common commercial anti-cancer drugs have been encapsulated in the hydrophobic cavity of several metalla-cages and cubes. The first host-guest system was obtained in 2008. It consists of the encapsulation of the platinum and palladium acetylacetonate ([Pt(acac)$_2$], [Pd(acac)$_2$]), a hydrophobic anti-cancer drugs, inside the cavity of the [(η^6-*p*-cym)$_6$Ru$_6$(tpt)$_2$(dobq)$_3$]$^{6+}$ metalla-prism. The synthesis of this new hybrid supramolecular system was confirmed by X-ray analysis, revealing the encapsulation of guest molecule inside the hydrophobic cavity of host (Fig. 22). This supramolecular host-guest

system showed good water solubility allowing high intrinsic cytotoxicity as compared to the empty initial metalla-prism and the initial hydrophobic guest molecule.[127]

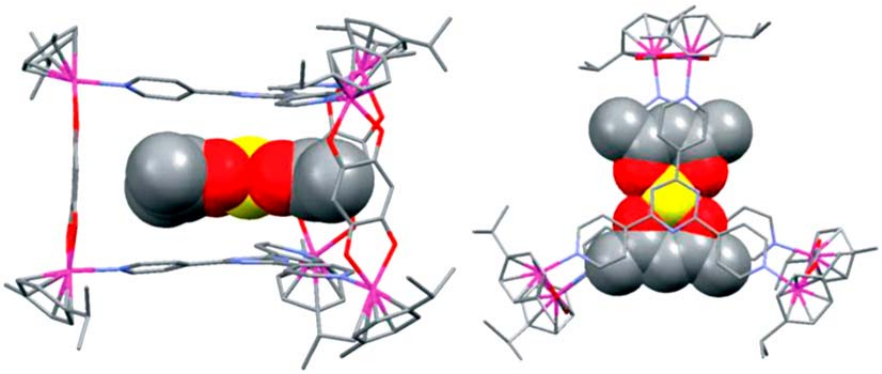

Figure 22. Molecular structure of the host-guest system $[Pt(acac)_2 \subset (\eta^6\text{-}p\text{-}cym)_6Ru_6(tpt)_2(dobq)_3]^{6+}$.[100]

On the other hand, the pyrene derivative, (1-(4,6-dichloro-1,3,5-triazin-2-yl) pyrene) which possesses good fluorescent properties was used as guest-molecule to confirm the efficiency of this host system to deliver drugs into cancer cells (Fig. 23). Therefore, fluorescence-captured images from tumor cells, show high fluorescent intensity for the host-guest system as compared to the guest molecule alone. This result confirms the release of the guest-molecule, and reflects the improvement of the uptake of the active species, which is a crucial element to improve the efficiency of the cancer treatments.[132]

Pyrene, which is a flat hydrophobic molecule, shows very good accessibility to ingress and egress within the cavity of the metalla-prisms. Many factors contribute to stabilize it inside such as the hydrophobic and the π-π stacking interactions. In addition, several biological active functions such as floxuridine (2'-deoxy-5-fluorouridine) were attached to this polyaromatic hydrocarbon molecule (Fig. 23). The new derivatives have been transported preferentially by the vectors into the cancer cells allowing high anti-cancer activity.[133]

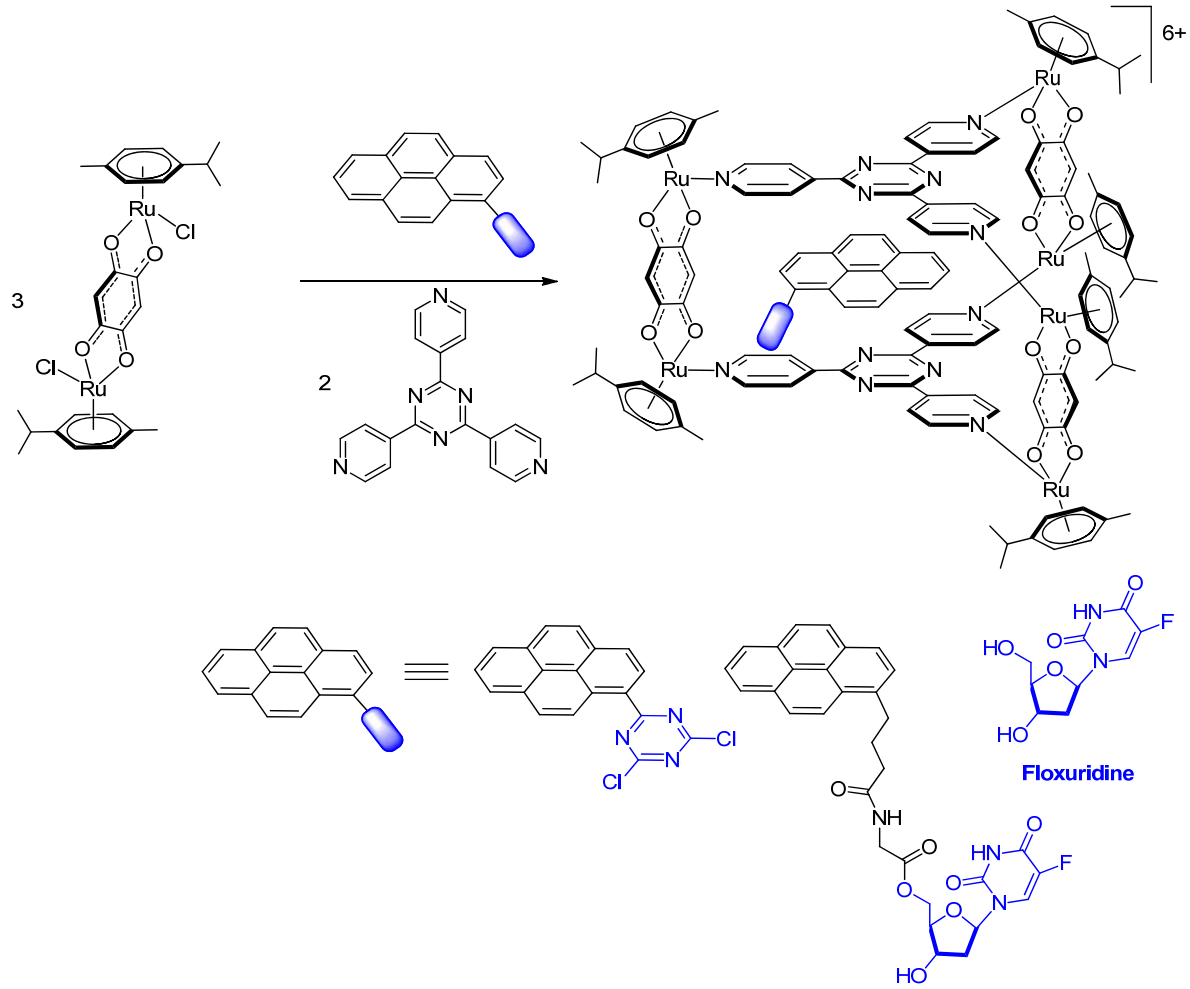

Figure 23. Pyrene derivatives encapsulated in $[(\eta^6\text{-p-cym})_6Ru_6(tpt)_2(dobq)_3]^{6+}$ metalla-prism.

Interestingly, when these planar aromatic molecules get trapped inside the cavity of metlla-cages, they lose their fluorescent properties. The spectroscopic analysis confirmed the quenching of the fluorescence light emitted by these guest molecules gradually after the addition of the host complex. The degradation of the intensity was proportional to the host, guest ratio, probably due to the electronic interactions between the two systems. Two putative approaches could explain this behavior. One possibility is that the host complex behaves like an umbrella limiting the penetration of the excitation light into the guest, like a greenhouse which absorbs the fluorescence response of the molecules.[134]

Recently, the investigation of this new finding was extended to the hydrophobic photosensitizers, targeting a safety photodynamic therapy (PDT) treatment. Indeed, protecting the photo-active guest molecules from undesirable light excitation, potentially avoid the skin photosensitivity, the main side effect in (PDT).[135] Several arene ruthenium metalla-prisms

and cubes with different portal size were found to be excellent nano-carriers to deliver photosensitizers (eg. porphin) into cancer cells (Fig. 24).[136]

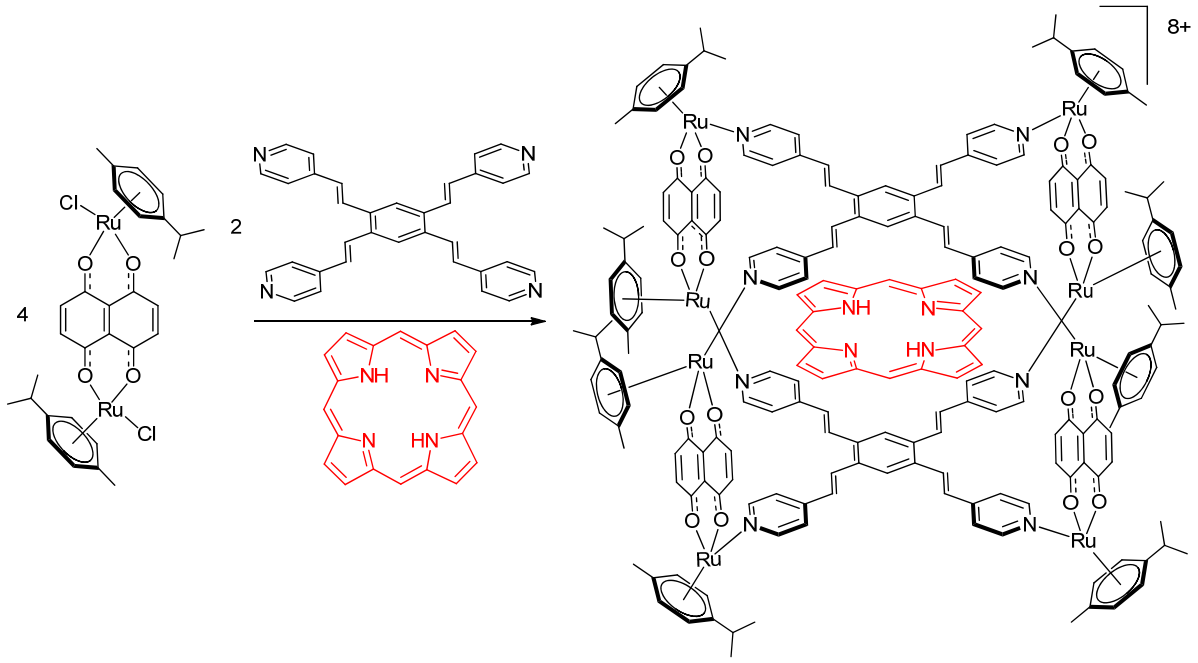

Figure 24. Synthesis of the host-guest system [porphi⊂(η^6-p-cym)$_8$Ru$_8$(tpvb)$_2$(dhnq)$_4$]$^{8+}$, (tpvb: 1,3,5-tris{2-(4- pyridyl)vinyl}benzene).[137]

1.4 Aims of this Work

Ruthenium – the latest transition metal to be discovered and used in organometallic chemistry has an increasing number of papers making it one of the most studied elements. Introduction of ruthenium as key element in the coordination driven self-assembling supramolecular systems dates back to the pioneering work by Süss-Fink in 1997, resulting in the discovery of first arene ruthenium metalla-rectangle. This work allowed the discovery of new series of tetranuclear, hexanuclear and octanuclear metalla-assemblies, their anticancer activities and drug delivery abilities to treat cancers, making it an interdisciplinary field gathering chemistry and biology. However, little is known about the dynamic behavior of these systems in solution.

The aim of this thesis was to rationalize the thermodynamic and kinetic rules directing the formation of this family of metalla-assemblies. In the first part of the work the dynamic ligand exchange behavior of cationic arene ruthenium metalla-rectangles of the type $[(p\text{-cymene})_4Ru_4(OO\cap OO)_2(N\cap N)_2]^{4+}$ (OO∩OO = oxalato, 2,5-dioxydo-1,4-benzoquinonato, 5,8-dioxydo-1,4-naphthoquinonato; N∩N = 4,4'-bipyridine-H_8, 4,4'-bipyridine-D_8) have been explored in solution using $^1H/^2D$ isotope labeling of the 4,4'-bipyridine connectors. In addition to the formation mechanism of this type of metalla-cycles, which have been investigated by NMR spectroscopy.

The second part, a series of new tetracationic metalla-rectangles and hexacationic metalla-prisms were prepared and characterized. Their biological activities as anticancer drugs and drug delivery vectors have been developed. Some were found to show remarkable selectivity to cancer cells and high efficiency in PDT treatment.

2

Insight into the Dynamic Ligand Exchange Process Involved in Bipyridyl-Linked Arene Ruthenium Metalla-Rectangles

As mentioned in sections 1.3.1 and 1.3.2, arene ruthenium metalla-assemblies built from stable dinuclear metalla-clips and polypyridyl donor ligands have attracted a great deal of attention due to their intriguing structure and potential applications. While most investigations have largely focused on the synthetic routes and the structural features of these supramolecular assemblies, there are no reports dealing with the dynamic characteristics of such structures. Isotope labeling is an appropriate tool for characterizing dynamic exchange in metalla-supramolecular assemblies.[138] With this technique, the dynamic ligand exchange processes in arene ruthenium metalla rectangles as well as the subsequent equilibrium under thermodynamic control were successfully studied. Moreover, on the basis of quantitative mass-spectroscopic results, the kinetics of the exchange process are discussed.

2.1 Approaches to Directly and Quantitatively Evidence the Dynamic Behavior of Coordination-Driven Metalla-Assemblies

As mentioned in section 1.2, a fundamental facet of coordination-driven self-assemblies is the possible dynamic exchange process of the different building blocks involved.[87a, 139] Self-repairing, self-recognition, and self-rearrangement are frequently encountered in metalla-assemblies, and these dynamic behaviors have been used to explain experimental results, even in many occasions without supporting experimental data. Indeed, examples that directly and quantitatively evidence the dynamic behavior of coordination-driven metalla-assemblies remain scarce.[140]

This limited number of studies is partially due to the difficulty of finding an appropriate method of characterization. Among these methods, isotope labeling is potentially the easiest one to utilize; being compatible with NMR spectroscopy and mass spectrometry. However, the preparation of isotope-labeled compounds is not always trivial and can be expensive. Zheng and Stang employed $^{1}H/^{2}D$ 4,4'-bipyridine ligands (bpy-H_8 and bpy-D_8) to study the dynamic ligand exchange behavior of platinum-based supramolecular metalla-cycles.[138] A mixture of the homo-isotopic tetranuclear complexes [(1,8-bis(*trans*-Pt(PEt_3)$_2$)anthracene)$_2$(bpy-H_8)$_2$]$^{4+}$ and [(1,8-bis(*trans*-Pt(PEt_3)$_2$)anthracene)$_2$(bpy-D_8)$_2$]$^{4+}$ was heated to 64°C and the dynamic ligand exchange process was monitored by ESI mass spectrometry for a prolonged period. After several days, the reaction has reached equilibrium and a final 1:2:1 ratio between the homo-H_{16}:hetero-H_8/D_8:homo-D_{16} metalla-rectangles was observed (Fig. 25). The dynamic exchange behavior of the Pt-N bonding assemblies was established, confirming the self-assembled nature of this system and the effectiveness of the $^{1}H/^{2}D$ isotope labeling methodology.

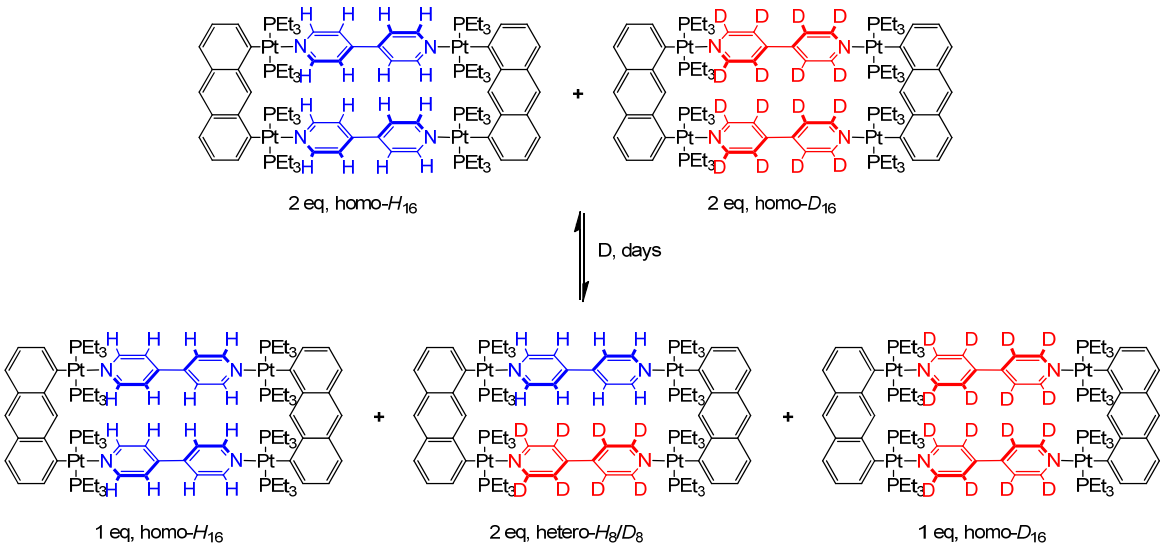

Figure 25. Homo- and hetero-metalla-rectangles of the general formula [(1,8-bis(trans-Pt(PEt$_3$)$_2$)anthracene)$_2$(bpy)$_2$]$^{4+}$ obtained after mixing equimolar amounts of the homo-H_{16} and homo-D_{16} metalla-rectangles, adapted from reference.[138]

Another approach to study dynamic ligand exchange processes consists of adding to a well-defined metalla-assembly a competing ligand or competing metal ion, and after reorganization and equilibrium, to analyze the new species formed.[141] Recently, Neogi and co-workers studied the response of defined heteroleptic metalla-supramolecular racks, rectangles, and trigonal prisms through the addition of pyridyl-based donor ligands. For example, excess of 1,2-di(pyridine-4-yl)ethyne forces a metalla-rectangle to alter into a rack architecture in solution.[89] Dynamic exchange processes can also be initiated by adding a competing metal ion as elegantly demonstrated by Hiraoka and Shionoya.[142] This kind of studies not only allows a better understanding of the dynamic behavior of these metalla-assemblies in solution but also a perspective of new synthetic routes to construct varying structural motifs.

In this chapter, a combination of these two methods, addition of competing ligands and isotope labeling, has been used to study the dynamic ligand exchange behaviors of arene ruthenium metalla-rectangles containing bipyridyl linkers. Moreover, on the basis of quantitative mass spectral measurements and NMR spectroscopy, the kinetics of the stimuli-triggered ligand exchange process have been investigated.

2.2 Synthesis and Characterization of the Arene Ruthenium Metalla-Rectangles

Six isotopical (isolated and purified) and three heteroisotopic (not isolated) arene ruthenium metalla-rectangles (see Fig. 26) of the general formula $[(p\text{-cymene})_4Ru_4(OO\cap OO)_2(N\cap N)_2]^{4+}$ (OO∩OO = oxalato, 2,5-dioxydo-1,4-benzoquinonato, 5,8-dioxydo-1,4-naphthoquinonato; N∩N = 4,4'-bipyridine-H_8, 4,4'-bipyridine-D_8) have been synthesized using the $^1H/^2D$ isotope-labeled 4,4'-bipyridine linkers. ESI-MS and ^1H NMR are used to observe and characterize the dynamic ligand exchange process operating in these cationic arene ruthenium metalla-assemblies.

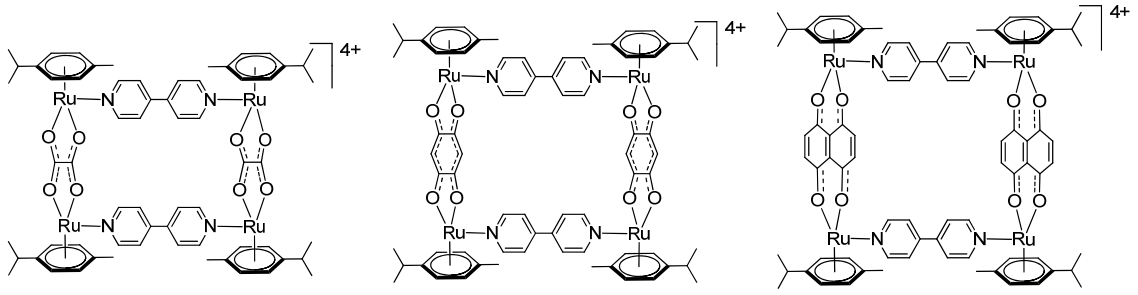

Figure 26. Molecular structures of the cationic arene ruthenium metalla-rectangles.

The synthesis of the isotopical metalla-rectangles, $[(p\text{-cymene})_4Ru_4(OO\cap OO)_2(bpy\text{-}H_8)_2]^{4+}$ and $[(p\text{-cymene})_4Ru_4(OO\cap OO)_2(bpy\text{-}D_8)_2]^{4+}$, has been performed following published methods using the corresponding dinuclear clips and bpy-H_8 or bpy-D_8, respectively.[113a, 116, 143]

On the other hand, two equivalents of the arene ruthenium metalla-clips $\{(p\text{-cymene})_2Ru_2(OO\cap OO)\}^{2+}$ react with a mixture of one equivalent of 4,4'-bipyridine-H_8 (bpy-H_8) and one equivalent of 4,4'-bipyridine-D_8 (bpy-D_8) to form a combination of the homo- and hetero-metalla-rectangles. The resulting mixture of each metalla-rectangle represents a statistical product distribution (theoretical value 1:2:1, homo-H_{16}, hetero-H_8/D_8, homo-D_8) (Fig. 27). In the case of the oxalato derivative, we were unable to confirm the formation of the hetero-H_8/D_8 metalla-rectangle; no peak corresponding to the intact arene ruthenium metalla-rectangles being observed by ESI-MS. Nevertheless, considering the behavior of the other two metalla-rectangles, a mixture of $[(p\text{-cymene})_4Ru_4(oxalato)_2(bpy\text{-}H_8)_2]^{4+}$, $[(p\text{-cymene})_4Ru_4(oxalato)_2(bpy\text{-}D_8)_2]^{4+}$ and $[(p\text{-cymene})_4Ru_4(oxalato)_2(bpy\text{-}H_8)(bpy\text{-}D_8)]^{4+}$ is certainly obtained.

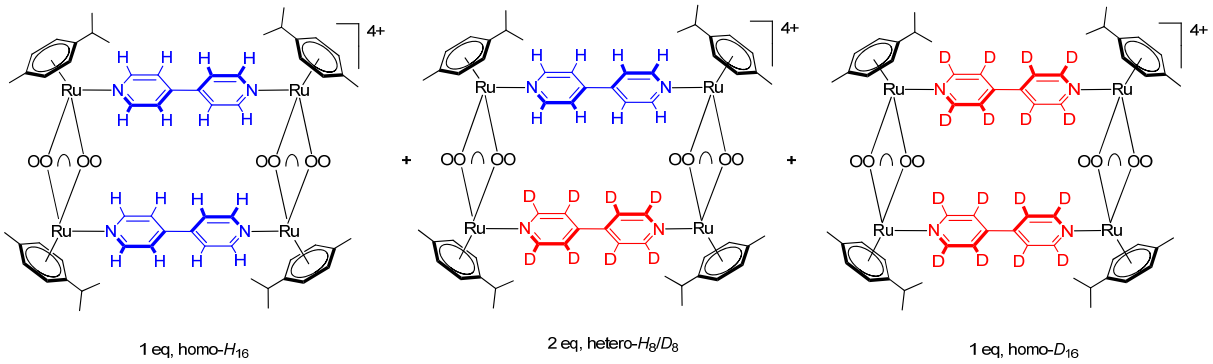

Figure 27. Resulting statistical mixture of the homo- and hetero-metalla-rectangles (OO∩OO = oxalato, 2,5-dioxydo-1,4-benzoquinonato, 5,8-dioxydo-1,4-naphthoquinonato).

2.3 Characterization of the Dynamic Ligand Exchange

2.3.1 Dynamic Ligand Exchange between Homo- and Hetero-Metalla-Rectangles

In order to observe a possible dynamic ligand exchange process between the homo-H_{16} and homo-D_{16} metalla-rectangles, as previously performed by Zheng and Stang with the metalla-rectangle $[(1,8\text{-bis}(trans\text{-}Pt(PEt_3)_2)\text{anthracene})_2(bpy)_2]^{4+}$ (Fig. 25),[138] we first mixed in methanol-d_4 the protonated metalla-rectangles and and their corresponding deuterated analogues in a 1:1 ratio. The evolution of the mixtures was then followed for 14 days by ^{1}H NMR and ESI-MS (methanol-d_4, 40°C). From the ^{1}H NMR spectrum we can notice in all cases the absence of signals associated to uncoordinated 4,4'-bipyridine-H_8 ligands. For metalla-rectangles $[(p\text{-cymene})_4Ru_4(2,5\text{-dioxydo-}1,4\text{-benzoquinonato})_2(bpy)_2]^{4+}$ and $[(p\text{-cymene})_4Ru_4(5,8\text{-dioxydo-}1,4\text{-naphthoquinonato})_2(bpy)_2]^{4+}$, ESI-MS confirms that both protonated and deuterated metalla-rectangles are intact with no peak corresponding to the hetero-H_8/D_8 metalla-rectangles, thus suggesting no exchange of the 4,4'-bipyridine ligands. Selected peaks from the ESI-MS spectrum of $[(p\text{-cymene})_4Ru_4(2,5\text{-dioxydo-}1,4\text{-benzoquinonato})_2(bpy)_2]^{4+}$ and $[(p\text{-cymene})_4Ru_4(5,8\text{-dioxydo-}1,4\text{-naphthoquinonato})_2(bpy)_2]^{4+}$, at the beginning, after 14 days, and from the mixed metalla-rectangles synthesized in a statistical 1:2:1 ratio, are presented in Figure 28. (Calculated ESI-MS peaks are presented in Fig. 29). The absence of the peaks corresponding to the hetero-derivatives $[M(H_8/D_8) - 2\ CF_3SO_3]^{2+}$ at m/z = 918 and 968, respectively, is clearly evidenced from these ESI-MS measurements (Fig. 28)

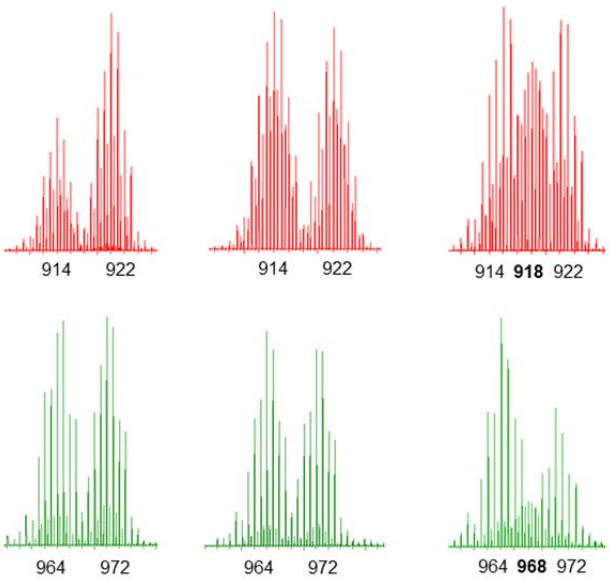

Figure 28. ESI-MS spectra of $[(p\text{-cymene})_4Ru_4(2,5\text{-dioxydo-}1,4\text{-benzoquinonato})_2(bpy)_2]^{4+}$ (top) and $[(p\text{-cymene})_4Ru_4(5,8\text{-dioxydo-}1,4\text{-naphthoquinonato})_2(bpy)_2]^{4+}$ (bottom), at the beginning after mixing the two homo-rectangles (left), after 14 days in solution at 40°C (middle), and from the mixed metalla-rectangles synthesized in a 1:2:1 ratio (right).

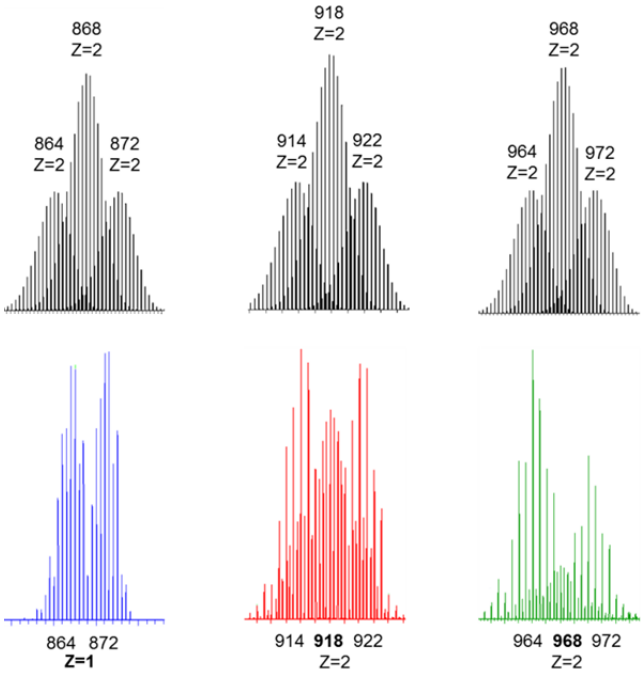

Figure 29. Calculated (up) and experimental (down) ESI-MS spectra of mixed metalla-rectangles synthesized in a 1:2:1 ratio: $[(p\text{-cymene})_4Ru_4(oxalato)_2(bpy)_2]^{4+}$ (left), $[(p\text{-cymene})_4Ru_4(2,5\text{-dioxydo-}1,4\text{-benzoquinonato})_2(bpy)_2]^{4+}$ (middle) and $[(p\text{-cymene})_4Ru_4(5,8\text{-dioxydo-}1,4\text{-naphthoquinonato})_2(bpy)_2]^{4+}$ (right).

We also tried to initiate the exchange process by exposing the mixtures of the homo-metalla-rectangles under UV light and heating. After 24 hours in methanol-d_4 under UV irradiation (λ = 375 nm), we did not observe any exchange (^{1}H NMR and ESI-MS), only the apparition of free *p*-cymene molecules by ^{1}H NMR spectroscopy, suggesting decomposition of the arene ruthenium units. Similarly, after 48 hours at 65°C in methanol-d_4, no evidence for the formation of the hetero-derivatives was observed, only slow decomposition of the metalla-rectangles.

2.3.2 Dynamic Ligand Exchange in the Presence of Competing Ligand

The absence of spontaneous ligand exchange process by simply mixing two isotopical metalla-rectangles forced us to modify our strategy. We decided to add to the homo-metalla-rectangles one equivalent of the free 4,4'-bipyridine ligand of the opposite labeling. First, we added one equivalent of 4,4'-bipyridine-H_8 to the smallest deuterated metalla-rectangle [(*p*-cymene)$_4$Ru$_4$(oxalato)$_2$(bpy-D_8)$_2$]$^{4+}$ in methanol-d_4. Instantly, signals corresponding to coordinated bpy-H_8 appear (H′$_\alpha$ and H′$_\beta$) in the ^{1}H NMR spectrum (Fig. 30).

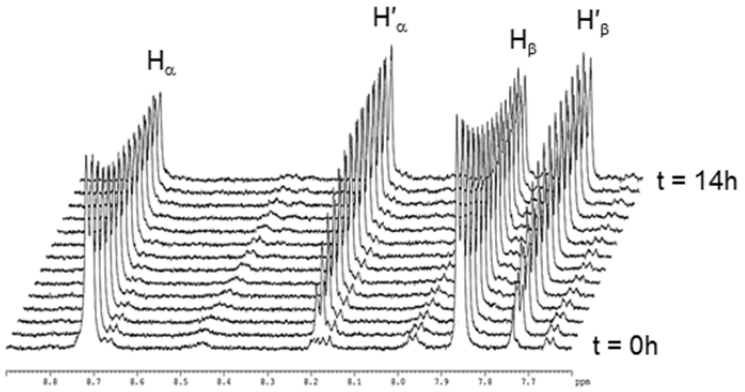

Figure 30. Representative ^{1}H NMR spectra following the ligand exchange process with metalla-rectangle [(p-cymene)$_4$Ru$_4$(oxalato)$_2$(bpy-D_8)$_2$]$^{4+}$ in methanol-d_4 (23 °C) upon addition of bpy-H_8.

In parallel, a decrease in the intensity of the signals (H$_\alpha$ and H$_\beta$) of the free bpy-H_8 was observed. After 24 hours, the mixture had reached equilibrium and no more changes were observed in the ^{1}H NMR spectrum. The opposite experiment, addition of one equivalent of 4,4'-bipyridine-D_8 to the metalla-rectangle [(*p*-cymene)$_4$Ru$_4$(oxalato)$_2$(bpy-H_8)$_2$]$^{4+}$ in methanol-d_4, shows exactly the opposite behavior, which is in this case an increase of free bpy-H_8 signals and a decrease of the signals associated to the coordinated bpy-H_8 protons.

The presence of free bpy-H_8 and a larger complex with coordinated bpy-H_8 ligand was confirmed by diffusion-ordered NMR spectroscopy (DOSY). The DOSY spectrum of the mixture obtained after addition of bpy-H_8 to $[(p\text{-cymene})_4Ru_4(oxalato)_2(bpy\text{-}D_8)_2]^{4+}$ in methanol-d_4 shows two species (Fig. 31), with a larger coefficient for the newly formed species, confirming the coordination of bpy-H_8 to ruthenium.

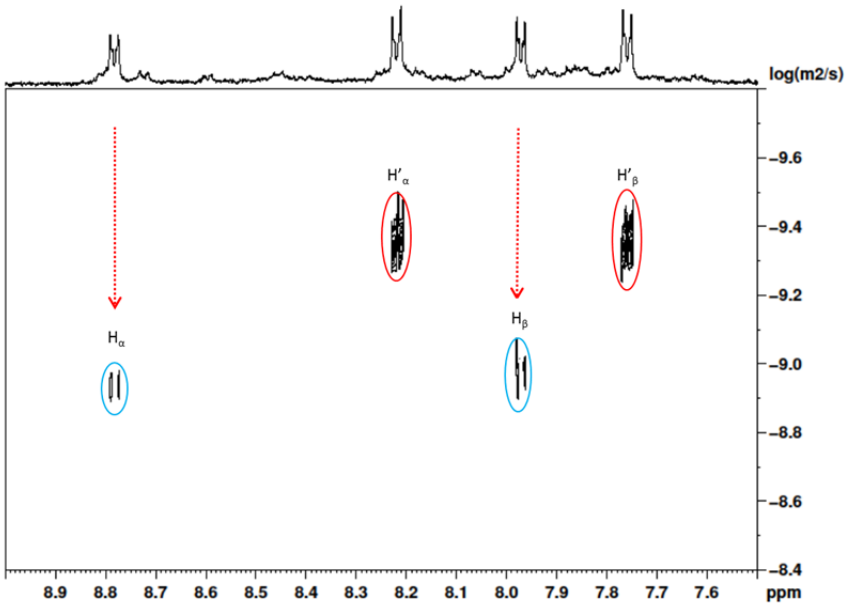

Figure 31. ^1H NMR and DOSY spectra (methanol-d_4, 23°C) after addition of bpy-H_8 to $[(p\text{-cymene})_4Ru_4(oxalato)_2(bpy\text{-}D_8)_2]^{4+}$ showing the resonances of the free bpy-H_8 (highlighted with red ovals) and the protons of the coordinated bpy-H_8 (blue ovals).

To identify the nature of these new species, the two mixtures obtained after 24 hours were studied by ESI-MS. In both cases, the ESI mass spectra show two distinctive fragments incorporating both bpy ligands in their core (bpy-H_8 or bpy-D_8), a di-cationic fragment with peaks at m/z = 786 and 790, and a mono-cationic fragment with peaks at m/z = 864 and 872 (Fig. 32).

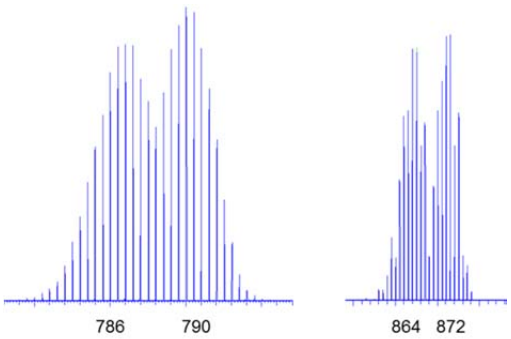

Figure 32. ESI-MS peaks corresponding to the species $[(p\text{-cymene})_4Ru_4(oxalato)_2(bpy) + 2\ CF_3SO_3]^{2+}$ and $[(p\text{-cymene})_2Ru_2(oxalato)(bpy) + CF_3SO_3]^{+}$ (right).

Despite similar behaviors, the kinetics of the ligand exchange processes before reaching equilibrium are different in these two experiments. The exchange process has been followed by ^{1}H NMR spectroscopy for 6 hours (Fig. 33), the rate of increase in the intensity of the coordinated bpy-H_8 signals in the first experiment is slower as compared to the rate of increase in intensity of the signals of free bpy-H_8 in the second experiment (Fig. 33a). This is due to the fact that in the first case, to exchange a Ru-N(bpy-D_8) bond with a Ru-N(bpy-H_8) bond, the disassembly of the metalla-rectangle $[(p\text{-cymene})_4Ru_4(oxalato)_2(bpy\text{-}D_8)_2]^{4+}$ has to take place first. In other words, two kinetic constants, a dissociative (k_d) and an associative (k_a) one, are operating. In the second case (Fig. 33b), the appearance of free bpy-H_8 signals is due to the disassembly of the metalla-rectangle $[(p\text{-cymene})_4Ru_4(oxalato)_2(bpy\text{-}H_8)_2]^{4+}$, thus involving only a dissociative process.

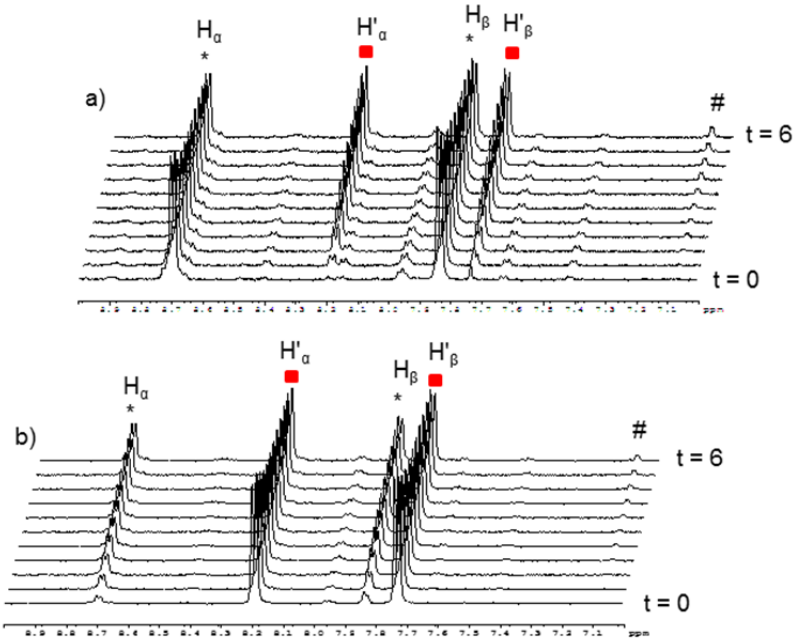

Figure 33. Representative ^{1}H NMR spectra (6 hours) following the kinetic exchange between $[(p\text{-cymene})_4Ru_4(oxalato)_2(bpy)_2]^{4+}$ (■) and 4,4'-bipyridine (*) (methanol-d_4, 23 °C); a) $[(p\text{-cymene})_4Ru_4(oxalato)_2(bpy\text{-}D_8)_2]^{4+}$ + bpy-H_8; b) $[(p\text{-cymene})_4Ru_4(oxalato)_2(bpy\text{-}H_8)_2]^{4+}$ + bpy-D_8 (# = free p-cymene).

In the case of the $[(p\text{-cymene})_4Ru_4(2,5\text{-dioxydo-}1,4\text{-benzoquinonato})_2(bpy)_2]^{4+}$ metalla-rectangle, a different behavior has been observed. In fact, when one equivalent of bpy-H_8 is added to $[(p\text{-cymene})_4Ru_4(2,5\text{-dioxydo-}1,4\text{-benzoquinonato})_2(bpy\text{-}D_8)_2]^{4+}$ in methanol-d_4 (Fig. 34a), the intensity of the signals corresponding to the protons of the free bpy-H_8 (*) decreases, accompanied by the apparition of a signal at δ = 7.1 ppm associated to

free *p*-cymene (#). However, no formation of [(*p*-cymene)$_4$Ru$_4$(2,5-dioxydo-1,4-benzoquinonato)$_2$(bpy-H_8)$_2$]$^{4+}$ or other {(*p*-cymene)Ru(bpy-H_8)} species is observed. It is worth mentioning here that upon addition of 4,4'-bipyridine to all metalla-rectangles, apparition of free *p*-cymene was observed by ^{1}H NMR spectroscopy. On the other hand, the opposite experiment, addition of bpy-D_8 to [(*p*-cymene)$_4$Ru$_4$(2,5-dioxydo-1,4-benzoquinonato)$_2$(bpy-H_8)$_2$]$^{4+}$, shows that the intensity of the signals corresponding to the protons of free bpy-H_8 increases and the intensity of the signals associated to coordinated bpy-H_8 decreases as expected (Fig. 34b). In terms of kinetics, the same behavior has been observed, a faster appearance of the signals associated to free bpy-H_8 after disassembly of the proteomic metalla-rectangle.

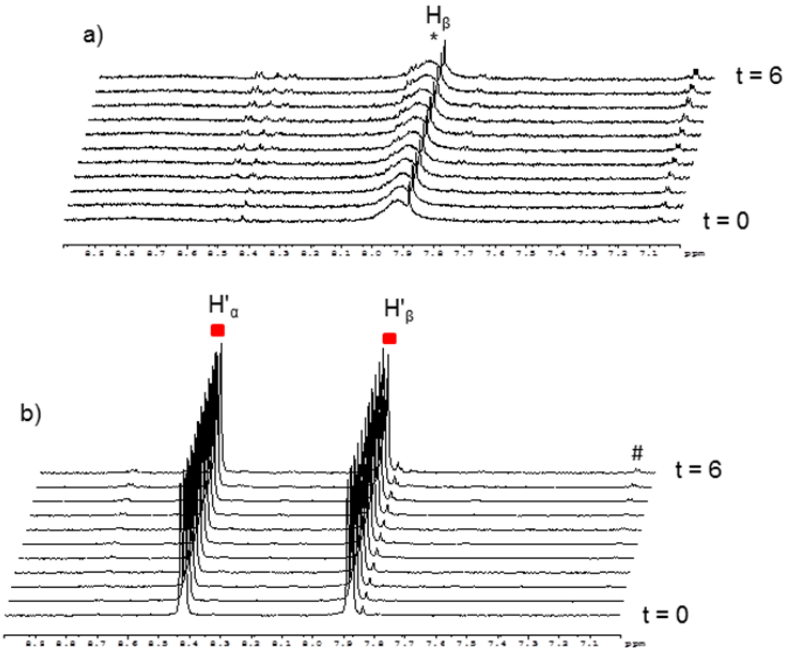

Figure 34. Representative ^{1}H NMR spectra (6 hours) following the kinetic exchange between [(p-cymene)$_4$Ru$_4$(2,5-dioxydo-1,4-benzoquinonato)$_2$(bpy)$_2$]$^{4+}$ (■) and 4,4'-bipyridine (*) (methanol-d_4, 23 °C); a) [(p-cymene)$_4$Ru$_4$(2,5-dioxydo-1,4-benzoquinonato)$_2$(bpy-D_8)$_2$]$^{4+}$ + bpy-H_8; b) [(p-cymene)$_4$Ru$_4$(2,5-dioxydo-1,4-benzoquinonato)$_2$(bpy-H_8)$_2$]$^{4+}$ + bpy-D_8 (# = free p-cymene).

In the case of [(*p*-cymene)$_4$Ru$_4$(5,8-dioxydo-1,4-naphthoquinonato)$_2$(bpy)$_2$]$^{4+}$, the dynamic ligand exchange process in methanol-d_4 upon addition of bpy is similar to that observed with the oxalato metalla-rectangles: A rapid exchange of the bpy ligands in solution after disassembly of the metalla-rectangle (Fig. 35). On the other hand, as opposed to the oxalato and 2,5-dioxydo-1,4-benzoquinonato derivatives, the presence of free *p*-cymene molecules is not detected in solution, thus suggesting a more robust metalla-assembly. On the

^{1}H NMR spectrum, the protons associated to the 5,8-dioxydo-1,4-naphthoquinonato bridging ligand are observed as a singlet at δ = 7.24 ppm.

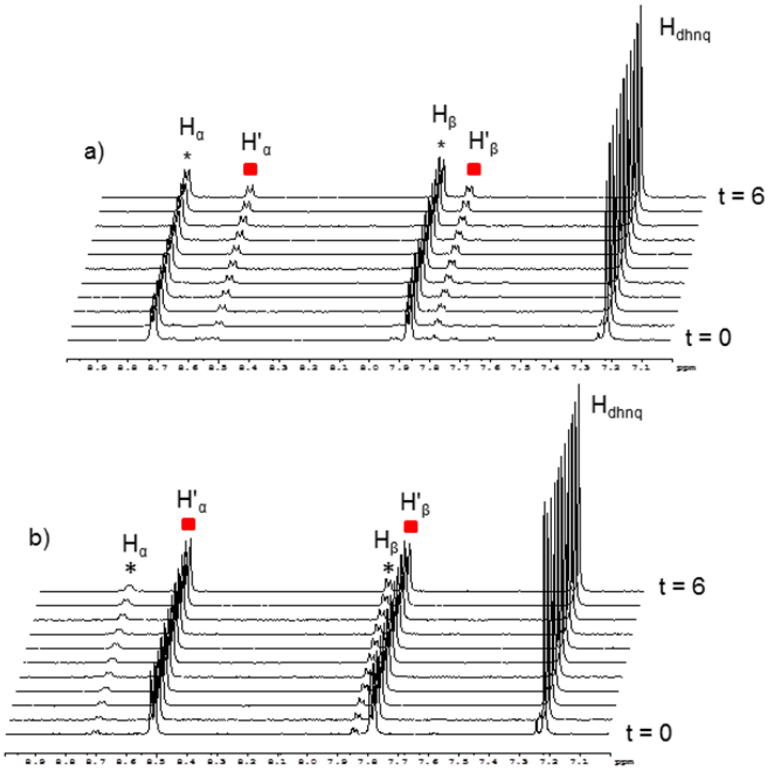

Figure 35. Representative ^{1}H NMR spectra (6 hours) following the kinetic exchange between [(p-cymene)$_4$Ru$_4$(5,8-dioxydo-1,4-naphthoquinonato)$_2$(bpy)$_2$]$^{4+}$ (■) and 4,4'-bipyridine (*) (methanol-d$_4$, 23 °C); a) [(p-cymene)$_4$Ru$_4$(5,8-dioxydo-1,4-naphthoquinonato)$_2$(bpy-D$_8$)$_2$]$^{4+}$ + bpy-H$_8$; b) [(p-cymene)$_4$Ru$_4$(5,8-dioxydo-1,4-naphthoquinonato)$_2$(bpy-H$_8$)$_2$]$^{4+}$ + bpy-D$_8$.

Interestingly, the ESI mass spectra of the solutions isolated after 6 hours reaction time show peaks corresponding to all metalla-rectangles at m/z = 964, 968 and 972, [M(H_{16}) - 2 CF_3SO_3]$^{2+}$, [M(H_8/D_8) - 2 CF_3SO_3]$^{2+}$ and [M(D_{16}) - 2 CF_3SO_3]$^{2+}$, respectively. The intensity of the peak corresponding to the mixed metalla-rectangle is nonetheless very low. Otherwise, peaks corresponding to fragments incorporating a bpy ligand in their core (bpy-H_8 or bpy-D_8) and {(*p*-cymene)$_2$Ru$_2$(5,8-dioxydo-1,4-naphthoquinonato)}$^{2+}$ units are also observed; a di-cationic fragment with peaks at m/z = 886 and 890, and a mono-cationic fragment with peaks at m/z = 964 and 972. These fragments have been attributed to the two species [(*p*-cymene)$_4$Ru$_4$(5,8-dioxydo-1,4-naphthoquinonato)$_2$(bpy) + 2 CF_3SO_3]$^{2+}$ and [(*p*-cymene)$_2$Ru$_2$(5,8-dioxydo-1,4-naphthoquinonato)(bpy) + CF_3SO_3]$^+$, respectively (Fig. 36).

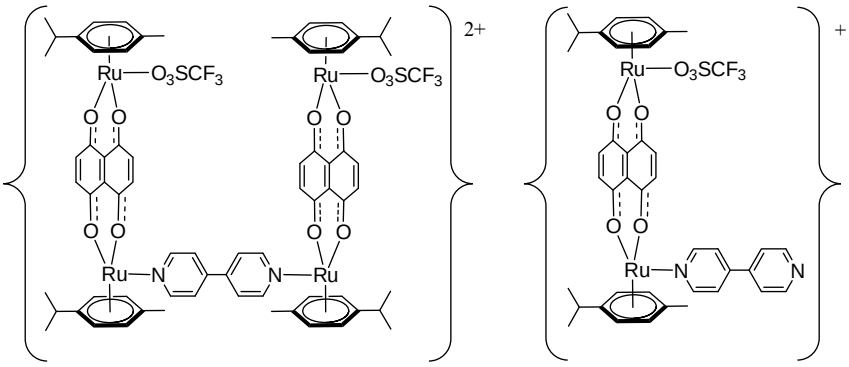

Figure 36. Molecular structure of the two fragments [(p-cymene)$_4$Ru$_4$(5,8-dioxydo-1,4-naphthoquinonato)$_2$(bpy) + 2 CF_3SO_3]$^{2+}$ and [(p-cymene)$_2$Ru$_2$(5,8-dioxydo-1,4-naphthoquinonato)(bpy) + CF_3SO_3]$^+$

2.4 Determination of the Initial Rate of the Exchange

As previously observed by NMR and mass spectrometry, addition of bpy to the metalla-rectangles produces several intermediates, thus obscuring the kinetics of the assembly-disassembly processes of the metalla-rectangles. Therefore, we chose to determine the initial rate of the reaction, when the initial concentrations of the metalla-rectangle and bpy are known and when the exchange processes follow a linear response (Fig. 37).

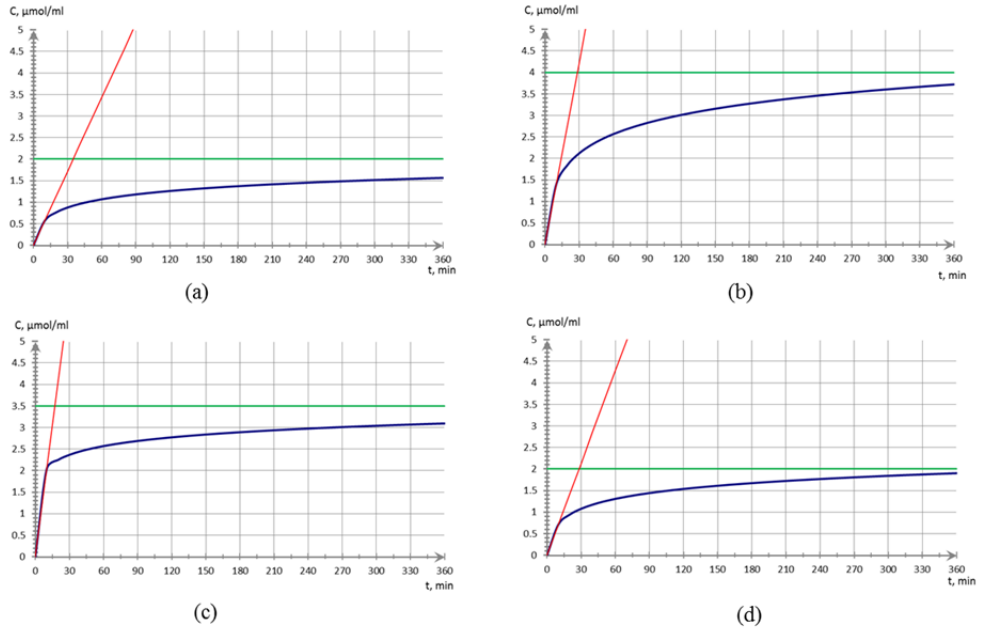

Figure 37. Initial rates of the exchange processes between the homo oxalato-metalla-rectangles and the free 4,4'-bipyridine of the opposite labeling, {homo-D_{16} + bpy-H_8: (a) 1:1 ratio (23 °C); (b) 1:10 ratio (23 °C),(c) 1:1 ratio (40 °C), homo-H_{16} + bpy-D_8: 1:10 ratio (23 °C)}.

These initial rates values of the exchange processes at room temperature with a 1:1 and 1:10 ratio (metalla-rectangle:bpy) and at 40°C with a 1:1 ratio are given in Table 4.

Table 4. Initial rates of the exchange processes between the homo-metalla-rectangles and the free 4,4'-bipyridine of the opposite labeling, (homo-D_{16} + bpy-H_8 = $V_{0'}$, homo-H_{16} + bpy-D_8 = $V_{0''}$).

metalla-rectangle [(*p*-cymene)$_4$Ru$_4$(OO∩OO)$_2$(bpy)$_2$]$^{4+}$	initial rate × 10^{-5} $V_{0'}$ (mol·L^{-1}·min^{-1})			initial rate × 10^{-5} $V_{0''}$ (mol·L^{-1}·min^{-1})		
OO∩OO =	1 eq	10 eq	1 eq (40°C)	1 eq	10 eq	1 eq (40°C)
oxalato	5.8	14.1	20.4	3.8	7.2	14.8
2,5-dioxydo-1,4-benzoquinonato	-	-	1.9	-	-	-
5,8-dioxydo-1,4-naphthoquinonato	4.7	8.2	7.1	4.4	9.6	17.4

For the 2,5-dioxydo-1,4-benzoquinonato metalla-rectangle, the initial rate of the exchange process was only determined upon addition of bpy-H_8 to [(*p*-cymene)$_4$Ru$_4$(2,5-dioxydo-1,4-benzoquinonato)$_2$(bpy-D_8)$_2$]$^{4+}$ at 40°C. The coordination of bpy-H_8 to the ruthenium atom is quite slow at this temperature and suggests a good stability of the metalla-rectangle. On the other hand, the initial rates of the exchange processes involving the other metalla-rectangles are faster and follow a similar trend. In both cases, the exchange process is more rapid when a 10 fold excess of bpy is added and when the temperature of the reaction is raised to 40°C.

Finally, when the addition of one equivalent of the free 4,4'-bipyridine ligand to the six homo-metalla-rectangles is performed at -20°C in methanol-d_4, no exchange occurs: All ^{1}H NMR spectra remaining identical for several hours, confirming the relative stability of these arene ruthenium metalla-rectangles in solution.

2.5 Conclusions

The dynamic ligand exchange behavior of cationic arene ruthenium metalla-rectangles of the type [(*p*-cymene)$_4$Ru$_4$(OO∩OO)$_2$(N∩N)$_2$]$^{4+}$ (OO∩OO = oxalato, 2,5-dioxydo-1,4-benzoquinonato, 5,8-dioxydo-1,4-naphthoquinonato; N∩N = 4,4'-bipyridine-H_8, 4,4'-bipyridine-D_8) has been studied in solution. The robustness of the rectangular architecture has been evidenced by NMR and ESI mass spectrometry. Thermodynamic and kinetic aspects of the ligand exchange process have been explored using ^{1}H/^{2}D isotope labeling of the 4,4'-

bipyridine connectors. This study shows that ligand exchange does not proceed spontaneously for these metalla-assemblies, even at high temperature, unless an external stimulus is applied.

3

Investigating the Formation Mechanism of Arene Ruthenium Metalla-Cycles by NMR Spectroscopy

As demonstrated previously, the arene ruthenium metalla-rectangles built with 4,4'-bipyridine linkers and the OO∩OO bridging units are robust and inert to ligand exchange unless an external stimulus is applied. However, one question remains: These structures constructed via a self-assembling process, are they kinetic or thermodynamic products?

In this chapter, the synthesis and characterization of twelve dinuclear arene ruthenium complexes as models of the intermediate species formed during the supramolecular assembly of arene ruthenium metalla-cycles have been reported. The kinetic and thermodynamic aspects dictating the formation of these dinuclear complexes, in addition to their stereochemical properties have been studied in solution using NMR spectroscopy. Several experiments, including an intramolecular [2+2] photochemical cycloaddition, gave valuable answers regarding the probable mechanism leading to the formation of arene ruthenium metalla-cycles and concerning the nature of the intermediate species.

3.1 Preparation of Dimetallic Arene Ruthenium Complexes

A series of dinuclear arene ruthenium complexes has been synthesized in methanol (RT, 24 h) by mixing in the presence of $AgCF_3SO_3$ (Scheme 7) one equivalent of a metalla-clip [(*p*-cymene)$_2$Ru$_2$(OO∩OO)Cl$_2$] (OO∩OO = oxalato; 2,5-dioxydo-1,4-benzoquinonato (dobq); 5,8-dioxydo-1,4-naphthoquinonato (donq)) with two equivalents of a monodentate N-ligand (L^n) (L^1 = 4-phenylpyridine; L^2 = 4-styrylpyridine, L^3 = 4-methylpyridine, L^4 = 4-^{t}butylpyridine). Consequently, twelve dinuclear arene ruthenium complexes of the general formula [(*p*-cymene)$_2$Ru$_2$(OO∩OO)$(L^n)_2$]$^{2+}$ were obtained in good yields (OO∩OO = donq, $L^n = L^1$, **[1]**$^{2+}$; OO∩OO = donq, $L^n = L^2$, **[2]**$^{2+}$; OO∩OO = donq, $L^n = L^3$, **[3]**$^{2+}$; OO∩OO = donq, $L^n = L^4$, **[4]**$^{2+}$; OO∩OO = dobq, $L^n = L^1$, **[5]**$^{2+}$; OO∩OO = dobq, $L^n = L^2$, **[6]**$^{2+}$; OO∩OO = dobq, $L^n = L^3$, **[7]**$^{2+}$; OO∩OO = dobq, $L^n = L^4$, **[8]**$^{2+}$; OO∩OO = oxalato, $L^n = L^1$, **[9]**$^{2+}$; OO∩OO = oxalato, $L^n = L^2$, **[10]**$^{2+}$; OO∩OO = oxalato, $L^n = L^3$, **[11]**$^{2+}$; OO∩OO = oxalato, $L^n = L^4$, **[12]**$^{2+}$).

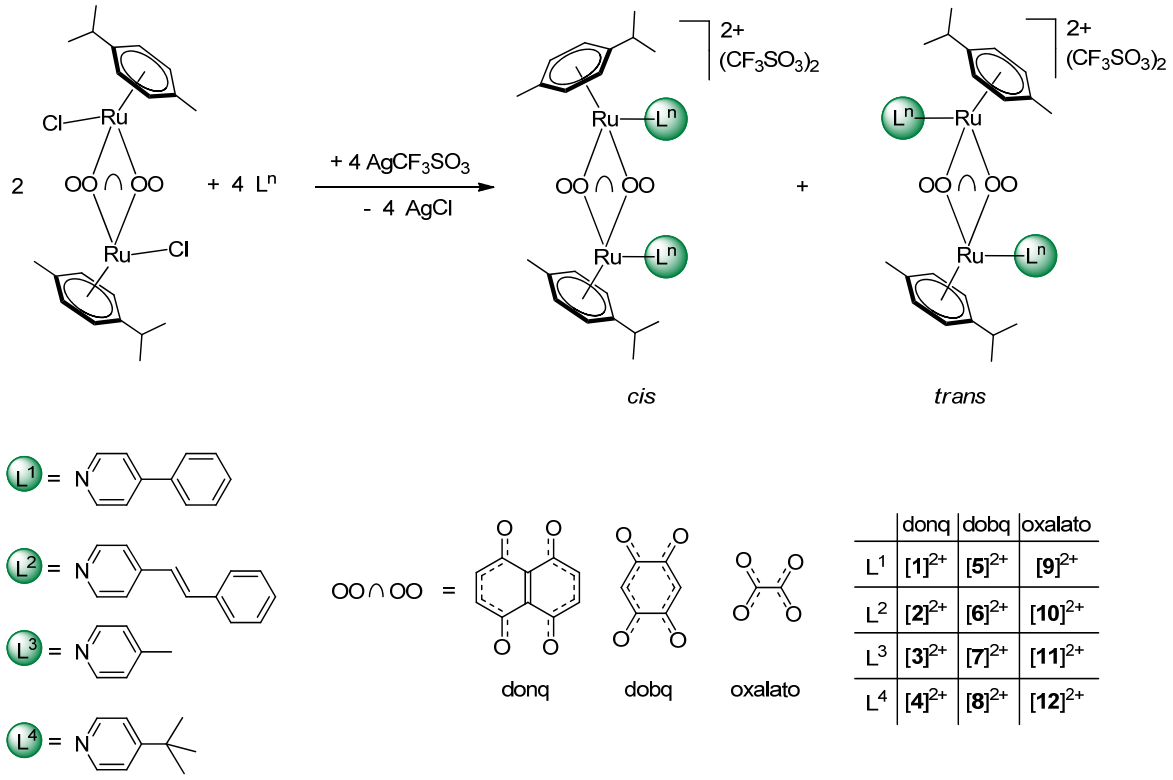

	donq	dobq	oxalato
L^1	**[1]**$^{2+}$	**[5]**$^{2+}$	**[9]**$^{2+}$
L^2	**[2]**$^{2+}$	**[6]**$^{2+}$	**[10]**$^{2+}$
L^3	**[3]**$^{2+}$	**[7]**$^{2+}$	**[11]**$^{2+}$
L^4	**[4]**$^{2+}$	**[8]**$^{2+}$	**[12]**$^{2+}$

Scheme 7. Synthesis of the dinuclear arene ruthenium complexes ***[1]***$^{2+}$*–****[12]***$^{2+}$.

All complexes were isolated as their triflate salts and as mixtures of *cis* and *trans* isomers (Scheme 7). The presence of *cis* and *trans* isomers can be expected and was not surprising, however, only the *cis* isomer is consistent with the formation of discrete metalla-assemblies.

The choice of 4-phenylpyridine (L^1), 4-styrylpyridine (L^2) and 4-*t*butylpyridine (L^4) as monodentate N-ligand was not accidental. The L^1 and L^2 derivatives are closely related to respectively 4,4'-bipyridyne and 1,2-bis(pyridine-4-yl)ethylene, two linkers commonly used to prepare metalla-rectangles,[144] while the *t*butyl derivative adds steric repulsions and accordingly should favor the formation of *trans* isomers.

3.2 X-ray Analysis Characterization

Despite having mixtures of the *cis* and *trans* isomers for all complexes, two *trans* derivatives have been isolated by crystallization of their triflate salts. These two crystalline structures allowed confirmation of the proposed complexes and subsequently allowed assignment to the corresponding isomers (*cis* and *trans*) for the two sets of signals observed in the ^{1}H NMR spectra. The molecular structures of [*trans*-**4**]$^{2+}$ and [*trans*-**7**]$^{2+}$ are presented in Figures 38 and 39, respectively.

In both structures, the ruthenium atoms adopted the typical three-legged piano-stool geometry with a metal···metal separation of 8.3958(6) and 8.4132(6) Å in [*trans*-**4**]$^{2+}$ and 7.9389(4) Å in [*trans*-**7**]$^{2+}$. Despite the presence of two crystallographically independent dinuclear complexes in the crystal packing of [*trans*-**4**]$(CF_3SO_3)_2$ 2 $(CH_3)_2CO$, the two dicationic complexes were found to be geometrically identical. Moreover, the geometrical parameters observed in [*trans*-**4**]$^{2+}$ and [*trans*-**7**]$^{2+}$ were comparable to those observed in the related complexes [(*p*-cymene)$_2$Ru$_2$(donq)$(OH_2)_2$]$^{2+}$,[145] and [(*p*-cymene)$_4$Ru$_4$(dobq)$_2$(4,4'-bipyridyne)$_2$]$^{4+}$.[146]

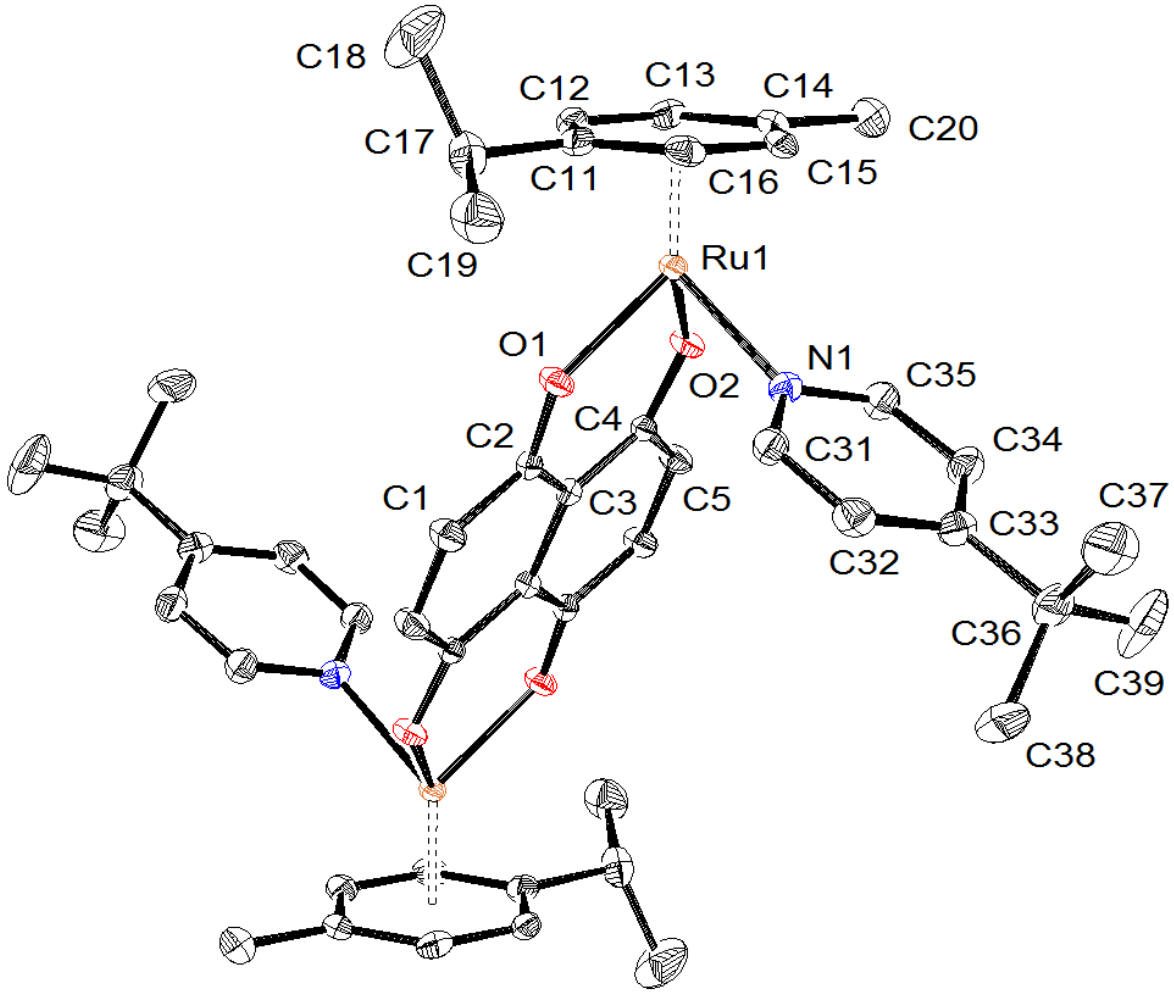

*Figure 38. ORTEP drawing of the cation [trans-**4**]$^{2+}$ at the 50% probability level ellipsoids, with hydrogen atoms, triflate anions and acetone molecules omitted for clarity. Selected bond lengths (Å) and angles (°): Ru1-N1 2.115(2), Ru1-O1 2.052(2), Ru1-O2 2.048(2), O1-C2 1.284(3), O2-C4 1.285(3); O1-Ru1-O2 86.84(6), O1-Ru1-N1 84.02(7), O2-Ru1-N1 84.42(7).*

In both structures, the angle observed between the plane defined by the OO∩OO bridging ligand and the plane formed by the adjacent pyridyl ring was < 90°. This deviation from 90° was more pronounced in [*trans*-**7**]$^{2+}$ with an angle of 79.54(6)°, while in [*trans*-**4**]$^{2+}$ these angles were found at 86.08(6) and 87.50(6)°, respectively.

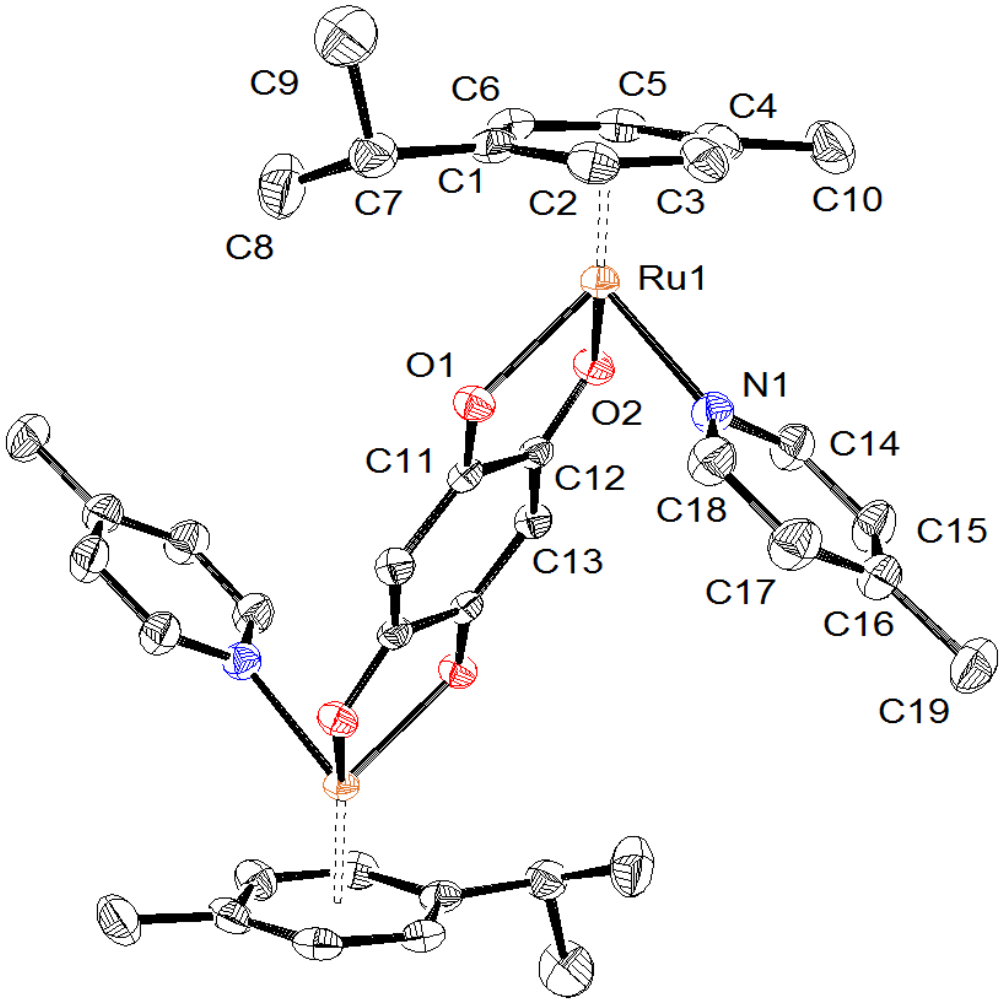

*Figure 39. ORTEP drawing of the cation [trans-**7**]$^{2+}$ at the 50% probability level ellipsoids, with hydrogen atoms and triflate anions omitted for clarity. Selected bond lengths (Å) and angles (°): Ru1-N1 2.111(2), Ru1-O1 2.094(1), Ru1-O2 2.077(1), O1-C11 1.274(2), O2-C12 1.283(2); O1-Ru1-O2 77.16(5), O1-Ru1-N1 84.14(6), O2-Ru1-N1 84.32(6).*

3.3 Investigation of the Stereochemical Properties of the Dinuclear Complexes in Solution Using NMR Spectroscopy

ROESY measurements have clearly confirmed the existence of two isomers in solution (Fig. 40). Furthermore, the assignment of the ^{1}H and ^{13}C NMR spectroscopy signals to the corresponding *cis* and *trans* isomers was based on the X-ray structures of *[trans-***4**](CF$_3$SO$_3$)$_2$ and [*trans*-**7**](CF$_3$SO$_3$)$_2$, and similar behavior was assumed for [**1**]$^{2+}$ to [**8**]$^{2+}$; NOE experiments were used for the oxalato derivatives [**9**]$^{2+}$ to [**12**]$^{2+}$.

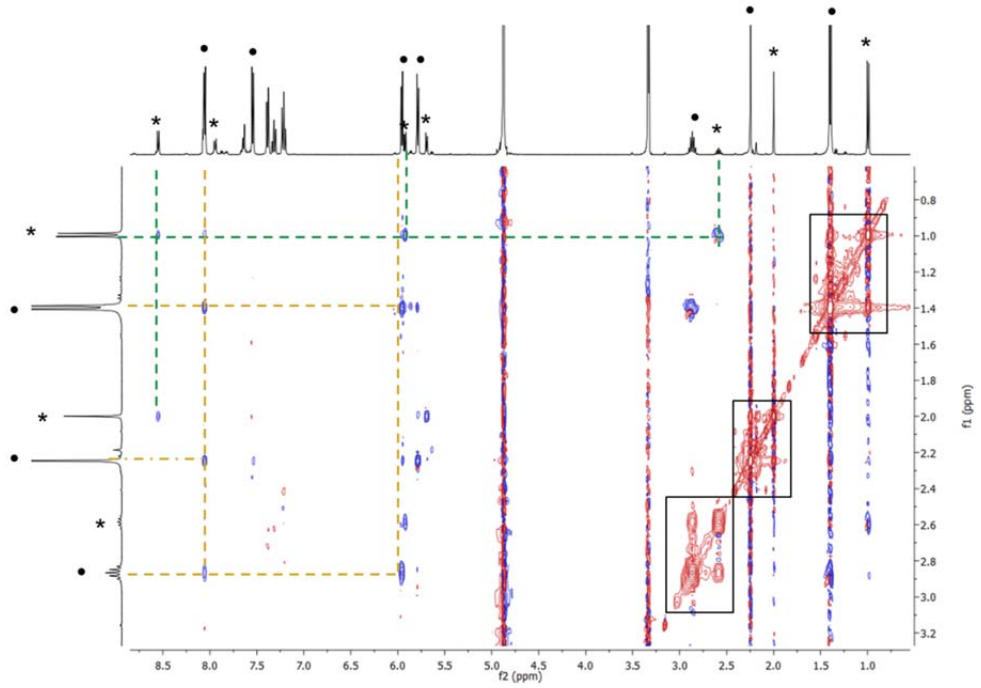

Figure 40. ROESY NMR spectrum of the complex ***[9]***$^{2+}$ *in CD_3OD (cis •, trans *, 23°C). The exchange cross peaks observed between the cis and trans conformers are highlighted by rectangles.*

In all complexes, the ^{1}H NMR spectra show the signals of the aromatic protons associated to the *p*-cymene moieties and to the pyridyl groups of the L^n ligands to be more downfield shifted for the *trans* isomer as compared to the corresponding signals of the *cis* isomer. For the donq and dobq derivatives the shift (Δδ) is around 0.15 ppm. As an example, HSQC spectra of the complex [**4**]$^{2+}$ is presented in Figure 41.

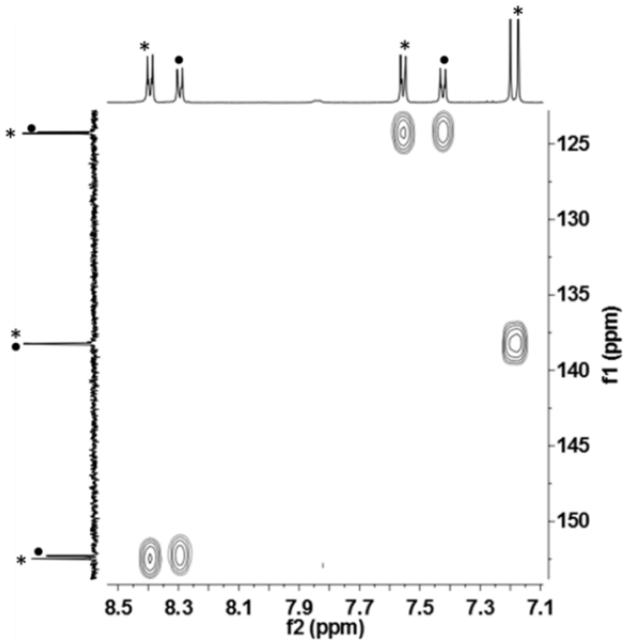

*Figure 41. ^{1}H NMR, ^{13}C NMR – HSQC spectra of the complex [**4**]$^{2+}$ in CD_3OD (pyridyl region; cis •, trans *, 23°C).*

This difference between the ^{1}H signals of the *cis* and *trans* isomers is more pronounced for the oxalato derivatives, in which a $\Delta\delta$ of roughly 0.5 ppm is observed between the two sets of signals (Fig. 42).

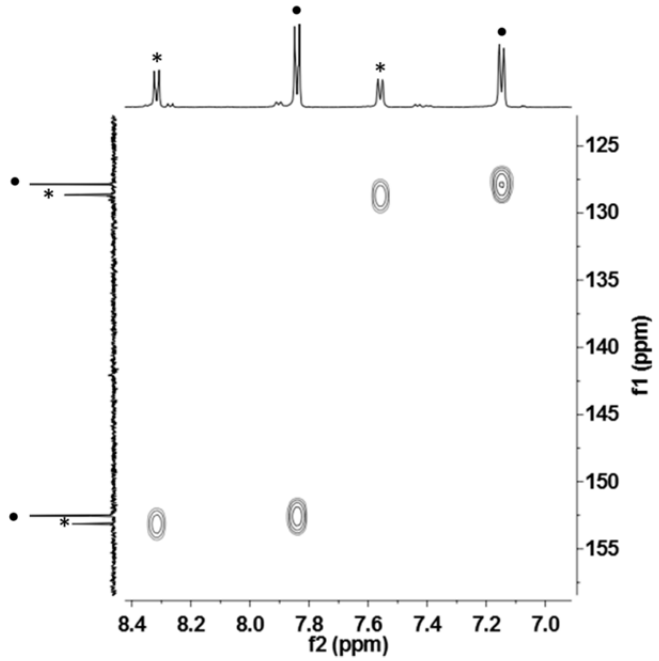

*Figure 42. ^{1}H NMR, ^{13}C NMR – HSQC spectra of the complex $[\mathbf{11}]^{2+}$ in CD_3OD (pyridyl region; cis •, trans *, 23°C).*

Interestingly, for the cations $[cis\text{-}\mathbf{10}]^{2+}$ and $[cis\text{-}\mathbf{12}]^{2+}$, several ^{1}H NMR signals show diastereotopic behavior, this suggests that the *cis* conformer has a lower symmetry. Indeed, the presence of two tert-butyl or two styryl groups in relatively close proximity forces the two adjacent pyridyl ligands to adopt a staggered conformation (Fig. 44), which reduces the symmetry of the dinuclear complexes. Consequently, the pyridyl and *p*-cymene aromatic protons appear as two sets of four doublets, as emphasized in the inset of Figure 43. However, in $[cis\text{-}\mathbf{12}]^{2+}$, the methyl groups of the tert-butyl groups and the methyl group of the *p*-cymene ligands are also nonequivalent, which suggests the loss of the C2 symmetry. This can be rationalized from a steric perspective, as the tert-butyl groups are not free to rotate (Fig. 44).

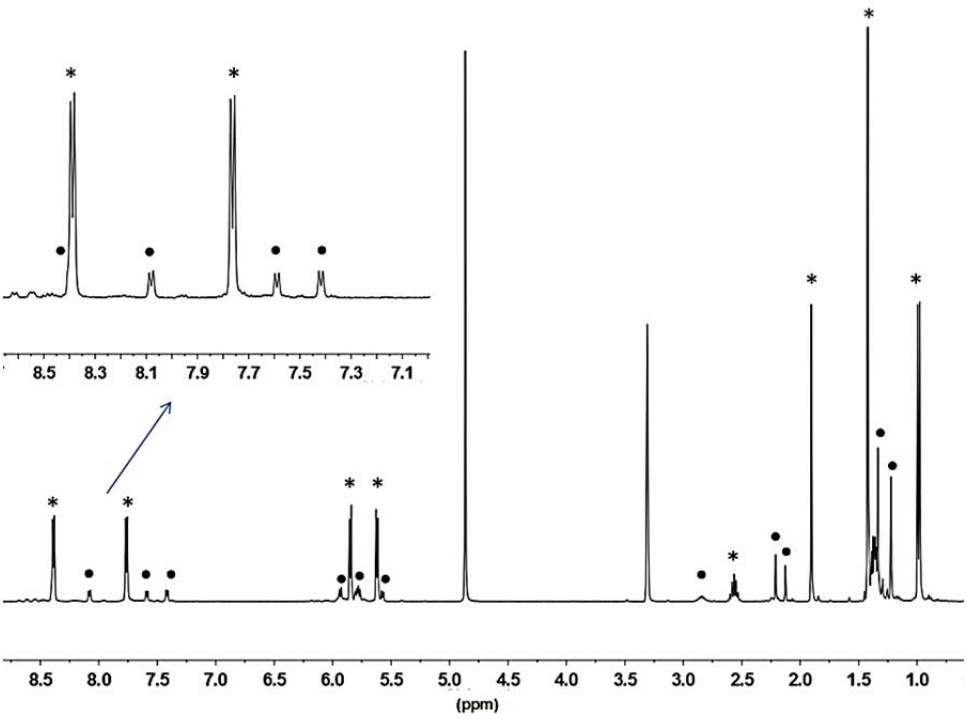

*Figure 43. ^{1}H NMR spectrum of the cation [**12**]$^{2+}$ in CD_3OD (cis •, trans *, 23°C).*

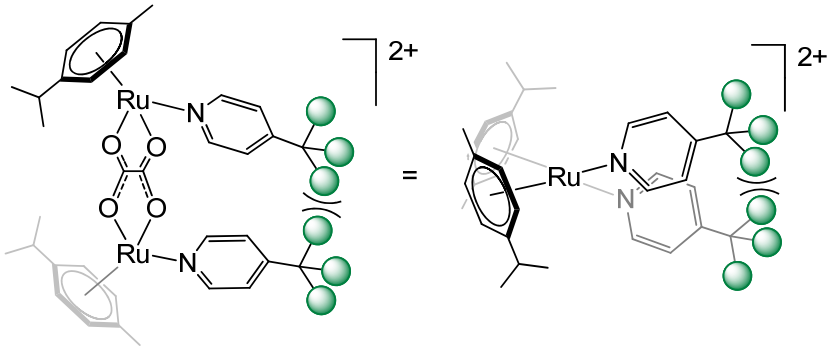

*Figure 44. Schematic representation of the cation [cis-**12**]$^{2+}$ showing the staggered conformation and the steric hindrance of the 4-tertbutylpyridine ligands (side and top views).*

The *cis-trans* ratio was generally close to 50:50 with slightly more of the *trans* isomers for the donq and dobq dinuclear complexes [**1**]$^{2+}$–[**8**]$^{2+}$, whereas the *cis* isomers dominated for the oxalato derivatives [**9**]$^{2+}$ and [**11**]$^{2+}$, and the *trans* isomer prevailed in [**10**]$^{2+}$ and [**12**]$^{2+}$ (Table 5).

Table 5. Cis-trans isomer ratio in a CD_3OD solution (23°C, determined by ^1H NMR) for cations $[\mathbf{1}]^{2+}$–$[\mathbf{12}]^{2+}$ after 1 hour and after 1 week.

	1 hours (CD_3OD)		**1 week** (CD_3OD)	
	cis	*trans*	*cis*	*trans*
$[\mathbf{1}]^{2+}$	46	54	45	55
$[\mathbf{2}]^{2+}$	41	59	40	60
$[\mathbf{3}]^{2+}$	47	53	46	54
$[\mathbf{4}]^{2+}$	42	58	41	59
$[\mathbf{5}]^{2+}$	39	61	37	63
$[\mathbf{6}]^{2+}$	38	62	39	61
$[\mathbf{7}]^{2+}$	38	62	38	62
$[\mathbf{8}]^{2+}$	32	68	31	69
$[\mathbf{9}]^{2+}$	78	22	80	20
$[\mathbf{10}]^{2+}$	20	80	20	80
$[\mathbf{11}]^{2+}$	70	30	69	31
$[\mathbf{12}]^{2+}$	24	76	38	62

This isomer distribution was rationalized from the shorter Ru···Ru separation found in the oxalato derivatives (ca. 5.5 Å),[147] which resulted in additional π-π stacking interactions between the adjacent N-ligands in $[\textit{cis}\text{-}\mathbf{9}]^{2+}$ and $[\textit{cis}\text{-}\mathbf{11}]^{2+}$, whereas steric hindrance of the L^n ligands favored the formation of $[\textit{trans}\text{-}\mathbf{10}]^{2+}$ and $[\textit{trans}\text{-}\mathbf{12}]^{2+}$.

3.4 Thermodynamic and Kinetics Aspects Dictating the Formation of the Dinuclear Complexes

The *cis*-*trans* ratios determined from the ^1H NMR spectroscopic data were used to estimate the standard free energy change (ΔG°) of the *cis* and *trans* conformers ($\Delta G° = -RT \cdot \ln K$). The higher concentration of the *cis* isomer in the oxalato derivatives $[\mathbf{9}]^{2+}$ and $[\mathbf{11}]^{2+}$ was attributed to a π-π stacking contribution. This contribution was estimated by comparing the ΔG° of the donq derivatives $[\mathbf{1}]^{2+}$ and $[\mathbf{3}]^{2+}$, for which no π-π interactions are possible owing to the longer Ru···Ru separation (> 8.3 Å),[134a] than those of the oxalato derivatives. As expected, the stabilization was higher for 4-phenylpyridine (0.9 kcal · mol^{-1}) than for 4-

methylpyridine (0.6 kcal · mol^{-1}; Table 6). These values are consistent with the planar aromatic surface of the respective pyridyl ligands.

Table 6. Estimated π-π stacking contribution in cations $[\mathbf{9}]^{2+}$ and $[\mathbf{11}]^{2+}$, favoring the cis isomers.

	$[\mathbf{1}]^{2+}$	$[\mathbf{9}]^{2+}$	$[\mathbf{3}]^{2+}$	$[\mathbf{11}]^{2+}$
cis-trans ratio	45 / 55	80 / 20	46 / 54	69 / 31
ΔG° (kcal · mol^{-1})	0.1	-0.8	0.1	-0.5
π - π stacking contribution in kcal · mol^{-1}, calculated from the Δ(ΔG°)	-0.9		-0.6	

The kinetics of the *cis-trans* interconversion for the oxalato derivatives were also studied in solution by ^{1}H NMR spectroscopy. The results showed that the *cis-trans* ratio remained almost unchanged for days, except for $[\mathbf{12}]^{2+}$ for which an increase of the *cis* isomer ratio was observed over a 1 week period (Table 5), thus suggesting a longer period to reach equilibrium for this system.

The presence of the ^{t}butyl group kinetically favors the formation of the *trans* isomer. However, the concentration of the *cis* isomer increased over time, and after reaching a dynamic equilibrium (CD_3OD, 23°C), the steric contribution of the ^{t}butyl group was estimated (Table 7). The difference in the ΔG° between the 4-methylpyridine derivative $[\mathbf{11}]^{2+}$ and the 4-^{t}butylpyridine derivative $[\mathbf{12}]^{2+}$ was 0.8 kcal · mol^{-1}.

Table 7. Estimated steric hindrance contribution in $[\mathbf{12}]^{2+}$, favoring the trans isomer.

	$[\mathbf{12}]^{2+}$	$[\mathbf{11}]^{2+}$
cis-trans ratio	38 / 62	69 / 31
ΔG° (kcal · mol^{-1})	0.3	-0.5
steric contribution in kcal · mol^{-1}, calculated from the Δ(ΔG°)	-0.8	

3.5 Plausible Mechanism of the *Cis–Trans* Conversion

ROESY experiments confirmed the dynamic exchange between the *cis* and *trans* isomers. Indeed, for all complexes, exchange cross peaks between the pyridyl protons of the terminal N-ligands of the *cis* and of the *trans* isomer were observed. As an example, the ROESY spectrum of $[\mathbf{12}]^{2+}$ is presented in Figure 45. Additionally, weak signals associated with free N-ligands, also exchanging with the two isomers, were noticed in the ^{1}H NMR spectra, supporting the dynamic nature of the Ru-N bond in these dinuclear arene ruthenium complexes.

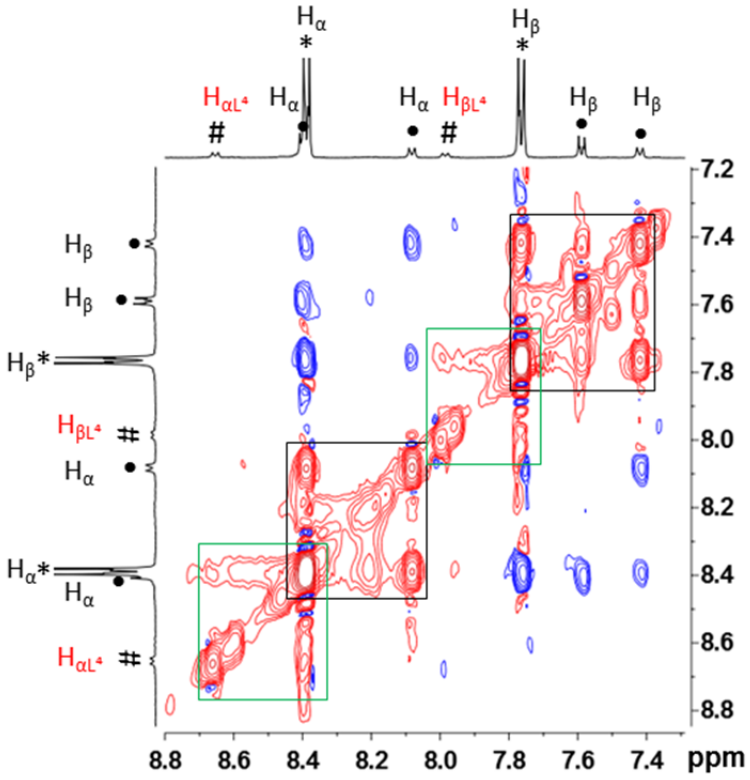

Figure 45. ROESY NMR spectrum of the cation $[\mathbf{12}]^{2+}$ in CD_3OD (23°C). The exchange cross peaks observed between the pyridyl protons of the cis (•) and trans (*) conformers and between the trans and free 4-^{t}butylpyridine (#) are highlighted by black and green rectangles, respectively.

The presence of weak signals assigned to non-coordinated N-ligands in the ^{1}H NMR spectra of $[\mathbf{1}]^{2+}$ to $[\mathbf{12}]^{2+}$, together with the clear correlation between the pyridyl-protons of the free N-ligand, the *cis* and the *trans* isomers in the ROESY experiments, suggest a *cis-trans* conversion involving decomplexation of a N-ligand followed by racemization at the metal center, and re-coordination of the N-ligand to generate the opposite conformer. Therefore, in analogy to a S_N1 type reaction, a mechanism for the *cis-trans* conversion was

proposed, see Figure 46. As previously studied by Ward and Hofmann,[148] the energy associated to an inversion of configuration for a two-legged piano stool intermediate (16e species) is estimated to be lower than 15 kcal · mol^{-1}. Such 16 valence electron species have been occasionally isolated and characterized.[149]

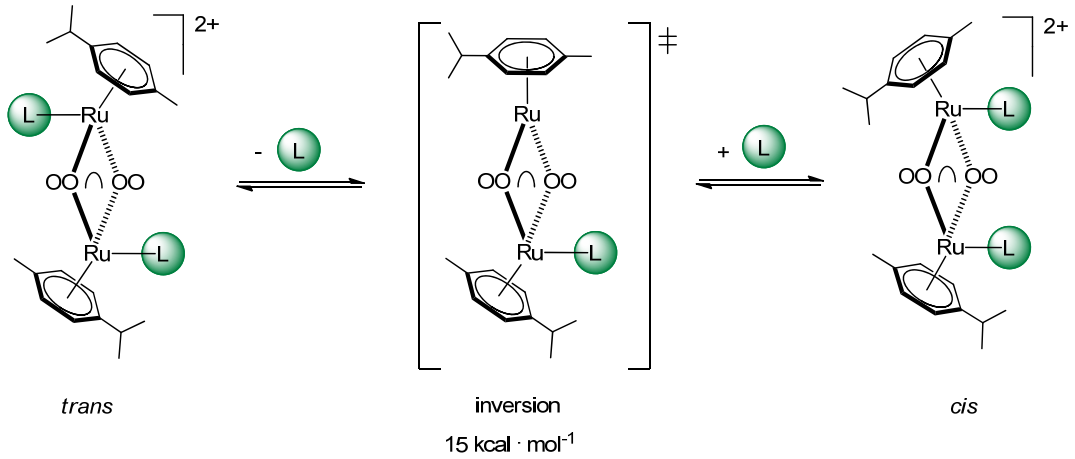

Figure 46. Proposed mechanism of the cis-trans conversion involving a 16e intermediate.

3.6 Dinuclear Arene Ruthenium Complexes as Template for [2+2] Cycloaddition

The presence of two parallel 4-styrylpyridine ligands in the oxalato derivative [*cis*-**10**]$^{2+}$ implied that a [2+2] cycloaddition reaction might occur between, as previously observed with the oxalato-bridged metalla-rectangle [(*p*-cymene)$_4$Ru$_4$(oxalato)$_2$(4,4'-bipyridylethylene)$_2$]$^{4+}$.[150] Accordingly, when a methanol solution of [**10**]$^{2+}$ was irradiated with a UV lamp (λ_{exc} = 365 nm), a photochemical [2+2] cycloaddition reaction was observed, forming quantitatively the dicationic cyclobutane derivative [**13**]$^{2+}$ (Scheme 8). The complete conversion of [**10**]$^{2+}$ to [**13**]$^{2+}$ was observed after 60 hours and confirm the dynamic nature of the Ru-N bond and the *cis-trans* interconversion in solution. During the photochemical [2+2] cycloaddition reaction in methanol, the initial orange solution of [**10**]$^{2+}$ has turned dark red upon formation of [**13**]$^{2+}$ (see insert in Scheme 8).

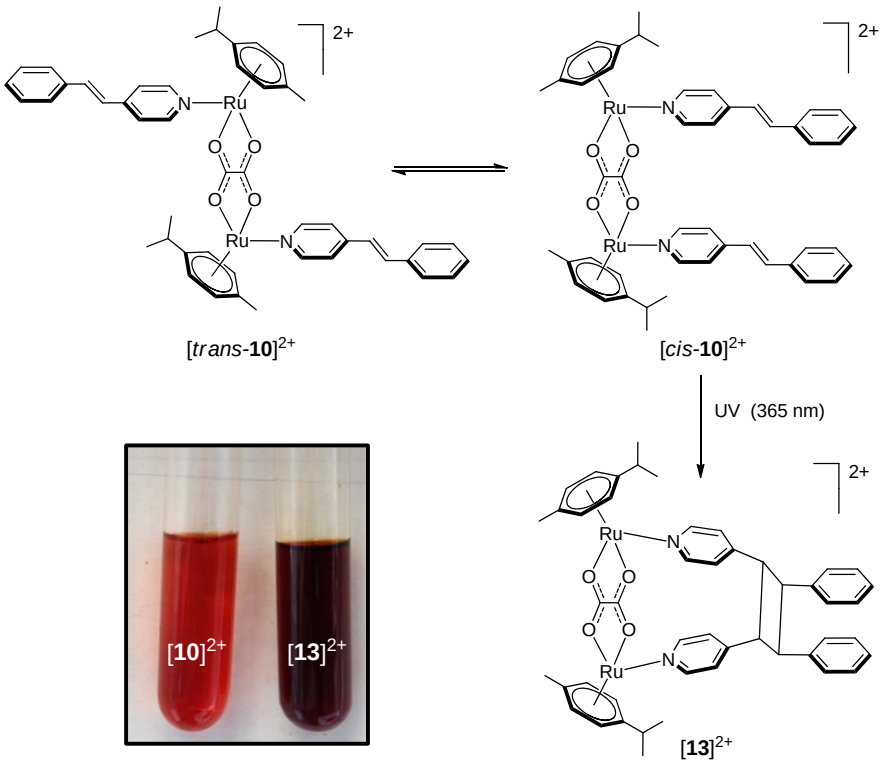

*Scheme 8. Synthesis of the [2+2] cycloaddition product [**13**]$^{2+}$ from [**10**]$^{2+}$.*

However, in the solid state, only partial conversion of the orange powder of [**10**]$^{2+}$ was observed (up to 30%), even after a prolonged UV-irradiation (3 days). This result is not surprising as the *cis-trans* conversion was only expected to occur in solution. The formation of [**13**]$^{2+}$ was further confirmed by multiple one-dimensional and two-dimensional NMR experiments (^{1}H, HSQC) (Fig. 47, 48) and by ESI mass spectrometry (Fig. 49).

The [2+2] cycloaddition reaction of the olefinic bonds was followed by ^{1}H NMR spectroscopy. The appearance of two doublets at δ = 4.78 and 4.65 ppm assigned to the cyclobutane protons, and the disappearance of the two doublets of the olefinic protons of the *cis* isomer at δ = 7.45 and 6.89 ppm together with the disappearance of the four doublets of the *trans* isomer at δ = 7.77, 7.64, 7.35 and 7.25 ppm confirmed the formation of [**13**]$^{2+}$ (Fig. 47).

These observations are consistent with the previously reported [2+2] cycloaddition of 4-styrylpyridine in di-silver complexes.[151] The ^{13}C NMR spectrum of complex [**13**]$^{2+}$ also showed two signals corresponding to the cyclobutane carbon atoms at δ 48.94 ppm and δ 45.14 ppm, respectively (Fig. 48).

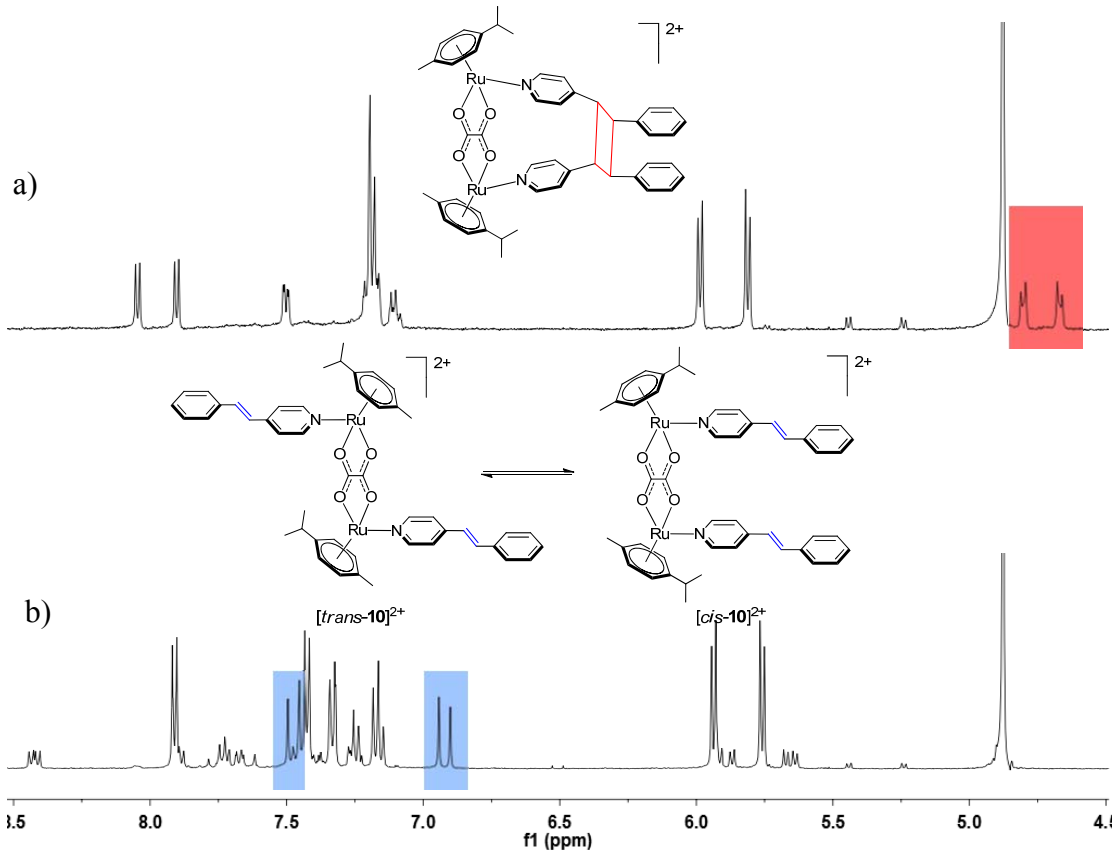

Figure 47. ^{1}H NMR spectra of cations $[\mathbf{10}]^{2+}$ and $[\mathbf{13}]^{2+}$ in CD_3OD (aromatic region, 23°C).

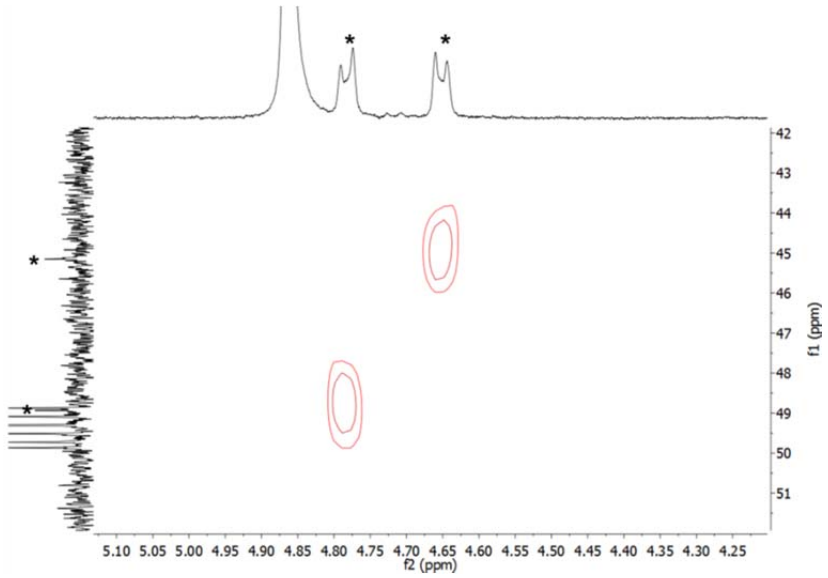

Figure 48. HSQC NMR spectrum of the complex $[\mathbf{13}]^{2+}$ in CD_3OD

The presence of only two ^{13}C signals for the cyclobutane ring suggests the formation of a single cyclobutane-isomer: The *cis* coordination of the two 4-styrylpyridine precursors controlling the stereo-chemistry of the [2+2] cycloaddition product. It is noteworthy to

mention from the infrared spectra, that the band corresponding to the stretching vibration of the ethylene groups ($\nu_{CH=CH}$), centered at 1595(s) cm^{-1} in the free 4-styrylpyridine,[152] which is also observed in $[\mathbf{10}]^{2+}$, disappeared during the formation of $[\mathbf{13}]^{2+}$.

ESI mass spectrometry was employed to further confirm the cycloaddition process in $[cis\text{-}\mathbf{10}]^{2+}$. In fact, the mass spectrum of the compound $[\mathbf{10}](CF_3SO_3)_2$ before the cycloaddition had two major peaks at m/z = 708 (#) and 890 (•) attributed to the fragments [(*p*-cymene)$_2$Ru$_2$(oxalato) + $CF_3SO_3]^+$ (#) and [(*p*-cymene)$_2$Ru$_2$(oxalato)(4-styrylpyridine) + $CF_3SO_3]^+$ (•), respectively (Fig. 8), with no sign of the intact complex $[\mathbf{10}]^{2+}$. After 24 h of UV-irradiation (365 nm), we observed the appearance of a new peak at m/z = 1071 (*) corresponding to the fragment [(*p*-cymene)$_2$Ru$_2$(oxalato){di(4-styrylpyridine)cyclobutane} + $CF_3SO_3]^+$ coupled with the decrease of the other two peaks.

However, as the time increased to 60 h, we observed the disappearance of the peaks corresponding to [(*p*-cymene)$_2$Ru$_2$(oxalato)(4-styrylpyridine) + $CF_3SO_3]^+$ (•) and [(*p*-cymene)$_2$Ru$_2$(oxalato) + $CF_3SO_3]^+$ (#) with a clean mass spectrum containing only a major peak at m/z = 1071 corresponding to [(*p*-cymene)$_2$Ru$_2$(oxalato){di(4-styrylpyridyl)cyclobutane} + $CF_3SO_3]^+$ (*), which further supports the formation of the [2+2] cycloaddition complex $[\mathbf{13}]^{2+}$.

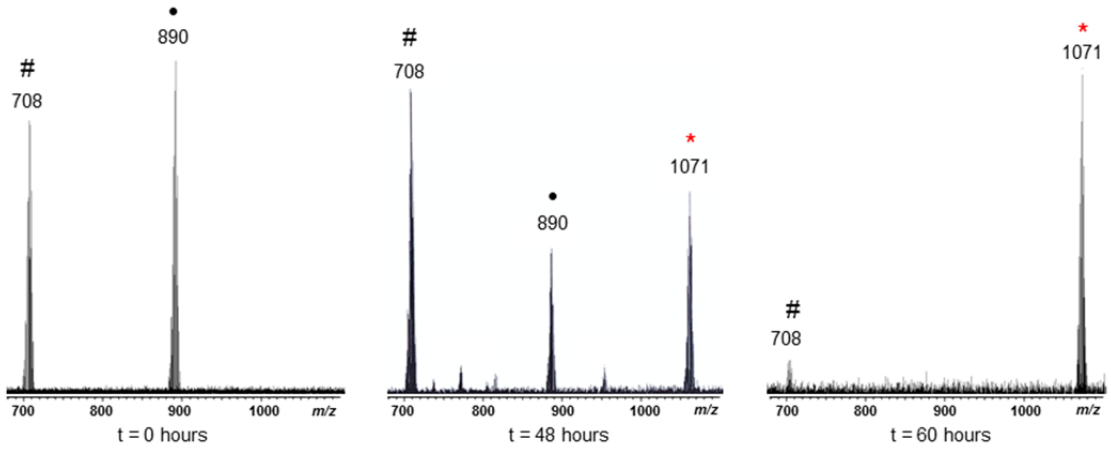

Figure 49. ESI-MS of complex $[\mathbf{10}]^{2+}$ before irradiation (left), after 48 hours (middle) of UV-irradiation (365 nm) and after 60 hours of UV-irradiation (right).

The [2+2] cycloaddition adduct $[\mathbf{13}]^{2+}$ mimics the final step during the formation of metalla-rectangles, namely the closure of the metalla-assembly. Overall, the stability of metalla-cycle $[\mathbf{13}]^{2+}$ was found to be extremely high, as already indicated by ESI mass spectrometry. All attempts to isolate the di(4-styrylpyridyl)cyclobutane molecule have failed

in our hands, such as refluxing complex $[\mathbf{13}]^{2+}$ in acetonitrile or dmso, even in the presence of triphenylphosphine, a strong coordinating agent.

The stability of $[\mathbf{13}]^{2+}$ is in agreement with our recent finding that arene ruthenium metalla-rectangles build with 4,4'-bipyridine linkers and the same OO∩OO bridging units are inert to ligand exchange unless an external stimulus is applied.[153] Obviously, the formation of a metalla-cycle in $[\mathbf{13}]^{2+}$ has introduced an additional stability to the system, similar to the stability obtained when forming metalla-cycles.

3.7 Conclusions

The stereochemical properties of twelve dinuclear arene ruthenium complexes have been studied in solution. The dinuclear complexes of the general formula $[(p\text{-cymene})_2\text{-}Ru_2(OOOO)(L^n)_2](CF_3SO_3)_2$ (OOOO = oxalato, 2,5-dioxido-1,4-benzoquinonato, 5,8-dioxido-1,4-naphthoquinonato; L^n = 4-phenylpyridine, 4-styrylpyridine, 4-methylpyridine, 4-tert-butylpyridine) have been isolated as mixtures of the *cis* and *trans* isomers. All of the complexes showed a noticeable lability of the pyridyl-based ligands (L^n) in solution and rapid exchange between the *cis* and *trans* isomers. The equilibrium between the *cis* and *trans* isomers was confirmed by ^{1}H NMR spectroscopy, and the intermediate species were identified and, thus, provided valuable insights into the formation mechanism of arene ruthenium metalla-assemblies.

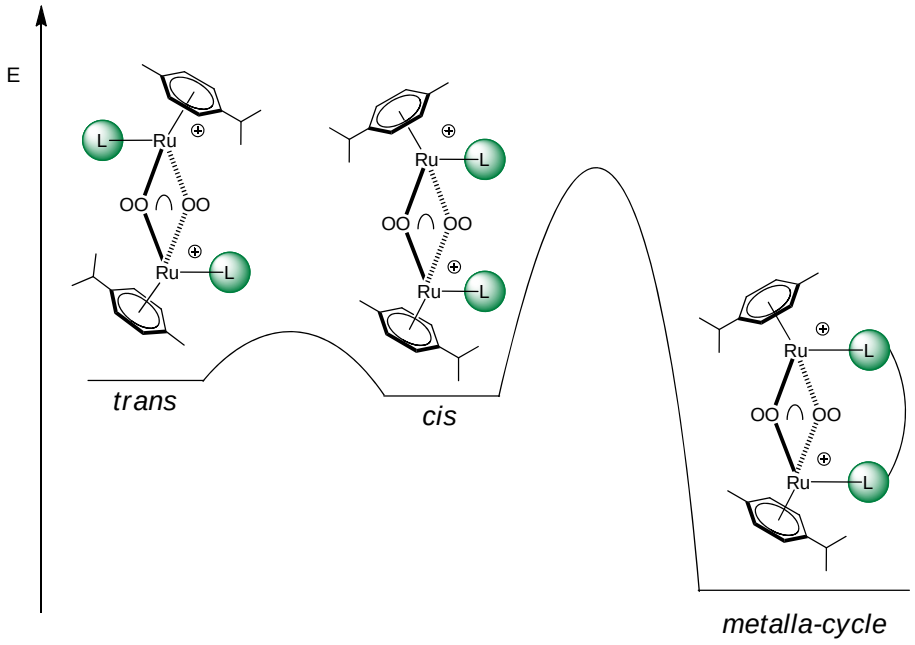

4

Strategy to Optimize the Biological Activity of Arene Ruthenium Metalla-Assemblies

Modification of the structural integrity of an active parent agent by functionalization or grafting hydrophilic groups or lipophilic motifs is an efficient approach usually used to enhance the biological activity of such compounds.[106, 154]

In this chapter, three new dinuclear arene ruthenium metalla-clips of the general formula [(*p*-cymene)$_2$Ru$_2$Cl$_2$(μ-L)], which have been prepared by Arion group in the university of Vienna, from [(*p*-cymene)$_2$Ru$_2$Cl$_2$(μ-Cl)$_2$] and H_2L organic linkers (H_2L^a = diethyl-1,2-diazenedicarboxylate, H_2L^b = N,N′-bis(2-hydroxyethyl)oxamide, H_2L^c = N,N′-bis{2-(2- hydroxyethoxy)ethyl}ethanediamide) are described. The bis-chelating bridging-linkers possess two functional groups that can be synthetically modified for physico-chemical optimizations. Reaction of these three dinuclear metalla-clips with 4,4′-bipyridine, 1,2-bis(4-pyridyl)ethylene, and 4,4′-azopyridine affords, in the presence of $AgCF_3SO_3$, nine tetracationic tetranuclear metalla-rectangles. Similarly, the tridentate ligands 2,4,6-tris(4-pyridyl)-1,3,5-triazine and 1,3,5-tris{2-(4-pyridyl)vinyl}benzene were used to generate six hexacationic hexanuclear metallaprisms. All metalla-assemblies and the dinuclear complexes were evaluated by the Dyson group in the Ecole Polytechnique Fédérale de Lausanne as

anticancer agents against cancerous (A2780) and noncancerous (HEK293) cell lines, showing an excellent selectivity for cancer cells.

4.1 Ruthenium Complexes as Anticancer Drugs

Cancer is one of the most common causes of death in the modern world.[155] In cancer, an estrange tissue is formed from a single defected cell (germ) due to genetic mutation. This genetic problem, manifested by rapid DNA replication, gives rise to cellular multiplication process resulting a big tumor tissue. This dangerous tissue ultimately leads toward metastases, i.e. its rapid widespread in the body. The type of treatment usually depends on the size and the region effected. In early stages, it is removed by surgery, followed by radiotherapy or/and chemotherapy to eliminate the remaining traces of tumor. The second treatment plays a significant to inhibit the re-germination of cancer from an eventual remaining affected cell. The radiotherapy implies the ionizing light to destroy the tumor cells but kills the surrounding normal tissues as well. Chemotherapy is considered as viable alternative to inhibit the proliferation of the cancer cells by apoptosis in second stage.

The active molecules in chemotherapy come from organic frameworks type background. They are either extracted from plants or designed / synthesized in laboratories. Some metal-based drugs also manifest good therapeutic activities such as Salvarsan and its arsenical derivatives developed in the early 20th century by Paul Ehrlich.[156] *Cis-diamminedichloroplatinium* (II) (cisplatin), a planar square platinium complex, discovered by Rosenberg in 1967 was the first metalo-drug approved for clinical use.[157] This drug showed good efficiency to treat ovarian, head-and-neck, bladder and testicular cancers by inhibiting the DNA replication, thus uncontrolled growth of cells.[158] However, the treatments with cisplatin suffer many shortcomings such as the side effects due to the lack of selectivity, and the resistance from some cancer types due to the specificity problems.[159]

Other transition metal-based drug analogues such as copper, palladium, gold, iridium, and rhodium have also been developed to kill cancer cells.[160] Among these active compounds, ruthenium complexes proved their ability to compete the commercial drugs by providing a new kind of actions *vs* tumor cells.[161] The first ruthenium complexes having good biological activities were neutral. Their design mimicked the structure of cisplatin. For example, the (*cis*-$Ru(NH_3)_3Cl_3$) developed by Durig[162] in 1976 or the (*cis*-$Ru(NH_3)_4Cl_2$) discovered by

Clark[163] in 1980. However, the solubility related issues in these complexes limited their further use.[164]

Recently two compounds containing ionic Ru(III) complexes, NAMI-A and KP 10 19, successfully passed through the second clinical phase. NAMI-A is highly effective against lung metastasis but low activity against primary tumors (Fig. 50).[165] KP 10 19, is, however, very active against colon carcinomas but is not anti-metastatic.[166] Recent studies suggest that the anticancer activities of these complexes are based on the redox behavior of ruthenium in biological medium. Indeed, the Ru(III) inorganic compounds become active only after their reduction to Ru (II) species.[161]

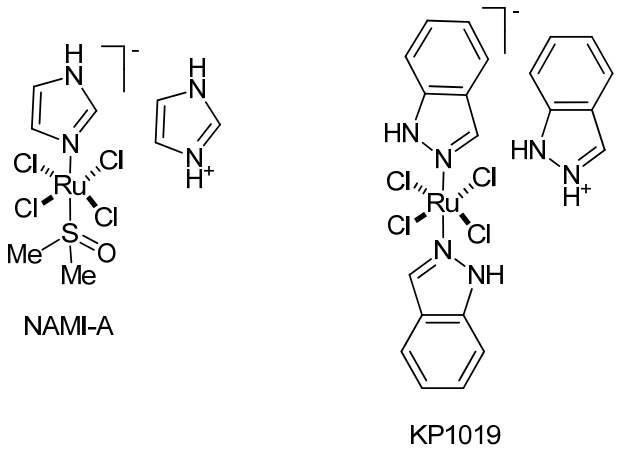

Figure 50. NAMI-A and KP1019, two ruthenium compounds in phase (II) of clinical trials.[167, 168]

In order to exploit this finding, a collection of highly cytotoxic arene ruthenium (II) complexes of type $[(\eta^6\text{-arene})Ru(\eta^2\text{-}N,N\text{-L})Cl]^+$ (e.g.; L= ethylendiamine) and $[(\eta^6\text{-arene})Ru(pta)X_2]$ (pta= 1,3,5-triaza-7-phosphatricyclo[3.3.1.1]decane, X= Cl, Br, I) have been developed by Sadler[169] and Dyson[106, 170], respectively. Among these, RM175 and RAPTA-C are the most promising arene ruthenium compounds for anticancer chemotherapy (Fig. 51).[171, 172]

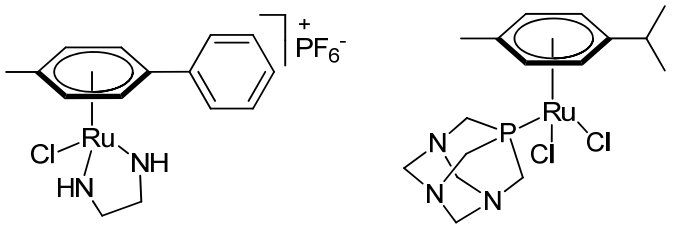

Figure 51. Molecular structure of [(η^6-biphenyl)Ru(μ-ethylendiamine)Cl][PF_6] (RM175)[171] and [(η^6-arene)Ru(pta)Cl_2] (RAPTA-C)[172] arene ruthenium complexes.

Stimulated by the promising anticancer activity of arene ruthenium complexes,[160, 173] related studies of arene ruthenium metalla-assemblies have become a flourishing area.[90b, 174] A great majority of these metalla-assemblies are derived from dinuclear arene ruthenium clips and poly-pyridyl connectors. The dinuclear metalla-clips are generally composed of two arene ruthenium units bridged by bis-chelating OO∩OO ligands, such as oxalato, 2,5-dioxido-1,4-benzoquinonato, 5,8-dioxido-1,4-naphthoquinonato, or 6,11-dioxido-5,12-naphthacenedionato ligands.[116, 175]

However, a few arene ruthenium metalla-clips have also been prepared using NN∩NN,[176] and NO∩NO[177] bis-chelating bridging-linkers. These bis-chelating bridging-linkers provide the dinuclear metalla-clips with robustness and inertness[153] and play a structural role in the successful synthesis of arene ruthenium metalla-assemblies by introducing a directional-bonding feature. In addition, they can also add functionality to the supramolecular systems, and accordingly, they can enhance the biological activity of the metalla-assemblies by modifying their physical and/or chemical properties.

Recently, we have demonstrated that embelin can be used as a bis-chelating OO∩OO linker to generate, in combination with 2,4,6-tris(4-pyridyl)-1,3,5-triazine (tpt), metalla-prisms with three lipophilic arms (Fig. 52).[131a]

Embelin (H_2L) is a quinonoid natural product with a C11 alkyl chain.[178] It was also shown that the pentamethylcyclopentadienyl (Cp*) rhodium analogue $[(Cp^*)_6Rh_6(\mu\text{-tpt})_2(\mu\text{-L})_3]^{6+}$, possesses interesting in vitro and in vivo activity,[129] implying that these linkers can enhance the biological properties of half-sandwich metalla-assemblies.

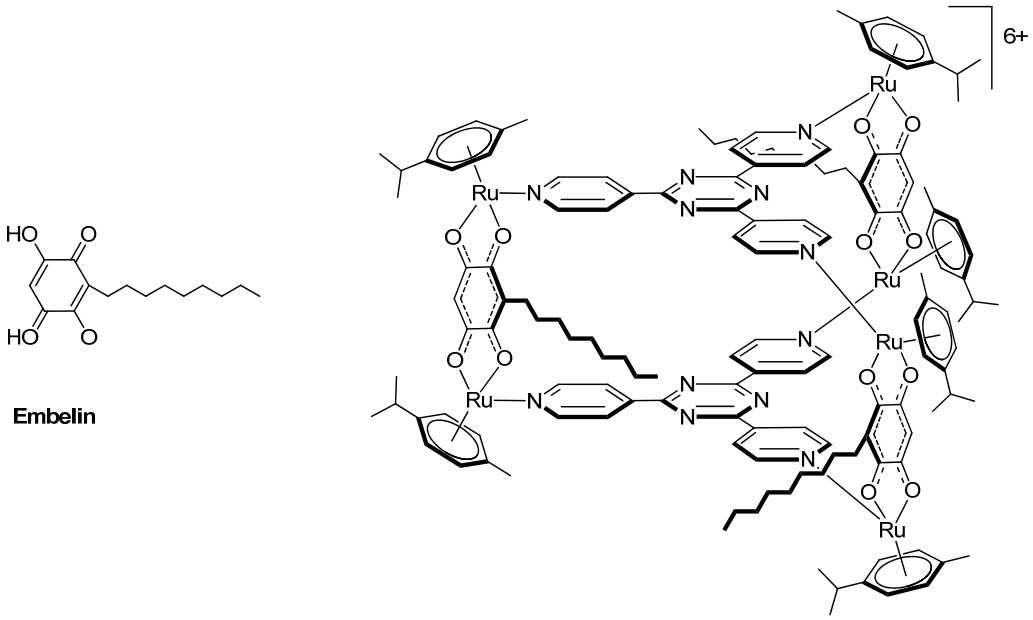

Figure 52. A metalla-prism assembled from embelin linkers, arene ruthenium corners, and 2,4,6-tris(4-pyridyl)-1,3,5-triazine panels.[131a]

Herein, we present a series of arene ruthenium metalla-clips incorporating a new family of ON∩NO bis-chelating bridging-linkers. The physico-chemical property of the metalla-assemblies can be easily modified by the introduction on these linkers of various functional groups. Therefore, from the three *p*-cymene ruthenium metalla-clips, nine tetracationic metalla-rectangles and six hexacationic metalla-prisms were prepared and characterized. All 18 compounds were evaluated for their cytotoxicity against cancerous (human ovarian cancer cells A2780) and noncancerous (kidney embryonic cells HEK293) cells, and some were found to show remarkable selectivity for the former.

4.2 Synthesis and Characterization of the Dinuclear Arene Ruthenium Metalla-Clips

Dinuclear arene ruthenium metalla-clips (**14a**−**14c**) of the general formula [(*p*-cymene)$_2$Ru$_2$Cl$_2$(μ-L)] (Fig. 53) were obtained in methanol by reacting diethyl-1,2-diazenedicarboxylate (H_2L^a), N,N′-bis(2-hydroxyethyl)oxamide (H_2L^b), or N,N′-bis{2-(2-hydroxyethoxy)ethyl}ethanediamide (H_2L^c) with [(*p*-cymene)$_2$Ru$_2$Cl$_2$(μ-Cl)$_2$] in the presence of triethylamine.

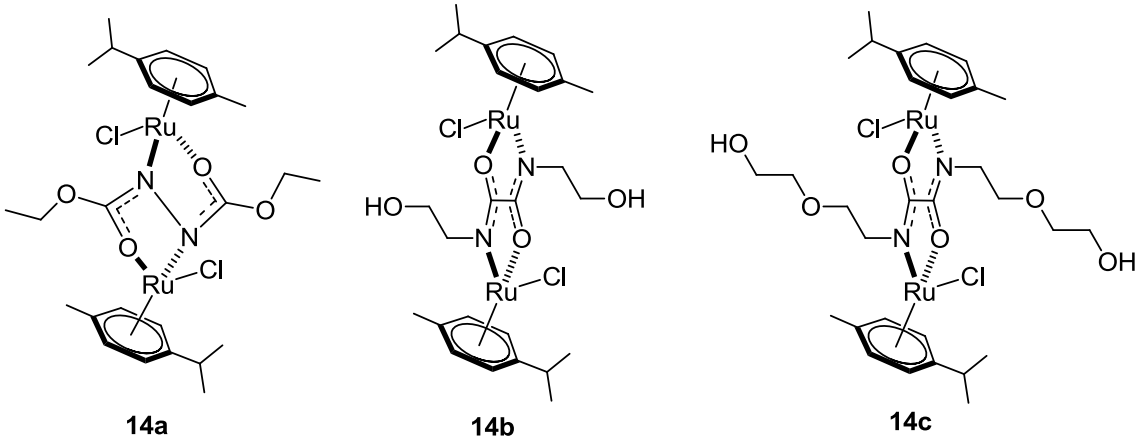

*Figure 53. Molecular structures of the dinuclear arene ruthenium metalla-clips **14a**−**14c**.*

The coordination of the ON∩NO bis-chelating bridging-linker between the two arene ruthenium units was confirmed by ^{1}H NMR spectroscopy and mass spectrometry (see the Experimental Section).

Furthermore, the molecular structure of complexes **14a** and **14c** was established by single-crystal X-ray structure analysis. Crystals of **14a** and **14c** were grown in chloroform. Despite the presence of two stereogenic centers in **14a**−**14c**, the dinuclear complexes are not chiral, with only the meso isomer being formed, as confirmed by single-crystal structure analyses. The inversion center was perfectly positioned halfway between the two metals. The molecular structures of **14a** and **14c** are shown in Figures 54 and 55, respectively, together with selected geometrical parameters. In **14a**, the Ru···Ru distance is 4.9411(5) Å, whereas, in **14c**, the same Ru···Ru distance is slightly longer, 5.5716(3) Å. The Ru−N and Ru−O bond lengths are identical in both structures and are comparable to those found in pentamethylcyclopentadienyl rhodium and iridium oxamidato derivatives.[179]

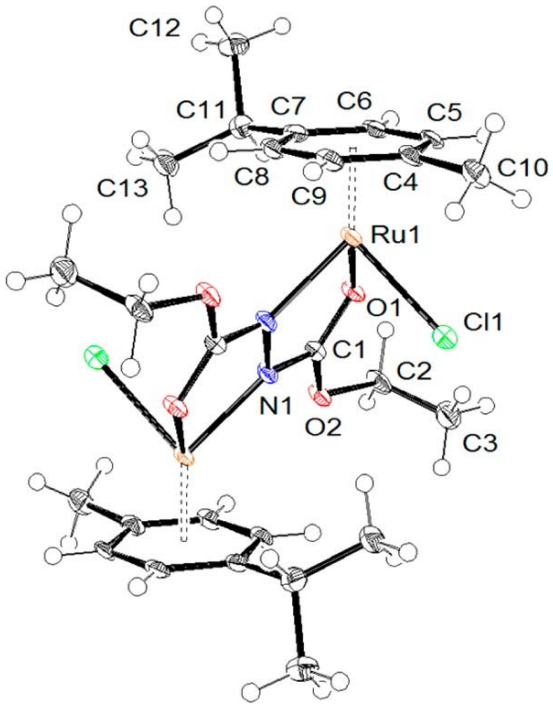

*Figure 54. ORTEP drawing of **14a** at 50% probability level ellipsoids. Selected bond distances (Å) and angles (deg): Ru1−N1^{i} = 2.090(2), Ru1−O1 = 2.110(2), Ru1−Cl1 = 2.4301(8), N1−N1^{i} = 1.422(5), Ru1−C4 = 2.209(3), Ru1−C5 = 2.200(3), Ru1−C6 = 2.165(3), Ru1−C7 = 2.177(3), Ru1−C8 = 2.147(3), Ru1−C9 = 2.175(3); O1−Ru1−N1i = 75.58(9), (i = 1 − x, 1 − y, 1 − z).*

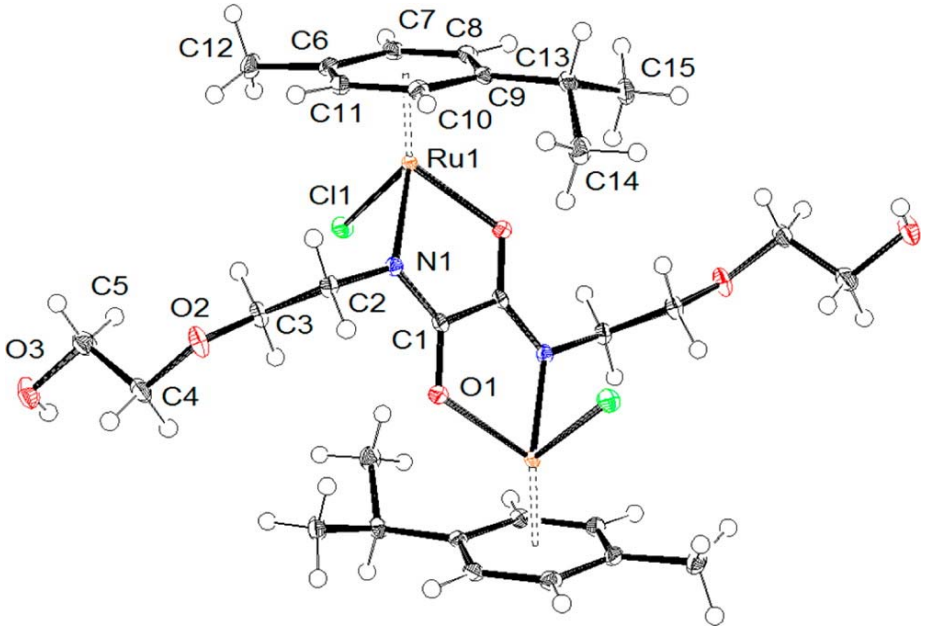

*Figure 55. ORTEP drawing of **14c** at 50% probability level ellipsoids. Selected bond distances (Å) and angles (deg): Ru1−N1 = 2.0901(15), Ru1−O1^{i} = 2.1094(13), Ru1−Cl1 = 2.4220(5), C1−O1 = 1.279(2), C1−N1 = 1.307(2), Ru1−C6 = 2.193(2), Ru1−C7 = 2.205(2), Ru1−C8 = 2.200(2), Ru1−C9 = 2.187(2), Ru1−C10 = 2.158(2), Ru1−C11= 2.174(2); N1−Ru1−O1i = 77.86(5), (i = 1 − x, 1 − y, −z).*

In **14a**, the N1−N1^{i} bond distance is 1.422(5) Å, which corresponds to a N−N single bond. Similarly, in **14c**, the central C1−C1^{i} bond length is 1.493(3) Å, consistent with a C−C single bond. However, in both cases, the bond lengths in the bridging ON∩NO ligands were found to be somewhere between single and double bonds, suggesting electronic delocalization along the two N−C−O units.

4.3 Synthesis and Characterization of a Series of Tetranuclear Arene Ruthenium Metalla-Rectangles

The dinuclear arene ruthenium metalla-clips **14a**−**14c** were reacted with 4,4′-bipyridine (bpy), 1,2-bis(4-pyridyl)ethylene (bpe), or 4,4′-azopyridine (bpa) in the presence of $AgCF_3SO_3$ to afford the corresponding tetracationic metalla-rectangles, [(*p*-cymene)$_4$Ru$_4$(μ-bpy)$_2$(μ-L)$_2$]$^{4+}$ ([**15a**]$^{4+}$−[**15c**]$^{4+}$), [(*p*-cymene)$_4$-Ru$_4$(μ-bpe)$_2$(μ-L)$_2$]$^{4+}$ ([**16a**]$^{4+}$−[**16c**]$^{4+}$), and [(*p*-cymene)$_4$Ru$_4$(μ-bpa)$_2$- (μ-L)$_2$]$^{4+}$ ([**17a**]$^{4+}$−[**17c**]$^{4+}$) in good yield. The structures of these cationic tetranuclear arene ruthenium metalla-rectangles are presented in Figure 56.

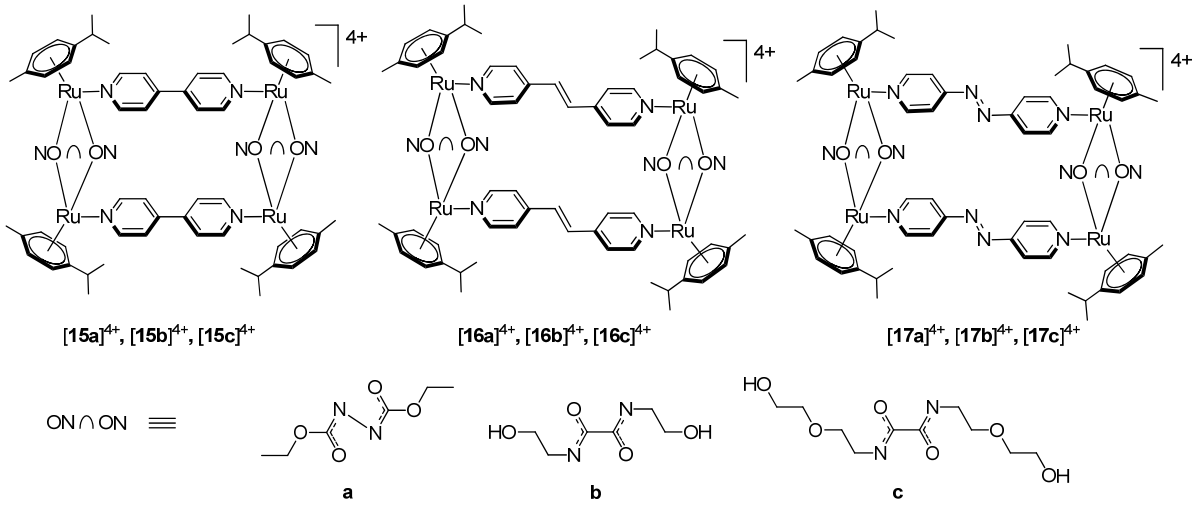

*Figure 56. Structures of the arene ruthenium metalla-rectangles [**15a**]$^{4+}$−[**17c**]$^{4+}$.*

All complexes were isolated and characterized as their triflate salts. The presence of two ON∩NO bis-chelating bridging-linkers within the metalla-rectangles [**15a**]$^{4+}$−[**17c**]$^{4+}$ gave rise to different isomers: the dinuclear arene ruthenium units being either of the same or of the opposite configurations. As previously mentioned, the metalla-clips [**14a**]$^{4+}$−[**14c**]$^{4+}$ were isolated as the *meso* form, the chloride atoms being *trans* from each other. However, upon formation of discrete metalla-assemblies, a *cis* orientation of the N-based connecting-

ligands is necessary, thus adding chirality to these systems. Indeed, three isomers were observed for each metalla-rectangle, a pair of enantiomers and a *meso* form (Fig. 57).

The ^{1}H NMR data of all metalla-rectangles showed two sets of signals, in agreement with the expected isomers. In all cases, the ratio between the *racemic* and the *meso* isomer was essentially 50:50, in accordance with a statistical distribution. Unfortunately, we were unable to associate a set of signals with a specific isomer. The chemical shifts of the different protons are listed in the Experimental Section.

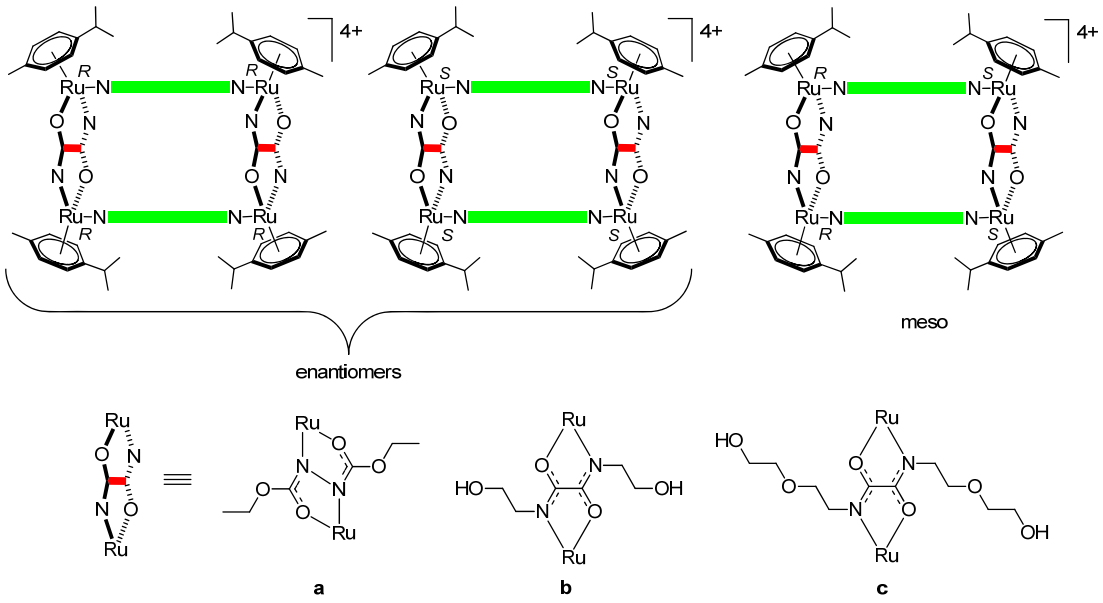

*Figure 57. Schematic representations of the different isomers observed in metalla-rectangles ([**15a**]$^{4+}$–[**17c**]$^{4+}$).*

All ^{1}H NMR spectra were recorded in CD_3OD or CD_2Cl_2 at 23 °C, and as previously mentioned, two sets of signals were observed for these metalla-rectangles (Experimental sections), with noticeable overlap for the signals of the peripheral protons. In metalla-rectangle [**17b**]$^{4+}$, eight doublets were observed between 5.4 and 6.2 ppm for the diastereotopic protons of the *p*-cymene rings (Fig. 58), which were associated with eight ^{13}C signals (Fig. 59).

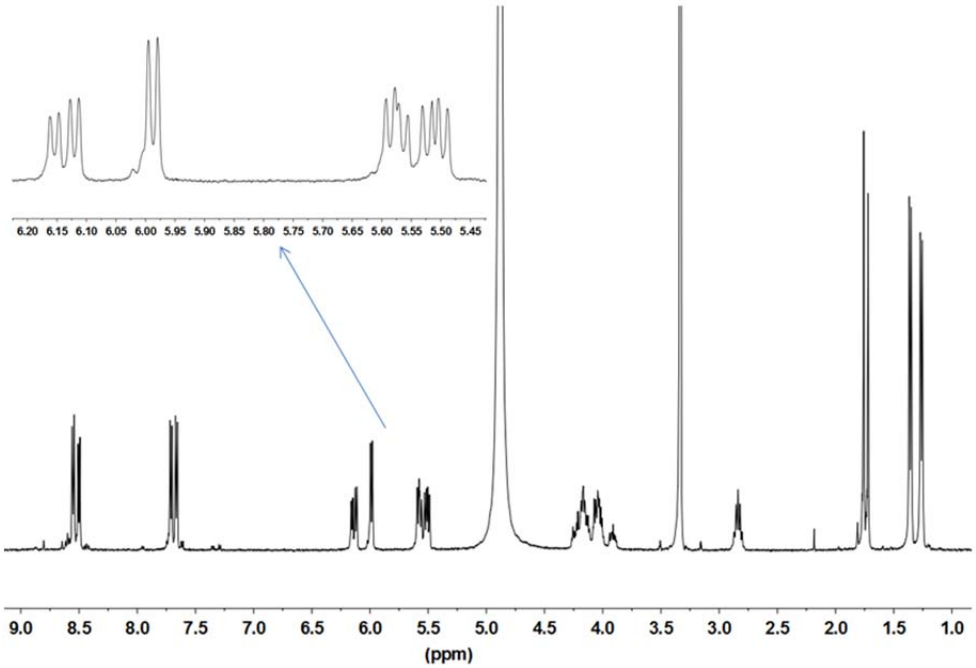

Figure 58. ^{1}H *NMR spectrum* (CD_2Cl_2, *23°C) of the complex [**17b**]*($CF_3SO_3)_4$.

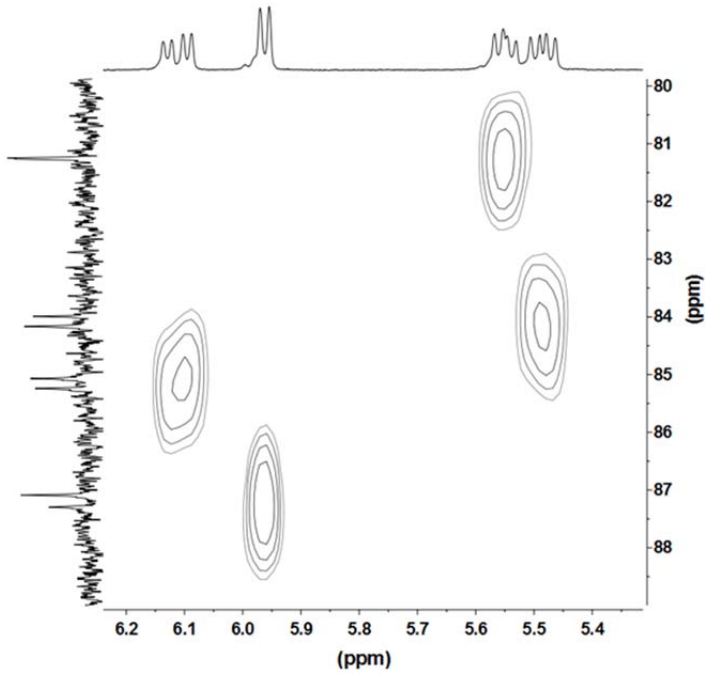

Figure 59. ^{1}H *NMR,* ^{13}C *NMR – HSQC spectra* (CD_2Cl_2, *23°C) of the complex [**17b**]*($CF_3SO_3)_4$ *(p-cymen region).*

4.4 Synthesis and Characterization of a Series of Hexanuclear Arene Ruthenium Metalla-Prisms

The dinuclear arene ruthenium metalla-clips **14a**−**14c** were also reacted with 2,4,6-tris(4-pyridyl)-1,3,5-triazine (tpt) or 1,3,5- tris{2-(4-pyridyl)vinyl}benzene (tpv) in the presence of $AgCF_3SO_3$ to afford in good yield the corresponding hexacationic hexanuclear metalla prisms, $[(p\text{-cymene})_6Ru_6(\mu\text{-tpt})_2(\mu\text{-L})_3]^{6+}$ ($[\mathbf{18a}]^{6+}$–$[\mathbf{18c}]^{6+}$) and $[(p\text{-cymene})_6Ru_6(\mu\text{-tpv})_2(\mu\text{-L})_3]^{6+}$ ($[\mathbf{19a}]^{6+}$–$[\mathbf{19c}]^{6+}$). All complexes were isolated and characterized as their triflate salts. The proposed structures of these cationic arene ruthenium metalla-prisms are presented in Figure 60.

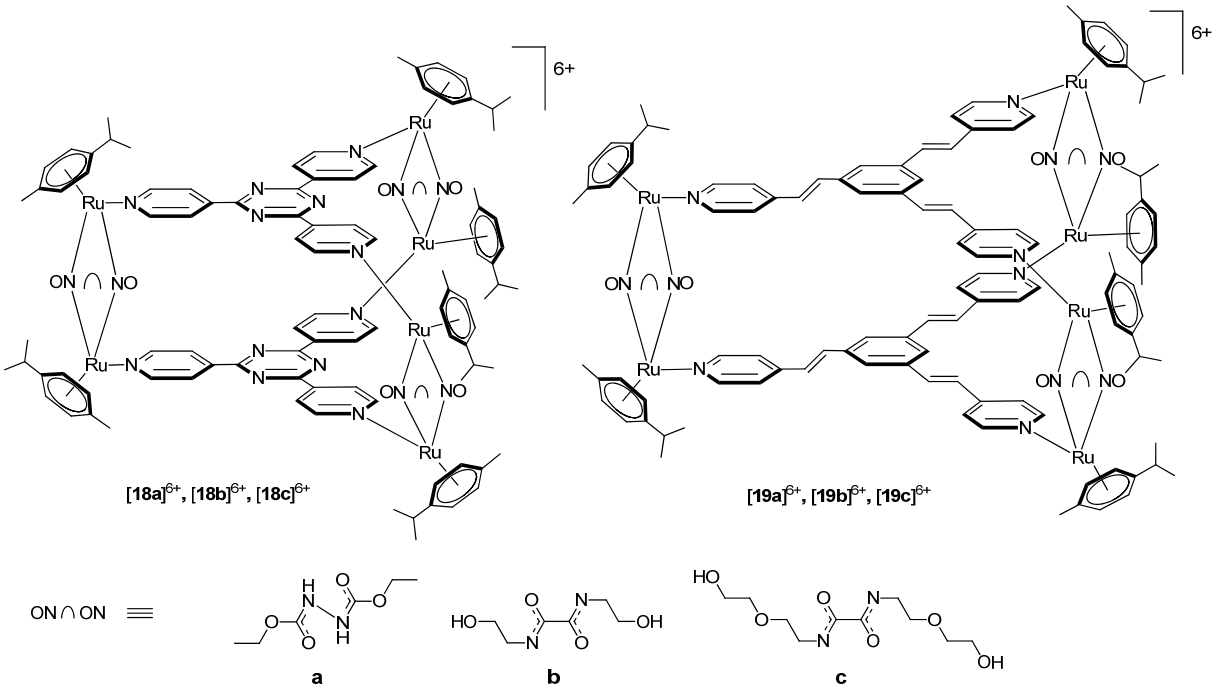

Figure 60. Structures of the arene ruthenium metalla-prisms ***[18a]***$^{6+}$–***[19c]***$^{6+}$.

By analogy with the metalla-rectangles $[\mathbf{15a}]^{4+}$–$[\mathbf{17c}]^{4}$, the ^{1}H NMR spectra of the metalla-prisms $[\mathbf{18a}]^{6+}$–$[\mathbf{19c}]^{6+}$ showed several sets of signals. As an example, the ^{1}H NMR spectrum of $[\mathbf{18a}]^{6+}$ is presented in Figure 61.

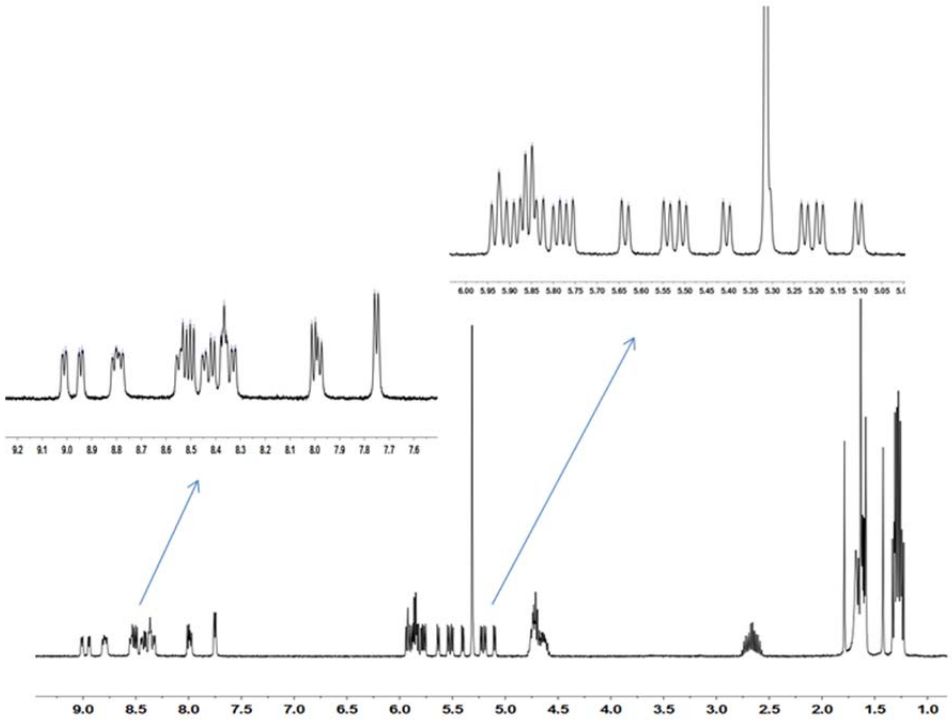

*Figure 61. ^{1}H NMR spectrum (CD_2Cl_2, 23°C) of the complex [**18a**]$(CF_3SO_3)_6$.*

The fixed R,R or S,S configuration of the dinuclear arene ruthenium units should, in principle, give rise to only two pairs of enantiomers for these metalla-prisms: the homochiral R,R−R,R−R,R and S,S−S,S−S,S enantiomers as well as the mixed enantiomers R,R−R,R−S,S and S,S−S,S−R,R. However, four sets of signals were observed for the metalla-prisms [**18a**]$^{6+}$–[**19c**]$^{6+}$, thus suggesting an additional element of chirality. In these metalla-prisms, the side arms of the ON∩NO bis-chelating ligands are certainly forcing the tridentate panels to adopt a staggered conformation, thus adding helical chirality to these systems: helical chirality being commonly observed in arene ruthenium metalla-prisms[180] and other metalla-assemblies.[131b, 181] As shown in Figure 62, the four isomers were clearly observed in the NMR spectra of metalla-prism [**18a**]$^{6+}$, in which 16 doublets associated with 16 individual carbons were observed for the aromatic CH groups of the *p*-cymene ligands.

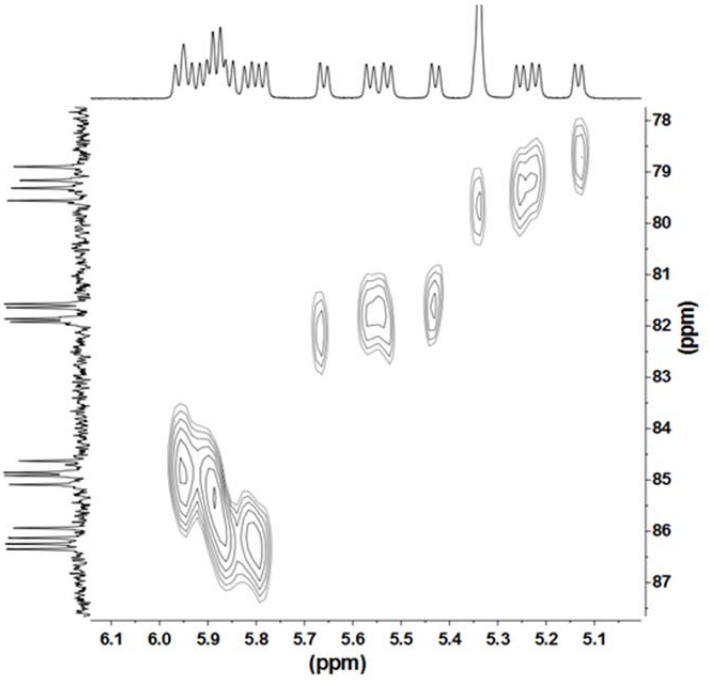

*Figure 62. ^{1}H NMR and ^{13}C NMR−HSQC spectra (CD_2Cl_2, 23 °C) of [**18a**]$(CF_3SO_3)_6$ (p-cymene region).*

4.5 Antiproliferative Activity Studies of the Arene Ruthenium Metalla-Assemblies

The antiproliferative activity of all the complexes was evaluated against human ovarian (A2780) carcinoma cells and nontumorigenic human embryonic (HEK293) kidney cells using the MTT assay.[182] The IC_{50} values after 72 h of exposure to the compounds are listed in Table 8, and for comparison, the biological activity of cisplatin is also reported. All tetracationic metalla-rectangles [**15a**]$^{4+}$−[**17c**]$^{4+}$and metalla-prisms [**18a**]$^{6+}$−[**19c**]$^{6+}$, except for metalla-rectangles [**16a**]$^{4+}$ and [**17b**]$^{4+}$, exhibit IC_{50} values in the submicromolar range against the A2780 human ovarian cancer cells, and their activities are comparable to those of previously describedhexacationic thiolato-bridged ruthenium complexes (IC_{50} from 0.2−0.6 μM).[125] Interestingly, the hexacationic metalla-prisms [**19a**]$^{4+}$−[**19c**]$^{4+}$were less active and the neutral dinuclear metalla-clips **14a**−**14c** were essentially inactive.

Table 8. IC_{50} values (μM) of the complexes after 72 h exposure on human ovarian (A2780) carcinoma cells and noncancerous human embryonic kidney (HEK293) cells.

Compound	HEK293 cells	A2780 cells	SC[a]
14a	>100	>100	
14b	>100	>100	
14c	>100	>100	
[**15a**]$(CF_3SO_3)_4$	4.7 ± 1.2	0.7 ± 0.1	6.6
[**15b**]$(CF_3SO_3)_4$	7.2 ± 1.2	0.8 ± 0.3	8.5
[**15c**]$(CF_3SO_3)_4$	4.5 ± 0.3	0.4 ± 0.1	13
[**16a**]$(CF_3SO_3)_4$	25.3 ± 0.7	3.1 ± 0.6	8.2
[**16b**]$(CF_3SO_3)_4$	7.0 ± 0.2	0.8 ± 0.2	8.5
[**16c**]$(CF_3SO_3)_4$	2.4 ± 0.1	0.5 ± 0.1	5
[**17a**]$(CF_3SO_3)_4$	2.9 ± 0.4	0.8 ± 0.1	3.5
[**17b**]$(CF_3SO_3)_4$	7.3 ± 0.7	2.0 ± 0.2	3.6
[**17c**]$(CF_3SO_3)_4$	4.9 ± 0.2	0.9 ± 0.1	5.3
[**18a**]$(CF_3SO_3)_6$	7.2 ± 0.1	0.6 ± 0.1	11.1
[**18b**]$(CF_3SO_3)_6$	1.6 ± 0.3	0.3 ± 0.1	5.4
[**18c**]$(CF_3SO_3)_6$	2.4 ± 0.2	0.3 ± 0.1	7.3
[**19a**]$(CF_3SO_3)_6$	16.7 ± 0.2	7.3 ± 0.3	2.3
[**19b**]$(CF_3SO_3)_6$	6.4 ± 0.5	>20	0.3
[**19c**]$(CF_3SO_3)_6$	11.6 ± 1.5	4.59 ± 0.2	2.5
Cisplatin	8.4 ± 1.2	1.4 ± 0.2	6

[a]SC = selectivity coefficient = IC_{50} HEK293/IC_{50} A2780.

The selectivity coefficients (SC = IC_{50} on HEK293/IC_{50} on A2780) of the tetracationic metalla-rectangles [**15a**]$^{4+}$–[**17c**]$^{4+}$and of the hexacationic metalla-prisms [**18a**]$^{6+}$–[**18c**]$^{6+}$are good; i.e., these complexes are ca. 1 order of magnitude more cytotoxic toward cancer cells than the noncancerous cells studied. In contrast, the hexanuclear metalla-prisms [**19a**]$^{6+}$–[**19c**]$^{6+}$ bridged by the tpv panels show higher IC50 values and less favorable selectivity coefficients, in accordance to previously reported hexacationic metalla-assemblies bearing benzoquinonato (IC_{50} ≈ 25 μM) and naphtoquinonato bridges (IC_{50} ≈ 5 μM).[133]

The nature of the substituent of the ON∩NO bridging-linker strongly influences the cytotoxicity of the complexes. A trend can be observed for metalla-assemblies with the N-(2-ethoxy)ethanol side arms ([**15c**]$^{4+}$–[**19c**]$^{6+}$), which generally exhibited lower IC_{50} values compared to other metalla-assemblies of the same series. In addition, as control experiments, the antiproliferative activity of the dinuclear arene ruthenium metalla-clips **14a**−**14c** was

evaluated, and all three compounds show IC_{50} values > 100 μM, 2 orders of magnitude higher than their corresponding metalla-assemblies. These observations are in agreement with previous reports describing a series of neutral and cationic dithiolato and cationic trithiolato-bridged arene ruthenium complexes.[125, 113b] A plausible reason for the higher cytotoxicity of the cationic species may be the better uptake of positively charged molecules into cells compared to their neutral counterparts.[183]

4.6 Conclusions

A new family of ON∩NO bis-chelating linkers has been used to generate dinuclear, tetranuclear, and hexanuclear arene ruthenium complexes incorporating functional groups. The neutral dinuclear complexes show no antiproliferative activity, while the cationic metalla-assemblies are all cytotoxic with IC_{50} values in the lower μM range. Interestingly, the cationic metalla-assemblies with the N-(2-ethoxy) ethanol functional groups on the ON∩NO linkers possess excellent selectivity for cancerous over noncancerous cells, suggesting that functionalization at the bridging-linkers offers great potential for the biological optimization of metalla-assemblies.

5

Arene Ruthenium Metalla-Prisms as Photosensitizer Delivery Vehicles into Cancer Cells

Porphyrins and phthalocyanines are the common photosensitizers usually employed in photodynamic therapy (PDT). These photo-active agents, in general, have poorly water-solubility and limited selectivity thus affecting overall photosensitivity.[184] Functionalization, substitution with hydrophilic groups of the parent agent or hiding inside a nano-carrier to be deliver into their target, are the promising strategies developed, in recent years, to enhance the biological activity of these PDT drugs.[185]

Among these nano-transporters, water-soluble metalla-cages developed in our group since 2008, have been found excellent nano-vectors for the delivery of guest molecules into cancer cells.[127] In addition to the transport and the selective delivery, shielding of the photo-activity in the presence of light is a new opportunity offered by these metalla-assemblies thus resulting in limited skin photosensitivity – a major drawbacks encountered in PDT.[137]

As a continuation of the investigation in our group, herein we report the synthesis and characterization of three arene ruthenium metalla-prisms with different portal size of the general formula $[(p\text{-cymene})_6Ru_6(\mu\text{-tpt})_2(\mu\text{-L})_3]^{6+}$ (2,5-dihydroxy-3-phenyl-1,4-benzoquinone (H_2L^d) (**d**), 2,5-dihydroxy-3,6-diphenyl-1,4-benzoquinone (H_2L^e) (**e**) and 2,5-dihydroxy-3,6-dimesityl-1,4-benzoquinone (H_2L^f) (**f**)). The encapsulation of the porphin guest-molecule inside the cavities of these host systems have been confirmed using different analytical measurements. The photodynamic activities of two host-guest systems have been evaluated in the group of Prof. Vincent Sol at Université de Limoges on the human colon cancer cell line HT-29. An excellent photo-toxicity was noteworthy with a potential of intracellular release of photosensitizers by these nano-organometallic cages.

5.1 Arene Ruthenium Metalla-Prisms: A New Approach in Photodynamic Therapy (PDT)

Photodynamic therapy (PDT) is a novel method with proven ability to treat the prostate, skin, lung, head and neck cancers. It can be employed as an alternative strategy to compete with conventional clinical treatment of cancers.[186] Since the hematoporphyrin derivative (Photofrin) became the first PTD agent approved for clinical use (1995) to treat bladder cancer in Canada,[187] many new photosensitizer formulations have made entry to the clinical prescription e.g. Verteporfin – a benzoporphyrin derivative (trade name Visudyne) in the US, metatetrahydroxyphenyl chlorin (trade name Foscan) in Europe (Fig. 63).[188]

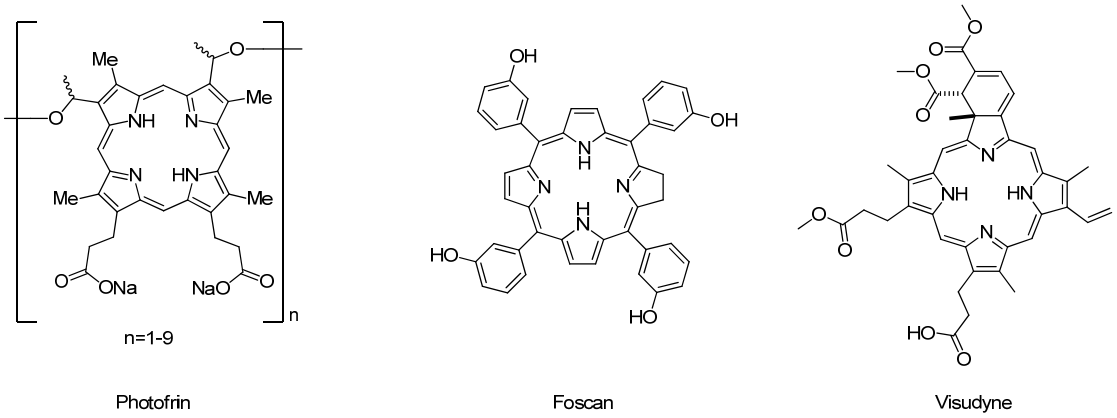

Figure 63. Typically photosensitizers clinically used in PDT.[189]

Photodynamic therapy (PDT) involves the administering of a non-toxic, light sensitive compound in the tumor cells. This photoactive compound, when exposed selectively to visible light irradiation, becomes toxic to malignant cancerous tissues via generation of singlet oxygen and other reactive oxygen species (Fig. 64).[190] Accumulation of the photosensitizer (PS) in nonspecific targets are considered to be less toxic for the healthy tissues, compared to the anticancer drugs being used in chemotherapy which have proven track record to be aggressive and invasive for the human body. Another advantage of this technique is the use of activating light which has inert nature vis-à-vis the ionizing light in radiotherapy with destructive effects.[191]

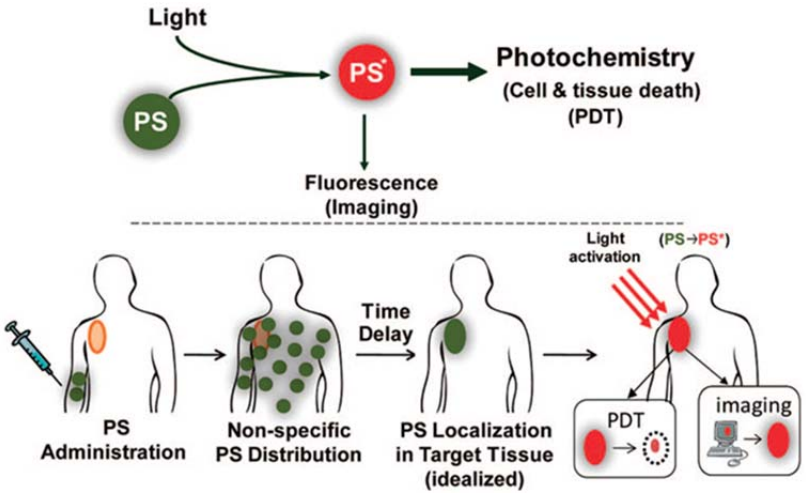

Figure 64. An overview of the photodynamic therapy treatment.[191]

To enhance the efficiency of PDT treatment, many improvements are sought by different research groups, which can be classified in two main strategies:

- The first strategy involves the development of a combination therapy by using a second modality or increasing the susceptibility of the tumor prior to PDT.[192]
- The second approach focuses more on the specificity and the selectivity of the photosensitizer targeting. There are three basic approaches to improve these two factors; the first one consists of using an inactive PS prodrug which is inactive in the normal cells but it can be regained after linkage with a specific cancerous cellular function (such as enzymes) (Fig. 65).[193]

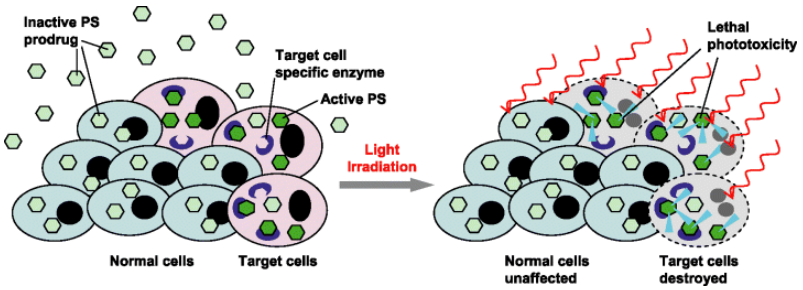

Figure 65. The photosensitizer prodrugs are distributed in both normal and affected cells, but it's activated only in the cancer cells in the presence of specific enzymes. Irradiation by a specific light destroys the target cells.[193]

The other approaches being employed involve the modification of structural integrity of the active parent agent by attaching a hydrophilic group or a lipophilic motif like cell-penetrating peptide[194] and monoclonal antibodies,[195] thereby improving the specificity of the final pro-agents into cancer cells (just like a pro-drug strategy), or by enhancing the selectivity through the development of photosensitizer delivery vehicles such as gold nanoparticles,[196] liposome,[197] and even viruses[185a] that can internalize the selectively for a target tissue.

However, the missing link in both strategies is the photoprotection of photosensitizer molecules since their unexpected activation produce undesired skin lesions – the main side effect of PDT. Recently, our group observed that hiding planar aromatic molecules with good fluorescent properties inside a tetra-cationic arene ruthenium metallarectangles leads to the quenching of the fluorescence light emitted by these guest molecules.[198] We extended the study to large organometallic cages, and it is demonstrated that the photoactivity of the hydrophobic photosensitizers is inhibited by their encapsulation in these metalla-cages, thus potentially avoiding the side effect of skin photosensitivity. As mentioned in the section 1.3.4, several arene ruthenim metalla-prisms and cubes with different portal size were found to be excellent nano-carriers for the delivery of photosensitizers (porhyrins and phthalocyanines) into cancer cells (Fig. 24). These studies show an important correlation between the host portal size and the release of the guest molecules.[137, 199]

In this chapter, three arene ruthenium metalla-clips incorporating a new family of benzo-quinonato derivatives used as bis-chelating bridging linkers are described. These metalla-clips are used to synthesize three new metalla cages with different portal size. The

PDT activities of the porphin molecule trapped inside the cavity of theses host systems have been reported.

5.2 Synthesis and Characterization of the Arene Ruthenium Metalla-Clips

The design of the three hydroxybenzo-quinonato derivatives is based on the synthetic strategy reported by Grée which involves Suzuki–Miyaura coupling reactions, the key step to efficiently introduce all the desired functionalized aromatic substituents. Compounds **d** and **e** are known, but compound **f** is new (Fig. 66) (more details in experimental sections).[200]

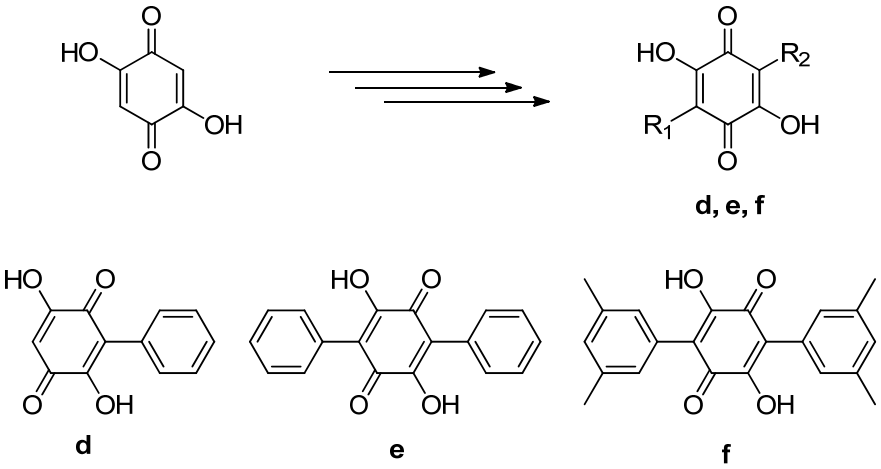

*Figure 66. Synthesis of the hydroxybenzo-quinonato derivatives (**e**–**f**).*[200]

The dinuclear arene ruthenium metalla-clips **20d**–**20f** with the general formula [(*p*-cymene)$_2$Ru$_2$Cl$_2$(μ-L)] (Fig. 67) have been obtained by reacting the corresponding benzoquinone derivatives, 2,5-dihydroxy-3-phenyl-1,4-benzoquinone (H_2L^d) (**d**), 2,5-dihydroxy-3,6-diphenyl-1,4-benzoquinone (H_2L^e) (**e**) and 2,5-dihydroxy-3,6-dimesityl-1,4-benzoquinone (H_2L^f) (**f**) with [(*p*-cymene)$_2$Ru$_2$Cl$_2$(μ-Cl)$_2$] in methanol at room temperature for 24 hours.

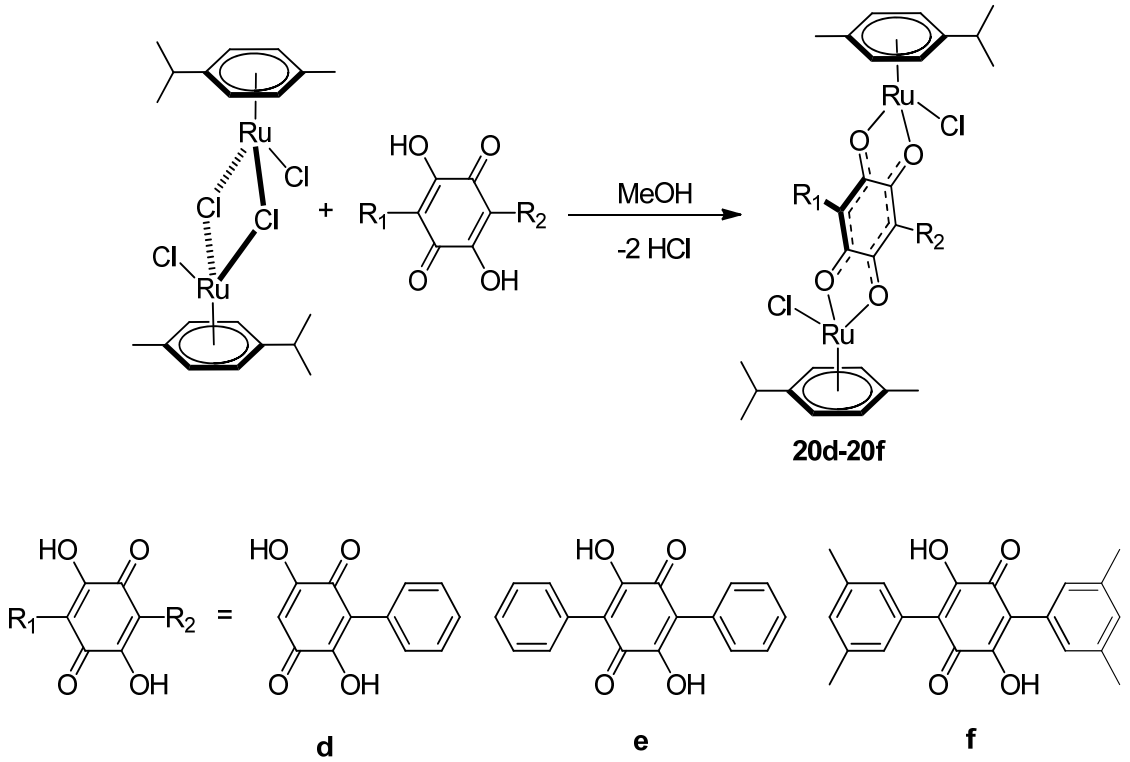

*Figure 67. Molecular structure of the dinuclear arene ruthenium metalla-clips **20d**−**20f**.*

The coordination of the quinonato bis-chelating bridging-linkers between the two arene ruthenium units was confirmed by NMR spectroscopy, mass spectrometry and elemental analysis (see Experimental Section). Furthermore, the molecular structure of complex **20e** was established by single-crystal X-ray structure analysis. The three complexes show good solubility in halogenated solvents such as chloroform and dichloromethane, but a limited solubility in methanol and ethanol.

The ^{1}H NMR spectra of the complexes **20d**−**20f**, realized in CD_2Cl_2 and $CDCl_3$, shows different signals at the interval [7.60 – 6.90 (ppm)] corresponds to the phenyl protons, along with the signals of the *p*-cymene groups; four doublets at {(5.66 ppm), (5.39 ppm); (5.68 ppm), (5.37 ppm)} associated to the complexes **20d** and **20e** respectively, and two multiplets at [(5.68 – 5.64 ppm), (5.36 – 5.32 ppm)] for the complex **20f**. Interestingly the benzo-quinonato proton (H_{dobq}) in the complex **20d** show two singlets at 5.79 ppm and 5.81 ppm with intensity 8:2 confirming the existence of two isomers with different proportions (Fig. 68).

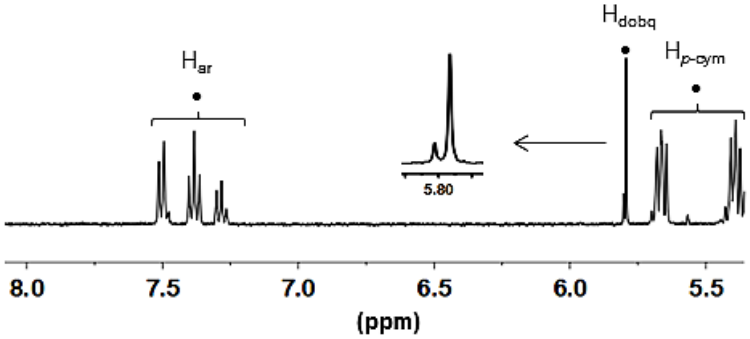

Figure 68. Excerpt of ^{1}H NMR spectrum of the complex ***20d****.*

Despite the presence of two isomers in solution, only one crystallizes as confirmed by the single-crystal structure analysis (Fig. 69).

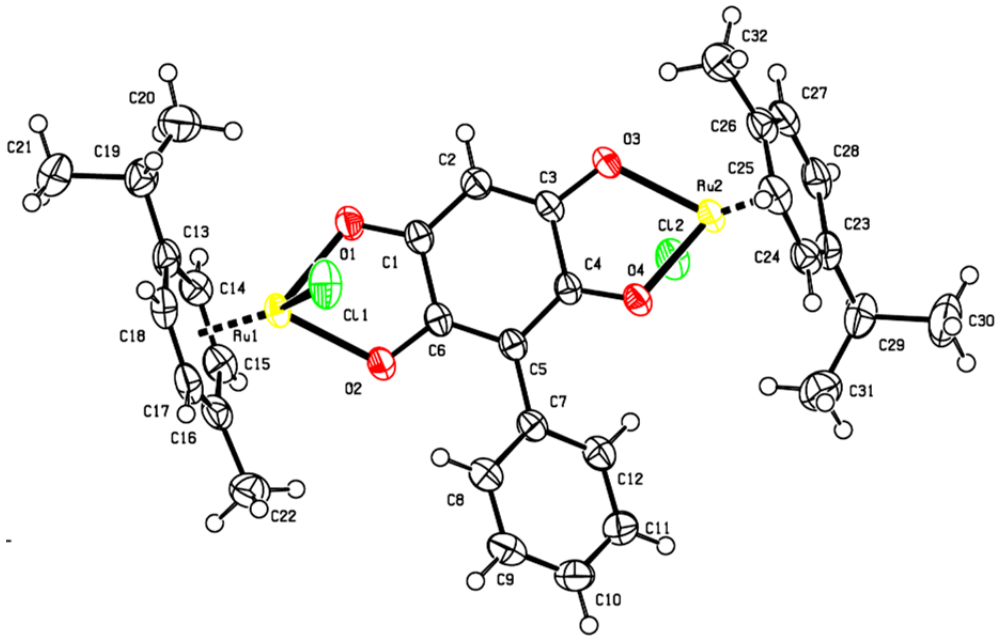

Figure 69. ORTEP drawing of ***20d*** *at 50% probability level ellipsoids.*

The existence of three mono-cationic fragments $[M - Cl]^{+}$ in the ESI-MS spectra at m/z = 723.3, 796.2, 852.5 respectively for the complex **20d**-**20f**, put forward the formation of metalla-clips.

5.3 Synthesis and Characterization of the Hexanuclear Arene Ruthenium Metalla-Prisms

The synthesis of the arene ruthenium metalla-assemblies followed a one-pot strategy in which the dinuclear arene ruthenium metalla-clips **20d**–**20f** reacted with 2,4,6-tris(4-pyridyl)-1,3,5-triazine (tpt) ligand in the presence of silver trifluoromethanesulfonate ($AgCF_3SO_3$) to afford the corresponding hexacationic metalla-prisms, $[(p\text{-cymene})_6Ru_6(\mu\text{-tpt})_2(\mu\text{-L})_3]^{6+}$ ($[\mathbf{21d}]^{6+}$–$[\mathbf{21f}]^{6+}$) in good yield. All complexes were isolated and characterized as their triflate salts. The formation of theses metalla-assemblies was confirmed by means of NMR spectroscopy, mass spectrometry and elemental analysis (see the Experimental Section). Furthermore, the proposed molecular structures of these cationic arene ruthenium metalla-prisms are presented in Figure 70.

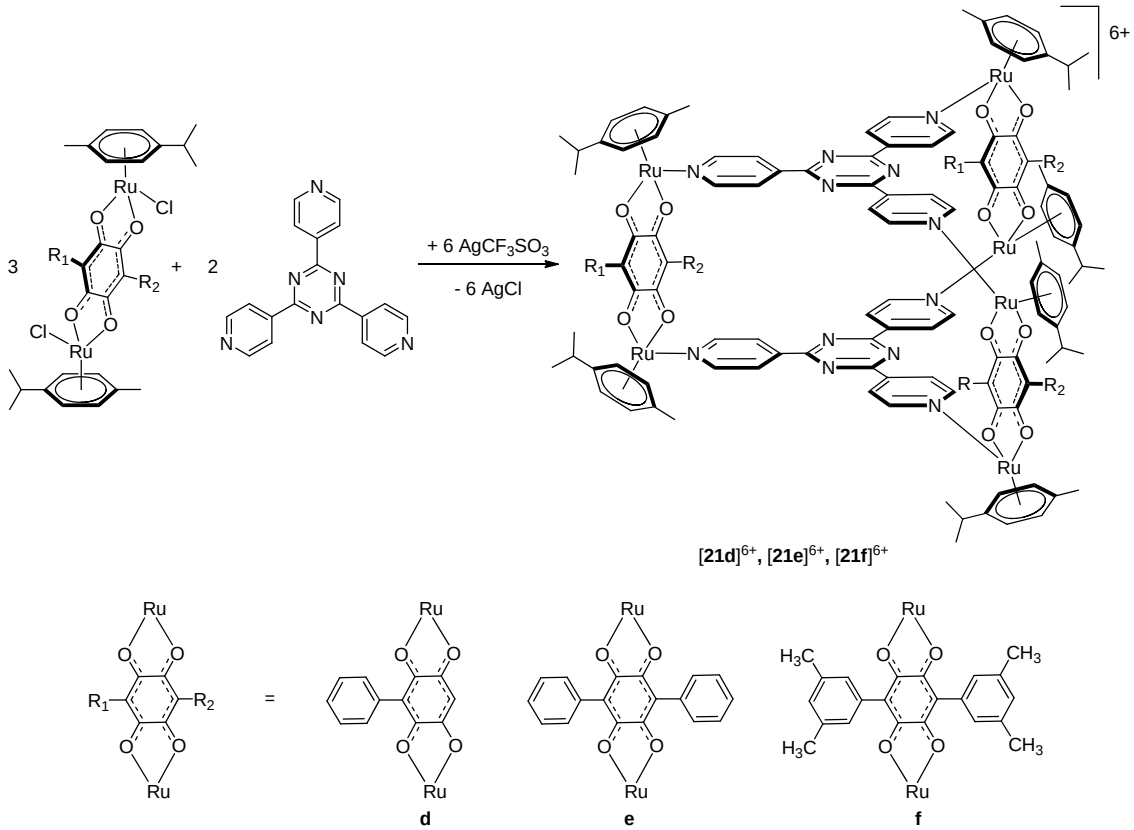

Figure 70. Synthesis of the hexa-cationic metalla-prisms $[\mathbf{21d}]^{6+}$–$[\mathbf{21f}]^{6+}$.

The addition of 1 equiv. of porphin during the synthesis of the three hexacationic metalla-prisms leads to the encapsulation of this photosensitizer inside the cavity of the host complexes (Fig. 71). The formation of the host-guest systems was single out and characterized by means of infrared, UV-visible, fluorescence and NMR spectroscopies as well as mass spectrometry. Moreover, the host-guest systems $[\mathbf{22d}]^{6+}$–$[\mathbf{22f}]^{6+}$ are alternatively accessible by reaction of the empty cages $[\mathbf{21d}]^{6+}$–$[\mathbf{21f}]^{6+}$ and one equivalent of porphine in methanol solution, as confirmed by NMR spectroscopy.

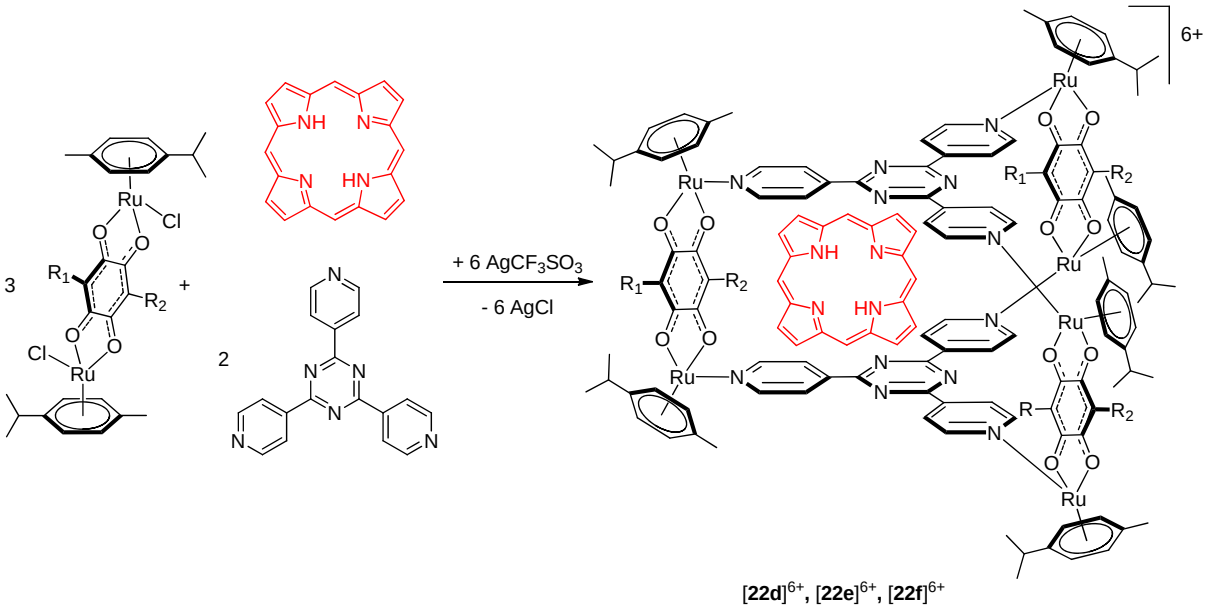

*Figure 71. Synthesis of the hexa-cationic host-guest systems ([porphin⊂cage]$^{6+}$) [**22d**]$^{6+}$–[**22f**]$^{6+}$.*

The Infra-red spectra of the complexes show a high absorption signal at around 1260 cm^{-1} associated to the trifluoromethanesulfonates anions ($CF_3SO_3^-$) together with absorptions at around 1600 cm^{-1} characteristics of the quinone functions (C=O) of the bis-chelating bridging linkers.

The UV-Visible absorption spectra of the metalla-prisms $[\mathbf{21d}]^{6+}$–$[\mathbf{22f}]^{6+}$ are characterized by an intense high-energy band centered at around 295 nm, which is assigned to a ligand-localized or intraligand $\pi \rightarrow \pi^*$ transition as well as broad low-energy bands related to metal-to-ligand charge transfer (MLCT) transitions. Furthermore, the formation of the host-guest systems ([porphin⊂cage]$^{6+}$) $[\mathbf{22d}]^{6+}$–$[\mathbf{22f}]^{6+}$ was further confirmed by the presence of an additional band absorption characteristic to porphin at around 395 nm (Fig. 72).[184]

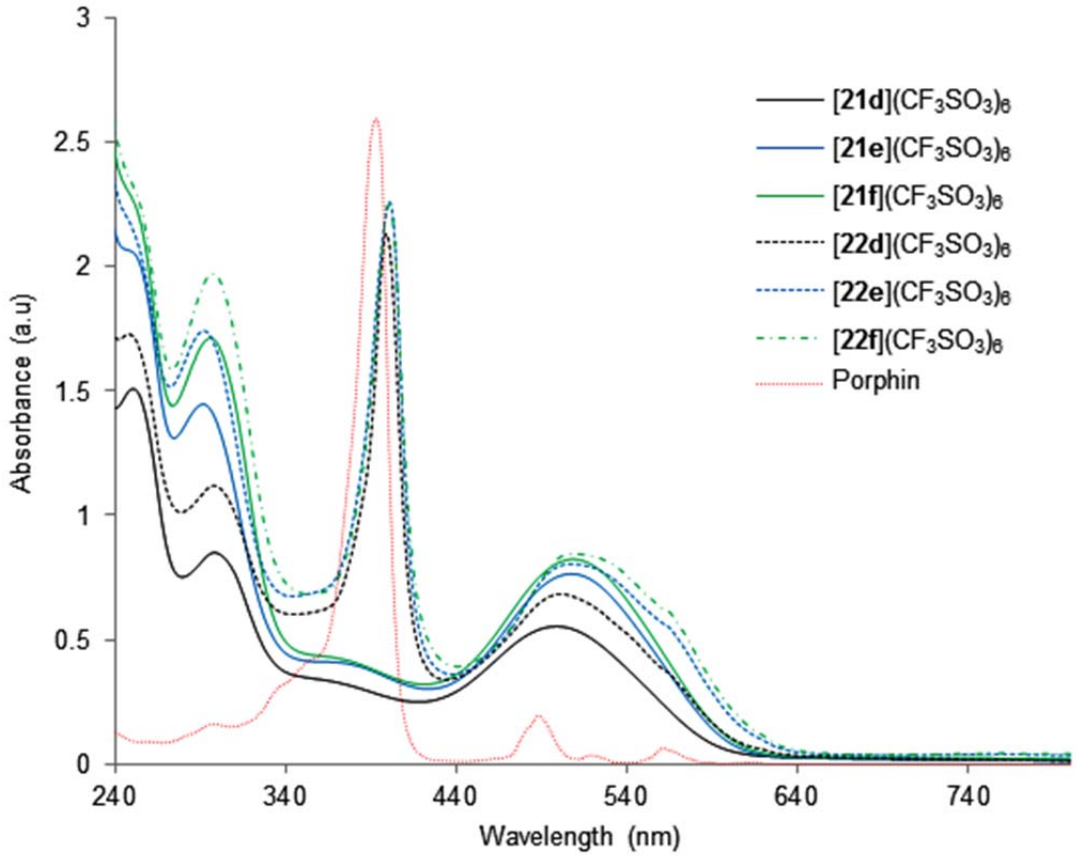

Figure 72. UV−visible spectra of porphin and complexes ***[21d]***$^{6+}$*−****[22f]***$^{6+}$ *(1.0 × 10^{-5} M in CH_2Cl_2).*

The ability of the metalla-prisms to protect porphin from light was tested, based on fluorescence spectroscopy measurements. In dichloromethane solution, the fluorescence emission of the porphin trapped inside the cages upon excitation at 405 nm is relatively quenched. However, the spectral features of the three host-guest systems are different. While for [**22d**]$^{6+}$ the fluorescence spectrum show a bathochromic shift as compared to porphin alone, no "shift" was observed for the two other systems. Moreover, the hypochromic effect was more important in these two complexes compared to the complex [**22d**]$^{6+}$ (Fig. 73).

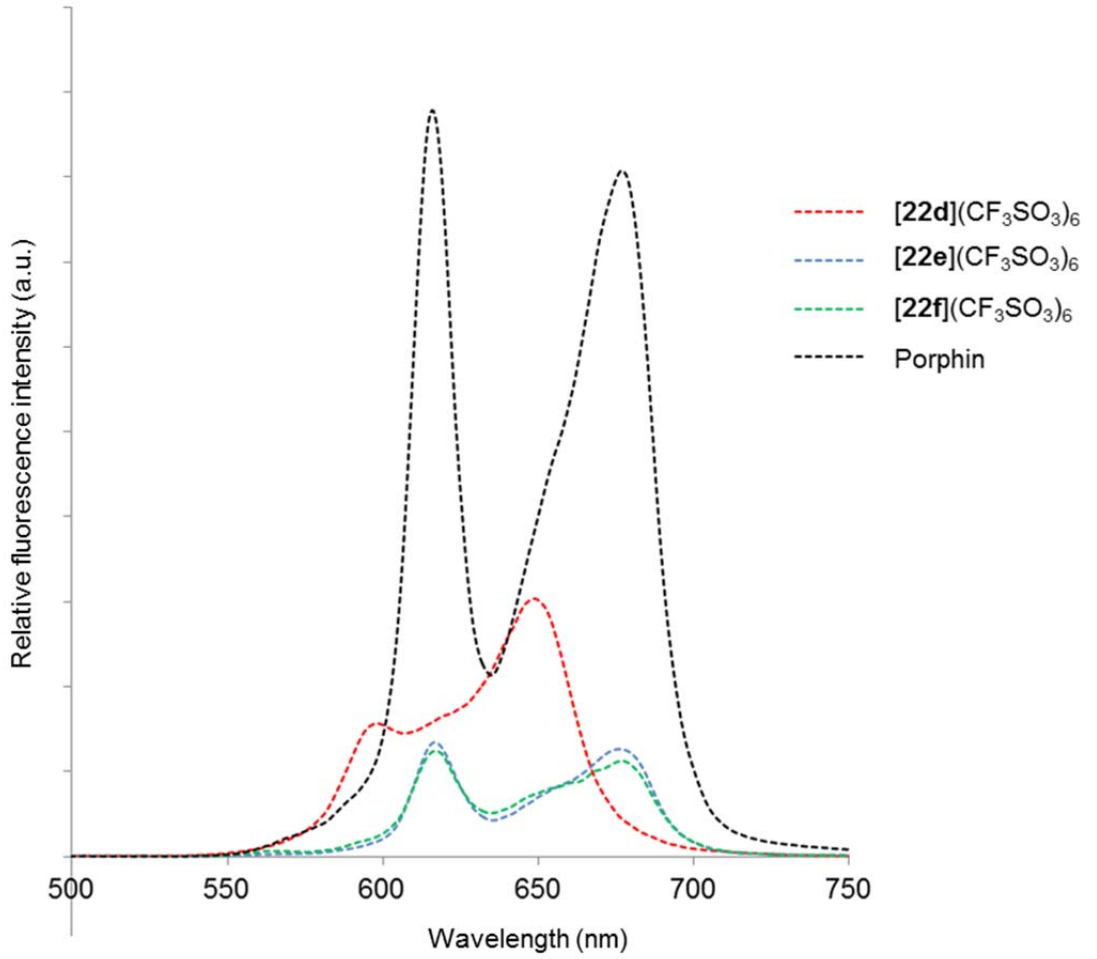

*Figure 73. Corrected emission spectra of [**22d**]$^{6+}$–[**22f**]$^{6+}$ and porphin (CH_2Cl_2, 25 °C, 10^{-6} M, λexc 405 nm).*

Evidence for host-guest systems was also established by the ^{1}H NMR spectroscopy results. For all the three systems [**22d**]$^{6+}$–[**22f**]$^{6+}$, the signals associated to the pyridyl protons of the 2,4,6-tris(4-pyridyl)-1,3,5-triazine (H_α and H_β) panels and the amine protons of the porphin (NH_{po}) are shifted upfield ($\Delta\delta_{H\alpha} \approx$ 0.5 ppm; $\Delta\delta_{H\beta} \approx$ 2.1 ppm; $\Delta\delta_{NHpo} \approx$ 2.5 ppm) in comparison to the protons of the empty host complexes. Signals of the aromatic ring in quinone derivatives shifted downfield ($\Delta\delta_{Har} \approx$ 0.6 ppm) for the three systems (Fig. 74). On the other hand, the two methyl groups on the phenyl ring in the system [**22f**]$^{6+}$ are consequently shifted downfield ($\Delta\delta_{CH3\text{-}ar} \approx$ 0.5 ppm) compared to the complex [**21f**]$^{6+}$. The signals corresponding to the *p*-cymene ligands are not affected by the presence of a guest molecule in the cavity due to their localization in the periphery of the metalla-assemblies as reported elsewhere.[184]

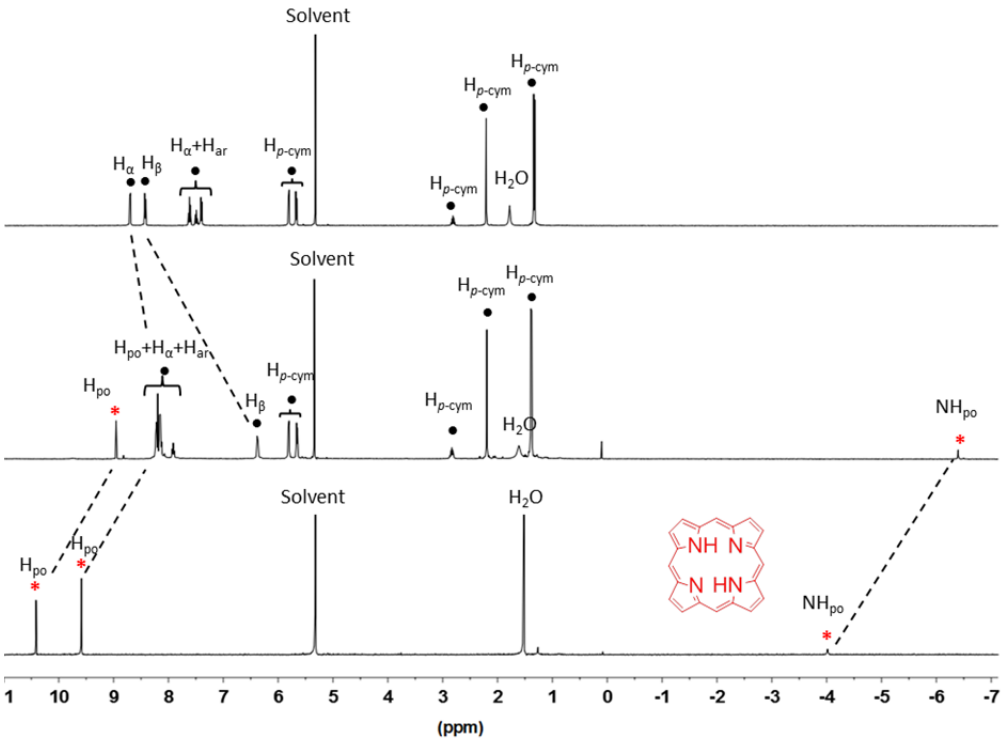

*Figure 74. ^{1}H NMR spectra of the porphin molecule (down), the complexes [**22e**]$^{6+}$ (middle) and [**21e**]$^{6+}$ (up) in (CD_2Cl_2, 23°C).*

Interestingly, upon formation of the metalla-prisms [**21d**]$^{6+}$ and [**22d**]$^{6+}$, the signal assigned to the aromatic proton of the quinonato derivative bridging units was divided into 3 signals with intensity 1:2:1 (for [**21d**]$^{6+}$), while in the host-guest system [**22d**]$^{6+}$, 4 signals were observed with intensity 1:1:1:1 (Fig. 75, 76). The splitting of this signal is associated to the presence of two isomers. Indeed, the presence of the phenyl group on the benzo-quinonato bridging linker decrease the symmetry in the metalla-prisms and give rise to symmetrical isomer and an unsymmetrical isomer in which the phenyl groups share the same quadrant (Fig. 75, 76).[131a]

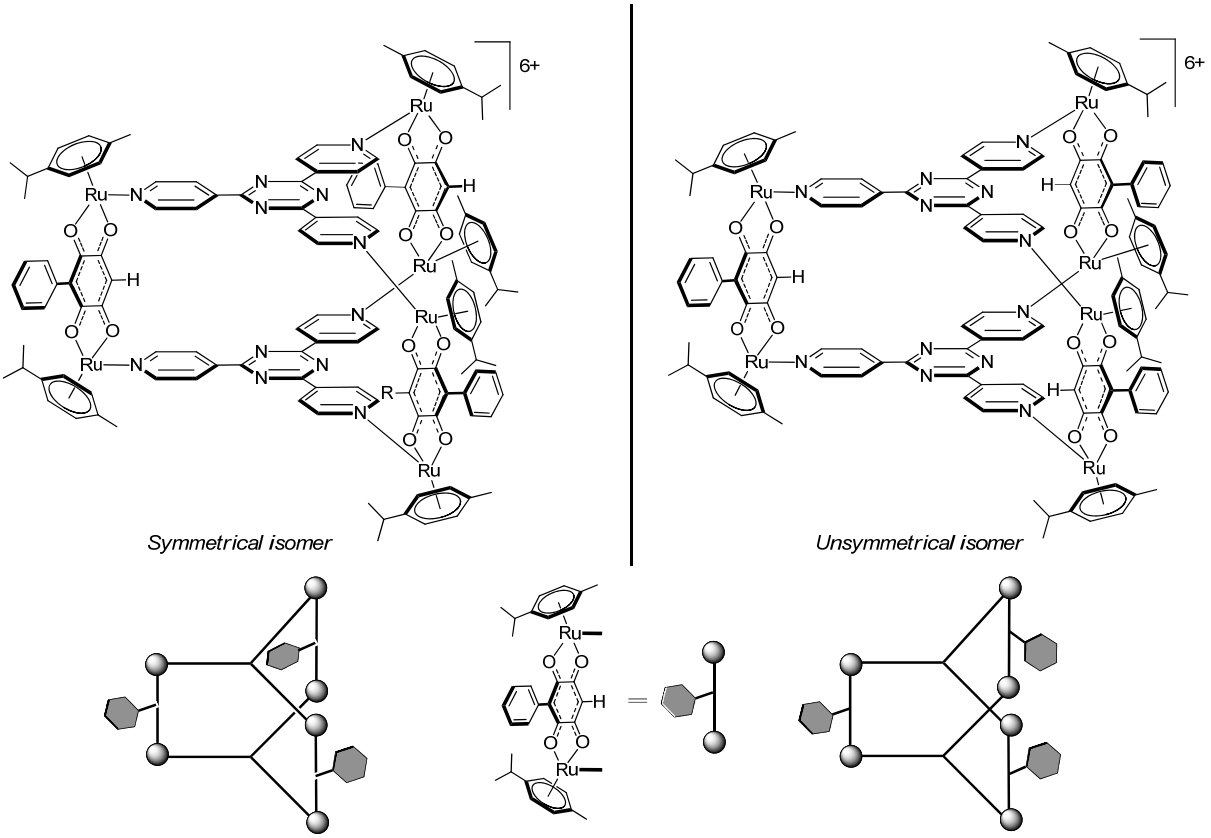

*Figure 75. Molecular structure of the two isomers of the metalla-prism [**21d**]$^{6+}$.*

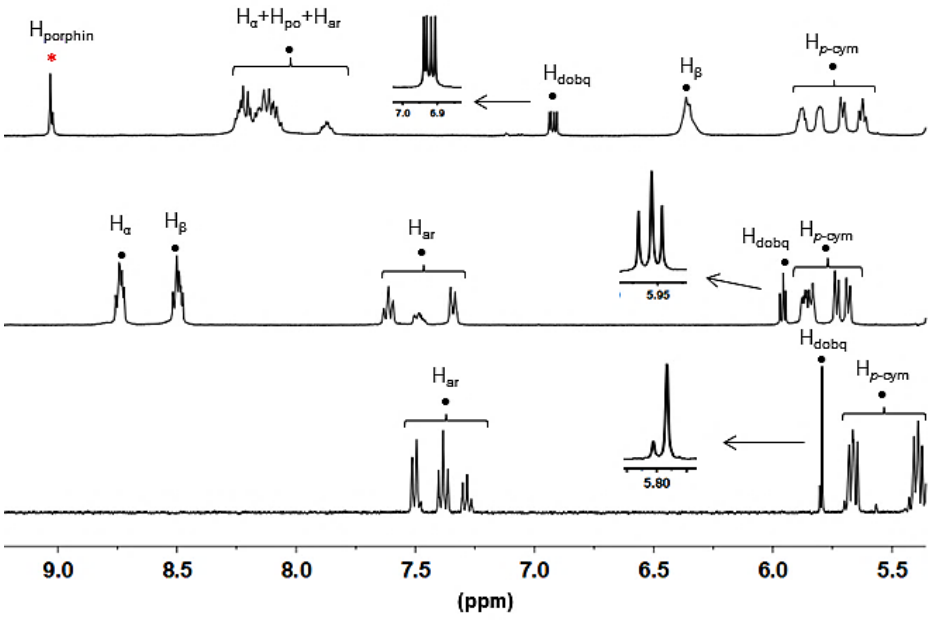

*Figure 76. Excerpts of ^{1}H NMR spectra of the complexes **20d** (down), [**21d**]$^{6+}$ (middle) and [**22d**]$^{6+}$ (up), in (CD_2Cl_2, 23°C).*

In order to further confirm the formation of the host–guest systems, a series of diffusion-ordered NMR (DOSY) spectra were recorded. These experiments show that the proton resonances of the host and the guest molecules possess the same diffusion coefficient ($D \approx$ -9.25 log (m^2/s)) for [porphin⊂cage]$^{6+}$ complexes, thus indicating the presence of only one associated specie in solution (Fig. 77). The diffusion coefficients of the three host–guest system ([porphin⊂cage]$^{6+}$) in CD_2Cl_2 are comparable to those found for similar analogues and consistent with the respective molecular sizes of the different species.[137, 184]

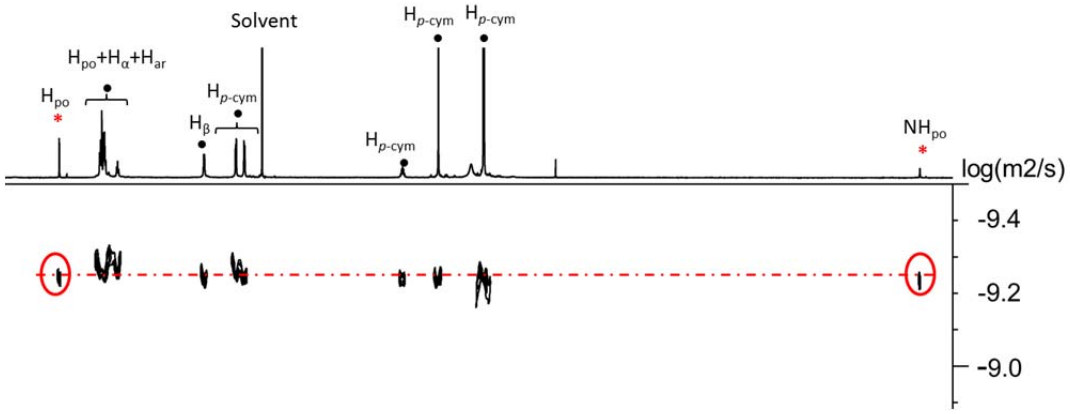

*Figure 77. ^{1}H NMR and DOSY spectra (CD_3OD, 23°C) of the complex [**22e**]$^{6+}$, showing the resonances of the encapsulated porphin (highlighted with red ovals).*

In these large systems, ROESY experiments perform an excellent technique for determining the host-guest interactions. In addition, these 2D spectra clearly show a strong nuclear Overhauser effect of the aromatic porphin protons (H_{po}) with the pyridyl protons (H_{α} and H_{β}) of the tpt panels. On the other hand, since no interaction between porphin and the *p*-cymene ligands is observed, we can conclude that the photosensitizer guest molecule is successfully encapsulated inside the cavity of the host complexes [**21d**]$^{6+}$–[**21f**]$^{6+}$ (Fig. 78).[184]

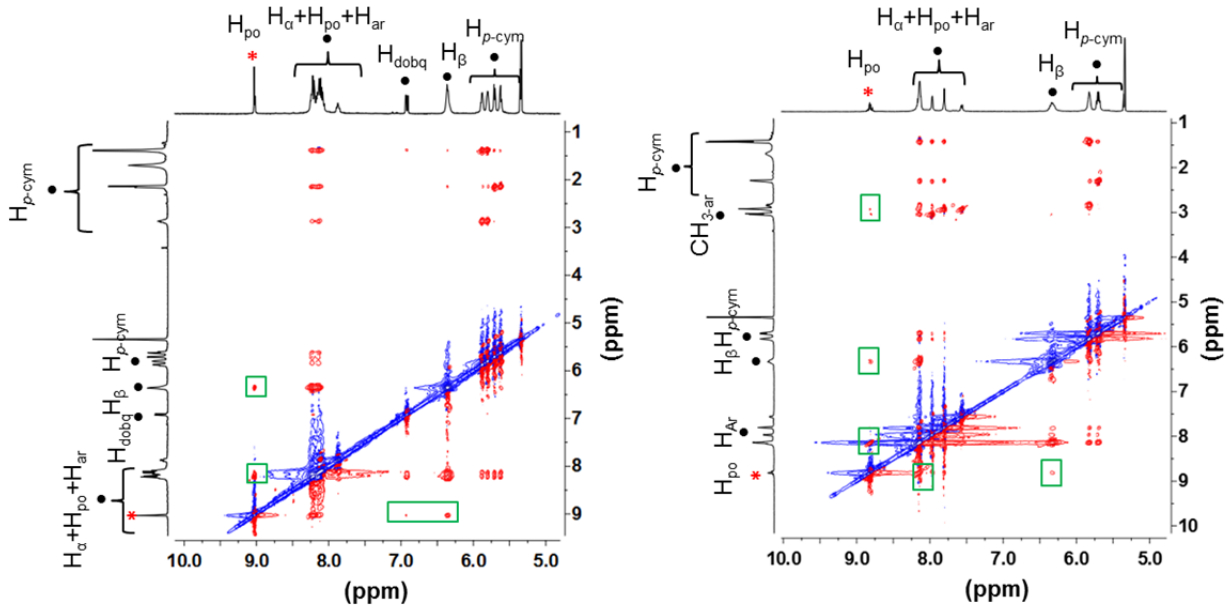

*Figure 78. 2D ROESY NMR spectra of the host-guest systems [**22d**]$^{6+}$ (left) and [**22f**]$^{6+}$ (right) in (CD_2Cl_2, 23°C). The ROEs cross peaks observed between the hosts and the guest are highlighted by green rectangles.*

The formation of the host–guest systems was further confirmed by electrospray ionization mass spectrometry (ESI-MS). All spectra showed different signals at m/z = 1146.1, 1221.2, 1329.5 corresponding respectively to the tri-cationic fragments [**22d** + 3 CF_3SO_3]$^{3+}$, [**22e** + 3 CF_3SO_3]$^{3+}$and [**22f** + 2CH_3OH + 3 CF_3SO_3]$^{3+}$ (Fig. 79).

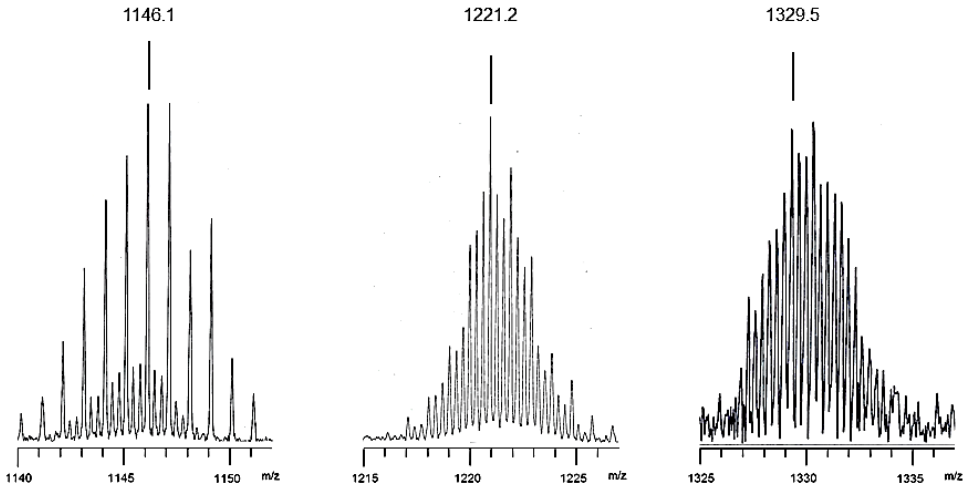

*Figure 79. Excerpts of the ESI-MS spectra corresponding to [**22d** + 3 CF_3SO_3]$^{3+}$ (left), [**22e** + 3 CF_3SO_3]$^{3+}$ (middle) and [**22f** + 2CH_3OH + 3 CF_3SO_3]$^{3+}$ (right).*

5.4 Application in Photodynamic Therapy

The photodynamic activity of the four compounds [**21e**]$^{6+}$, [**21f**]$^{6+}$, [**22e**]$^{6+}$ and [**22f**]$^{6+}$ were evaluated on human colorectal cancer cells (HT-29) with the concentration varying from 1 to 1000 nM at a fixed light dose of 20 J/cm^2. In the absence of porphin, the empty cages exposed to light show no photo-activity. However, the [porphin⊂cage]$^{6+}$ host-guest systems ([**22e**]$^{6+}$, [**22f**]$^{6+}$) exhibit an excellent photo-toxicity, hence proving the release of porphin in the illuminated cells. Moreover, a 10 nM concentration of the compound [**22f**]$^{6+}$ was sufficient to inhibit 50% of cells viability. Thus, the complex [**22f**]$^{6+}$ is ten times more active than the complex [**22e**]$^{6+}$ (Fig. 80). This difference may be related to the photosensitizer's release rate and the portal size of the two hosts.

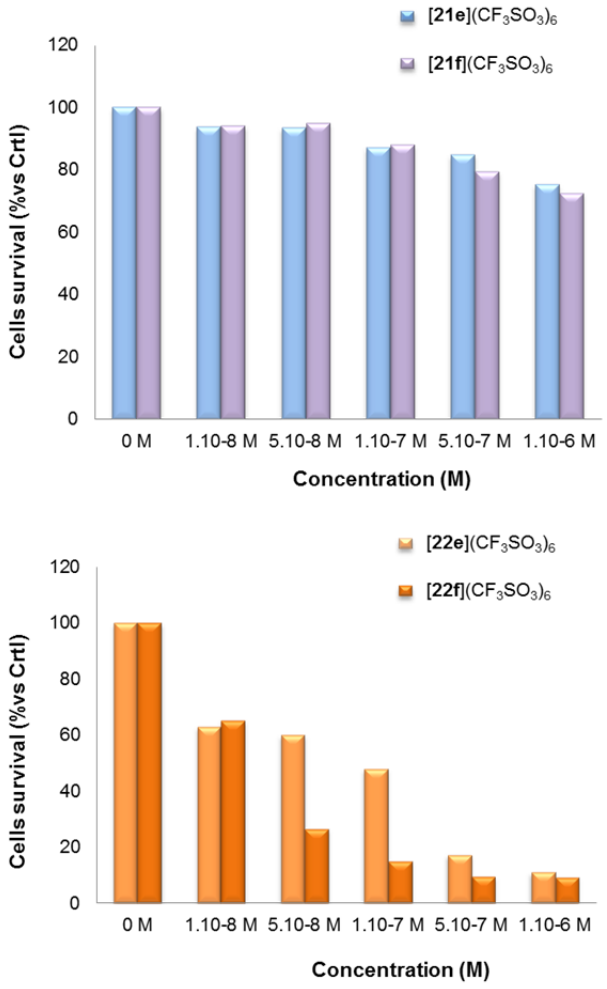

*Figure 80. Phototoxicity on human colorectal cancer cells (HT-29) from compounds [**21e**]$^{6+}$ and [**21f**]$^{6+}$ (top), [**22e**]$^{6+}$, and [**22f**]$^{6+}$ (bottom), at different concentrations (10 to 1000 nM), and after exposure to light (20 J/cm^2).*

5.5 Conclusions

A series of OO∩OO hydroxybenzo-quinonato bis-chelating bridging ligands have been used to generate dinuclear and hexanuclear arene ruthenium complexes incorporating either one or two phenyl groups. Despite the similarity in the dynamic host-guest behavior in NMR time scale, the fluorescence emissions of porphin and the photo-activity in the host-guest compounds are quite different. The metalla-prisms with relatively small portal size show an excellent photo-toxicity with half maximal inhibitory concentrations in the nM range.

6

General Conclusions and Perspectives

The thermodynamic and kinetic rules driving the formation of arene ruthenium metalla-assemblies constructed by a prearranged self-assembling process, in addition to the exploration of their anticancer activities as potential drugs and drugs delivery vectors are described in the present thesis.

6.1 Insight into the Thermodynamic and the Kinetic Aspects Dictating the Formation of Arene Ruthenium Metalla-Assemblies

The synthetic routes and empirical parameters allowing an efficient formation of arene ruthenium metalla-assemblies are now well established. However, the dynamic behavior of these structures and the exact thermodynamic and/or kinetic pathways were not known. The studies and results presented in this thesis have given some answers to these issues and have contributed to rationalizing the thermodynamic and kinetic aspects in coordination driven metalla-assemblies.

The first part of this work deals with the dynamic ligand exchange behavior of the arene ruthenium metalla-rectangles having the general formula $[(p\text{-cymene})Ru_4(OO\cap OO)_2(N\cap N)_2]^{4+}$ (OO∩OO = oxalato, 2,5-dioxydo-1,4-benzoquinonato, 5,8-dioxydo-1,4-naphthoquinonato; N∩N = 4,4'-bipyridine-H_8, 4,4'-bipyridine-D_8). The $^1H/^2D$ isotope labeling study of the 4,4'-bipyridine connectors shows that the ligand exchanges does not proceed spontaneously, even at high temperature. This exchange occurs only when an external stimulus is present (Scheme 9). This finding demonstrates the robustness of the matalla-cyclic architectures. This extra strength of metalla-assemblies favors their application in cancer treatment, where the stability is a crucial factor for drug delivery vectors.

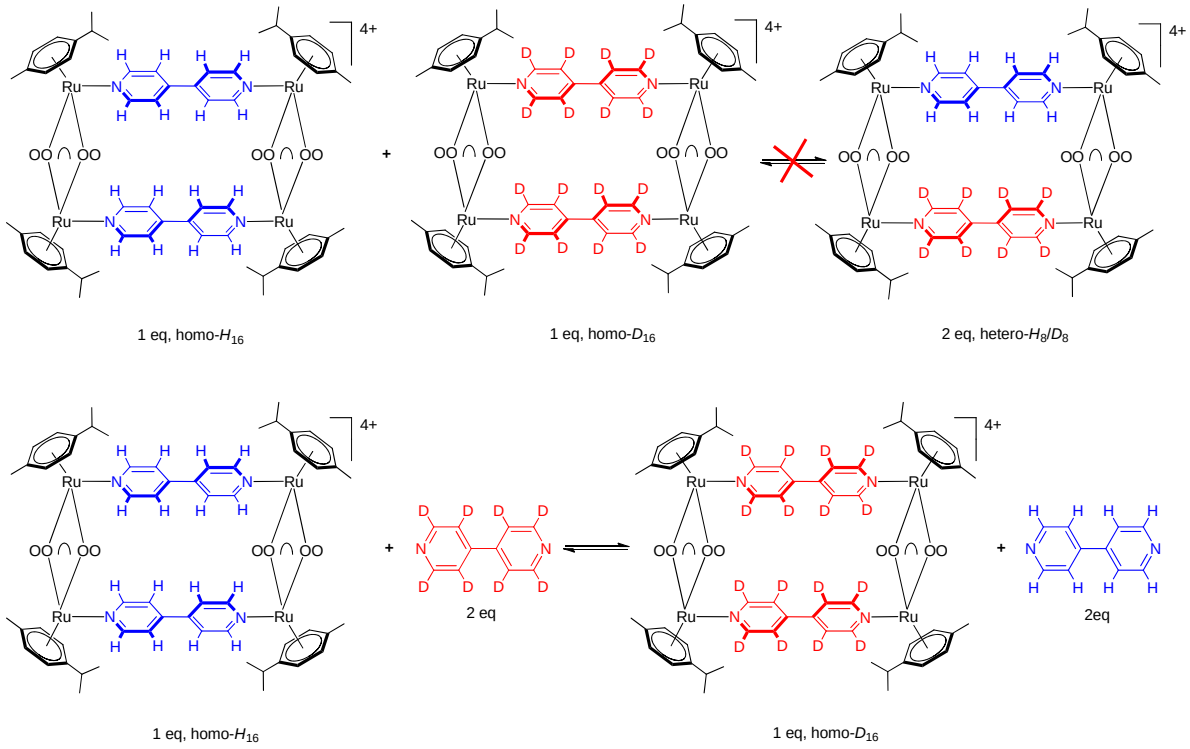

Scheme 9. Description of the dynamic ligand exchange of the arene ruthenium metalla-rectangles; absence of spontaneous ligand exchange process between two isotopical metalla-rectangles with the opposite labeling (up), putative dynamic ligand exchange behavior in the presence of 4,4'-bipyridine as competing ligand (down).

In the second part, the intermediary species leading to the formation of stable arene ruthenium metalla-assemblies built from OO∩OO bridging ligands and bi-pyridyl linkers are identified. The dynamic nature of the Ru-N bond in the solution before the closure of metalla-

cycle is confirmed by NMR experiments. This helped us to propose the formation mechanism of arene ruthenium metalla-assemblies (Scheme 10).

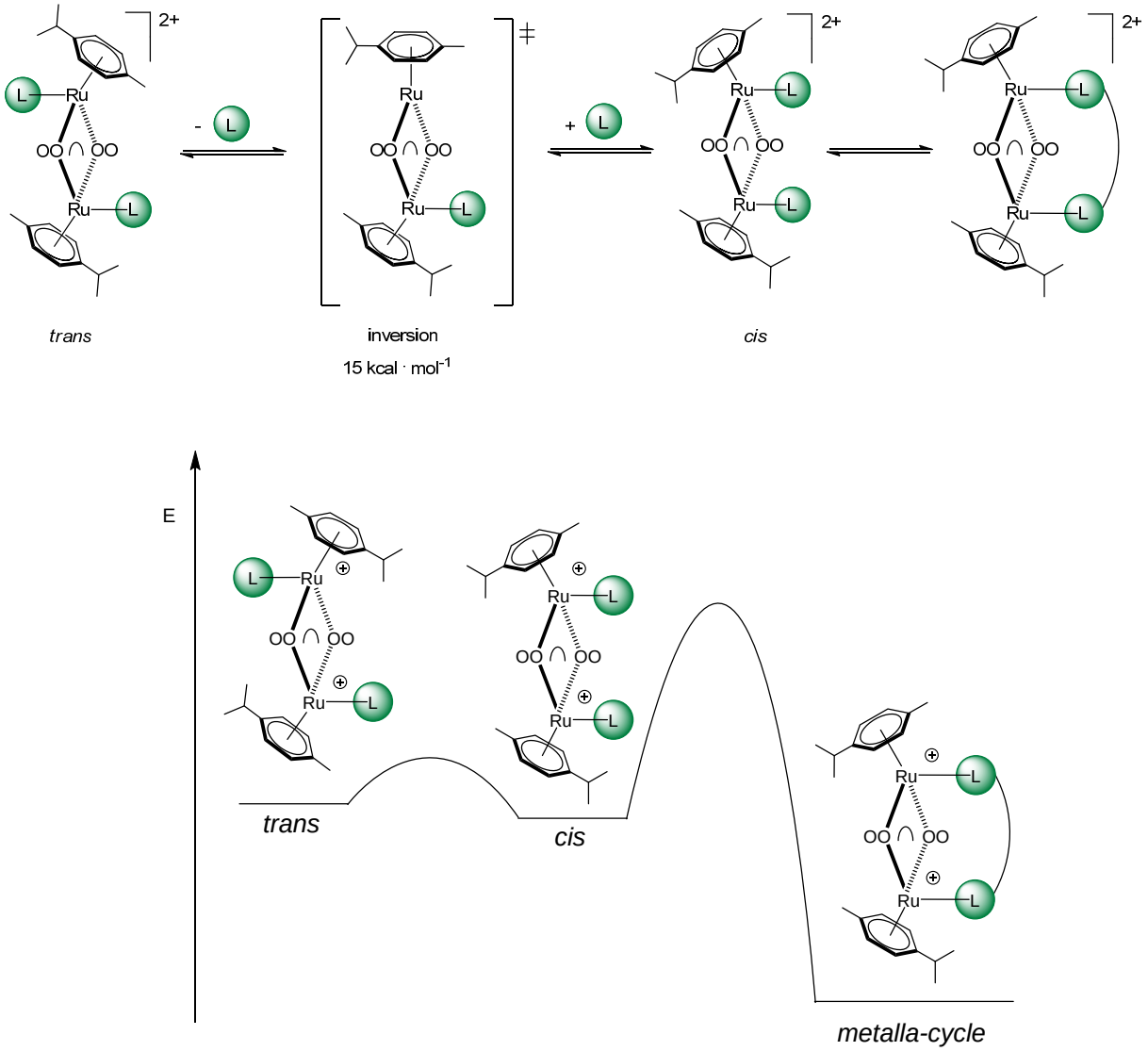

Scheme 10. Plausible self-assembling pathway leading to the formation of arene ruthenium metalla-cycles.

However, one question remains unanswered for arene ruthenium metalla-cycles linked with bi-pyridyl linkers: Does the final step involve two half-rectangles (Scheme 11A), or a fully occupied *cis* dinuclear metalla-clip with a naked metalla-clip (Scheme 11B), or a contribution of both? Hopefully, further studies will give the answer to this remaining question.

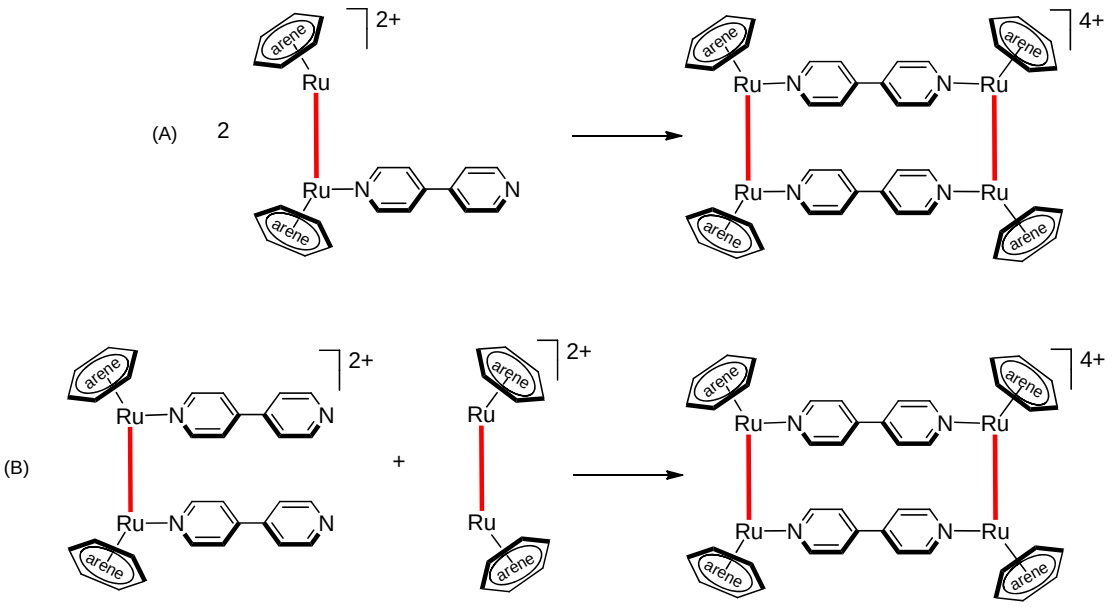

Scheme 11. Hypothetical steps leading to the formation of arene ruthenium metalla-cycles.

6.2 Arene Ruthenium Metalla-Prisms as Anticancer Drugs and Drug Delivery Vectors

Since the discovery of the "Enhanced permeability and retention" (EPR) effect in the 1980s by Maeda, structural factors, especially the influence of size and shapes have been examined in view of enhancing the biological activity of the chemotherapeutic agents. Among macromolecular compounds, water-soluble arene ruthenium metalla-prisms developed in our group since 2008, showed excellent antiproliferative activities against human ovarian cancer cells as well as great ability to deliver active species into tumor tissues. In order to improve these two main benefits, two new strategies have been developed and tested in this present work.

In addition, a new family of ON∩NO bis-chelating linkers has been used to generate a new family of dinuclear, tetranuclear, and hexanuclear arene ruthenium complexes incorporating different functional groups. The neutral dinuclear complexes have shown no antiproliferative activity, while the cationic metalla-assemblies were all cytotoxic with IC_{50} values in the lower µM range. Interestingly, the cationic metalla-assemblies with the N-(2-ethoxy)ethanol functional groups on the ON∩NO linkers possessed excellent selectivity for

cancerous over noncancerous cells, suggesting that functionalization at the bridging-linkers offers great potential for the biological optimization of metalla-assemblies (Fig. 81, Table 9).

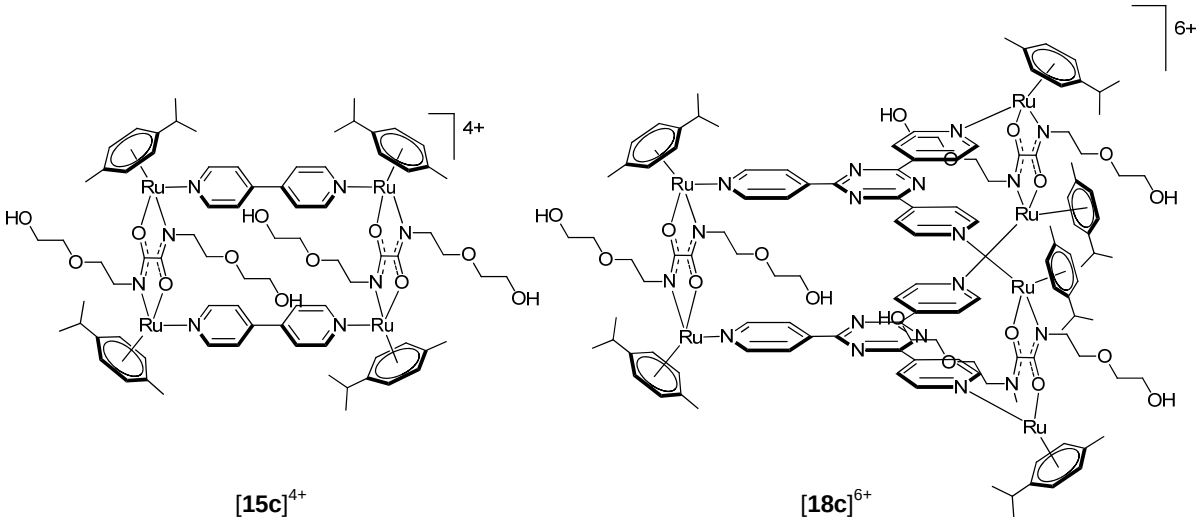

Figure 81. Molecular structures of the arene ruthenium metalla-assemblies ***[15c]***$^{4+}$ *and* ***[18c]***$^{6+}$ *incorporating N-(2-ethoxy)ethanol functional groups, possessing an excellent selectivity for cancerous over noncancerous cells.*

Table 9. IC_{50} *values (μM) of the complexes* ***[15c]***$^{4+}$, ***[18c]***$^{6+}$ *and cisplatin after 72 h exposure on human ovarian (A2780) carcinoma cells and noncancerous human embryonic kidney (HEK293) cells.*

Compound	HEK293 cells	A2780 cells	SC[a]
[15c]$(CF_3SO_3)_4$	4.5 ± 0.3	0.4 ± 0.1	**13**
[18c]$(CF_3SO_3)_6$	2.4 ± 0.2	0.3 ± 0.1	**7.3**
cisplatin	8.4 ± 1.2	1.4 ± 0.2	**6**

[a]*SC = selectivity coefficient =* IC_{50} *HEK293/*IC_{50} *A2780.*

The second part deals with the applications of the arene ruthenium metalla-prisms as vehicles for intracellular delivery of photosensitizers. Consequently, a series of OO∩OO hydroxybenzo-quinonato bis-chelating bridging ligands are used to build three hexanuclear arene ruthenium metalla-prisms with different portal sizes. The metalla-prism with relatively smaller portal size **[22f]**$^{6+}$ show good photo-protection ability of the porphin molecule, and an excellent photo-toxicity with half maximal inhibitory concentrations in nM range. This difference would be more highlighted *in vivo*, where the stability of the complex encapsulated

within the nano-transporter is crucial to inhibit the undesirable premature release of the guest molecule before reaching the target.

6.3 Perspectives

Arene ruthenium metalla-assemblies incorporating functional groups in their bis-chelating bridging ligands have been developed in this thesis. These assemblies demonstrated selective and efficient anticancer activities, thus opening a new area of research in our group.

Consequently, one possible new feature would be the incorporation of hydrophilic functions to the arene ligands to allow a better stability towards the final metalla-assemblies structures, along with a simple administration in the blood. On the other hand, segments of peptides or proteins such as transferrin can be attached to the bis-chelating linker's functional groups, providing better accessibility to the biological barriers and cells membranes.

Moreover, the Dyson group recently showed that a fluoroalkychain attached to mononuclear arene ruthenium complexes results in an excellent thermo-activity to these systems. Under mild hyperthermia, an excellent cytotoxicity and selectivity for cancerous over noncancerous cells was note-worthy for these compounds.[201] Extrapolation of this strategy to the tetranuclear, hexanuclear and octanuclear arene ruthenium metalla-assemblies by attaching the fluoroalkychain to the hydroxybenzo-quinonato bis-chelating bridging ligand is a possible perspective (Fig. 82).

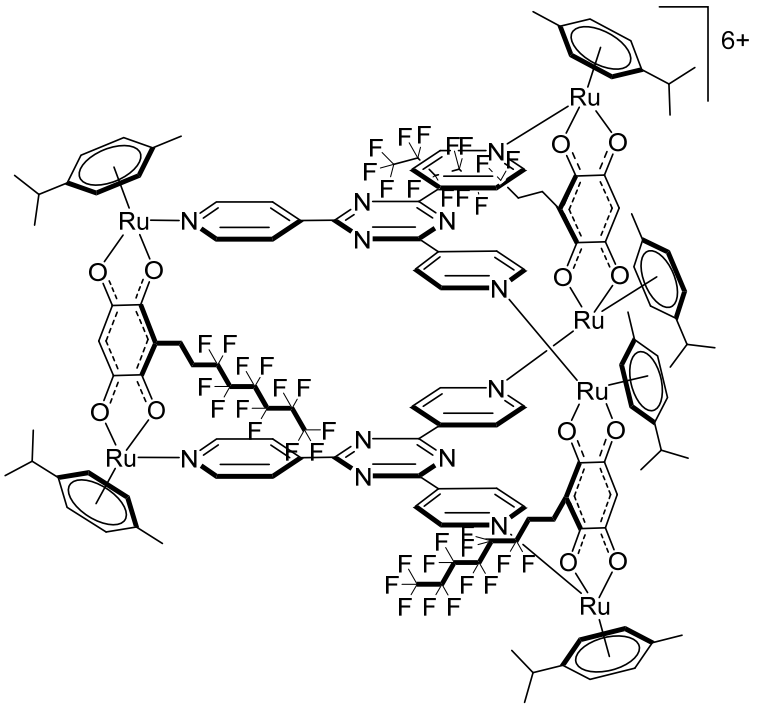

Figure 82. Structures of the targeted arene ruthenium metalla-prisms incorporating fluoroalkychain.

The arene ruthenium metalla-prisms synthesized in the present work are able to encapsulate a collection of different guest molecules. Among these active species, cisplatin prodrugs are very promising candidates (Fig. 83). In addition, their intracellular transportation by the metalla-cages could be a good strategy in order to mitigate the premature aquation and undesirable interactions, which are plausible limitations of the cisplatin.[202] Another possibility is the encapsulation of new highly efficient and photostable photosensitizers e.g. the ones based on BODIPY Chromophore for further two photon excitation PDT treatment purposes (Fig. 83).

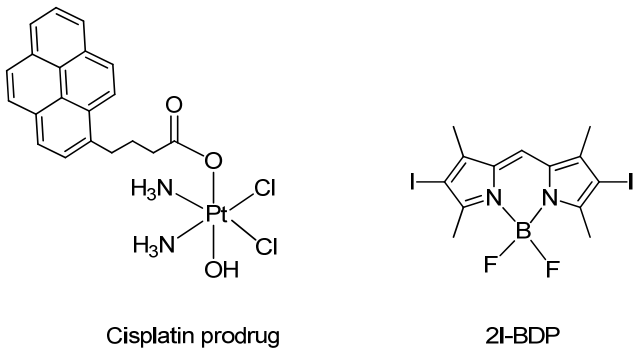

Figure 83. New cisplatin derived prodrug synthesized by the group of Dr. Wee Han Ang (National University of Singapore)(left), and 4,4-difluoro-2,6-diiodo-1,3,5,7-tetramethyl-4-bora-3a,4a-diaza-s-indacene (2I-BDP) photosensitizer.[203]

7 Experimental Section

7.1 General Remarks

7.1.1 Solvents, Lamp and Products

Solvents of analytical grade purchased from commercial sources (Acros organic, Honeywell solvents and VWR international) degassed and saturated with nitrogen prior to use, were employed for the synthesis of the starting organic compounds; they were used as received unless specified otherwise for the organometallic complexes. The photoreactions with UV light were performed with an UV reactor (Luzchem Research, photoreactor, λ = 365 nm). 4,4′-bipyridine-D_8 (bpy-D_8) (purity 98 atom % D), 4,4′-bipyridine (bpy), 1,2-bis(4-pyridyl)ethylene (bpe), 4,4′-azopyridine (bpa), 4-phenylpyridine (L^1), 4-styrylpyridine (L^2), 4-methylpyridine (L^3), 4-*tert*-butylpyridine (L^4) were purchased from Sigma-Aldrich, while the tridentate spacers 2,4,6-tris(4-pyridyl)-1,3,5-triazine (tpt)[204] and 1,3,5-tris{2-(4-pyridyl)vinyl}benzene (tpv)[205] were prepared according to published methods. Porphin is commercially available from Frontier Scientific. All other reagents were purchased from Alfa Aesar, Acros organics, TCI-Europe or Aldrich and used as received unless specified otherwise.

The arene ruthenium complexes $[(p\text{-cymene})_2Ru_2Cl_2(\mu\text{-}Cl)_2]$,[206] $[(p\text{-cymene})_2Ru_2(OO\cap OO)Cl_2]$ (OO∩OO = oxalato,[116] 2,5-dioxido-1,4-benzoquinonato,[127] 5,8-

dioxido-1,4-naphthoquinonato[207]), along with, the arene ruthenium metalla-rectangle [(*p*-cymene)Ru_4(OO∩OO)$_2$(bpy-H_8)$_2$](CF_3SO_3)$_4$ (OO∩OO = oxalato, 2,5-dioxydo-1,4-benzoquinonato, 5,8-dioxydo-1,4-naphthoquinonato) were prepared according to published methods.[11]

7.1.2 NMR Experiments

The ^{1}H, ^{13}C{^{1}H}, COSY, HSQC, HMBC, ROESY and DOSY NMR spectra were recorded with Bruker Avance II 400 spectrometers, and the residual protonated solvent was used as an internal standard. The 2D ROESY experiments were recorded with 8 or 16 scans for each of the 400 t_1 increments. The duration of the spin-lock time was 0.3 s, and the spin lock was performed with a train of 180 (x) – 180 ($-x$) pulses to reduce the TOCSY magnetization transfer.[208] The data were multiplied with a squared cosine window function in both dimensions before Fourier transformation and zero-filled to 2048 and 1024 points in ω_2 and ω_1 dimensions, respectively.

7.1.3 Analytical Instruments

Infrared spectra were recorded as KBr pellets on a Perkin-Elmer FTIR 1720 X spectrometer. UV/Visible absorption spectra were recorded with a Perkin–Elmer UV/Visible spectrophotometer Lambda 24 using precision cells made of quartz (1 cm). Fluorescence spectra were recorded on a Perkin-Elmer-LS50B luminescence spectrometer. Electrospray and nanoelectrospray mass spectra were recorded in the positive-ion mode with LCQ ion trap (Thermo Finnigan) and LTQ Orbitrap XL mass spectrometers (Thermo Scientific), respectively, and with a Bruker FTMS 4.7 T BioAPEX II mass spectrometer. The elemental analyses of **14a**–**14c** were performed at the Microanalytical Laboratory of the University of Vienna (Austria), while, for the other complexes [(**1–13**), (**15a–22f**)], the elemental analyses were carried out by the Mikroelementaranalytisches Laboratorium, ETH Zürich (Switzerland).

7.1.4 X-ray Crystallographic Details

X-ray diffraction measurements of **14a** and **14c** were performed on an X8 APEXII CCD diffractometer. Single crystals were positioned at 35 and 40 mm from the detector, and 2488 and 2098 frames were measured, each for 30 s over a 1° scan width, respectively. The data were processed using the SAINT software. X-Ray Crystallography. Crystals of [*trans*-**4**]$(CF_3SO_3)_2 \cdot 2\ (CH_3)_2CO$ and [*trans*-**7**]$(CF_3SO_3)_2$ were mounted on a Stoe Image Plate Diffraction system equipped with a ϕ circle goniometer, using Mo-Kα graphite monochromatic radiation (λ = 0.71073 Å) with ϕ range 0-200º. The structures were solved by direct methods using the program SHELXS-97, while the refinement and all further calculations were carried out using SHELXL-97.[209] The H atoms were included in calculated positions and treated as riding atoms using the SHELXL default parameters. The non-H atoms were refined anisotropically, using weighted full-matrix least-squares on F^2.

7.1.5 Biological Studies

Cytotoxicity Test (MTT assay) (performed by the group of Professor Dyson (EPFL))

Cell lines, Cell Culture, and Cell Viability Test; HEK293 human embryonic kidney cells (ATCC CRL-1573) were obtained from ATCC (Middlesex, U.K.), and the A2780 human ovarian carcinoma cell line was obtained from the European Collection of Cell Cultures (calatogue number 93112519, Salisbury, U.K.). All cell culture media were purchased from Life Technologies (Zug, Switzerland). A2780 cells were cultured in RPMI-1640 medium (Gibco, GlutaMax), while HEK293 cells were cultured in Dulbecco's Modified Eagle Medium (DMEM, Gibco, GlutaMax) supplemented with 10% fetal bovine serum (FBS, Sigma-Aldrich, Buchs, Switzerland) and 1% penicillin/streptomycin (Life Technologies, Zug, Switzerland). Cells were incubated in a CO_2 incubator with 5% CO_2 and 100% relative humidity at 37 °C. MTT (MTT = 3-(4,5-dimethyl-2-thiazolyl)-2,5-diphenyl-2*H*-tetrazolium bromide) was purchased from Calbiochem (Zug, Switzerland). The cell viability was determined by the MTT assay. The absorption was read using a SpectraMax M52 microplate reader (Molecular Devices, Sunnyvale, CA, USA). Cells were seeded in 96-well plates as monolayers with 100 µL of cell suspension (approximately 5000 cells) per well and preincubated for 24 h in medium supplemented with 10% FBS. All compounds were

dissolved in DMSO. The stock solutions were serially diluted in the culture medium to the appropriate concentration to give a final DMSO concentration of not higher than 0.5%. A 100 µL aliquot of the compound solution was added to each well, and the plates were incubated for another 72 h. Subsequently, MTT (5 mg/mL solution) was added to the cells, and the plates were incubated for a further 2 h. The culture medium was aspirated, and the purple formazan crystals, formed by the mitochondrial dehydrogenase activity of vital cells, were dissolved in DMSO. The optical density, directly proportional to the number of surviving cells, was quantified at 590 nm using a multiwell plate reader, and the fraction of surviving cells was calculated from the absorbance of untreated control cells. The evaluation was based on means from at least two independent experiments, each comprising triplicates per concentration level.

In vitro Phototoxicity Studies (MTT assay) (performed by the group of Prof. Vincent Sol at the Université de Limoges)

The cell viability was assessed by the 3-(4,5-dimethylthiazol-2-yl)-2,5-diphenyl tetrazolium bromide (MTT) staining method. 100 µL per well of cell suspension at 0.5 × 105 cells per mL were cultured in microplates (96 wells) in complete DMEM GlutamaxTM. After cells had grown for 24 h, the supernatant was removed and cells were incubated in the dark with different concentrations of compounds [**21e**][CF_3SO_3]$_6$, [**21f**][CF_3SO_3]$_6$, [**22e**][CF_3SO_3]$_6$ and [**22f**][CF_3SO_3]$_6$ ranging from 10 to 1000 nM for 24 h. Phototoxicity (with irradiation at a fluence of 20 J/cm^2) of the compounds was evaluated using the MTT assay, and control experiments were as follow: no treatment with light exposure and assays combining treatment and light. 15 µL of MTT (5 g MTT/L in H_2O) were added and cells incubated for 3 h. One hundred µl of DMSO were added to each well and mixed to dissolve the reduced MTT crystals and the absorbance read at 595 nm using a microplate spectrophotometer (Triad Serlabo Technologies). Each experiment was realized in triplicate and repeated four times.

7.2 Syntheses and Characterizations

7.2.1 Synthesis and Characterization of the Isotopic and Heteroisotopic Arene Ruthenium Metalla-Rectangles

General Synthetic Method for the Isotopic Metalla-Rectangles of the General Formula [(p-cymene)Ru_4(OO∩OO)$_2$(bpy-D_8)$_2$]$^{4+}$.

A mixture of the dinuclear clip [(*p*-cymene)$_2$Ru$_2$(OO∩OO)Cl$_2$] (OO∩OO = oxalato, 2,5-dioxydo-1,4-benzoquinonato, 5,8-dioxydo-1,4-naphthoquinonato) (0.16 mmol) and 2 equiv of $AgCF_3SO_3$ (0.32 mmol) in methanol (20 mL) was stirred at room temperature for 2 h and the solution was filtered to remove AgCl. To the filtrate, the corresponding 4,4′-bipyridine-D_8 (bpy-D_8) (0.16 mmol) was added. The mixture was stirred at room temperature for 24 h, and the solvent removed under vacuum. The residue was dissolved in dichloromethane (20 mL), the extract filtered and concentrated (3 mL), and diethyl ether was slowly added to initiate precipitation of the product as a dark orange or red solid.

[(*p*-cymene)$_4$Ru$_4$(oxalato)$_2$(bpy-D_8)$_2$](CF$_3$SO$_3$)$_4$ **(R-ox-homo-D_{16})**. Orange solid, Yield: 0.052 mmol (65%). ^{1}H NMR (400 MHz, MeOD): δ (ppm) , 5.96(d, 8H, $^3J_{H\text{-}H}$ = 6.2 Hz, C**H**$_{p\text{-}cym}$), 5.78 (d, 8H, $^3J_{H\text{-}H}$ = 6.2 Hz, C**H**$_{p\text{-}cym}$), 2.95 (sept, 4H, $^3J_{H\text{-}H}$ = 6.9 Hz, C**H**(CH$_3$)$_2$), 2.23 (s, 12H, C**H**$_3$), 1.39 (d, 24H, $^3J_{H\text{-}H}$ = 6.9 Hz, CH(C**H**$_3$)$_2$). ^{13}C{^{1}H} NMR (100 MHz, MeOD): δ (ppm) 172.5 (**C**=O), 149.27 (**C**$_{bpy}$), 142.12 (**C**$_{bpy}$), 125.6 (**C**$_{bpy}$), 103.97 (**C**$_{p\text{-}cym}$), 99.13 (**C**$_{p\text{-}cym}$), 83.61 (**C**H$_{p\text{-}cym}$), 82.99 (**C**H$_{p\text{-}cym}$), 32.48 (**C**H(CH$_3$)$_2$), 22.47 (CH(**C**H$_3$)$_2$), 18.02 (**C**H$_3$). IR (cm^{-1}): 3077 (w, CH$_{p\text{-}cym}$), 1634(s, C=O), 1578 (s, C=C$_{bpy}$), 1259 (s, CF$_3$). UV-visible: (1.0×10^{-5} M, CH_2Cl_2, 298 K): λ_{max} 241 nm (ε = 29 371 M^{-1} · cm^{-1}), 311 nm (ε = 25 684 M^{-1} · cm^{-1}). ESI-MS: 790 [M - bpy - 2 CF_3SO_3]$^{2+}$, 872 [1/2 M - CF_3SO_3]$^{1+}$, 708 [1/2 M – bpy – CF_3SO_3]$^{1+}$.

[(*p*-cymene)$_4$Ru$_4$(2,5-dioxydo-1,4-benzoquinonato)$_2$(bpy-D_8)$_2$](CF$_3$SO$_3$)$_4$ **(R-dobq-homo-D_{16})**. Red solid, Yield: 0.053 mmol (66%). ^{1}H NMR (400 MHz, MeOD): δ (ppm) , 6.02 (d, 8H, $^3J_{H\text{-}H}$ =6.4 Hz, C**H**$_{p\text{-}cym}$), 5.80 (d, 8H, $^3J_{H\text{-}H}$ = 6.4 Hz, C**H**$_{p\text{-}cym}$), 5.77 (s, 8 H, C**H**$_{dhbq}$), 2.87 (sep, 4H, $^3J_{H\text{-}H}$ = 6.9 Hz, C**H**(CH$_3$)$_2$), 2.17 (s, 12H, **C**H$_3$), 1.35 (d, 24H, $^3J_{H\text{-}H}$ = 6.9 Hz, CH(C**H**$_3$)$_2$). ^{13}C{^{1}H} NMR (100 MHz, MeOD): δ (ppm) 185.7 (**C**=O), 146.7 (**C**$_{bpy}$), 144.7 (**C**$_{bpy}$), 123.6 (**C**$_{bpy}$), 105.56 (**C**$_{p\text{-}cym}$), 103.00 (**C**H$_{dhbq}$), 100.35 (**C**$_{p\text{-}cym}$), 85.07 (**C**H$_{p\text{-}cym}$), 83.55 (**C**H$_{p\text{-}cym}$), 32.73 (**C**H(CH$_3$)$_2$), 22.68 (CH(**C**H$_3$)$_2$), 18.28 (**C**H$_3$). IR (cm^{-1}): 3066 (w, CH$_{p\text{-}cym}$),

1580 (s, C=C_{bpy}), 1527 (s, C=O), 1258 (s, CF_3). UV-visible: (1.0×10^{-5} M, CH_2Cl_2, 298 K): λ_{max} 308 nm (ε = 45 981 $M^{-1} \cdot cm^{-1}$), 491 nm (ε = 30 945 $M^{-1} \cdot cm^{-1}$). ESI-MS: 922 [M – 2 CF_3SO_3]$^{2+}$.

[(*p*-cymene)$_4$Ru$_4$(5,8-dioxydo-1,4-naphthoquinonato)$_2$(bpy-D_8)$_2$](CF_3SO_3)$_4$ **(R-donq-homo-D_{16})**. Dark green solid, Yield: 0.053 mmol (66%). ^{1}H NMR (400 MHz, MeOD): δ (ppm) , 7.24 (s, 8 H, C**H**$_{dhnq}$), 5.86 (d, 8H, $^3J_{H\text{-}H}$=6.4 Hz, C**H**$_{p\text{-}cym}$), 5.63 (d, 8H, $^3J_{H\text{-}H}$= 6.4 Hz, C**H**$_{p\text{-}cym}$), 2.83 (sep, 4H, $^3J_{H\text{-}H}$= 7 Hz, C**H**(CH_3)$_2$), 2.17 (s, 12H, C**H**$_3$), 1.35 (d, 24H, $^3J_{H\text{-}H}$= 7 Hz, CH(C**H**$_3$)$_2$). ^{13}C{1H} NMR (100 MHz, MeOD): δ (ppm) 172.26 (**C**=O), 153.49 (**C**$_{bpy}$), 138.62 (**C**$_{bpy}$), 124.15 (**C**$_{bpy}$), 112.58 (**C**$_{p\text{-}cym}$), 105.04 (**C**H$_{dhnq}$), 101.24 (**C**$_{p\text{-}cym}$), 85.96 (**C**H$_{p\text{-}cym}$), 84.03 (**C**H$_{p\text{-}cym}$), 31.98 (**C**H(CH_3)$_2$), 22.46 (CH(**C**H_3)$_2$), 17.31 (**C**H_3). IR (cm^{-1}): 3066 (w, $CH_{p\text{-}cym}$), 1578 (s, C=C_{bpy}), 1536 (s, C=O), 1259 (s, CF_3). UV-visible: (1.0×10^{-5} M, CH_2Cl_2, 298 K): λ_{max} 317 nm (ε = 33 470 $M^{-1} \cdot cm^{-1}$), 433 nm (ε = 17 300 $M^{-1} \cdot cm^{-1}$), 642 nm (ε = 1300 $M^{-1} \cdot cm^{-1}$), 695 nm (ε = 2863 $M^{-1} \cdot cm^{-1}$). ESI-MS: 972 [M – CF_3SO_3]$^{2+}$.

General Synthetic Method for the Heteroisotopic Metalla-Rectangles of the General Formula [(p-cymene)Ru$_4$(OO∩OO)$_2$(bpy-H$_8$)(bpy-D$_8$)]$^{4+}$.

A mixture of the dinuclear clip [(*p*-cymene)$_2$Ru$_2$(OO∩OO)Cl_2] (OO∩OO = oxalato, 2,5-dioxydo-1,4-benzoquinonato, 5,8-dioxydo-1,4-naphthoquinonato) (0.16 mmol) and 2 equiv of $AgCF_3SO_3$ (0.32 mmol) in methanol (20 mL) was stirred at room temperature for 2 h and the solution was filtered to remove AgCl. To the filtrate, a mixture of bpy-H_8 and bpy-D_8 (0.08 mmol + 0.08 mmol) was added. The mixture was stirred at room temperature for 24 h, and the solvent removed under vacuum. Then the residue was dissolved in dichloromethane (20 mL), the extract filtered and concentrated (3 mL), and diethyl ether was slowly added to initiate precipitation of the product as a dark orange or red solids, the average yield of the obtained metalla-rectangle mixtures being 63%.

All NMR data are consistent with the formation of the mixed metalla-rectangles (Figure 27), however, no chemical shifts of the protons between the ^{1}H/^{2}D species are observed, only the integration being consistent with the expected mixtures between the homo- and hetero-metalla-rectangles.

[(*p*-cymene)$_4$Ru$_4$(oxalato)$_2$(bpy-H_8)(bpy-D_8)](CF$_3$SO$_3$)$_4$ **(R-ox-hetero H_8-D_8)**. Orange solid. ESI-MS: 786 [M(D_8/H_8) – (bpy-D_8) – 2 CF$_3$SO$_3$]$^{2+}$, 790 [M(D_8/H_8) – (bpy-H_8) – 2 CF$_3$SO$_3$]$^{2+}$, 864 [1/2 M(D_8/H_8) – CF$_3$SO$_3$]$^{1+}$, 872 [1/2 M(D_8/H_8) – CF$_3$SO$_3$]$^{1+}$.

[(*p*-cymene)$_4$Ru$_4$(2,5-dioxydo-1,4-benzoquinonato)$_2$(bpy-H_8)(bpy-D_8)](CF$_3$SO$_3$)$_4$ **(R-dobq-hetero H_8-D_8).** Red solid. ESI-MS: 836 [M(D_8/H_8) – (bpy-D_8) – 2 CF$_3$SO$_3$]$^{2+}$, 840 [M(D_8/H_8) – (bpy-H_8) – 2 CF$_3$SO$_3$]$^{2+}$, 918 [M(D_8/H_8) – 2 CF$_3$SO$_3$]$^{2+}$.

[(*p*-cymene)$_4$Ru$_4$(5,8-dioxydo-1,4-naphthoquinonato)$_2$(bpy-H_8)(bpy-D_8)](CF$_3$SO$_3$)$_4$ **(R-dobq-hetero H_8-D_8)**. Dark green solid. ESI-MS: 886 [M(D_8/H_8) – (bpy-D_8) – 2 CF$_3$SO$_3$]$^{2+}$, 890 [M(D_8/H_8) – (bpy-H_8) – 2 CF$_3$SO$_3$]$^{2+}$, 968 [M(D_8/H_8) – 2 CF$_3$SO$_3$]$^{2+}$.

7.2.2 Preparation of the Arene Ruthenium Dimetallic Complexes

*General Synthetic Method for the Dinuclear Arene Ruthenium Complexes of the General Formula [(p-cymene)$_2$Ru$_2$(OO∩OO)(L^n)$_2$]$^{2+}$ [**1**]$^{2+}$–[**12**]$^{2+}$.*

A mixture of the dinuclear complex [(*p*-cymene)$_2$Ru$_2$(OO∩OO)Cl$_2$] (OO∩OO = oxalato, 2,5-dioxydo-1,4-benzoquinonato and 5,8-dioxydo-1,4-naphthoquinonato) (0.16 mmol) and 2 eq. of AgCF$_3$SO$_3$ (0.32 mmol) in methanol (20 mL) was stirred at room temperature for 2 h and the solution was filtered to remove AgCl. To the filtrate, the corresponding 4-phenylpyridine, 4-styrylpyridine, 4-methylpyridine and 4-^{t}butylpyridine (0.32 mmol) was added. The mixture was stirred at room temperature for 24 h, and the solvent removed under vacuum. The residue was dissolved in dichloromethane (20 mL), the extract filtered and concentrated (3 mL), and diethyl ether with pentane were slowly added to initiate precipitation of the product as an orange, green or red solid.

[1][CF$_3$SO$_3$]$_2$: Dark green solid, Yield: 0.09 mmol (56%). IR (cm^{-1}): 3066 (w, CH$_{p\text{-}cym}$), 1612 (s, C=C$_L$), 1534 (s, C=O), 1275 (s, CF$_3$). UV-visible: (1.0 × 10^{-5} M, CH$_2$Cl$_2$, 298 K): λ_{max} 554 nm (ε = 12 183 M^{-1} · cm^{-1}), 546 nm (ε = 12 129 M^{-1} · cm^{-1}), 237 nm (ε = 70545 M^{-1} · cm^{-1}), 695 nm (ε = 2863 M^{-1} · cm^{-1}). ESI-MS: 963 [M – L^1 – CF$_3$SO$_3$]$^+$, 807 [M – 2 L^1 – CF$_3$SO$_3$]$^{1+}$. Calcd for C$_{54}$H$_{52}$F$_6$N$_2$O$_{10}$Ru$_2$S$_2$ · CH$_2$Cl$_2$ · 2H$_2$O: C, 47.59; H, 4.07; N, 2.02. Found: C, 47.54; H, 3.72; N, 1.99.

[*cis*-1][CF_3SO_3]$_2$ (46%). ^{1}H NMR (400 MHz, CD_3OD): δ (ppm) 8.41 (d, 4H, $^3J_{H\text{-}H}$ = 6.8 Hz, C**H**$_\alpha$), 7.59 (d, 4H, $^3J_{H\text{-}H}$ = 6.8 Hz, C**H**$_\beta$), 7.53 (m, 4H, C**H**$_{ar}$), 7.35 (m, 4H, C**H**$_{ar}$), 7.26 (s, 4H, C**H**$_{donq}$), 5.87 (d, 4H, $^3J_{H\text{-}H}$ = 6.4 Hz, C**H**$_{p\text{-}cym}$), 5.60 (d, 4H, $^3J_{H\text{-}H}$ = 6.4 Hz, C**H**$_{p\text{-}cym}$), 2.79 (sept, 2H, $^3J_{H\text{-}H}$ = 7.0 Hz, C**H**$(CH_3)_2$), 2.14 (s, 6H, C**H**$_3$), 1.28 (d, 12H, $^3J_{H\text{-}H}$ = 7.0 Hz, CH(C**H**$_3)_2$). ^{13}C{1H} NMR (100 MHz, CD_3OD): δ (ppm) 172.36 (**C**=O), 153.18 (**C**$_L$), 138.61 (**C**$_L$), 131.42 (**C**H$_{ar}$), 130.37 (**C**H$_{ar}$), 128.09 (**C**H$_{ar}$), 124.52 (**C**$_L$), 104.81 (**C**H$_{donq}$), 100.91 (**C**$_{p\text{-}cym}$), 85.78 (**C**H$_{p\text{-}cym}$), 83.97 (**C**H$_{p\text{-}cym}$), 32.02 (**C**H$(CH_3)_2$), 22.42 (CH(**C**$H_3)_2$), 17.35 (**C**H_3).

[*trans*-1][CF_3SO_3]$_2$ (54%): ^{1}H NMR (400 MHz, CD_3OD): δ (ppm) 8.56 (d, 4H, $^3J_{H\text{-}H}$ = 6.8 Hz, C**H**$_\alpha$), 7.83 (d, 4H, $^3J_{H\text{-}H}$ = 6.8 Hz, C**H**$_\beta$), 7.79 (m, 4H, C**H**$_{ar}$), 7.55 (m, 6H, C**H**$_{ar}$), 7.23 (s, 4H, C**H**$_{donq}$), 5.81 (d, 4H, $^3J_{H\text{-}H}$ = 6.4 Hz, C**H**$_{p\text{-}cym}$), 5.60 (d, 4H, $^3J_{H\text{-}H}$ = 6.4 Hz, C**H**$_{p\text{-}cym}$), 2.86 (sept, 2H, $^3J_{H\text{-}H}$ = 7.0 Hz, C**H**$(CH_3)_2$), 2.12 (s, 6H, C**H**$_3$), 1.36 (d, 12H, $^3J_{H\text{-}H}$ = 7.0 Hz, CH(C**H**$_3)_2$). ^{13}C{1H} NMR (100 MHz, CD_3OD): δ (ppm) 172.64 (**C**=O), 153.48 (**C**$_L$), 138.57 (**C**$_L$), 131.67 (**C**H$_{ar}$), 130.56 (**C**H$_{ar}$), 128.29 (**C**H$_{ar}$), 124.58 (**C**$_L$), 104.86 (**C**H$_{donq}$), 100.78 (**C**$_{p\text{-}cym}$), 85.56 (**C**H$_{p\text{-}cym}$), 83.90 (**C**H$_{p\text{-}cym}$), 31.97 (**C**H$(CH_3)_2$), 22.48 (CH(**C**$H_3)_2$), 17.38 (**C**H_3).

[2][CF_3SO_3]$_2$: Dark green solid, Yield: 0.09 mmol (60%). IR (cm^{-1}): 3063 (w, $CH_{p\text{-}cym}$), 1609 (s, C=C$_L$), 1533 (s, C=O), 1274 (s, CF_3). UV-visible: (1.0×10^{-5} M, CH_2Cl_2, 298 K): λ_{max} 306 nm (ε = 61 955 $M^{-1} \cdot cm^{-1}$), 228 nm (ε = 76 676 $M^{-1} \cdot cm^{-1}$). ESI-MS: 989 $[M - L^2 - CF_3SO_3]^+$, 807 $[M - 2\ L^2 - CF_3SO_3]^+$. Calcd for $C_{58}H_{54}F_6N_2O_{10}Ru_2S_2 \cdot CH_2Cl_2$: C, 50.46; H, 4.02; N, 1.99. Found: C, 50.07; H, 3.95; N, 1.86.

[*cis*-2][CF_3SO_3]$_2$ (41%). ^{1}H NMR (400 MHz, CD_3OD): δ (ppm) 8.28 (d, 4H, $^3J_{H\text{-}H}$ = 6.8 Hz, C**H**$_\alpha$), 7.43 (m, 4H, C**H**$_\beta$), 7.41 (m, 4H, C**H**$_{ar}$), 7.22 (m, 6H, C**H**$_{ar}$), 7.36 (d, 2H, $^3J_{H\text{-}H}$ = 16.4 Hz, C**H**=CH), 6.92 (d, 2H, $^3J_{H\text{-}H}$ = 16.4 Hz, CH=C**H**), 7.26 (s, 4H, C**H**$_{donq}$), 5.85 (d, 4H, $^3J_{H\text{-}H}$ = 6.4 Hz, C**H**$_{p\text{-}cym}$), 5.61 (d, 4H, $^3J_{H\text{-}H}$ = 6.4 Hz, C**H**$_{p\text{-}cym}$), 2.84 (sept, 2H, $^3J_{H\text{-}H}$ = 7.0 Hz, C**H**$(CH_3)_2$), 2.12 (s, 6H, C**H**$_3$), 1.35 (d, 12H, $^3J_{H\text{-}H}$ = 7.0 Hz, CH(C**H**$_3)_2$). ^{13}C{1H} NMR (100 MHz, CD_3OD): δ (ppm) 172.36 (**C**=O), 153.18 (**C**$_L$), 138.61 (**C**$_L$), 131.42 (**C**H$_{ar}$), 130.37 (**C**H$_{ar}$), 128.09 (**C**H$_{ar}$), 124.52 (**C**$_L$), 104.81 (**C**H$_{donq}$), 100.91 (**C**$_{p\text{-}cym}$), 85.78 (**C**H$_{p\text{-}cym}$), 83.97 (**C**H$_{p\text{-}cym}$), 32.02 (**C**H$(CH_3)_2$), 22.42 (CH(**C**$H_3)_2$), 17.35 (**C**H_3).

[*trans*-2][CF_3SO_3]$_2$ (59%). ^{1}H NMR (400 MHz, CD_3OD): δ (ppm) 8.42 (d, 4H, $^3J_{H\text{-}H}$ = 6.8 Hz, C**H**$_\alpha$), 7.66 (m, 4H, C**H**$_\beta$), 7.62 (m, 4H, C**H**$_{ar}$), 7.60 (d, 2H, $^3J_{H\text{-}H}$ = 16.4 Hz, C**H**=CH), 7.42 (m, 6H, C**H**$_{ar}$), 7.21 (d, 2H, $^3J_{H\text{-}H}$ = 16.4 Hz, CH=C**H**), 7.25 (s, 4H, C**H**$_{donq}$), 5.80 (d, 4H, $^3J_{H\text{-}H}$ = 6.4 Hz, C**H**$_{p\text{-}cym}$), 5.58 (d, 4H, $^3J_{H\text{-}H}$ = 6.4 Hz, C**H**$_{p\text{-}cym}$), 2.78 (sept, 2H, $^3J_{H\text{-}H}$ = 7.0 Hz,

C**H**$(CH_3)_2$), 2.11 (s, 6H, C**H**$_3$), 1.27 (d, 12H, $^3J_{H\text{-}H}$ = 7.0 Hz, CH(C**H**$_3)_2$). ^{13}C{1H} NMR (100 MHz, CD_3OD): δ (ppm) 172.64 (**C**=O), 153.48 (**C**$_L$), 138.57 (**C**$_L$), 131.67 (**C**H_{ar}), 130.56 (**C**H_{ar}), 128.29 (**C**H_{ar}), 124.58 (**C**$_L$), 104.86 (**C**H_{donq}), 100.78 (**C**$_{p\text{-}cym}$), 85.56 (**C**$H_{p\text{-}cym}$), 83.90 (**C**$H_{p\text{-}cym}$), 31.97 (**C**$H(CH_3)_2$), 22.48 (CH(**C**$H_3)_2$), 17.38 (**C**H_3).

[3][CF_3SO_3]$_2$: Dark green solid, Yield: 0.11 mmol (68%). IR (cm^{-1}): 3070 (w, $CH_{p\text{-}cym}$), 1624 (s, C=C$_L$), 1532 (s, C=O), 1270 (s, CF_3). UV-visible: (1.0×10^{-5} M, CH_2Cl_2, 298 K): λ_{max} 439 nm (ε = 2 357 $M^{-1} \cdot cm^{-1}$), 318 nm (ε = 3 313 $M^{-1} \cdot cm^{-1}$), 229 nm (ε = 12 472 $M^{-1} \cdot cm^{-1}$), ESI-MS: 901 $[M - L^3 - CF_3SO_3]^+$, 807 $[M - 2\ L^3 - CF_3SO_3]^+$. Calcd for $C_{44}H_{46}F_6N_2O_{10}Ru_2S_2$: C, 46.23; H, 4.06; N, 2.45. Found: C, 45.65; H, 4.01; N, 2.36.

[*cis*-3][CF_3SO_3]$_2$ (47%). ^{1}H NMR (400 MHz, CD_3OD): δ (ppm) 8.23 (d, 4H, $^3J_{H\text{-}H}$ = 6.6 Hz, C**H**$_α$), 7.22 (d, 4H, $^3J_{H\text{-}H}$ = 6.6 Hz, C**H**$_β$), 7.18 (s, 4H, C**H**$_{donq}$), 5.80 (d, 4H, $^3J_{H\text{-}H}$ = 6.3 Hz, C**H**$_{p\text{-}cym}$), 5.57 (d, 4H, $^3J_{H\text{-}H}$ = 6.3 Hz, C**H**$_{p\text{-}cym}$), 2.77 (m, 2H, C**H**$(CH_3)_2$), 2.32 (s, 6H, $CH_βCCH_3$), 2.07 (s, 6H, C**H**$_3$), 1.31 (d, 12H, $^3J_{H\text{-}H}$ = 7.0 Hz, CH(C**H**$_3)_2$). ^{13}C{1H} NMR (100 MHz, CD_3OD): δ (ppm) 172.28 (**C**=O), 152.36 (**C**$_L$), 138.49 (**C**H_{donq}), 128.09 (**C**$_L$), 85.76 (**C**$H_{p\text{-}cym}$), 83.78 (**C**$H_{p\text{-}cym}$), 32.01 (**C**$H(CH_3)_2$), 22.46 (CH(**C**$H_3)_2$), 20.89 ($CH_βCCH_3$), 17.36 (**C**H_3).

[*trans*-3][CF_3SO_3]$_2$ (53%). ^{1}H NMR (400 MHz, CD_3OD): δ (ppm) 8.33 (d, 4H, $^3J_{H\text{-}H}$ = 6.8 Hz, C**H**$_α$), 7.34 (d, 4H, $^3J_{H\text{-}H}$ = 6.8 Hz, C**H**$_β$), 7.15 (s, 4H, C**H**$_{donq}$), 5.76 (d, 4H, $^3J_{H\text{-}H}$ = 6.3 Hz, C**H**$_{p\text{-}cym}$), 5.54 (d, 4H, $^3J_{H\text{-}H}$ = 6.3 Hz, C**H**$_{p\text{-}cym}$), 2.77 (m, 2H, C**H**$(CH_3)_2$), 2.43 (s, 6H, $CH_βCCH_3$), 2.07 (s, 6H, C**H**$_3$), 1.26 (d, 12H, $^3J_{H\text{-}H}$ = 7.0 Hz, CH(C**H**$_3)_2$). ^{13}C{1H} NMR (100 MHz, CD_3OD): δ (ppm) 172.55 (**C**=O), 152.57 (**C**$_L$), 138.49 (**C**H_{donq}), 128.16 (**C**$_L$), 85.49 (**C**$H_{p\text{-}cym}$), 83.83 (**C**$H_{p\text{-}cym}$), 31.97 (**C**$H(CH_3)_2$), 22.42 (CH(**C**$H_3)_2$), 20.92 ($CH_βC\mathbf{C}H_3$), 17.32 (**C**H_3).

[4][CF_3SO_3]$_2$: Dark green solid, Yield: 0.10 mmol (62%). IR (cm^{-1}): 3065 (w, $CH_{p\text{-}cym}$), 1637 (s, C=C$_L$), 1537 (s, C=O), 1275 (s, CF_3). UV-visible: (1.0×10^{-5} M, CH_2Cl_2, 298 K): λ_{max} 554 nm (ε = 12 183 $M^{-1} \cdot cm^{-1}$), 546 nm (ε = 12 129 $M^{-1} \cdot cm^{-1}$), 237 nm (ε = 70545 $M^{-1} \cdot cm^{-1}$), 695 nm (ε = 2863 $M^{-1} \cdot cm^{-1}$). ESI-MS: 943 $[M - L^4 - CF_3SO_3]^+$, 807 $[M - 2\ L^4 - CF_3SO_3]^+$. Calcd for $C_{50}H_{58}F_6N_2O_{10}Ru_2S_2$: C, 48.93; H, 4.76; N, 2.28. Found: C, 48.71; H, 4.74; N, 2.18.

[*cis*-4][CF_3SO_3]$_2$ (42%). ^{1}H NMR (400 MHz, CD_3OD): δ (ppm) 8.32 (d, 4H, $^3J_{H\text{-}H}$ = 6.8 Hz, C**H**$_α$), 7.45 (d, 4H, $^3J_{H\text{-}H}$ = 6.8 Hz, C**H**$_β$), 7.20 (s, 4 H, C**H**$_{donq}$), 5.78 (d, 4H, $^3J_{H\text{-}H}$ = 6.4 Hz, C**H**$_{p\text{-}cym}$), 5.57 (d, 4H, $^3J_{H\text{-}H}$ = 6.4 Hz, C**H**$_{p\text{-}cym}$), 2.83 (sept, 2H, $^3J_{H\text{-}H}$ = 7.0 Hz, C**H**$(CH_3)_2$),

2.11 (s, 6H, C**H**$_3$), 1.34 (d, 12H, $^3J_{H\text{-}H}$ = 7.0 Hz, CH(C**H**$_3$)$_2$), 1.22 (s, 18H, C(C**H**$_3$)$_3$). ^{13}C{1H} NMR (100 MHz, CD_3OD): δ (ppm) 172.35 (**C**=O), 165.57 (**C**=O), 152.58 (**C**$_L$), 138.54 (**C**H$_{donq}$), 124.52 (**C**$_L$), 104.74 (**C**$_{p\text{-}cym}$), 100.71 (**C**$_{p\text{-}cym}$), 85.66 (**C**H$_{p\text{-}cym}$), 83.95 (**C**H$_{p\text{-}cym}$), 36.02 (**C**(CH$_3$)$_3$), 31.99 (**C**H(CH$_3$)$_2$), 30.41 (C(**C**H$_3$)$_3$), 22.45 (CH(**C**H$_3$)$_2$), 17.31 (**C**H$_3$).

[*trans*-4][CF$_3$SO$_3$]$_2$ (58%). ^{1}H NMR (400 MHz, CD_3OD): δ (ppm) 8.42 (d, 4H, $^3J_{H\text{-}H}$ = 6.8 Hz, C**H**$_\alpha$), 7.58 (d, 4H, $^3J_{H\text{-}H}$ = 6.8 Hz, C**H**$_\beta$), 7.22 (s, 4H, C**H**$_{donq}$), 5.83 (d, 4H, $^3J_{H\text{-}H}$ = 6.4 Hz, C**H**$_{p\text{-}cym}$), 5.60 (d, 4H, $^3J_{H\text{-}H}$ = 6.4 Hz, C**H**$_{p\text{-}cym}$), 2.79 (sept, 2H, $^3J_{H\text{-}H}$ = 7.0 Hz, C**H**(CH$_3$)$_2$), 2.10 (s, 6H, C**H**$_3$), 1.35 (s, 18H, C(C**H**$_3$)$_3$), 1.29 (d, 12H, $^3J_{H\text{-}H}$ = 7.0 Hz, CH(C**H**$_3$)$_2$). ^{13}C{1H} NMR (100 MHz, CD_3OD): δ (ppm) 172.57 (**C**=O), 165.81 (**C**=O), 152.76 (**C**$_L$), 138.51 (**C**H$_{donq}$), 124.58 (**C**$_L$), 104.77 (**C**$_{p\text{-}cym}$), 100.57 (**C**$_{p\text{-}cym}$), 85.40 (**C**H$_{p\text{-}cym}$), 83.99 (**C**H$_{p\text{-}cym}$), 36.15 (**C**(CH$_3$)$_3$), 31.95 (**C**H(CH$_3$)$_2$), 30.52 (C(**C**H$_3$)$_3$), 22.42 (CH(**C**H$_3$)$_2$), 17.27 (**C**H$_3$).

[5][CF$_3$SO$_3$]$_2$: Red solid, Yield: 0.09 mmol (56%). IR (cm^{-1}): 3064 (w, CH$_{p\text{-}cym}$), 1613 (s, C=C$_L$), 1523 (s, C=O), 1258 (s, CF$_3$). UV-visible: (1.0×10^{-5} M, CH_2Cl_2, 298 K): λ_{max} 237 nm (ε = 46 681 M^{-1} · cm^{-1}), 418 nm (ε = 11 262 M^{-1} · cm^{-1}), 484 nm (ε = 11 088 M^{-1} · cm^{-1}). ESI-MS: 922 [M – 2 CF_3SO_3]$^+$, 758 [M – 2 L^1 – CF_3SO_3]$^+$. Calcd for $C_{50}H_{48}F_6N_2O_{10}Ru_2S_2$: C, 49.34; H, 3.97; N, 2.30. Found: C, 49.48; H, 3.99; N, 2.21.

[*cis*-5][CF$_3$SO$_3$]$_2$ (39%). ^{1}H NMR (400 MHz, CD_3OD): δ (ppm) 8.25 (d, 4H, $^3J_{H\text{-}H}$ = 6.8 Hz, C**H**$_\alpha$), 7.64 (d, 4H, $^3J_{H\text{-}H}$ = 6.8 Hz, C**H**$_\beta$), 7.53 (m, 4H, C**H**$_{ar}$), 7.40 (m, 6H, C**H**$_{ar}$), 7.42 (m, 2H, C**H**$_{ar}$), 6.04 (d, 4H, $^3J_{H\text{-}H}$ = 6.3 Hz, C**H**$_{p\text{-}cym}$), 5.84 (d, 4H, $^3J_{H\text{-}H}$ = 6.3 Hz, C**H**$_{p\text{-}cym}$), 5.83 (s, 2H, C**H**$_{dobq}$), 2.91 (sept, 2H, $^3J_{H\text{-}H}$ = 6.9 Hz, C**H**(CH$_3$)$_2$), 2.23 (s, 6H, C**H**$_3$), 1.39 (d, 12H, $^3J_{H\text{-}H}$ = 6.9 Hz, CH(C**H**$_3$)$_2$). ^{13}C{^{1}H} NMR (100 MHz, CD_3OD): δ (ppm) 185.42 (**C**=O), 154.03 (**C**$_L$), 152.78 (**C**$_L$), 131.80 (**C**H$_{ar}$), 130.49 (**C**H$_{ar}$), 128.10 (**C**H$_{ar}$), 124.68 (**C**$_L$), 105.01 (**C**$_{p\text{-}cym}$), 102.75 (**C**H$_{dobq}$), 99.96 (**C**$_{p\text{-}cym}$), 84.81 (**C**H$_{p\text{-}cym}$), 83.29 (**C**H$_{p\text{-}cym}$), 32.73 (**C**H(CH$_3$)$_2$), 22.53 (CH(**C**H$_3$)$_2$), 18.20 (**C**H$_3$).

[*trans*-5][CF$_3$SO$_3$]$_2$ (61%). ^{1}H NMR (400 MHz, CD_3OD): δ (ppm) 8.38 (d, 4H, $^3J_{H\text{-}H}$ = 6.8 Hz, C**H**$_\alpha$), 7.89 (d, 4H, $^3J_{H\text{-}H}$ = 6.8 Hz, C**H**$_\beta$), 7.83 (m, 4H, C**H**$_{ar}$), 7.58 (m, 6H, C**H**$_{ar}$), 7.36 (m, 2H, C**H**$_{ar}$), 5.98 (d, 4H, $^3J_{H\text{-}H}$ = 6.3 Hz, C**H**$_{p\text{-}cym}$), 5.79 (d, 4H, $^3J_{H\text{-}H}$ = 6.3 Hz, C**H**$_{p\text{-}cym}$), 5.78 (s, 2H, C**H**$_{dobq}$), 2.86 (sept, 2H, $^3J_{H\text{-}H}$ = 6.9 Hz, C**H**(CH$_3$)$_2$), 2.24 (s, 6H, C**H**$_3$), 1.32 (d, 12H, $^3J_{H\text{-}H}$ = 6.9 Hz, CH(C**H**$_3$)$_2$). ^{13}C{^{1}H} NMR (100 MHz, CD_3OD): δ (ppm) 185.5 (**C**=O), 154.31 (**C**$_L$), 152.98 (**C**$_L$), 131.99 (**C**H$_{ar}$), 130.72 (**C**H$_{ar}$), 128.39 (**C**H$_{ar}$), 124.85 (**C**$_L$), 105.19 (**C**$_{p\text{-}cym}$),

102.62 (**C**H_{dobq}), 99.84 (**C**$_{p\text{-}cym}$), 84.71 (**C**$H_{p\text{-}cym}$), 83.49 (**C**$H_{p\text{-}cym}$), 32.73 (**C**$H(CH_3)_2$), 22.53 ($CH(\mathbf{C}H_3)_2$), 18.20 (**C**H_3).

[6][CF_3SO_3]$_2$: Red solid, Yield: 0.1 mmol (62%). IR (cm^{-1}): 3066 (w, $CH_{p\text{-}cym}$), 1611 (s, C=C_L), 1520 (s, C=O), 1256 (s, CF_3). UV-visible: (1.0×10^{-5} M, CH_2Cl_2, 298 K): λ_{max} 319 nm (ε = 94 518 $M^{-1} \cdot cm^{-1}$). ESI-MS: 1120 [M – CF_3SO_3]$^+$, 939 [M – L^2 – CF_3SO_3]$^+$, 758 [M – 2 L^2 – CF_3SO_3]$^+$. Calcd for $C_{54}H_{52}F_6N_2O_{10}Ru_2S_2$: C, 51.10; H, 4.13; N, 2.21. Found: C, 51.36; H, 3.97; N, 2.43.

[*cis*-6][CF_3SO_3]$_2$ (38%). ^{1}H NMR (400 MHz, CD_3OD): δ (ppm) 8.10 (d, 4H, $^3J_{H\text{-}H}$ = 6.8 Hz, C**H**$_\alpha$), 7.65 (m, 4H, C**H**$_{ar}$), 7.44 (d, 4H, $^3J_{H\text{-}H}$ = 6.8 Hz, C**H**$_\beta$), 7.40 (m, 6H, C**H**$_{ar}$), 7.36 (d, 2H, $^3J_{H\text{-}H}$ = 16.4 Hz, C**H**=CH), 6.87 (d, 2H, $^3J_{H\text{-}H}$ = 16.4 Hz, CH=C**H**), 6.03 (d, 4H, $^3J_{H\text{-}H}$ = 6.3 Hz, C**H**$_{p\text{-}cym}$), 5.84 (s, 2H, C**H**$_{dobq}$), 5.80 (d, 4H, $^3J_{H\text{-}H}$ = 6.3 Hz, C**H**$_{p\text{-}cym}$), 2.90 (sept, 2H, $^3J_{H\text{-}H}$ = 6.9 Hz, C**H**$(CH_3)_2$), 2.20 (s, 6H, C**H**$_3$), 1.38 (d, 12H, $^3J_{H\text{-}H}$ = 6.9 Hz, $CH(\mathbf{C}H_3)_2$). ^{13}C{^{1}H} NMR (100 MHz, CD_3OD): δ(ppm) 185.44 (**C**=O), 153.61 (**C**$_L$), 149.89 (**C**$_L$), 130.56 (**C**H_{ar}), 129.90 (**C**H_{ar}), 128.61 (**C**H_{ar}), 124.58 (**C**$_L$), 105.13 (**C**$_{p\text{-}cym}$), 102.66 (**C**H_{dobq}), 100.01 (**C**$_{p\text{-}cym}$), 84.85 (**C**$H_{p\text{-}cym}$), 83.16 (**C**$H_{p\text{-}cym}$), 32.62 (**C**$H(CH_3)_2$), 22.56 ($CH(\mathbf{C}H_3)_2$), 18.20 (**C**H_3).

[*trans*-6][CF_3SO_3]$_2$ (62%). ^{1}H NMR (400 MHz, CD_3OD): δ (ppm) 8.24 (d, 4H, $^3J_{H\text{-}H}$ = 6.8 Hz, C**H**$_\alpha$), 7.71 (d, 4H, $^3J_{H\text{-}H}$ = 6.8 Hz, C**H**$_\beta$), 7.65 (d, 2H, $^3J_{H\text{-}H}$ = 16.4 Hz, C**H**=CH), 7.38 (m, 4H, C**H**$_{ar}$), 7.20 (m, 6H, C**H**$_{ar}$), 7.25 (d, 2H, $^3J_{H\text{-}H}$ = 16.4 Hz, CH=C**H**), 5.97 (d, 4H, $^3J_{H\text{-}H}$ = 6.3 Hz, C**H**$_{p\text{-}cym}$), 5.77 (d, 4H, $^3J_{H\text{-}H}$ = 6.3 Hz, C**H**$_{p\text{-}cym}$), 5.76 (s, 2H, C**H**$_{dobq}$), 2.84 (sept, 2H, $^3J_{H\text{-}H}$ = 6.9 Hz, C**H**$(CH_3)_2$), 2.22 (s, 6H, C**H**$_3$), 1.32 (d, 12H, $^3J_{H\text{-}H}$ = 6.9 Hz, $CH(\mathbf{C}H_3)_2$). ^{13}C{^{1}H} NMR (100 MHz, CD_3OD): δ (ppm) 185.44 (**C**=O), 153.96 (**C**$_L$), 150.19 (**C**$_L$), 130.83 (**C**H_{ar}), 130.05 (**C**H_{ar}), 128.78 (**C**H_{ar}), 124.78 (**C**$_L$), 104.92 (**C**$_{p\text{-}cym}$), 102.54 (**C**H_{dobq}), 99.91 (**C**$_{p\text{-}cym}$), 84.75 (**C**$H_{p\text{-}cym}$), 83.16 (**C**$H_{p\text{-}cym}$), 32.57 (**C**$H(CH_3)_2$), 22.53 ($CH(\mathbf{C}H_3)_2$), 18.20 (**C**H_3).

[7][CF_3SO_3]$_2$: Red solid, Yield: 0.11 mmol (68%). IR (cm^{-1}): 3070 (w, $CH_{p\text{-}cym}$), 1616 (s, C=C_L), 1521 (s, C=O), 1259 (s, CF_3). UV-visible: (1.0×10^{-5} M, CH_2Cl_2, 298 K): λ_{max} 237 nm (ε = 46 681 $M^{-1} \cdot cm^{-1}$), 418 nm (ε = 11 262 $M^{-1} \cdot cm^{-1}$), 484 nm (ε = 11 088 $M^{-1} \cdot cm^{-1}$). ESI-MS: 944 [M – CF_3SO_3]$^+$, 851 [M – L^3 – CF_3SO_3]$^+$. Calcd for $C_{40}H_{44}F_6N_2O_{10}Ru_2S_2 \cdot H_2O$: C, 43.24; H, 4.17; N, 2.52. Found: C, 43.04; H, 3.97; N, 2.79.

[*cis*-7][CF_3SO_3]$_2$ (38%). ^{1}H NMR (400 MHz, CD_3OD): δ (ppm) 8.07 (d, 4H, $^3J_{H\text{-}H}$ = 6.6 Hz, C**H**$_\alpha$), 7.26 (d, 4H, $^3J_{H\text{-}H}$ = 6.6 Hz, C**H**$_\beta$), 5.99 (d, 4H, $^3J_{H\text{-}H}$ = 6.4 Hz, C**H**$_{p\text{-}cym}$), 5.76 (s, 2H, C**H**$_{dobq}$), 5.73 (d, 4H, $^3J_{H\text{-}H}$ = 6.4 Hz, C**H**$_{p\text{-}cym}$), 2.80 (m, 2H, C**H**$(CH_3)_2$), 2.36 (s, 6H,

$CH_\beta CC\mathbf{H}_3$), 2.16 (s, 6H, C$\mathbf{H}_3$), 1.38 (d, 12H, $^3J_{H\text{-}H}$ = 6.9 Hz, CH(C$\mathbf{H}_3$)$_2$). $^{13}C\{^1H\}$ NMR (100 MHz, CD_3OD): δ (ppm) 185.31 (**C**=O), 153.88 ($\mathbf{C}_L$), 153.23 ($\mathbf{C}_L$), 128.47 ($\mathbf{C}_L$), 105.03 ($\mathbf{C}_{p\text{-}cym}$), 102.53 ($\mathbf{C}H_{dobq}$), 99.94 ($\mathbf{C}_{p\text{-}cym}$), 84.75 ($\mathbf{C}H_{p\text{-}cym}$), 83.05 ($\mathbf{C}H_{p\text{-}cym}$), 32.57 ($\mathbf{C}H(CH_3)_2$), 22.52 (CH($\mathbf{C}H_3$)$_2$), 21.00 ($CH_\beta CC\mathbf{H}_3$), 18.13 ($\mathbf{C}H_3$).

[*trans*-7][CF_3SO_3]$_2$ (62%). ^{1}H NMR (400 MHz, CD_3OD): δ (ppm) 8.15 (d, 4H, $^3J_{H\text{-}H}$ = 6.6 Hz, C$\mathbf{H}_\alpha$), 7.41 (d, 4H, $^3J_{H\text{-}H}$ = 6.6 Hz, C$\mathbf{H}_\beta$), 5.93 (d, 4H, $^3J_{H\text{-}H}$ = 6.4 Hz, C$\mathbf{H}_{p\text{-}cym}$), 5.76 (d, 4H, $^3J_{H\text{-}H}$ = 6.4 Hz, C$\mathbf{H}_{p\text{-}cym}$), 5.69 (s, 2H, C$\mathbf{H}_{dobq}$), 2.80 (m, 2H, C$\mathbf{H}$(CH$_3$)$_2$), 2.47 (s, 6H, $CH_\beta CC\mathbf{H}_3$), 2.18 (s, 6H, C$\mathbf{H}_3$), 1.30 (d, 12H, $^3J_{H\text{-}H}$ = 6.9 Hz, CH(C$\mathbf{H}_3$)$_2$). $^{13}C\{^1H\}$ NMR (100 MHz, CD_3OD): δ (ppm) 185.38 (**C**=O), 154.07 ($\mathbf{C}_L$), 153.42 ($\mathbf{C}_L$), 128.37 ($\mathbf{C}_L$), 104.84 ($\mathbf{C}_{p\text{-}cym}$), 102.44 ($\mathbf{C}H_{dobq}$), 99.78 ($\mathbf{C}_{p\text{-}cym}$), 84.61 ($\mathbf{C}H_{p\text{-}cym}$), 83.35 ($\mathbf{C}H_{p\text{-}cym}$), 32.54 ($\mathbf{C}H(CH_3)_2$), 22.50 (CH($\mathbf{C}H_3$)$_2$), 21.02 ($CH_\beta C\mathbf{C}H_3$), 18.14 ($\mathbf{C}H_3$).

[8][CF_3SO_3]$_2$: Red solid, Yield: 0.09 mmol (56%). IR (cm^{-1}): 3066 (w, $CH_{p\text{-}cym}$), 1622 (s, C=C_L), 1515 (s, C=O), 1263 (s, CF_3). UV-visible: (1.0×10^{-5} M, CH_2Cl_2, 298 K): λ_{max} 228 nm (ε = 9 889 $M^{-1} \cdot cm^{-1}$), 307 nm (ε = 4 947 $M^{-1} \cdot cm^{-1}$), 501 nm (ε = 4 101 $M^{-1} \cdot cm^{-1}$). ESI-MS: 1028 $[M - CF_3SO_3]^+$, 893 $[M - L^4 - CF_3SO_3]^+$. Calcd for $C_{46}H_{56}F_6N_2O_{10}Ru_2S_2$: C, 46.93; H, 4.79; N, 2.38. Found: C, 46.54; H, 4.87; N, 2.26.

[*cis*-8][CF_3SO_3]$_2$ (32%). ^{1}H NMR (400 MHz, CD_3OD): δ (ppm) 8.15 (d, 4H, $^3J_{H\text{-}H}$ = 6.9 Hz, C$\mathbf{H}_\alpha$), 7.47 (d, 4H, $^3J_{H\text{-}H}$ = 6.9 Hz, C$\mathbf{H}_\beta$), 5.98 (d, 4H, $^3J_{H\text{-}H}$ = 6.4 Hz, C$\mathbf{H}_{p\text{-}cym}$), 5.78 (d, 4H, $^3J_{H\text{-}H}$ = 6.4 Hz, C$\mathbf{H}_{p\text{-}cym}$), 5.77 (s, 2H, C$\mathbf{H}_{dobq}$), 2.83 (m, 2H, C$\mathbf{H}$(CH$_3$)$_2$), 2.16 (s, 6H, C$\mathbf{H}_3$), 1.34 (d, 12H, $^3J_{H\text{-}H}$ = 6.9 Hz, CH(C$\mathbf{H}_3$)$_2$) 1.22 (s, 18H, C(C$\mathbf{H}_3$)$_3$). $^{13}C\{^1H\}$ NMR (100 MHz, CD_3OD): δ (ppm) 185.45 (**C**=O), 153.49($\mathbf{C}_L$), 124.76 ($\mathbf{C}_L$), 105.05 ($\mathbf{C}_{p\text{-}cym}$), 102.63 ($\mathbf{C}H_{dobq}$), 99.78 ($\mathbf{C}_{p\text{-}cym}$), 84.71 ($\mathbf{C}H_{p\text{-}cym}$), 83.28 ($\mathbf{C}H_{p\text{-}cym}$), 36.30 ($\mathbf{C}(CH_3)_3$), 32.55 ($\mathbf{C}H(CH_3)_2$), 30.48 (C($\mathbf{C}H_3$)$_3$), 22.51 (CH($\mathbf{C}H_3$)$_2$), 18.12 ($\mathbf{C}H_3$).

[*trans*-8][CF_3SO_3]$_2$ (68%). ^{1}H NMR (400 MHz, CD_3OD): δ (ppm) 8.22 (d, 4H, $^3J_{H\text{-}H}$ = 6.9 Hz, C$\mathbf{H}_\alpha$), 7.61 (d, 4H, $^3J_{H\text{-}H}$ = 6.9 Hz, C$\mathbf{H}_\beta$), 5.92 (d, 4H, $^3J_{H\text{-}H}$ = 6.4 Hz, C$\mathbf{H}_{p\text{-}cym}$), 5.73 (d, 4H, $^3J_{H\text{-}H}$ = 6.4 Hz, C$\mathbf{H}_{p\text{-}cym}$), 5.72 (s, 2H, C$\mathbf{H}_{dobq}$), 2.83 (m, 2H, C$\mathbf{H}$(CH$_3$)$_2$), 2.19 (s, 6H, C$\mathbf{H}_3$), 1.35 (s, 18H, C(C$\mathbf{H}_3$)$_3$), 1.30 (d, 12H, $^3J_{H\text{-}H}$ = 6.9 Hz, CH(C$\mathbf{H}_3$)$_2$). $^{13}C\{^1H\}$ NMR (100 MHz, CD_3OD): δ (ppm) 185.47 (**C**=O), 153.66 ($\mathbf{C}_L$), 124.89 ($\mathbf{C}_L$), 104.83 ($\mathbf{C}_{p\text{-}cym}$), 102.48 ($\mathbf{C}H_{dobq}$), 99.64 ($\mathbf{C}_{p\text{-}cym}$), 84.61 ($\mathbf{C}H_{p\text{-}cym}$), 83.51 ($\mathbf{C}H_{p\text{-}cym}$), 36.17 ($\mathbf{C}(CH_3)_3$), 32.59 ($\mathbf{C}H(CH_3)_2$), 30.41 (C($\mathbf{C}H_3$)$_3$), 22.51 (CH($\mathbf{C}H_3$)$_2$), 18.14 ($\mathbf{C}H_3$).

[9][CF_3SO_3]$_2$: Orange solid, Yield: 0.12 mmol (75%). IR (cm^{-1}): 3068 (w, $CH_{p\text{-}cym}$), 1630 (s, C=C_L), 1540 (s, C=O), 1264 (s, CF_3). UV-visible: (1.0×10^{-5} M, CH_2Cl_2, 298 K): λ_{max} 241 nm (ε = 29 371 $M^{-1} \cdot cm^{-1}$), 311 nm (ε = 25 684 $M^{-1} \cdot cm^{-1}$). ESI-MS: 863 [M – L^1 – $CF_3SO_3]^+$, 708 [M – 2 L^1 – $CF_3SO_3]^+$. Calcd for $C_{46}H_{46}F_6N_2O_{10}Ru_2S_2 \cdot H_2O$: C, 46.62; H, 4.08; N, 2.36. Found: C, 46.64; H, 3.84; N, 2.30.

[*cis*-9][CF_3SO_3]$_2$ (78%). ^{1}H NMR (400 MHz, CD_3OD): δ (ppm) 8.03 (d, 4H, $^3J_{H\text{-}H}$ = 6.8 Hz, C**H**$_\alpha$), 7.52 (d, 4H, $^3J_{H\text{-}H}$ = 6.8 Hz, C**H**$_\beta$), 7.36 (m, 4H, C**H**$_{ar}$), 7.29 (m, 2H, C**H**$_{ar}$), 7.19 (m, 4H, C**H**$_{ar}$), 5.93 (d, 4H, $^3J_{H\text{-}H}$ = 6.4 Hz, C**H**$_{p\text{-}cym}$), 5.76 (d, 4H, $^3J_{H\text{-}H}$ = 6.4 Hz, C**H**$_{p\text{-}cym}$), 2.84 (sept, 2H, $^3J_{H\text{-}H}$ = 6.9 Hz, C**H**$(CH_3)_2$), 2.22 (s, 6H, C**H**$_3$), 1.37 (d, 12H, $^3J_{H\text{-}H}$ = 6.9 Hz, CH(C**H**$_3)_2$). ^{13}C{^{1}H} NMR (100 MHz, CD_3OD): δ (ppm) 172.25 (**C**=O), 153.67 (**C**$_L$), 152.56 (**C**$_L$), 131.92 (**C**H_{ar}), 130.50 (**C**H_{ar}), 127.85 (**C**H_{ar}), 124.31 (**C**$_L$), 98.69 (**C**$_{ar}$), 83.58 (**C**$H_{p\text{-}cym}$), 83.03 (**C**$H_{p\text{-}cym}$), 32.33 (**C**$H(CH_3)_2$), 22.51 (CH(**C**$H_3)_2$), 18.08 (**C**H_3).

[*trans*-9][CF_3SO_3]$_2$ (22%). ^{1}H NMR (400 MHz, CD_3OD): δ (ppm) 8.52 (d, 4H, $^3J_{H\text{-}H}$ = 6.8 Hz, C**H**$_\alpha$), 8.03 (m, 4H, C**H**$_\beta$), 7.92 (d, 4H, $^3J_{H\text{-}H}$ = 7.9 Hz, C**H**$_{ar}$), 7.61 (m, 6H, C**H**$_{ar}$), 5.90 (d, 4H, $^3J_{H\text{-}H}$ = 6.4 Hz, C**H**$_{p\text{-}cym}$), 5.67 (d, 4H, $^3J_{H\text{-}H}$ = 6.4 Hz, C**H**$_{p\text{-}cym}$), 2.56 (sept, 2H, $^3J_{H\text{-}H}$ = 6.9 Hz, C**H**$(CH_3)_2$), 1.97 (s, 6H, C**H**$_3$), 0.97 (d, 12H, $^3J_{H\text{-}H}$ = 6.9 Hz, CH(C**H**$_3)_2$). ^{13}C{^{1}H} NMR (100 MHz, CD_3OD): δ (ppm) 172.25 (**C**=O), 154.38 (**C**$_L$), 151.56 (**C**$_L$), 132.18 (**C**H_{ar}), 130.85 (**C**H_{ar}), 128.46 (**C**H_{ar}), 125.30 (**C**$_L$), 99.28 (**C**$_{ar}$), 83.98 (**C**$H_{p\text{-}cym}$), 81.08 (**C**$H_{p\text{-}cym}$), 32.56 (**C**$H(CH_3)_2$), 22.13 (CH(**C**$H_3)_2$), 17.96 (**C**H_3).

[10][CF_3SO_3]$_2$: Orange solid, Yield: 0.11 mmol (68%). IR (cm^{-1}): 3067 (w, $CH_{p\text{-}cym}$), 1632 (s, C=C_L), 1618 (s, C_H=C_H), 1259 (s, CF_3). UV-visible: (1.0×10^{-5} M, CH_2Cl_2, 298 K): λ_{max} 320 nm (ε = 83 197 $M^{-1} \cdot cm^{-1}$). ESI-MS: 889 [M – L^2 – $CF_3SO_3]^+$, 708 [M – 2 L^2 – $CF_3SO_3]^+$. Calcd for $C_{50}H_{50}F_6N_2O_{10}Ru_2S_2$: C, 49.26; H, 4.13; N, 2.30. Found: C, 49.21; H, 4.11; N, 2.19.

[*cis*-10][CF_3SO_3]$_2$ (20%). ^{1}H NMR (400 MHz, CD_3OD): δ (ppm) 8.41 (d, 2H, $^3J_{H\text{-}H}$ = 6.5 Hz, C**H**$_\alpha$), 8.39 (d, 2H, $^3J_{H\text{-}H}$ = 6.5 Hz, C**H**$_\alpha$), 7.86 (d, 2H, $^3J_{H\text{-}H}$ = 6.5 Hz, C**H**$_\beta$), 7.77 (d, 1H, $^3J_{H\text{-}H}$ = 16.4 Hz, C**H**=CH), 7.70 (m, 4H, C**H**$_{ar}$), 7.69 (d, 2H, $^3J_{H\text{-}H}$ = 6.5 Hz, C**H**$_\beta$), 7.65 (m, 2H, C**H**$_{ar}$), 7.64 (d, 1H, $^3J_{H\text{-}H}$ = 16.4 Hz, C**H**=CH), 7.44 (m, 2H, C**H**$_{ar}$), 7.40 (m, 2H, C**H**$_{ar}$), 7.35 (d, 1H, $^3J_{H\text{-}H}$ = 16.4 Hz, C**H**=CH), 7.25 (d, 1H, $^3J_{H\text{-}H}$ = 16.4 Hz, CH=C**H**), 5.88 (d, 2H, $^3J_{H\text{-}H}$ = 6.8 Hz, C**H**$_{p\text{-}cym}$), 5.84 (d, 2H, $^3J_{H\text{-}H}$ = 6.8 Hz, C**H**$_{p\text{-}cym}$), 5.65 (d, 2H, $^3J_{H\text{-}H}$ = 6.8 Hz, C**H**$_{p\text{-}cym}$), 5.61 (d, 2H, $^3J_{H\text{-}H}$ = 6.8 Hz, C**H**$_{p\text{-}cym}$), 2.55 (sept, 2H, $^3J_{H\text{-}H}$ = 6.9 Hz, C**H**$(CH_3)_2$), 2.15 (s, 3H, C**H**$_3$), 1.96 (s, 3H, C**H**$_3$),1.31 (d, 6H, $^3J_{H\text{-}H}$ = 6.9 Hz, CH(C**H**$_3)_2$), 1.01 (d, 6H, $^3J_{H\text{-}H}$ = 6.9 Hz,

$CH(C\mathbf{H}_3)_2$). $^{13}C\{^1H\}$ NMR (100 MHz, CD_3OD): δ (ppm) 172.32 (**C**=O), 153.78 ($\mathbf{C}_L$), 153.68 ($\mathbf{C}_L$), 138.01 (**C**H=CH), 129.80 ($\mathbf{C}H_{ar}$), 128.40 ($\mathbf{C}H_{ar}$), 124.71 (**C**H=CH), 124.51 (**C**H=CH), 124.42 ($\mathbf{C}_L$), 123.92 ($\mathbf{C}_L$), 98.91 ($\mathbf{C}_{ar}$), 83.54 ($\mathbf{C}H_{p\text{-}cym}$), 82.83 ($\mathbf{C}H_{p\text{-}cym}$), 32.47 ($\mathbf{C}H(CH_3)_2$), 22.46 ($CH(\mathbf{C}H_3)_2$), 18.06 ($\mathbf{C}H_3$).

[*trans*-10][CF_3SO_3]$_2$ (80%). ^1H NMR (400 MHz, CD_3OD): δ (ppm) 7.89 (d, 4H, $^3J_{H\text{-}H}$ = 6.7 Hz, $C\mathbf{H}_\alpha$), 7.45 (d, 2H, $^3J_{H\text{-}H}$ = 16.4 Hz, C**H**=CH), 7.40 (d, 4H, $^3J_{H\text{-}H}$ = 6.7 Hz, $C\mathbf{H}_\beta$), 7.31 (m, 4H, $C\mathbf{H}_{ar}$),7.22 (m, 2H, $C\mathbf{H}_{ar}$), 7.14 (d, 4H, $^3J_{H\text{-}H}$ = 6.8 Hz, $C\mathbf{H}_{ar}$), 6.89 (d, 2H, $^3J_{H\text{-}H}$ = 16.4 Hz, CH=C**H**), 5.91 (d, 4H, $^3J_{H\text{-}H}$ = 6.4 Hz, $C\mathbf{H}_{p\text{-}cym}$), 5.73 (d, 4H, $^3J_{H\text{-}H}$ = 6.4 Hz, $C\mathbf{H}_{p\text{-}cym}$), 2.82 (sept, 2H, $^3J_{H\text{-}H}$ = 6.9 Hz, $C\mathbf{H}(CH_3)_2$), 2.19 (s, 6H, $C\mathbf{H}_3$), 1.36 (d, 12H, $^3J_{H\text{-}H}$ = 6.9 Hz, $CH(C\mathbf{H}_3)_2$). $^{13}C\{^1H\}$ NMR (100 MHz, CD_3OD): δ (ppm) 172.32 (**C**=O), 153.29 ($\mathbf{C}_L$), 150.11 ($\mathbf{C}_L$), 139.12 (**C**H=CH), 130.72 ($\mathbf{C}H_{ar}$), 130.04 ($\mathbf{C}H_{ar}$), 128.71 ($\mathbf{C}H_{ar}$), 124.35 (**C**H=CH), 123.97 ($\mathbf{C}_L$), 98.91 ($\mathbf{C}_{ar}$), 83.54 ($\mathbf{C}H_{p\text{-}cym}$), 82.83 ($\mathbf{C}H_{p\text{-}cym}$), 32.47 ($\mathbf{C}H(CH_3)_2$), 22.46 ($CH(\mathbf{C}H_3)_2$), 18.06 ($\mathbf{C}H_3$).

[11][CF_3SO_3]$_2$: Orange solid, Yield: 0.13 mmol (81%). IR (cm^{-1}): 3069 (w, $CH_{p\text{-}cym}$), 1627 (s, C=C_L), 1537 (s, C=O), 1267 (s, CF_3). UV-visible: (1.0×10^{-5} M, CH_2Cl_2, 298 K): λ_{max} 254 nm (ε = 2 180 $M^{-1} \cdot cm^{-1}$), 307 nm (ε = 4 947 $M^{-1} \cdot cm^{-1}$), 501 (ε = 4 101 $M^{-1} \cdot cm^{-1}$). ESI-MS: 801 $[M - L^3 - CF_3SO_3]^+$, 708 $[M - 2\ L^3 - CF_3SO_3]^+$. Calcd for $C_{36}H_{42}F_6N_2O_{10}Ru_2S_2$: C, 41.46; H, 4.06; N, 2.69. Found: C, 41.24; H, 4.05; N, 2.61.

[*cis*-11][CF_3SO_3]$_2$ (70%). ^1H NMR (400 MHz, CD_3OD): δ (ppm) 7.84 (d, 4H, $^3J_{H\text{-}H}$ = 6.6 Hz, $C\mathbf{H}_\alpha$), 7.15 (m, 4H, $C\mathbf{H}_\beta$), 5.89 (d, 4H, $^3J_{H\text{-}H}$ = 6.4 Hz, $C\mathbf{H}_{p\text{-}cym}$), 5.72 (d, 4H, $^3J_{H\text{-}H}$ = 6.4 Hz, $C\mathbf{H}_{p\text{-}cym}$), 2.80 (m, 2H, $C\mathbf{H}(CH_3)_2$), 2.40 (s, 6H, $CH_\beta CC\mathbf{H}_3$), 2.18 (s, 6H, $C\mathbf{H}_3$), 1.34 (d, 12H, $^3J_{H\text{-}H}$ = 6.9 Hz, $CH(C\mathbf{H}_3)_2$). $^{13}C\{^1H\}$ NMR (100 MHz, CD_3OD): δ (ppm) 172.10 (**C**=O), 153.63 ($\mathbf{C}_L$), 152.85 ($\mathbf{C}_L$), 103.45 ($\mathbf{C}_L$), 99.68 ($\mathbf{C}H_{p\text{-}cym}$), 83.53 ($\mathbf{C}H_{p\text{-}cym}$), 82.82 ($\mathbf{C}H_{p\text{-}cym}$), 32.45 ($\mathbf{C}H(CH_3)_2$), 22.47 ($CH(\mathbf{C}H_3)_2$), 21.30 ($CH_\beta\mathbf{C}CH_3$), 18.02 ($\mathbf{C}H_3$).

[*trans*-11][CF_3SO_3]$_2$ (30%). ^1H NMR (400 MHz, CD_3OD): δ (ppm) 8.32 (d, 4H, $^3J_{H\text{-}H}$ = 6.6 Hz, $C\mathbf{H}_\alpha$), 7.56 (m, 4H, $C\mathbf{H}_\beta$), 5.86 (d, 4H, $^3J_{H\text{-}H}$ = 6.4 Hz, $C\mathbf{H}_{p\text{-}cym}$), 5.62 (d, 4H, $^3J_{H\text{-}H}$ = 6.4 Hz, $C\mathbf{H}_{p\text{-}cym}$), 2.80 (m, 2H, $C\mathbf{H}(CH_3)_2$), 2.56 (s, 6H, $CH_\beta CC\mathbf{H}_3$), 1.92 (s, 6H, $C\mathbf{H}_3$), 0.99 (d, 12H, $^3J_{H\text{-}H}$ = 6.9 Hz, $CH(C\mathbf{H}_3)_2$). $^{13}C\{^1H\}$ NMR (100 MHz, CD_3OD): δ (ppm) 171.68 (**C**=O), 154.52 ($\mathbf{C}_L$), 153.45 ($\mathbf{C}_L$), 104.96 ($\mathbf{C}_L$), 99.17 ($\mathbf{C}H_{p\text{-}cym}$), 83.85 ($\mathbf{C}H_{p\text{-}cym}$), 80.98 ($\mathbf{C}H_{p\text{-}cym}$), 32.23 ($\mathbf{C}H(CH_3)_2$), 22.12 ($CH(\mathbf{C}H_3)_2$), 21.13 ($CH_\beta\mathbf{C}CH_3$), 17.87 ($\mathbf{C}H_3$).

[12][CF_3SO_3]$_2$: Orange solid, Yield: 0.12 mmol (75%). IR (cm^{-1}): 3069 (w, $CH_{p\text{-}cym}$), 1630 (s, C=C_L), 1538 (s, C=O), 1274 (s, CF_3). UV-visible: (1.0×10^{-5} M, CH_2Cl_2, 298 K): λ_{max} 227 nm (ε = 4 589 $M^{-1} \cdot cm^{-1}$), 259 nm (ε = 3 429 $M^{-1} \cdot cm^{-1}$). ESI-MS: 843 $[M - L^4 - CF_3SO_3]^+$, 708 $[M - 2\ L^4 - CF_3SO_3]^+$. Calcd for $C_{42}H_{54}F_6N_2O_{10}Ru_2S_2$: C, 44.76; H, 4.83; N, 2.49. Found: C, 44.86; H, 4.81; N, 2.46.

[*cis*-12][CF_3SO_3]$_2$ (38%). ^{1}H NMR (400 MHz, CD_3OD): δ (ppm) 8.40 (d, 2H, $^3J_{H\text{-}H}$ = 6.8 Hz, C**H**$_\alpha$), 8.08 (d, 2H, $^3J_{H\text{-}H}$ = 6.8 Hz, C**H**$_\beta$), 7.59 (d, 2H, $^3J_{H\text{-}H}$ = 6.8 Hz, C**H**$_\alpha$), 7.42 (d, 2H, $^3J_{H\text{-}H}$ = 6.8 Hz, C**H**$_\beta$), 5.95 (d, 2H, $^3J_{H\text{-}H}$ = 6.4 Hz, C**H**$_{p\text{-}cym}$), 5.79 (d, 2H, $^3J_{H\text{-}H}$ = 6.4 Hz, C**H**$_{p\text{-}cym}$), 5.76 (d, 2H, $^3J_{H\text{-}H}$ = 6.4 Hz, C**H**$_{p\text{-}cym}$), 5.57 (d, 2H, $^3J_{H\text{-}H}$ = 6.4 Hz, C**H**$_{p\text{-}cym}$), 2.85 (m, 2H, C**H**$(CH_3)_2$), 2.21 (s, 3H, C**H**$_3$), 2.13 (s, 3H, C**H**$_3$), 1.37 (d, 6H, $^3J_{H\text{-}H}$ = 6.9 Hz, CH(C**H**$_3)_2$), 1.34 (d, 6H, $^3J_{H\text{-}H}$ = 6.9 Hz, CH(C**H**$_3)_2$), 1.33 (s, 12H, C(C**H**$_3)_3$), 1.23 (s, 6H, C(C**H**$_3)_3$). ^{13}C{^{1}H} NMR (100 MHz, CD_3OD): δ (ppm) 171.68 (**C**=O), 153.69 (**C**$_L$), 125.39 (**C**$_L$), 98.90 (**C**H$_{p\text{-}cym}$), 83.74 (**C**H$_{p\text{-}cym}$), 82.02 (**C**H$_{p\text{-}cym}$), 36.43 (**C**$(CH_3)_3$), 32.48 (**C**H$(CH_3)_2$), 32.32 (**C**H$(CH_3)_2$), 30.51 (C(**C**$H_3)_3$), 22.62 (**C**$(CH_3)_3$), 22.45 (CH(**C**H_3)), 17.88 (**C**H_3).

[*trans*-12][CF_3SO_3]$_2$ (62%). ^{1}H NMR (400 MHz, CD_3OD): δ (ppm) 8.39 (d, 4H, $^3J_{H\text{-}H}$ = 6.8 Hz, C**H**$_\alpha$), 7.76 (d, 4H, $^3J_{H\text{-}H}$ = 6.8 Hz, C**H**$_\beta$), 5.85 (d, 4H, $^3J_{H\text{-}H}$ = 6.4 Hz, C**H**$_{p\text{-}cym}$), 5.52 (d, 4H, $^3J_{H\text{-}H}$ = 6.4 Hz, C**H**$_{p\text{-}cym}$), 2.57 (m, 2H, C**H**$(CH_3)_2$), 1.91 (s, 6H, C**H**$_3$), 1.42 (s, 18H, C(C**H**$_3)_3$), 0.99 (d, 12H, $^3J_{H\text{-}H}$ = 6.9 Hz, CH(C**H**$_3)_2$). ^{13}C{^{1}H} NMR (100 MHz, CD_3OD): δ (ppm) 171.68 (**C**=O), 153.17 (**C**$_L$), 124.42 (**C**$_L$), 98.90 (**C**H$_{p\text{-}cym}$), 83.60 (**C**H$_{p\text{-}cym}$), 81.30 (**C**H$_{p\text{-}cym}$), 36.43 (**C**$(CH_3)_3$), 32.22 (**C**H$(CH_3)_2$), 30.57 (C(**C**$H_3)_3$), 22.19 (CH(**C**H_3)), 17.84 (**C**H_3).

[13][CF_3SO_3]$_2$: A CD_3OD solution (10 mL) of [**10**][CF_3SO_3]$_2$ (50 mg, 0.04 mmol) was placed in a UV reactor (Luzchem Research, photoreactor, λ = 365 nm) for 60 hours. Then the solvent was removed under vacuum to isolate [**13**][CF_3SO_3]$_2$ as a red solid, yield: 0.04 mmol (98%). ^{1}H NMR (400 MHz, CD_3OD): δ (ppm) 8.05 (d, 2H, $^3J_{H\text{-}H}$ = 6.1 Hz, C**H**$_\alpha$), 7.90 (d, 2H, $^3J_{H\text{-}H}$ = 6.0 Hz, C**H**$_\alpha$), 7.50 (d, 2H, $^3J_{H\text{-}H}$ = 6.1 Hz, C**H**$_\beta$), 7.18 (m, 10H, C**H**$_{ar}$), 7.11 (m, 2H, C**H**$_\beta$), 5.99 (d, 4H, $^3J_{H\text{-}H}$ = 6.1 Hz, C**H**$_{p\text{-}cym}$), 5.81 (d, 4H, $^3J_{H\text{-}H}$ = 6.1 Hz, C**H**$_{p\text{-}cym}$), 4.81 (d, 2H, $^3J_{H\text{-}H}$ = 6.6 Hz, C**H**CH), 4.68 (d, 2H, $^3J_{H\text{-}H}$ = 6.6 Hz, CHC**H**), 2.87 (sept, 2H, $^3J_{H\text{-}H}$ = 6.9 Hz, C**H**$(CH_3)_2$), 2.24 (s, 6H, C**H**$_3$), 1.40 (d, 12H, $^3J_{H\text{-}H}$ = 6.9 Hz, CH(C**H**$_3)_2$). ^{13}C{^{1}H} NMR (100 MHz, CD_3OD): δ (ppm) 172.32 (**C**=O), 154.02 (**C**$_L$), 152.68 (**C**$_L$), 129.26 (**C**H$_{ar}$), 129.19 (**C**H$_{ar}$), 128.98 (**C**H$_{ar}$), 127.63 (**C**$_L$), 125.55 (**C**$_L$), 123.97 (**C**$_L$), 83.14 (**C**H$_{p\text{-}cym}$), 82.85 (**C**H$_{p\text{-}cym}$), 48.94 (**C**HCH), 45.14(CH**C**H), 32.55 (**C**H$(CH_3)_2$), 22.46 (CH(**C**$H_3)_2$), 18.06 (**C**H_3). IR

(cm^{-1}): 3067 (w, $CH_{p\text{-}cym}$), 1632 (s, C=C_L), 1259 (s, CF_3). UV-visible: (1.0×10^{-5} M, CH_2Cl_2, 298 K): λ_{max} 310 nm (ε = 17 266 $M^{-1} \cdot cm^{-1}$). ESI-MS: 1070 $[M - CF_3SO_3]^+$, 708 $[M - C_{26}H_{22}N_2 - CF_3SO_3]^+$. Calcd for $C_{50}H_{50}F_6N_2O_{10}Ru_2S_2 \cdot CH_2Cl_2$: C, 46.97; H, 4.02; N, 2.15. Found: C, 47.51; H, 4.00; N, 2.79.

7.2.4 Synthesis and Characterisation of the ON∩NO bis-chelating Organic Linkers and the Dinuclear, Tetranuclear, and Hexanuclear Arene Ruthenium Complexes

Synthesis of N,N'-Bis{2-(2-hydroxyethoxy)ethyl}ethanediamide **(H_2L^c)**. To a cooled solution of 2-aminoethoxyethanol (−10 °C, 10 mL, 0.1 mol) and triethylamine (13.85 mL, 0.1 mol) in methylene chloride (120 mL) under an inert atmosphere was added dropwise over 1.5 h a solution of oxalyl chloride (4.25 mL, 0.05 mol) in methylene chloride (20 mL). The mixture was stirred overnight, and the precipitated triethylammonium chloride was filtered off. The volume of the mother liquor was reduced to ca. 30 mL, and then THF (60 mL) was added. The precipitated triethylammonium hydrochloride was filtered off. The solvent was removed under reduced pressure, and the residue was washed with THF and dried under vacuum. Yield: 7.2 g, 27 mmol (49%). ^{1}H NMR (500 MHz, $CDCl_3$): δ (ppm), 7,85 (br. s, 2H, N*H*), 3.73–3.75 (m, 4H, OCH_2), 3.60 (t, $^3J_{H-H}$ = 5.25 Hz, 4H, OCH_2), 3.58–3.60 (m, 4H, OCH_2), 3.51–3.54 (m, 4H, OCH_2), 3.11 (q, $^3J_{H-H}$ = 7.3 Hz, 0.6H, [(CH_3CH_2)$_3$NH]Cl), 3.10 (q, $^3J_{H-H}$ = 7.2 Hz, 0.6H, [(CH_3CH_2)$_3$NH]Cl), 2.40 (br.s, 3H, CH_2OH + H_2O), 1.41 (t, $^3J_{H-H}$ = 7.3 Hz, 1.7H, [(CH_3CH_2)$_3$NH]Cl). ESI–MS: *m*/*z* = 265 $[M + H]^+$, 287 $[M + Na]^+$. Elemental Analysis (%): Calcd. for $C_{10}H_{20}N_2O_6 \cdot 0.2[(C_2H_5)_3NH]Cl$: C, 46.10; H, 8.01; N, 10.56 Found: C, 46.49; H, 7.78; N, 10.06. The compound was used without further purification for the synthesis of the dinuclear arene ruthenium complex **14c**.

Synthesis of the Metalla-Clip [(p-Cymene)$_2$Ru$_2$Cl$_2$(μ-L^a)] **(14a)**. To a solution of diethyl-1,2-diazenedicarboxylate (0.35 g, 2.0 mmol) in methanol (10 mL) was added [(*p*-cymene)$_2$Ru$_2$Cl$_2$(μ-Cl)$_2$] (1.1 g, 1.8 mmol) and a solution of triethylamine (0.6 mL, 4.3 mmol) in methanol (7 mL), and the mixture was left to stand overnight at room temperature. The crystalline product formed was filtered off, washed with methanol, and dried in air. Yield: 1.1 g, 1.6 mmol (85.0%). ^{1}H NMR (500 MHz, $CDCl_3$): δ (ppm), 5.44 (d, $^3J_{H-H}$ = 5.5 Hz, 2H,

C**H**$_{p\text{-}cym}$), 5.37 (d, $^3J_{H-H}$ = 5.5 Hz, 2H, C**H**$_{p\text{-}cym}$), 5.32 (d, $^3J_{H-H}$ = 5.5 Hz, 2H, C**H**$_{p\text{-}cym}$), 5.08 (d, $^3J_{H-H}$ = 5.5 Hz, 2H, C**H**$_{p\text{-}cym}$), 4.32 and 4.34 (two overlapped q, $^3J_{H-H}$ = 7.0 Hz, 2 H, OC**H**$_2$CH$_3$), 4.19 and 4.21 (two overlapped q, $^3J_{H-H}$ = 7.0 Hz, 2 H, OC**H**$_2$CH$_3$), 2.74 (sept, $^3J_{H-H}$ = 6.5 Hz, 2H, C**H**(CH$_3$)$_2$), 2.17 (s, 6H, C**H**$_3$), 1.32 (t, $^3J_{H-H}$ = 7.0 Hz, 6H, OCH$_2$C**H**$_3$), 1.20 (t, $^3J_{H-H}$ = 6.5 Hz, 12H, CH(C**H**$_3$)$_2$). IR (cm^{-1}): 1551, 1420, 1337, 1075. ESI–MS: *m*/*z* = 680 [M – Cl]$^+$, 702 [M – HCl + Na]$^+$. Elemental Analysis (%): Calcd. for $C_{26}H_{38}Cl_2N_2O_4Ru_2$: C, 43.64; H, 5.35; N, 3.91. Found: C, 43.29; H, 5.29; N, 4.03.

Synthesis of the Metalla-Clip [(p-Cymene)$_2$Ru$_2$Cl$_2$(μ-L^b)] **(14b)**. To a solution of [(*p*-cymene)$_2$Ru$_2$Cl$_2$(μ-Cl)$_2$] (1.85 g, 3.0 mmol) in warm methanol (80 mL) were added a solution of *N*,*N*′-bis(2-hydroxyethyl)oxamide (0.53 g, 3.0 mmol) in warm methanol (25 mL) and triethylamine (0.85 mL, 6.1 mmol), and the mixture was refluxed overnight. The volume of solvent was reduced to ca. 30 mL, and the precipitate formed was filtered off, washed with methanol, and dried in air. Yield: 2.0 g, 2.8 mmol (93.0%). ^{1}H NMR (500 MHz, CDCl$_3$): δ (ppm), 5.41 (d, $^3J_{H-H}$ = 6.0 Hz, 2H, C**H**$_{p\text{-}cym}$), 5.35 (d, $^3J_{H-H}$ = 6.0 Hz, 2H, C**H**$_{p\text{-}cym}$), 5.33 (d, $^3J_{H-H}$ = 6.0 Hz, 2H, C**H**$_{p\text{-}cym}$), 4.99 (d, $^3J_{H-H}$ = 5.5 Hz, 2H, C**H**$_{p\text{-}cym}$), 4.43–4.47 (m, 2H, OC**H**$_2$), 3.68–3.81 (m, 6H, OC**H**$_2$), 3.31–3.35 (m, 2H, CH$_2$O**H**), 2.68 (sept, $^3J_{H-H}$ = 7.0 Hz, 6H, C**H**(CH$_3$)$_2$), 2.21 (s, 6H, C**H**$_3$), 1.21 (d, $^3J_{H-H}$ = 7.0 Hz, 6H, CH(C**H**$_3$)$_2$), 1.16 (d, $^3J_{H-H}$ = 7.0 Hz, 6H, CH(C**H**$_3$)$_2$). IR (cm^{-1}): 3397, 1594, 1055, 1025, 788. ESI–MS: *m*/*z* = 680 [M – Cl]$^+$, 644 [M – Cl – HCl]$^+$, 322.5 [M – 2Cl]$^{2+}$. Elemental Analysis (%): Calcd. for $C_{26}H_{38}Cl_2N_2O_4Ru_2$: C, 43.64; H, 5.35; N, 3.91. Found: C, 43.60; H, 5.26; N, 3.99.

Synthesis of the Metalla-Clip [(p-Cymene)$_2$Ru$_2$Cl$_2$(μ-L^c)] **(14c)**. To a solution of [(*p*-cymene)$_2$Ru$_2$Cl$_2$(μ-Cl)$_2$] (0.2 g, 0.33 mmol) in methanol (12 mL) were added a solution of *N*,*N*′-bis[2-(2-hydroxyethoxy)ethyl]ethanediamide (0.09 g, 0.33 mmol) in methanol (2 mL) and triethylamine (0.12 mL, 0.7 mmol), and the mixture was refluxed for 20 h. The solvent was removed, and the residue was washed with THF and water and recrystallized from chloroform. Yield: 211 mg, 0.27 mmol (41%). ^{1}H NMR (500 MHz, CDCl$_3$): δ (ppm), 5.41 (d, $^3J_{H-H}$ = 5.5 Hz, 2H, C**H**$_{p\text{-}cym}$), 5.37 (d, $^3J_{H-H}$ = 5.5 Hz, 4H, C**H**$_{p\text{-}cym}$), 5.17 (d, $^3J_{H-H}$ = 5.5 Hz, 2H, C**H**$_{p\text{-}cym}$), 4.09–4.15 (m, 2H, OC**H**$_2$), 3.59–3.77 (m, 14H, OC**H**$_2$), 3.09 (m, 2H, O**H**), 2.73 (sept, $^3J_{H-H}$ = 7.0 Hz, 6H, C**H**(CH$_3$)$_2$), 2.16 (s, 6H, C**H**$_3$), 1.22 (d, $^3J_{H-H}$ = 7.0 Hz, 6H, CH(C**H**$_3$)$_2$), 1.20 (d, $^3J_{H-H}$ = 7.0 Hz, 6H, CH(C**H**$_3$)$_2$). IR (cm^{-1}): 3423, 1597, 1335, 1108, 1052, 876. ESI–MS: *m*/*z* = 768 [M – Cl]$^+$, 733 [M – Cl – HCl]$^+$. Elemental Analysis (%): Calcd. for $C_{30}H_{46}Cl_2N_2O_6Ru_2$: C, 44.83; H, 5.77; N, 3.49. Found: C, 45.36; H, 5.71; N, 3.62.

General Synthetic Method for the Tetracationic Metalla-Rectangles of the General Formula [(p-cymene)$_4$Ru$_4$(μ-bpy)$_2$(μ-L)$_2$]$^{4+}$ ***([15a]$^{4+}$-[15c]$^{4+}$)****, [(p-cymene)$_4$Ru$_4$(μ-bpe)$_2$(μ-L)$_2$]$^{4+}$* ***([16a]$^{4+}$-[16c]$^{4+}$)*** *and [(p-cymene)$_4$Ru$_4$(μ-bpa)$_2$(μ-L)$_2$]$^{4+}$* ***([17a]$^{4+}$-[17c]$^{4+}$)****.*

A mixture of the dinuclear clip (**14a-14c**) of the general formula [(p-cymene)$_2$Ru$_2$Cl$_2$(μ-L)] (0.16 mmol) and 2 equiv of $AgCF_3SO_3$ (0.32 mmol) in methanol (20 mL) was stirred at room temperature for 2 h and the solution was filtered to remove AgCl. To the filtrate, the corresponding 4,4'-bipyridine, 1,2-bis(4-pyridyl)ethylene and 4,4'-azopyridine (0.16 mmol) were added. The mixture was stirred at at room temperature for 24 h, and the solvent removed under vacuum. The residue was dissolved in dichloromethane (20 mL), the extract filtered and concentrated (3 mL) and diethyl ether was slowly added to initiate precipitation of the product as a black, brown, yellow, orange or red solid.

[15a][CF$_3$SO$_3$]$_4$: Orange solid, Yield: 0.055 mmol (68%). ^{1}H NMR (400 MHz, CD_2Cl_2): δ (ppm), 8.00 (d, 8H, $^3J_{H\text{-}H}$ = 5.6 Hz, C**H**$_\alpha$), 7.81 (d, 4H, $^3J_{H\text{-}H}$ = 3.3 Hz, C**H**$_\beta$), 7.67 (d, 4H, $^3J_{H\text{-}H}$ = 5.8 Hz, C**H**$_\beta$), 5.87 – 5.83 (m, 4H, C**H**$_{p\text{-}cym}$), 5.83 – 5.79 (m, 4H, C**H**$_{p\text{-}cym}$), 5.58 – 5.45 (m, 4H, C**H**$_{p\text{-}cym}$), 5.30 – 5.17 (m, 4H, C**H**$_{p\text{-}cym}$), 4.66 (q, 4H, $^3J_{H\text{-}H}$ = 3.1 Hz, C**H$_2$**CH$_3$), 4.62 (q, 4H, $^3J_{H\text{-}H}$ = 3.1 Hz, C**H$_2$**CH$_3$), 2.70 – 2.63 (m, 4H, C**H**(CH$_3$)$_2$), 1.66 (s, 6H, C**H**$_3$), 1.63 (s, 6H, C**H**$_3$), 1.57 (m, 12H, CH$_2$C**H$_3$**), 1.31 (d, 12H, $^3J_{H\text{-}H}$ = 7.0 Hz, CH(C**H**$_3$)$_2$), 1.28 (d, 12H, $^3J_{H\text{-}H}$ = 6.9 Hz, CH(C**H**$_3$)$_2$). ^{13}C{^{1}H} NMR (100 MHz, CD_2Cl_2): δ (ppm), 165.44 (**C**=O), 165.36 (**C**=O), 152.77 (**C**$_{bpy}$), 152.73 (**C**$_{bpy}$), 124.78 (**C**$_{bpy}$), 123.94 (**C**$_{bpy}$), 86.42 (**C**H$_{p\text{-}cym}$), 86.22 (**C**H$_{p\text{-}cym}$), 85.07 (**C**H$_{p\text{-}cym}$), 84.97 (**C**H$_{p\text{-}cym}$), 82.38 (**C**H$_{p\text{-}cym}$), 82.36 (**C**H$_{p\text{-}cym}$), 79.71 (**C**H$_{p\text{-}cym}$), 79.62 (**C**H$_{p\text{-}cym}$), 65.97 (**C**H$_2$CH$_3$), 31.51(**C**H(CH$_3$)$_2$), 22.61 (CH(**C**H$_3$)$_2$), 22.58 (CH(**C**H$_3$)$_2$), 17.91 (**C**H$_3$), 17.87 (**C**H$_3$), 15.39 (CH$_2$**C**H$_3$), 15.37 (CH$_2$**C**H$_3$). IR: υ (cm^{-1}): 3073.9 (w, CH$_{p\text{-}cym}$), 1610 (s, C=O), 1262 (s, CF$_3$). UV-visible: (1.0 × 10^{-5} M, CH_3CN, 298 K): λ_{max} 242 nm (ε = 121 665 M^{-1} · cm^{-1}), 383 nm (ε = 16 285 M^{-1} · cm^{-1}). ESI-MS: 2050 [M – CF_3SO_3]$^+$, 950 [M – 2CF_3SO_3]$^{2+}$. Elemental Analysis (%): Calc. for $C_{76}H_{92}F_{12}N_8O_{20}Ru_4S_4$ ·3 CH_2Cl_2: C, 38.68; H, 4.03; N, 4.57. Found: C, 38.72; H, 4.15; N, 4.76.

[15b][CF$_3$SO$_3$]$_4$: Yellow solid, Yield: 0.06 mmol (75%). ^{1}H NMR (400 MHz, CD_2Cl_2): δ (ppm), 8.48 (d, 8H, $^3J_{H\text{-}H}$ = 6.5 Hz, C**H**$_\alpha$), 7.69 (d, 8H, $^3J_{H\text{-}H}$ = 6.8 Hz, C**H**$_\beta$), 5.79 (d, 4H, $^3J_{H\text{-}H}$ = 5.8 Hz, C**H**$_{p\text{-}cym}$), 5.74 (d, 4H, $^3J_{H\text{-}H}$ = 5.8 Hz, C**H**$_{p\text{-}cym}$), 5.47 (d, 4H, $^3J_{H\text{-}H}$ = 5.8 Hz, C**H**$_{p\text{-}cym}$), 5.29 (d, 4H, $^3J_{H\text{-}H}$ = 5.8 Hz, C**H**$_{p\text{-}cym}$), 4.51 – 4.46 (m, 8H, C**H$_2$**CH$_2$), 4.51 – 4.46 (m, 8H, CH$_2$C**H$_2$**), 2.83 – 2.76 (m, 4H, C**H**(CH$_3$)$_2$), 1.76 (s, 12H, C**H**$_3$), 1.32 (d, 12H, $^3J_{H\text{-}H}$ = 7.0 Hz,

CH(C**H**$_3$)$_2$), 1.23 (d, 12H, $^3J_{H\text{-}H}$ = 6.9 Hz, CH(C**H**$_3$)$_2$). ^{13}C{^{1}H} NMR (100 MHz, CD_2Cl_2): δ (ppm), 177.57 (**C**=O), 158.31 (**C**$_{bpy}$), 154.84 (**C**$_{bpy}$), 124.03 (**C**$_{bpy}$), 104.11 (**C**$_{p\text{-}cym}$), 85.58 (**C**H$_{p\text{-}cym}$), 83.54 (**C**H$_{p\text{-}cym}$), 83.01 (**C**H$_{p\text{-}cym}$), 80.91 (**C**H$_{p\text{-}cym}$), 61.98 (**C**H$_2$CH$_2$), 31.03(**C**H(CH$_3$)$_2$), 22.63 (CH(**C**H$_3$)$_2$), 21.78 (CH(**C**H$_3$)$_2$), 17.52 (**C**H$_3$). IR: υ (cm^{-1}): 3071.5 (w, CH$_{p\text{-}cym}$), 1602 (s, C=O), 1258.2 (s, CF_3). UV-visible: (1.0×10^{-5} M, CH_3CN, 298 K): λ_{max} 309 nm (ε = 64 003 M^{-1} · cm^{-1}). ESI-MS: 950 [M – 2CF_3SO_3]$^{2+}$, 2049 [M – CF_3SO_3]$^+$. Elemental Analysis (%): Calc. for $C_{76}H_{92}O_{20}Ru_4F_{12}S_4N_8$ ·2 CH_2Cl_2: C, 39.56; H, 4.09; N, 4.73. Found: C, 39.76; H, 4.18; N, 4.86.

[15c][CF_3SO_3]$_4$: Brown solid, Yield: 0.051 mmol (63%). ^{1}H NMR (400 MHz, CD_2Cl_2): δ (ppm), 8.44 (d, 4H, $^3J_{H\text{-}H}$ = 6.6 Hz, C**H**$_\alpha$), 8.35 (d, 4H, $^3J_{H\text{-}H}$ = 6.6 Hz, C**H**$_\alpha$), 7.81 (d, 4H, $^3J_{H\text{-}H}$ = 6.8 Hz, C**H**$_\beta$), 7.72 (d, 4H, $^3J_{H\text{-}H}$ = 6.8 Hz, C**H**$_\beta$), 5.93 (d, 2H, $^3J_{H\text{-}H}$ = 5.9 Hz, C**H**$_{p\text{-}cym}$), 5.81 (d, 2H, $^3J_{H\text{-}H}$ = 5.9 Hz, C**H**$_{p\text{-}cym}$), 5.78 (d, 4H, $^3J_{H\text{-}H}$ = 5.9 Hz, C**H**$_{p\text{-}cym}$), 5.50 – 5.46 (d, 2H, $^3J_{H\text{-}H}$ = 5.9 Hz, C**H**$_{p\text{-}cym}$), 5.34 (d, 2H, $^3J_{H\text{-}H}$ = 5.9 Hz, C**H**$_{p\text{-}cym}$), 5.28 (d, 2H, $^3J_{H\text{-}H}$ = 5.9 Hz, C**H**$_{p\text{-}cym}$), 4.39 – 3.74 (m, 16H, C**H$_2$**CH$_2$), 2.80 – 2.73 (m, 4H, C**H**(CH$_3$)$_2$), 1.71 (s, 12H, C**H**$_3$), 1.32 (d, 12H, $^3J_{H\text{-}H}$ = 7.0 Hz, CH(C**H**$_3$)$_2$), 1.23 (d, 12H, $^3J_{H\text{-}H}$ = 6.9 Hz, CH(C**H**$_3$)$_2$). ^{13}C{^{1}H} NMR (100 MHz, CD_2Cl_2): δ (ppm), 176.57 (**C**=O), 154.80 (**C**$_{bpy}$), 154.13 (**C**$_{bpy}$), 123.75 (**C**$_{bpy}$), 85.76 (**C**H$_{p\text{-}cym}$), 84.93 (**C**H$_{p\text{-}cym}$), 84.73 (**C**H$_{p\text{-}cym}$), 82.63 (**C**H$_{p\text{-}cym}$), 80.59 (**C**H$_{p\text{-}cym}$), 73.66 (**C**H$_2$CH$_2$), 70.62 (**C**H$_2$CH$_2$), 61.79 (**C**H$_2$CH$_2$), 31.44 (**C**H(CH$_3$)$_2$), 22.46 (CH(**C**H$_3$)$_2$), 22.29 (CH(**C**H$_3$)$_2$), 17.84 (**C**H$_3$). IR: υ (cm^{-1}): 3069.3 (w, CH$_{p\text{-}cym}$), 1599.3 (s, C=O), 1258.7 (s, CF_3). UV-visible: (1.0×10^{-5} M, CH_3CN, 298 K): λ_{max} 306 nm (ε = 110 994 M^{-1} · cm^{-1}). ESI-MS: 1038 [M – CF_3SO_3]$^{2+}$, 2225 [M – CF_3SO_3]$^+$. Elemental Analysis (%): Calc. for $C_{84}H_{108}O_{24}Ru_4F_{12}S_4N_8$ · 3 CH_2Cl_2: C, 39.74; H, 4.37; N, 4.26. Found: C, 39.76; H, 4.28; N, 4.56.

[16a][CF_3SO_3]$_4$: Orange solid, Yield: 0.053 mmol (67%). ^{1}H NMR (400 MHz, CD_2Cl_2): δ (ppm), 7.75 (d, 8H, J = 6.1 Hz, C**H**$_\alpha$), 7.52 – 7.50 (m, 8H, C**H**$_\beta$), 7.49 (d, 4H, $^3J_{H\text{-}H}$ = 7.2 Hz, C**H**=C**H**), 5.86 – 5.74 (m, 8H, C**H**$_{p\text{-}cym}$), 5.49 – 5.45 (m,4H, C**H**$_{p\text{-}cym}$), 5.20 – 5.17 (m,4H, C**H**$_{p\text{-}cym}$), 4.78 – 4.49 (m, 8H, C**H$_2$**CH$_3$), 2.68 – 2.61 (m, 4H, C**H**(CH$_3$)$_2$), 1.66 (s, 4H, C**H**$_3$), 1.64 (s, 4H, C**H**$_3$), 1.62 (s, 4H, C**H**$_3$), 1.58 – 1.53 (m, 12H, CH$_2$C**H$_3$**), 1.30 (d, 12H, $^3J_{H\text{-}H}$ = 6.9, CH(C**H**$_3$)$_2$), 1.26 (d, 12H, $^3J_{H\text{-}H}$ = 6.9 Hz, CH(C**H**$_3$)$_2$). ^{13}C{^{1}H} NMR (100 MHz, CD_2Cl_2): δ (ppm), 165.35 (**C**=O), 165.28 (**C**=O), 151.56 (**C**$_{bpe}$), 132.79 (**C**H=CH), 132.39 (CH=**C**H), 124.58 (**C**$_{bpe}$), 86.21 (**C**H$_{p\text{-}cym}$), 86.05 (**C**H$_{p\text{-}cym}$), 85.04 (**C**H$_{p\text{-}cym}$), 84.92 (**C**H$_{p\text{-}cym}$), 82.26 (**C**H$_{p\text{-}cym}$), 79.67 (**C**H$_{p\text{-}cym}$), 79.56 (**C**H$_{p\text{-}cym}$), 65.72 (**C**H$_2$CH$_3$), 31.49 (**C**H(CH$_3$)$_2$), 22.65

($CH(\mathbf{C}H_3)_2$), 22.54 ($CH(\mathbf{C}H_3)_2$), 17.93 ($\mathbf{C}H_3$), 17.90 ($\mathbf{C}H_3$), 15.42 ($CH_2\mathbf{C}H_3$), 15.35 ($CH_2\mathbf{C}H_3$). IR: υ (cm^{-1}): 3071.9 (w, $CH_{p\text{-}cym}$), 1611.6 (s, C=O), 1263.1 (s, CF_3). UV-visible: (1.0×10^{-5} M, CH_3CN, 298 K): λ_{max} 234 nm ($\varepsilon = 100\,117\ M^{-1} \cdot cm^{-1}$), 312 nm ($\varepsilon = 60\,999\ M^{-1} \cdot cm^{-1}$). ESI-MS: 2101 $[M - CF_3SO_3]^+$, 976 $[M - 2CF_3SO_3]^{2+}$. Elemental Analysis (%): Calc. for $C_{80}H_{96}F_{12}N_8O_{20}Ru_4S_4$: C, 42.70; H, 4.30; N, 4.98. Found: C, 42.38; H, 4.56; N, 4.88.

[16b][CF_3SO_3]$_4$: Yellow solid, Yield: 0.056 mmol (70%). ^{1}H NMR (400 MHz, CD_2Cl_2): δ (ppm), 8.06 (d, 4H, $^3J_{H\text{-}H}$ = 6.8 Hz, C$\mathbf{H}_\alpha$), 7.96 (d, 4H, $^3J_{H\text{-}H}$ = 6.8 Hz, C$\mathbf{H}_\alpha$), 7.60 (d, 4H, $^3J_{H\text{-}H}$ = 6.8 Hz, C$\mathbf{H}_\beta$), 7.57 (d, 4H, $^3J_{H\text{-}H}$ = 6.8 Hz, C$\mathbf{H}_\beta$), 7.50 (d, 4H, $^3J_{H\text{-}H}$ = 22.2 Hz, C**H**=C**H**), 5.72 – 5.62 (m, 12H, C$\mathbf{H}_{p\text{-}cym}$), 5.31 (d, 2H, $^3J_{H\text{-}H}$ = 5.8 Hz, C$\mathbf{H}_{p\text{-}cym}$), 5.28 (d, 2H, $^3J_{H\text{-}H}$ = 5.8 Hz, C$\mathbf{H}_{p\text{-}cym}$), 4.34 – 4.29 (m, 8H, C$\mathbf{H_2}CH_2$), 3.99 – 3.89 (m, 8H, $CH_2C\mathbf{H_2}$), 2.82 – 2.77 (m, 4H, C**H**$(CH_3)_2$), 1.97 (s, 6H, C$\mathbf{H}_3$), 1.91 (s, 6H, C$\mathbf{H}_3$), 1.32 (d, 12H, $^3J_{H\text{-}H}$ = 7.0 Hz, $CH(C\mathbf{H}_3)_2$), 1.20 (d, 6H, $^3J_{H\text{-}H}$ = 6.9 Hz, $CH(C\mathbf{H}_3)_2$), 1.17 (d, 6H, $^3J_{H\text{-}H}$ = 6.9 Hz, $CH(C\mathbf{H}_3)_2$). $^{13}C\{^1H\}$ NMR (100 MHz, CD_2Cl_2): δ (ppm), 172.04 (**C**=O), 153.22 ($\mathbf{C}_{bpe}$), 153.02 ($\mathbf{C}_{bpe}$), 146.49 ($\mathbf{C}_{bpe}$), 149.39 ($\mathbf{C}_{bpe}$), 132.73 (**C**H=CH), 132.67 (CH=**C**H), 104.11 ($\mathbf{C}_{p\text{-}cym}$), 83.87 ($\mathbf{C}H_{p\text{-}cym}$), 83.84 ($\mathbf{C}H_{p\text{-}cym}$), 83.69 ($\mathbf{C}H_{p\text{-}cym}$), 83.62 ($\mathbf{C}H_{p\text{-}cym}$), 60.86 ($\mathbf{C}H_2CH_2$), 31.23 ($\mathbf{C}H(CH_3)_2$), 31.09 ($\mathbf{C}H(CH_3)_2$), 22.65 ($CH(\mathbf{C}H_3)_2$), 22.25 ($CH(\mathbf{C}H_3)_2$), 17.83 ($\mathbf{C}H_3$), 17.53 ($\mathbf{C}H_3$). IR: υ ($cm^{-1}$): 3070.5 (w, $CH_{p\text{-}cym}$), 1601.9 (s, C=O), 1258.1 (s, CF_3). UV-visible: (1.0×10^{-5} M, CH_3CN, 298 K): λ_{max} 307 nm ($\varepsilon = 86\,769\ M^{-1} \cdot cm^{-1}$). ESI-MS: 976 $[M - 2CF_3SO_3]^{2+}$, 2101 $[M - CF_3SO_3]^+$. Elemental Analysis (%): Calc. for $C_{80}H_{96}F_{12}N_8O_{20}Ru_4S_4 \cdot 2\ CH_2Cl_2$: C, 40.70; H, 4.16; N, 4.63. Found: C, 40.10; H, 4.43; N, 4.67.

[16c][CF_3SO_3]$_4$: Yellow solid, Yield: 0.048 mmol (60%). ^{1}H NMR (400 MHz, CD_2Cl_2): δ (ppm), 8.17 (d, 6H, $^3J_{H\text{-}H}$ = 6.1 Hz, C$\mathbf{H}_\alpha$), 8.11 (d, 2H, $^3J_{H\text{-}H}$ = 6.1 Hz, C$\mathbf{H}_\alpha$), 7.64 (d, 8H, $^3J_{H\text{-}H}$ = 6.1 Hz, C$\mathbf{H}_\beta$), 7.49 (d, 4H, $^3J_{H\text{-}H}$ = 3.2 Hz, C**H**=C**H**), 5.90 (d, 1H, $^3J_{H\text{-}H}$ = 5.9 Hz, C$\mathbf{H}_{p\text{-}cym}$), 5.81 (d, 3H, $^3J_{H\text{-}H}$ = 5.9 Hz, C$\mathbf{H}_{p\text{-}cym}$), 5.75 (d, 4H, $^3J_{H\text{-}H}$ = 6.2 Hz, C$\mathbf{H}_{p\text{-}cym}$), 5.46 (d, 1H, $^3J_{H\text{-}H}$ = 6.0 Hz, C$\mathbf{H}_{p\text{-}cym}$), 5.43 (d, 3H, $^3J_{H\text{-}H}$ = 6.0 Hz, C$\mathbf{H}_{p\text{-}cym}$), 5.30 (d, 1H, $^3J_{H\text{-}H}$ = 6.0 Hz, C$\mathbf{H}_{p\text{-}cym}$), 5.24 (d, 3H, $^3J_{H\text{-}H}$ = 6.0 Hz, C$\mathbf{H}_{p\text{-}cym}$), 4.45 – 3.52 (m, 32H, C$\mathbf{H_2}CH_2$), 2.76 – 2.72 (m, 4H, C**H**$(CH_3)_2$), 1.68 (s, 12H, C$\mathbf{H}_3$), 1.29 (d, 12H, $^3J_{H\text{-}H}$ = 7.0 Hz, $CH(C\mathbf{H}_3)_2$), 1.21 (d, 6H, $^3J_{H\text{-}H}$ = 6.9 Hz, $CH(C\mathbf{H}_3)_2$), 1.17 (d, 6H, $^3J_{H\text{-}H}$ = 6.9 Hz, $CH(C\mathbf{H}_3)_2$). $^{13}C\{^1H\}$ NMR (100 MHz, CD_2Cl_2): δ (ppm), 172.04 (**C**=O), 153.63 ($\mathbf{C}_{bpe}$), 153.12 ($\mathbf{C}_{bpe}$), 146.49 ($\mathbf{C}_{bpe}$), 132.87 (**C**H=CH), 104.23 ($\mathbf{C}_{p\text{-}cym}$), 85.90 ($\mathbf{C}H_{p\text{-}cym}$), 85.83 ($\mathbf{C}H_{p\text{-}cym}$), 85.10 ($\mathbf{C}H_{p\text{-}cym}$), 82.41 ($\mathbf{C}H_{p\text{-}cym}$), 79.99 ($\mathbf{C}H_2CH_2$), 74.05 ($\mathbf{C}H_2CH_2$), 61.99 ($\mathbf{C}H_2CH_2$), 31.40 ($\mathbf{C}H(CH_3)_2$), 22.57 ($CH(\mathbf{C}H_3)_2$), 22.23 ($CH(\mathbf{C}H_3)_2$), 17.81 ($\mathbf{C}H_3$). IR: υ ($cm^{-1}$): 3069.1 (w, $CH_{p\text{-}cym}$), 1599.3 (s,

C=O), 1259.3 (s, CF_3). UV-visible: (1.0×10^{-5} M, CH_3CN, 298 K): λ_{max} 307 nm (ε = 73 065 $M^{-1} \cdot cm^{-1}$). ESI-MS: 1064 $[M - CF_3SO_3]^{2+}$, 2278 $[M - CF_3SO_3]^{+}$. Elemental Analysis (%): Calc. for $C_{80}H_{96}F_{12}N_8O_{20}Ru_4S_4 \cdot 2\ CH_2Cl_2$: C, 40.70; H, 4.16; N, 4.63. Found: C, 40.42; H, 4.49; N, 4.26.

[17a][CF_3SO_3]$_4$: Black solid, Yield: 0.056 mmol (70%). ^{1}H NMR (400 MHz, MeOD): δ (ppm), 8.25 (d, 8H, $^3J_{H\text{-}H}$ = 5.6 Hz, C**H**$_\alpha$), 7.81 (d, 4H, $^3J_{H\text{-}H}$ = 6.8 Hz, C**H**$_\beta$), 7.63 (d, 4H, $^3J_{H\text{-}H}$ = 6.8 Hz, C**H**$_\beta$), 6.13 – 6.04 (m, 8H, C**H**$_{p\text{-}cym}$), 5.72 – 5.70 (m, 4H, C**H**$_{p\text{-}cym}$), 5.44 – 5.41 (m, 4H, C**H**$_{p\text{-}cym}$), 4.76 – 4.58 (m, 8H, C**H$_2$**CH$_3$), 2.76 – 2.72 (m, 4H, C**H**(CH$_3$)$_2$), 1.68 (s, 6H, C**H**$_3$), 1.65 (s, 6H, C**H**$_3$), 1.63 – 1.58 (m, 12H, CH$_2$C**H$_3$**), 1.35 (d, 12H, $^3J_{H\text{-}H}$ = 6.9, CH(C**H**$_3$)$_2$), 1.32 (d, 12H, $^3J_{H\text{-}H}$ = 6.9 Hz, CH(C**H**$_3$)$_2$). ^{13}C{^{1}H} NMR (100 MHz, MeOD): δ (ppm), 166.54 (**C**=O), 166.51 (**C**=O), 158.52 (**C**$_{bpa}$), 158.19 (**C**$_{bpa}$), 155.48 (**C**$_{bpa}$), 155.42 (**C**$_{bpa}$), 119.86 (**C**$_{bpa}$), 119.63 (**C**$_{bpa}$), 103.76 (**C**$_{p\text{-}cym}$), 103.72 (**C**$_{p\text{-}cym}$), 102.94 (**C**$_{p\text{-}cym}$), 87.90 (**C**H$_{p\text{-}cym}$), 87.81 (**C**H$_{p\text{-}cym}$), 86.66 (**C**H$_{p\text{-}cym}$), 86.61 (**C**H$_{p\text{-}cym}$), 83.33 (**C**H$_{p\text{-}cym}$), 83.22 (**C**H$_{p\text{-}cym}$), 80.53 (**C**H$_{p\text{-}cym}$), 80.46 (**C**H$_{p\text{-}cym}$), 66.33 (**C**H$_2$CH$_3$), 32.49 (**C**H(CH$_3$)$_2$), 22.86 (CH(**C**H$_3$)$_2$), 17.78 (**C**H$_3$), 17.73 (**C**H$_3$), 15.60 (CH$_2$**C**H$_3$). IR: υ (cm^{-1}): 3073.9 (w, CH$_{p\text{-}cym}$), 1602.6 (s, C=O), 1264.2 (s, CF_3). UV-visible: (1.0×10^{-5} M, CH_3CN, 298 K): λ_{max} 245 nm (ε = 144 942 $M^{-1} \cdot cm^{-1}$), 308 nm (ε = 52 738 $M^{-1} \cdot cm^{-1}$). ESI-MS: 794 $[M - 3CF_3SO_3 - 2L]^{+}$. Elemental Analysis (%): Calc. for $C_{76}H_{92}F_{12}N_{12}O_{20}Ru_4S_4$: C, 40.50; H, 4.11; N, 7.46. Found: C, 40.05; H, 4.16; N, 7.45.

[17b][CF_3SO_3]$_4$: Brown solid, Yield: 0.056 mmol (70%). ^{1}H NMR (400 MHz, MeOD): δ (ppm), 8.55 (d, 4H, $^3J_{H\text{-}H}$ = 6.8 Hz, C**H**$_\alpha$), 8.50 (d, 4H, $^3J_{H\text{-}H}$ = 6.8 Hz, C**H**$_\alpha$), 7.71 (d, 4H, $^3J_{H\text{-}H}$ = 6.8 Hz, C**H**$_\beta$), 7.66 (d, 4H, $^3J_{H\text{-}H}$ = 6.8 Hz, C**H**$_\beta$), 6.15 (d, 2H, $^3J_{H\text{-}H}$ = 5.9 Hz, C**H**$_{p\text{-}cym}$), 6.12 (d, 2H, $^3J_{H\text{-}H}$ = 5.9 Hz, C**H**$_{p\text{-}cym}$), 5.99 (d, 4H, $^3J_{H\text{-}H}$ = 6.2 Hz, C**H**$_{p\text{-}cym}$), 5.63 – 5.44 (m, 8H, C**H**$_{p\text{-}cym}$), 4.26 – 4.09 (m, 8H, C**H$_2$**CH$_2$), 4.10 – 4.00 (m, 8H, CH$_2$C**H$_2$**), 2.85 – 2.82 (m, 4H, C**H**(CH$_3$)$_2$), 1.76 (s, 6H, C**H**$_3$), 1.72 (s, 6H, C**H**$_3$), 1.36 (d, 12H, $^3J_{H\text{-}H}$ = 7.0 Hz, CH(C**H**$_3$)$_2$), 1.26 (d, 12H, $^3J_{H\text{-}H}$ = 6.9 Hz, CH(C**H**$_3$)$_2$). ^{13}C{^{1}H} NMR (100 MHz, MeOD): δ (ppm), 172.79 (**C**=O), 156.91 (**C**$_{bpa}$), 156.78 (**C**$_{bpa}$), 146.49 (**C**$_{bpa}$), 149.39 (**C**$_{bpa}$), 119.55 (**C**$_{bpa}$), 119.30 (**C**$_{bpa}$), 104.11 (**C**$_{p\text{-}cym}$), 87.40 (**C**H$_{p\text{-}cym}$), 87.61 (**C**H$_{p\text{-}cym}$), 85.56 (**C**H$_{p\text{-}cym}$), 85.39 (**C**H$_{p\text{-}cym}$), 84.48 (**C**H$_{p\text{-}cym}$), 84.30 (**C**H$_{p\text{-}cym}$), 81.62 (**C**H$_{p\text{-}cym}$), 81.57 (**C**H$_{p\text{-}cym}$), 61.93 (**C**H$_2$CH$_2$), 61.77 (**C**H$_2$CH$_2$), 56.13 (CH$_2$**C**H$_2$), 56.13 (CH$_2$**C**H$_2$), 32.40 (**C**H(CH$_3$)$_2$), 23.13 (CH(**C**H$_3$)$_2$), 23.05 (CH(**C**H$_3$)$_2$), 22.24 (CH(**C**H$_3$)$_2$), 17.76 (**C**H$_3$), 17.71 (**C**H$_3$). IR: υ (cm^{-1}): 3072.1 (w, CH$_{p\text{-}cym}$), 1601.3 (s, C=O), 1258.4 (s, CF_3). UV-visible: (1.0×10^{-5} M, CH_3CN, 298 K): λ_{max} 285 nm (ε

= 86 769 $M^{-1} \cdot cm^{-1}$). ESI-MS: 978 $[M - 2CF_3SO_3]^{2+}$, 2105 $[M - CF_3SO_3]^{+}$. Elemental Analysis (%): Calc. for $C_{76}H_{92}F_{12}N_{12}O_{20}Ru_4S_4 \cdot CH_2Cl_2$: C, 39.54; H, 4.05; N, 7.19. Found: C, 39.71; H, 4.33; N, 6.64.

[17c][CF_3SO_3]$_4$: Red solid, Yield: 0.048 mmol (60%). ^{1}H NMR (400 MHz, MeOD): δ (ppm), 8.49 (d, 8H, $^3J_{H\text{-}H}$ = 6.1 Hz, C**H**$_\alpha$), 7.73 (d, 8H, $^3J_{H\text{-}H}$ = 6.8 Hz, C**H**$_\beta$), 6.27 (d, 4H, $^3J_{H\text{-}H}$ = 5.9 Hz, C**H**$_{p\text{-}cym}$), 6.00 (d, 4H, $^3J_{H\text{-}H}$ = 5.9 Hz, C**H**$_{p\text{-}cym}$), 5.62 (d, 4H, $^3J_{H\text{-}H}$ = 5.9 Hz, C**H**$_{p\text{-}cym}$), 5.52 (d, 4H, $^3J_{H\text{-}H}$ = 5.9 Hz, C**H**$_{p\text{-}cym}$), 4.30 – 3.80 (m, 32H, C**H$_2$**CH$_2$), 2.87 – 2.80 (m, 4H, C**H**(CH$_3$)$_2$), 1.72 (s, 12H, C**H**$_3$), 1.37 (d, 12H, $^3J_{H\text{-}H}$ = 7.0 Hz, CH(C**H**$_3$)$_2$), 1.27 (d, 12H, $^3J_{H\text{-}H}$ = 6.9 Hz, CH(C**H**$_3$)$_2$). ^{13}C{^{1}H} NMR (100 MHz, MeOD): δ (ppm), 176.57 (**C**=O), 154.80 (**C**$_{bpa}$), 154.13 (**C**$_{bpa}$), 123.75 (**C**$_{bpa}$), 85.76 (**C**H$_{p\text{-}cym}$), 84.93 (**C**H$_{p\text{-}cym}$), 84.73 (**C**H$_{p\text{-}cym}$), 82.63 (**C**H$_{p\text{-}cym}$), 80.59 (**C**H$_{p\text{-}cym}$), 73.66 (**C**H$_2$CH$_2$), 70.62 (**C**H$_2$CH$_2$), 61.79 (**C**H$_2$CH$_2$), 31.44 (**C**H(CH$_3$)$_2$), 22.46 (CH(**C**H$_3$)$_2$), 22.29 (CH(**C**H$_3$)$_2$), 17.84 (**C**H$_3$). IR: υ (cm^{-1}): 3072 (w, CH$_{p\text{-}cym}$), 1601.5 (s, C=O), 1258.4 (s, CF_3). UV-visible: (1.0×10^{-5} M, CH_3CN, 298 K): λ_{max} 284 nm (ε = 73 905 $M^{-1} \cdot cm^{-1}$). ESI-MS: 1066 $[M - CF_3SO_3]^{2+}$. Elemental Analysis (%):Calc. for $C_{84}H_{108}F_{12}N_{12}O_{24}Ru_4S_4 \cdot CH_2Cl_2$: C, 40.59; H, 4.41; N, 6.68. Found: C, 40.58; H, 4.48; N, 6.70.

General Synthetic Method for the Hexacationic Metalla-Prisms of the General Formulas [(p-cymene)$_6$Ru$_6$(μ-tpt)$_2$(μ-L)$_3$]$^{6+}$ ***([18a]$^{6+}$-[18c]$^{6+}$)*** *and [(p-cymene)$_6$Ru$_6$(μ-tpv)$_2$(μ-L)$_3$]$^{6+}$* ***([19a]$^{6+}$-[19c]$^{6+}$).***

A mixture of the dinuclear clip (1a-1c) of the general formula [(p-cymene)$_2$Ru$_2$Cl$_2$(μ-L)] (0.16 mmol) and 2 equiv of $AgCF_3SO_3$ (0.32 mmol) in methanol (20 mL) was stirred at room temperature for 2 h and the solution was filtered to remove AgCl. To the filtrate, the corresponding 2,4,6-tris(4-pyridyl)-1,3,5-triazine and 1,3,5-tris{2-(4-pyridyl)vinyl}benzene (0.11 mmol) were added. The mixture was stirred at 60°C for 24 h, and the solvent removed under vacuum. The residue was dissolved in dichloromethane (20 mL), the extract filtered and concentrated (3 mL) and diethyl ether was slowly added to initiate precipitation of the product as a brown or red solid.

[18a][CF_3SO_3]$_6$: Brown solid, Yield: 0.037 mmol (70%). ^{1}H NMR (400 MHz, CD_2Cl_2): δ (ppm), 9.03 (d, 3H, $^3J_{H\text{-}H}$ = 4.5 Hz, C**H**$_{tpt}$), 8.96 (d, 3H, $^3J_{H\text{-}H}$ = 4.7 Hz, C**H**$_{tpt}$), 8.84 – 8.77 (m, 6H, C**H**$_{tpt}$), 8.59 – 8.49 (m, 12H, C**H**$_{tpt}$), 8.47 – 8.43 (m, 6H, C**H**$_{tpt}$), 8.40 – 8.34 (m, 6H, C**H**$_{tpt}$), 8.04 – 8.00 (m, 6H, C**H**$_{tpt}$), 7.78 (d, 6H, $^3J_{H\text{-}H}$ = 5.8 Hz, C**H**$_{tpt}$), 5.97 –5.93 (m, 6H,

C**H**$_{p\text{-}cym}$), 5.91 (d, 3H, $^{3}J_{H\text{-}H}$ = 5.9 Hz, C**H**$_{p\text{-}cym}$), 5.88 (d, 3H, $^{3}J_{H\text{-}H}$ = 5.9 Hz, C**H**$_{p\text{-}cym}$), 5.86 (d, 6H, $^{3}J_{H\text{-}H}$ = 6.3 Hz, C**H**$_{p\text{-}cym}$), 5.82 (d, 3H, $^{3}J_{H\text{-}H}$ = 6.2 Hz, C**H**$_{p\text{-}cym}$), 5.79 (d, 3H, $^{3}J_{H\text{-}H}$ = 6.2 Hz, C**H**$_{p\text{-}cym}$), 5.66 (d, 3H, $^{3}J_{H\text{-}H}$ = 6.1 Hz, C**H**$_{p\text{-}cym}$), 5.56 (d, 3H,$^{3}J_{H\text{-}H}$ = 6.2 Hz, C**H**$_{p\text{-}cym}$), 5.53 (d, 3H, $^{3}J_{H\text{-}H}$ = 6.2 Hz, C**H**$_{p\text{-}cym}$), 5.43 (d, 3H, $^{3}J_{H\text{-}H}$ = 6.1 Hz, C**H**$_{p\text{-}cym}$), 5.34 (d, 3H, $^{3}J_{H\text{-}H}$ = 6.1 Hz, C**H**$_{p\text{-}cym}$), 5.25 (d, 3H, $^{3}J_{H\text{-}H}$ = 6.0 Hz, C**H**$_{p\text{-}cym}$), 5.22 (d, 3H, $^{3}J_{H\text{-}H}$ = 6.0 Hz, , C**H**$_{p\text{-}cym}$), 5.13 (d, 3H, $^{3}J_{H\text{-}H}$ = 5.9 Hz, C**H**$_{p\text{-}cym}$), 4.76 – 4.58 (m, 24H, C**H$_2$**CH$_3$), 2.79 – 2.60 (m, 12H, C**H**(CH$_3$)$_2$), 1.81 (s, 12H, C**H**$_3$), 1.66 (s, 12H, C**H$_3$**), 1.62 (s, 12H, C**H$_3$**), 1.63 – 1.58 (m, 18H, CH$_2$C**H$_3$**), 1.45 (s, 12H, C**H**$_3$), 1.33 – 123 (m, 72H, CH(C**H**$_3$)$_2$). ^{13}C{^{1}H} NMR (100 MHz, CD_2Cl_2): δ (ppm), 170.18 (**C**=O), 169.95 (**C**=O), 169.90 (**C**=O), 169.57 (**C**=O), 153.70 (**C**H$_{tpt}$), 153.36 (**C**$_{tpt}$), 153.13 (**C**$_{tpt}$), 152.65 (**C**$_{tpt}$), 152.40 (**C**$_{tpt}$), 152.20 (**C**$_{tpt}$), 152.03 (**C**$_{tpt}$), 143.70 (**C**$_{tpt}$), 143.42 (**C**$_{tpt}$), 143.37 (**C**$_{tpt}$), 143.01 (**C**$_{tpt}$), 125.70 (**C**$_{tpt}$), 125.67 (**C**$_{tpt}$), 125.49 (**C**$_{tpt}$),125.34 (**C**$_{tpt}$), 125.16 (**C**$_{tpt}$), 125.01 (**C**$_{tpt}$), 125.23 (**C**$_{tpt}$),122.65 (**C**$_{tpt}$), 102.94 (**C**$_{p\text{-}cym}$), 102.60 (**C**$_{p\text{-}cym}$), 102.52 (**C**$_{p\text{-}cym}$), 102.17 (**C**$_{p\text{-}cym}$), 101.89 (**C**$_{p\text{-}cym}$), 101.57 (**C**$_{p\text{-}cym}$), 101.24 (**C**$_{p\text{-}cym}$), 101.02 (**C**$_{p\text{-}cym}$), 86.35 (**C**H$_{p\text{-}cym}$), 86.25 (**C**H$_{p\text{-}cym}$), 86.13 (**C**H$_{p\text{-}cym}$), 85.94 (**C**H$_{p\text{-}cym}$), 85.09 (**C**H$_{p\text{-}cym}$), 84.92 (**C**H$_{p\text{-}cym}$), 84.85 (**C**H$_{p\text{-}cym}$), 84.63 (**C**H$_{p\text{-}cym}$), 81.92 (**C**H$_{p\text{-}cym}$), 81.86 (**C**H$_{p\text{-}cym}$), 81.64 (**C**H$_{p\text{-}cym}$), 81.57 (**C**H$_{p\text{-}cym}$), 79.56 (**C**H$_{p\text{-}cym}$), 79.32 (**C**H$_{p\text{-}cym}$), 79.16 (**C**H$_{p\text{-}cym}$), 78.90 (**C**H$_{p\text{-}cym}$), 65.71 (**C**H$_2$CH$_3$), 65.68 (**C**H$_2$CH$_3$), 31.16 (**C**H(CH$_3$)$_2$), 31.10 (**C**H(CH$_3$)$_2$), 31.04 (**C**H(CH$_3$)$_2$), 22.24 (CH(**C**H$_3$)$_2$), 22.22 (CH(**C**H$_3$)$_2$), 22.19 (CH(**C**H$_3$)$_2$), 22.13 (CH(**C**H$_3$)$_2$), 22.10 (CH(**C**H$_3$)$_2$), 22.17 (CH(**C**H$_3$)$_2$), 17.70 (**C**H$_3$), 17.50 (**C**H$_3$), 17.39 (**C**H$_3$), 17.18 (**C**H$_3$), 14.90 (CH$_2$**C**H$_3$), 14.86 (CH$_2$**C**H$_3$), 14.77 (CH$_2$**C**H$_3$). IR: υ (cm^{-1}): 3071.9 (w, CH$_{p\text{-}cym}$), 1611.6 (s, C=O), 1263.1 (s, CF$_3$). UV-visible: (1.0×10^{-5} M, CH_3CN, 298 K): λ_{max} 242 nm (ε = 179 448 $M^{-1} \cdot cm^{-1}$), 347 nm (ε = 40 018 $M^{-1} \cdot cm^{-1}$). ESI-MS: 1578 $[M - 3CF_3SO_3]^{3+}$, 1002 $[M - 2CF_3SO_3]^{2+}$. Elemental Analysis (%): Calc. for $C_{120}H_{138}F_{18}N_{18}O_{30}Ru_6S_6 \cdot 5\ CH_2Cl_2$: C, 38.71; H, 3.85; N, 6.50. Found: C, 38.71; H, 4.30; N, 6.80.

The number of protons of the compound ***[18a][CF$_3$SO$_3$]$_6$*** *is multiplied by two, because of the existence of four isomers in solution.*

[18b][CF$_3$SO$_3$]$_6$: Brown solid, Yield: 0.030 mmol (56%). ^{1}H NMR (400 MHz, CD_2Cl_2): δ (ppm), 8.68 (br, 24H, C**H**$_{tpt}$), 5.84 – 5.71 (m, 14H, C**H**$_{p\text{-}cym}$), 5.66 – 5.60 (m, 5H, C**H**$_{p\text{-}cym}$), 5.39 – 5.31 (m, 5H, C**H**$_{p\text{-}cym}$), 4.39 – 4.32 (m, 12H, C**H$_2$**CH$_2$), 4.06 – 4.00 (m, 12H, CH$_2$C**H$_2$**), 2.88 – 2.80 (m, 6H, C**H**(CH$_3$)$_2$), 1.91 – 1.83 (m, 18H, C**H**$_3$), 1.36 – 1.34 (m, 18H, CH(C**H**$_3$)$_2$), 1.27 – 1.19 (m, 18H, CH(C**H**$_3$)$_2$). ^{13}C{^{1}H} NMR (100 MHz, CD_2Cl_2): δ (ppm), 172.63

(**C**=O), 172.52 (**C**=O), 172.26 (**C**=O), 172.07 (**C**=O), 154.89 (**C**$_{tpt}$), 84.24 (**C**H$_{p\text{-}cym}$), 83.69 (**C**H$_{p\text{-}cym}$), 83.58 (**C**H$_{p\text{-}cym}$), 83.55 (**C**H$_{p\text{-}cym}$), 83.51 (**C**H$_{p\text{-}cym}$), 83.47 (**C**H$_{p\text{-}cym}$), 83.21 (**C**H$_{p\text{-}cym}$), 82.78 (**C**H$_{p\text{-}cym}$), 61.84 (**C**H$_2$CH$_2$), 31.36 (**C**H(CH$_3$)$_2$), 31.23 (CH(**C**H$_3$)$_2$), 22.40 (CH(**C**H$_3$)$_2$), 22.22 (CH(**C**H$_3$)$_2$), 17.73 (**C**H$_3$), 17.68 (**C**H$_3$). IR: υ (cm^{-1}): 3067.7 (w, CH$_{p\text{-}cym}$), 1606.9 (s, C=O), 1258.4 (s, CF$_3$). UV-visible: (1.0 × 10^{-5} M, CH$_3$CN, 298 K): λ_{max} 250 nm (ε = 155 922 M^{-1} · cm^{-1}), 310 nm (ε = 56 104 M^{-1} · cm^{-1}). ESI-MS: 1002 [M – 2CF$_3$SO$_3$]$^{3+}$, 1578 [M – CF$_3$SO$_3$]$^{2+}$. Elemental Analysis (%): Calc. for C$_{120}$H$_{138}$F$_{18}$N$_{18}$O$_{30}$Ru$_6$S$_6$ · 7 CH$_2$Cl$_2$: C, 37.68; H, 3.78; N, 6.23. Found: C, 37.32; H, 3.96; N, 6.59.

[18c][CF$_3$SO$_3$]$_6$: Yellow solid, Yield: 0.031 mmol (58%). ^{1}H NMR (400 MHz, CD$_2$Cl$_2$): δ (ppm), 8.71 (br, 24H, C**H**$_{tpt}$), 6.05 – 5.98 (m, 6H, C**H**$_{p\text{-}cym}$), 5.87 – 5.82 (m, 6H, C**H**$_{p\text{-}cym}$), 5.60 – 5.55 (m, 6H, C**H**$_{p\text{-}cym}$), 5.41 – 5.35 (m, 6H, C**H**$_{p\text{-}cym}$), 4.21 – 3.89 (m, 48H, C**H$_2$**CH$_2$), 2.82 – 2.77 (m, 6H, C**H**(CH$_3$)$_2$), 1.71 (s, 6H, C**H**$_3$), 1.67 (s, 4H, C**H**$_3$), 1.65 (s, 8H, C**H**$_3$), 1.34 – 1.32 (m, 18H, CH(C**H**$_3$)$_2$), 1.27 – 1.24 (m, 18H, CH(C**H**$_3$)$_2$). ^{13}C{^{1}H} NMR (100 MHz, CD$_2$Cl$_2$): δ (ppm), 176.48 (**C**=O), 155.83 (**C**$_{tpt}$), 132.02 (**C**$_{tpt}$), 125.66(**C**$_{tpt}$), 86.45 (**C**H$_{p\text{-}cym}$), 85.35 (**C**H$_{p\text{-}cym}$), 82.60 (**C**H$_{p\text{-}cym}$), 82.34 (**C**H$_{p\text{-}cym}$), 80.26 (**C**H$_{p\text{-}cym}$), 80.57 (**C**H$_{p\text{-}cym}$), 73.92 (**C**H$_2$CH$_2$), 70.84 (**C**H$_2$CH$_2$), 63.94 (**C**H$_2$CH$_2$), 62.30 (**C**H$_2$CH$_2$), 55.40 (**C**H$_2$CH$_2$), 53.75 (**C**H$_2$CH$_2$), 31.65 (**C**H(CH$_3$)$_2$), 22.42 (CH(**C**H$_3$)$_2$), 17.76 (**C**H$_3$). IR: υ (cm^{-1}): 3071 (w, CH$_{p\text{-}cym}$), 1600.9 (s, C=O), 1259.3 (s, CF$_3$). UV-visible: (1.0 × 10^{-5} M, CH$_3$CN, 298 K): λ_{max} 247 nm (ε = 144 942 M^{-1} · cm^{-1}), 308 nm (ε = 52 738 M^{-1} · cm^{-1}). ESI-MS: 1090 [M – 3CF$_3$SO$_3$]$^{3+}$, 1710 [M – 2CF$_3$SO$_3$]$^{3+}$. Calc. for C$_{132}$H$_{162}$F$_{18}$N$_{18}$O$_{36}$Ru$_6$S$_6$· 4 CH$_2$Cl$_2$: C, 40.26; H, 4.22; N, 6.21. Found: C, 40.19; H, 4.60; N, 6.38.

[19a][CF$_3$SO$_3$]$_6$: Yellow solid, Yield: 0.039 mmol (73%). ^{1}H NMR (400 MHz, MeOD): δ (ppm),), 7.95 (br, 2H, C**H**$_{ar}$), 7.88 – 7.80 (m, 12H, C**H**$_{\alpha}$), 7.65 (br, 2H, C**H**$_{ar}$), 7.63 (br, 1H, C**H**$_{ar}$), 7.47 – 7.41 (m, 12H, C**H**$_{\beta}$), 7.36 (br, 1H, C**H**$_{ar}$), 7.47 – 7.23 (m, 12H, C**H**=CH), 6.11 – 5.88 (m, 12H, C**H**$_{p\text{-}cym}$), 5.76 – 5.51 (m, 6H, C**H**$_{p\text{-}cym}$), 5.43 – 5.28 (m, 6H, C**H**$_{p\text{-}cym}$), 4.68 – 4.60 (m, 12H, C**H$_2$**CH$_3$), 2.74 – 2.67 (m, 6H, C**H**(CH$_3$)$_2$), 1.75 (s, 5H, C**H**$_3$), 1.68 (s, 8H, C**H**$_3$), 1.63 (s, 5H, C**H**$_3$), 1.61 – 1.56 (m, 12H, CH$_2$C**H$_3$**), 1.35 (m, 36H, CH(C**H**$_3$)$_2$). ^{13}C{^{1}H} NMR (100 MHz, MeOD): δ (ppm), 166.54 (**C**=O), 166.51 (**C**=O), 158.52 (**C**$_{tpv}$), 158.19 (**C**$_{tpv}$), 155.48 (**C**$_{tpv}$), 155.42 (**C**$_{tpv}$), 137.78 (C**H**=C**H**), 137.59 (C**H**=C**H**), 137.45 (C**H**=C**H**), 137.24 (C**H**=C**H**), 130.76 (**C**$_{ar}$), 128.54 (**C**$_{ar}$), 126.16 (**C**$_{ar}$), 126.07 (**C**$_{ar}$), 125.79 (C**H**=C**H**), 125.72 (C**H**=C**H**), 125.59 (C**H**=C**H**), 125.48 (C**H**=C**H**), 123.63(**C**$_{tpv}$), 119.86 (**C**$_{tpv}$), 119.63 (**C**$_{tpv}$), 103.76 (**C**$_{p\text{-}cym}$), 103.72 (**C**$_{p\text{-}cym}$), 102.94 (**C**$_{p\text{-}cym}$), (**C**$_{p\text{-}cym}$), 87.90 (**C**H$_{p\text{-}cym}$), 87.81 (**C**H$_{p\text{-}}$

$_{cym}$), 86.66 (**C**H$_{p\text{-}cym}$), 86.61 (**C**H$_{p\text{-}cym}$), 83.33 (**C**H$_{p\text{-}cym}$), 83.22 (**C**H$_{p\text{-}cym}$), 80.53 (**C**H$_{p\text{-}cym}$), 80.46 (**C**H$_{p\text{-}cym}$), 66.33 (**C**H$_2$CH$_3$), 32.49 (**C**H(CH$_3$)$_2$), 22.86 (CH(**C**H$_3$)$_2$), 17.78 (**C**H$_3$), 17.73 (**C**H$_3$), 15.60 (CH$_2$**C**H$_3$). IR: υ (cm^{-1}): 3070 (w, CH$_{p\text{-}cym}$), 1609 (s, C=O), 1263.1 (s, CF$_3$). UV-visible: (1.0 × 10^{-5} M, CH$_3$CN, 298 K): λ_{max} 237 nm (ε = 125 684 M^{-1} · cm^{-1}), 337 nm (ε = 332 425 M^{-1} · cm^{-1}). ESI-MS: 1052 [M – 3CF$_3$SO$_3$]$^{3+}$, 1653 [M – 2CF$_3$SO$_3$]$^{2+}$. Elemental Analysis (%):Calc. for C$_{138}$H$_{156}$F$_{18}$N$_{12}$O$_{30}$Ru$_6$S$_6$: C, 46.00; H, 4.36; N, 4.66. Found: C, 45.50; H, 4.41; N, 4.54.

[19b][CF$_3$SO$_3$]$_6$: Brown solid, Yield: 0.038 mmol (71%). ^{1}H NMR (400 MHz, MeOD): δ (ppm), 8.10 – 8.05 (m, 12H, C**H**$_\alpha$), 7.74 – 7.66 (m, 6H, C**H**$_{ar}$), 7.52 – 7.48 (m, 6H, C**H**=CH), 6.12 – 6.10 (m, 6H, C**H**=CH), 6.12 – 6.10 (m, 6H, C**H**$_{p\text{-}cym}$), 5.95 – 5.93 (m, 6H, C**H**$_{p\text{-}cym}$), 5.51 – 5.47 (m, 12H, C**H**$_{p\text{-}cym}$), 4.20 – 4.18 (m, 12H, C**H$_2$**CH$_2$), 4.09 – 4.05 (m, 6H, CH$_2$C**H$_2$**), 3.90 – 3.83 (m, 6H, CH$_2$C**H$_2$**), 2.86 – 2.79 (m, 6H, C**H**(CH$_3$)$_2$), 1.75 – 1.72 (m, 18H, C**H**$_3$), 1.36 (m, 18H, $^3J_{H\text{-}H}$ = 7.0 Hz, CH(C**H**$_3$)$_2$), 1.26 (m, 18H, $^3J_{H\text{-}H}$ = 7.0 Hz, CH(C**H**$_3$)$_2$). ^{13}C{^{1}H} NMR (100 MHz, MeOD): δ (ppm), 172.65 (**C**=O), 153.79 (**C**$_{tpv}$), 149.49 (**C**$_{tpv}$), 138.08 (C**H**=CH), 137.64 (C**H**=CH), 128.86 (C**H**$_{ar}$), 128.43 (C**H**$_{ar}$), 123.90 (**C**$_{tpv}$), 104.87 (**C**$_{p\text{-}cym}$), 87.27 (**C**H$_{p\text{-}cym}$), 85.54 (**C**H$_{p\text{-}cym}$), 84.06 (**C**H$_{p\text{-}cym}$), 80.98 (**C**H$_{p\text{-}cym}$), 61.77 (**C**H$_2$CH$_2$), 56.02 (**C**H$_2$CH$_2$), 32.39 (CH(**C**H$_3$)$_2$), 23.17 (CH(**C**H$_3$)$_2$), 22.30 (CH(**C**H$_3$)$_2$), 17.78 (**C**H$_3$). IR: υ (cm^{-1}): 3067.8 (w, CH$_{p\text{-}cym}$), 1601.3 (s, C=O), 1256.2 (s, CF$_3$). UV-visible: (1.0 × 10^{-5} M, CH$_3$CN, 298 K): λ_{max} 334 nm (ε = 243 433 M^{-1} · cm^{-1}). ESI-MS: 1002 [M – 2CF$_3$SO$_3$]$^{3+}$, 1578 [M – CF$_3$SO$_3$]$^{2+}$. Elemental Analysis (%): Calc. for C$_{138}$H$_{156}$F$_{18}$N$_{12}$O$_{30}$Ru$_6$S$_6$ · 2 CH$_2$Cl$_2$: C, 44.56; H, 4.27; N, 4.45. Found: C, 44.08; H, 4.33; N, 4.44.

[19c][CF$_3$SO$_3$]$_6$: Brown solid, Yield: 0.036 mmol (68%). ^{1}H NMR (400 MHz, MeOD): δ (ppm), 8.09 – 8.05 (m, 12H, C**H**$_{tpv}$), 7.75 – 7.67 (m, 6H, C**H**$_{ar}$), 7.55 – 7.53 (m, 12H, C**H**$_{tpv}$), 7.54 – 7.47 (m, 6H, C**H**=C**H**), 7.34 – 7.28 (m, 6H, C**H**=C**H**), (m, 6H, C**H**$_{p\text{-}cym}$), 5.87 – 5.82 (m, 6H, C**H**$_{p\text{-}cym}$), 5.60 – 5.55 (m, 6H, C**H**$_{p\text{-}cym}$), 5.41 – 5.35 (m, 6H, C**H**$_{p\text{-}cym}$), 4.23 – 3.80 (m, 48H, C**H$_2$**CH$_2$), 2.88 – 2.81 (m, 6H, C**H**(CH$_3$)$_2$), 1.74 (s, 6H, C**H**$_3$), 1.72 (s, 6H, C**H**$_3$), 1.71 (s, 6H, C**H**$_3$), 1.36 (d, 18H, $^3J_{H\text{-}H}$ = 6.9 Hz, CH(C**H**$_3$)$_2$), 1.27 (m, 18H, CH(C**H**$_3$)$_2$). ^{13}C{^{1}H} NMR (100 MHz, MeOD): δ (ppm), 172.71 (**C**=O), 153.93 (**C**$_{tpv}$), 137.65 (C**H**=C**H**), 137.76 (C**H**=C**H**), 138.07 (C**H**=C**H**), 141.69 (C**H**=C**H**), 127.67 (**C**$_{ar}$), 128.71(**C**$_{ar}$), 129.65(**C**$_{ar}$), 123.63(**C**$_{tpv}$), 104.67 (**C**$_{p\text{-}cym}$), 87.14 (**C**H$_{p\text{-}cym}$), 85.83 (**C**H$_{p\text{-}cym}$), 81.01 (**C**H$_{p\text{-}cym}$), 74.28 (**C**H$_2$CH$_2$), 71.46 (**C**H$_2$CH$_2$), 62.35 (**C**H$_2$CH$_2$), 54.08 (**C**H$_2$CH$_2$), 32.39 (**C**H(CH$_3$)$_2$), 23.23 (CH(**C**H$_3$)$_2$), 22.27 (CH(**C**H$_3$)$_2$), 17.76 (**C**H$_3$). IR: υ (cm^{-1}): 3067 (w, CH$_{p\text{-}cym}$), 1600.2 (s,

C=O), 1259.0 (s, CF_3). UV-visible: (1.0×10^{-5} M, CH_3CN, 298 K): λ_{max} 337 nm (ε = 294 472 $M^{-1} \cdot cm^{-1}$). ESI-MS: 1140 $[M - 3CF_3SO_3]^{3+}$, 1785 $[M - 2CF_3SO_3]^{3+}$. Elemental Analysis (%): Calc. for $C_{150}H_{180}F_{12}N_{12}O_{36}Ru_6S_6 \cdot 4\ CH_2Cl_2$: C, 43.96; H, 4.50; N, 3.99. Found: C, 43.57; H, 4.50; N, 3.87.

7.2.4 Synthesis and Characterisation of the OO∩OO Benzo-quinone Derivatives Organic Linkers and the Hexanuclear Arene Ruthenium Host and Host-Guest Complexes

Synthesis of 2,5-dihydroxy-3,6-dimesityl-2,4-dimethyl-1,4-benzoquinone ***($C_2H_6L^f$).*** Orange solid, Yield: 162 mg, 0.43 mmol (43%). A mixture of 2,5-Dibromo-3,6-dimethoxy-1,4-benzoquinone (326 mg, 1.0 mmol, 1.0 equiv.), dichlorobis(triphenylphosphane) palladium(II) (70 mg, 0.1 mmol, 0.1 equiv.), potassium carbonate (690 mg, 5.0 mmol, 5.0 equiv.), and phenylboronic acid (533 mg, 4.0 mmol, 4.0 equiv.) in dioxane (10 mL) was stirred at 110 °C for 24 h. The resulting dark solution was diluted with CH_2Cl_2 and dried with anhydrous $MgSO_4$. The mixture was filtered through a pad of Celite and concentrated under vacuum. The residue was dissolved in dichloromethane (5 mL), the extract filtered and concentrated and diethyl ether (50 mL) was slowly added to initiate precipitation of the product. ^{1}H NMR (400 MHz, $CDCl_3$): δ (ppm), 7.02 (s, 2H, C**H**$_{ar}$), 6.92 (s, 4H, C**H**$_{ar}$), 3.81 (s, 6H, OC**H**$_3$), 2.04 (s, 12H, CC**H**$_3$). ^{13}C{^{1}H} NMR (100 MHz, $CDCl_3$): δ (ppm), 183.69 (**C**=O), 154.57 (**C**−O), 137.39 (**C**CH_3), 130.35 (**C**$_{ar}$), 128.13 (**C**H_{ar}), 61.49 (O**C**H_3), 21.32 (C**C**H_3). ESI-MS: 399.6 $[M + Na]^+$. Elemental Analysis (%): Calc. for $C_{24}H_{24}O_4$: C, 76.57; H, 6.43. Found: C, 76.38; H, 6.30.

Synthesis of 2,5-dihydroxy-3,6-dimesityl-1,4-benzoquinone ***(H_2L^f)***. Black solid, Yield: 57 mg, 0.16 mmol (68%). To a solution of compound ($C_2H_6L^c$) (90 mg, 0.24 mmol) in anhydrous CH_2Cl_2 (8.0 mL) was added slowly a solution of BBr_3 in CH_2Cl_2 (1.0 M, 1.0 mL) at –78 °C. The reaction mixture was stirred under argon for 12 h until room temperature was attained. The reaction was quenched with methanol, and the resulting solution was concentrated under vacuum. The compound was obtained from dioxane. ^{1}H NMR (400 MHz, $CDCl_3$): δ (ppm), 8.15 (br, 2H, O**H**$_{ar}$), 7.26 – 7.05 (m, 6H, C**H**$_{ar}$), 2.38 (s, 12H, CC**H**$_3$). 347.6 $[M - H]^-$.

Elemental Analysis (%): Calc. for $C_{22}H_{20}O_4 \cdot 0.5\ Br_3$: C, 56.43; H, 4.31. Found: C, 56.58; H, 4.76.

General Synthetic Method for the Arene-Ruthenium Metalla-Clips of the General Formula [(p-cymene)$_2$Ru$_2$(μ-L^n)] **(20d-20f)**.

A mixture of (*p*-cymene)$_2$Ru$_2$(μ-Cl)$_2$Cl$_2$ (200 mg, 0.33 mmol), 2,5-Dihydroxy-3-phenyl-1,4-benzoquinone (71 mg, 0.33 mmol), 2,5-Dihydroxy-3,6-diphenyl-1,4-benzoquinone (96 mg, 0.33 mmol), 2,5-Dihydroxy-3,6-diphenyl-3,5-dimethyl-1,4-benzoquinone (114 mg, 0.33 mmol) in MeOH (30 mL) was stirred for 15 h at room temperature. The precipitate was filtered, washed with diethyl ether, pentane, and dried in vacuo.

[**20d**]**:** Black solid, Yield: 185 mg, 0.24 mmol (73%). ^{1}H NMR (400 MHz, CD_2Cl_2): δ (ppm), 7.53 – 7.47 (m, 2H, C**H**$_{ar}$), 7.40 – 7.36 (m, 2H, C**H**$_{ar}$), 7.30 – 7.26 (m, 1H, C**H**$_{ar}$), 5.79 (s, 1H, C**H**$_{dobq}$), 5.66 (d, 4H, $^3J_{H\text{-}H}$ = 5.9 Hz, C**H**$_{p\text{-}cym}$), 5.39 (d, 4H, $^3J_{H\text{-}H}$ = 5.9 Hz, C**H**$_{p\text{-}cym}$), 2.93 – 2.86 (m, 2H, C**H**(CH$_3$)$_2$), 2.27 (s, 6H, C**H**$_3$), 1.37 (d, 6H, $^3J_{H\text{-}H}$ = 7.0 Hz, CH(C**H**$_3$)$_2$), 1.35 (d, 6H, $^3J_{H\text{-}H}$ = 7.0 Hz, CH(C**H**$_3$)$_2$). ^{13}C{^{1}H} NMR (100 MHz, CD_2Cl_2): δ (ppm), 184.12 (**C**=O), 130.77 (**C**H$_{ar}$), 127.87 (**C**H$_{ar}$), 126.89 (**C**H$_{ar}$), 101.08 (C**H**$_{dobq}$) 82.34 (**C**H$_{p\text{-}cym}$), 79.54 (**C**H$_{p\text{-}cym}$), 31.73 (**C**H(CH$_3$)$_2$), 22.69 (CH(**C**H$_3$)$_2$), 22.48 (CH(**C**H$_3$)$_2$), 18.78 (**C**H$_3$). IR: υ (cm^{-1}): 3042 (w, CH$_{p\text{-}cym}$), 1520 (s, C=O).UV-visible: (1.0 × 10^{-5} M, CH_2Cl_2, 298 K): λ_{max} 507 nm (ε = 23 910 M^{-1} · cm^{-1}). ESI-MS: 779.5 [M + Na]$^+$, 723.3 [M – Cl]$^+$. Elemental Analysis (%): Calc. for $C_{32}H_{34}O_4Cl_2Ru_2 \cdot H_2O$: C, 49.68; H, 4.69. Found: C, 49.82; H, 4.74.

[20e]: Black solid, Yield: 192 mg, 0.23 mmol (70%). ^{1}H NMR (400 MHz, CD_2Cl_2): δ (ppm), 7.60 – 7.57 (m, 4H, C**H**$_{ar}$), 7.42 – 7.38 (m, 4H, C**H**$_{ar}$), 7.31 – 7.29 (m, 2H, C**H**$_{ar}$), 5.68 (d, 4H, $^3J_{H\text{-}H}$ = 5.9 Hz, C**H**$_{p\text{-}cym}$), 5.37 (d, 4H, $^3J_{H\text{-}H}$ = 5.9 Hz, C**H**$_{p\text{-}cym}$), 2.70 – 2.63 (m, 2H, C**H**(CH$_3$)$_2$), 2.30 (s, 2H, C**H**$_3$), 2.26 (s, 4H, C**H**$_3$), 1.36 (d, 12H, $^3J_{H\text{-}H}$ = 7.0 Hz, CH(C**H**$_3$)$_2$). ^{13}C{^{1}H} NMR (100 MHz, CD_2Cl_2): δ (ppm), 180.31 (**C**=O), 131.02 (**C**H$_{ar}$), 128.06 (**C**H$_{ar}$), 127.19 (**C**H$_{ar}$), 101.08 (C**H**$_{dobq}$), 83.29 (**C**H$_{p\text{-}cym}$), 79.58 (**C**H$_{p\text{-}cym}$), 31.52 (**C**H(CH$_3$)$_2$), 22.86 (CH(**C**H$_3$)$_2$), 18.56 (**C**H$_3$). IR: υ (cm^{-1}): 3050 (w, CH$_{p\text{-}cym}$), 1637 (s, C=O). UV-visible: (1.0 × 10^{-5} M, CH_2Cl_2, 298 K): λ_{max} 295 nm (ε = 32 480 M^{-1} · cm^{-1}), 515 nm (ε = 22 610 M^{-1} · cm^{-1}). ESI-MS: 854.2 [M + Na]$^+$, 796.2 [M – Cl]$^+$. Elemental Analysis (%): Calc. for $C_{38}H_{38}O_4Cl_2Ru_2$: C, 54.87; H, 4.60. Found: C, 54.36; H, 4.78.

[**20f**]**:** Black solid, Yield: 175 mg, 0.20 mmol (60%). ^{1}H NMR (400 MHz, $CDCl_3$): δ (ppm), 7.38 – 7.37 (m, 2H, C**H**$_{ar}$), 7.29 – 7.28 (m, 2H, C**H**$_{ar}$), 6.90 (br, 2H, C**H**$_{ar}$), 5.68 – 5.65 (m, 4H, C**H**$_{p\text{-}cym}$), 5.36 – 5.32 (m, 4H, C**H**$_{p\text{-}cym}$), 2.96 – 2.91 (m, 2H, C**H**$(CH_3)_2$), 2.44 (s, 4H, C**H**$_3$), 2.35 (s, 8H, C**H**$_3$), 2.29 (s, 6H, C**H**$_3$), 1.43 (d, 12H, $^{3}J_{H\text{-}H}$ = 7.0 Hz, CH(C**H**$_3)_2$). ^{13}C{^{1}H} NMR (100 MHz, $CDCl_3$): δ (ppm), 181.13 (**C**=O), 136.26 (**C**H$_{ar}$), 130.34 (**C**H$_{ar}$), 128.37 (**C**H$_{ar}$), 99.94 (**C**$_{dobq}$), 96.29 (**C**$_{dobq}$), 83.20 (**C**H$_{p\text{-}cym}$), 79.22 (**C**H$_{p\text{-}cym}$), 31.39 (**C**H$(CH_3)_2$), 23.88 (**C**H$_3$), 22.69 (CH(**C**H$_3)_2$), 21.49 (**C**H$_3$), 18.43 (**C**H$_3$). IR: υ (cm^{-1}): 3063 (w, CH$_{p\text{-}cym}$), 1600 (s, C=O). UV-visible: (1.0 × 10^{-5} M, CH_3CN, 298 K): λ_{max} 300 nm (ε = 20 262 M^{-1} · cm^{-1}), 520 nm (ε = 13 000 M^{-1} · cm^{-1}). ESI-MS: 852.5 [M – Cl]$^{+}$, 909.4 [M + Na]$^{+}$. Elemental Analysis (%): Calc. for $C_{42}H_{46}O_4Cl_2Ru_2 \cdot CH_2Cl_2$: C, 53.09; H, 4.97. Found: C, 53.00; H, 4.77.

General Synthetic Method for the Hexacationic Metalla-Prisms of the General Formula [(p-cymene)$_6$Ru$_6$(μ-tpt)$_2$(μ-L^n)$_3$]$^{6+}$ ***([21d]$^{6+}$-[21f]$^{6+}$)****.*

A mixture of the dinuclear clip (**20d**-**20f**) of the general formula [(*p*-cymene)$_2$Ru$_2$Cl$_2$(μ-L^n)] (0.16 mmol) and 2 equiv of $AgCF_3SO_3$ (0.32 mmol) in MeOH/ CH_2Cl_2, (1/1, 30 mL) was stirred at room temperature for 2 h and the solution was filtered to remove AgCl. To the filtrate 2,4,6-tris(4-pyridyl)-1,3,5-triazine (0.11 mmol) were added. The mixture was stirred at 60°C for 24 h, and the solvent removed under vacuum. The residue was dissolved in dichloromethane (20 mL), the extract filtered and concentrated (3 mL) and diethyl ether was slowly added to initiate precipitation of the product as a red solid.

[21d][CF$_3$SO$_3$]$_6$: Red solid, Yield: 111 mg, 0.031 mmol (58%). ^{1}H NMR (400 MHz, CD_2Cl_2): δ (ppm), 8.76 – 8.72 (m, 12H, C**H**$_{tpt}$), 8.52 – 8.48 (m, 12H, C**H**$_{tpt}$), 7.64 – 7.59 (m, 6H, C**H**$_{ar}$), 7.51 – 7.48 (m, 3H, C**H**$_{ar}$), 7.36 – 7.33 (m, 6H, C**H**$_{ar}$), 5.97 – 5.95 (m, 3H, C**H**$_{dobq}$), 5.88 – 5.83 (m, 12H, C**H**$_{p\text{-}cym}$), 5.73 (d, 6H, $^{3}J_{H\text{-}H}$ = 6.1 Hz, C**H**$_{p\text{-}cym}$), 5.69 (d, 6H, $^{3}J_{H\text{-}H}$ = 6.1 Hz, C**H**$_{p\text{-}cym}$), 2.90 – 2.83 (m, 6H, C**H**$(CH_3)_2$), 2.23 – 2.22 (m, 18H, C**H**$_3$), 1.38 – 1.36 (m, 36H, CH(C**H**$_3)_2$). ^{13}C{^{1}H} NMR (100 MHz, CD_2Cl_2): δ (ppm), 184.24 (**C**=O), 181.48 (**C**=O), 170.06 (**C**H$_{tpt}$), 154.43 (**C**$_{tpt}$), 144.94 (**C**$_{tpt}$), 130.40 (**C**H$_{ar}$), 128.69 (**C**H$_{ar}$), 128.26 (**C**H$_{ar}$), 125.61 (**C**H$_{tpt}$), 104.81 (**C**$_{p\text{-}cym}$), 102.44 (**C**H$_{dobq}$), 99.15 (**C**$_{p\text{-}cym}$), 83.17 (**C**H$_{p\text{-}cym}$), 82.93 (**C**H$_{p\text{-}cym}$), 82.66 (**C**H$_{p\text{-}cym}$), 31.83 (**C**H$(CH_3)_2$), 22.49 (CH(**C**H$_3)_2$), 22.37 (CH(**C**H$_3)_2$), 18.35 (**C**H$_3$). IR: υ (cm^{-1}): 2970 (w, CH$_{p\text{-}cym}$), 1630 (s, C=O), 1258 (s, CF_3). UV-

visible: (1.0×10^{-5} M, CH_2Cl_2, 298 K): λ_{max} 251 nm (ε = 150 910 $M^{-1} \cdot cm^{-1}$), 298 nm (ε = 85 020 $M^{-1} \cdot cm^{-1}$) , 498 nm (ε = 55 370 $M^{-1} \cdot cm^{-1}$). ESI-MS: 1041.7 $[M - 3\ CF_3SO_3]^{3+}$. Elemental Analysis (%): Calc. for $C_{138}H_{126}F_{18}N_{12}O_{30}Ru_6S_6 \cdot 7\ CH_2Cl_2$: C, 41.79; H, 3.39; N, 4.03. Found: C, 41.62; H, 3.49; N, 4.43.

[21e][CF_3SO_3]$_6$: Red solid, Yield: 124mg, 0.033 mmol (61%). ^{1}H NMR (400 MHz, CD_2Cl_2): δ (ppm), 8.74 (d, 12H, $^3J_{H\text{-}H}$ = 6.7 Hz, C**H**$_{tpt}$), 8.44 (d, 12H, $^3J_{H\text{-}H}$ = 6.6 Hz, C**H**$_{tpt}$), 7.65 – 7.62 (m, 12H, C**H**$_{ar}$), 7.53 – 7.49 (m, 6H, C**H**$_{ar}$), 7.43 – 7.40 (m, 12H, C**H**$_{ar}$), 5.82 (d, 12H, $^3J_{H\text{-}H}$ = 6.6 Hz, C**H**$_{p\text{-}cym}$), 5.68 (d, 12H, $^3J_{H\text{-}H}$ = 6.6 Hz, C**H**$_{p\text{-}cym}$), 2.83 (sep, 6H, $^3J_{H\text{-}H}$ = 6.8 Hz, C**H**$(CH_3)_2$), 2.22 (s, 18H, C**H**$_3$), 1.35 (d, 36H, $^3J_{H\text{-}H}$ = 6.9 Hz, CH(C**H**$_3)_2$). ^{13}C{^{1}H} NMR (100 MHz, CD_2Cl_2): δ (ppm), 181.49 (**C**=O), 170.10 (**C**=O), 154.29 (**C**H$_{tpt}$), 144.96(**C**$_{tpt}$), 130.41 (**C**H$_{ar}$), 129.84 (**C**H$_{ar}$), 128.59 (**C**H$_{ar}$), 128.19 (**C**H$_{ar}$), 125.62 (**C**H$_{ar}$), 104.52 (**C**$_{p\text{-}cym}$), 99.33(**C**$_{p\text{-}cym}$), 84.30 (**C**H$_{p\text{-}cym}$), 83.17 (**C**H$_{p\text{-}cym}$), 32.07 (**C**H$(CH_3)_2$), 22.62 (CH(**C**H$_3)_2$), 18.58 (**C**H$_3$). IR: υ (cm^{-1}): 2970 (w, CH$_{p\text{-}cym}$), 1637 (s, C=O), 1260 (s, CF_3). UV-visible: (1.0×10^{-5} M, CH_2Cl_2, 298 K): λ_{max} 232 nm (ε = 238 010 $M^{-1} \cdot cm^{-1}$), 292 nm (ε = 144 760 $M^{-1} \cdot cm^{-1}$), 508 nm (ε = 76 490 $M^{-1} \cdot cm^{-1}$). ESI-MS: 1118.1 $[M - 3\ CF_3SO_3]^{3+}$. Elemental Analysis (%): Calc. for $C_{156}H_{138}F_{18}N_{12}O_{30}Ru_6S_6 \cdot 3\ CH_2Cl_2$: C, 47.08; H, 3.58; N, 4.14. Found: C, 47.06; H, 3.78; N, 4.22.

[21f][CF_3SO_3]$_6$: Red solid, Yield: 119 mg, 0.030 mmol (56%). ^{1}H NMR (400 MHz, CD_2Cl_2): δ (ppm), 8.60 (br, 12H, C**H**$_{tpt}$), 8.41 (br, 12H, C**H**$_{tpt}$), 7.16 – 7.14 (m, 9H, C**H**$_{ar}$), 7.01 (br, 9H, C**H**$_{ar}$), 5.85 (d, $^3J_{H\text{-}H}$ = 5.9 Hz, C**H**$_{p\text{-}cym}$), 5.74 – 5.70 (m, 12H, C**H**$_{p\text{-}cym}$), 2.87 – 2.83 (m, 6H, C**H**$(CH_3)_2$), 2.61 – 2.59 (m, 12H, C**H**$_3$), 2.52 – 2.50 (m, 24H, C**H**$_3$), 2.30 – 2.27 (m, 18H, C**H**$_3$), 1.39 (d, 36H, $^3J_{H\text{-}H}$ = 6.9 Hz, CH(C**H**$_3)_2$). ^{13}C{^{1}H} NMR (100 MHz, CD_2Cl_2): δ (ppm), 180.71 (**C**=O), 180.60 (**C**=O), 180.57 (**C**=O), 180.47 (**C**=O),153.83 (**C**H$_{tpt}$), 143.89 (**C**$_{tpt}$), 137.34 (**C**$_{ar}$), 137.02 (**C**$_{ar}$), 129.67 (**C**H$_{ar}$), 128.72 (**C**H$_{ar}$), 127.58 (**C**H$_{ar}$), 124.13 (**C**H$_{tpt}$), 102.50 (**C**$_{p\text{-}cym}$), 102.50 (**C**$_{dobq}$), 98.72 (**C**$_{p\text{-}cym}$), 84.24 (**C**H$_{p\text{-}cym}$), 84.04 (**C**H$_{p\text{-}cym}$), 30.94 (**C**H$(CH_3)_2$), 23.13 (**C**H$_3$), 23.05 (**C**H$_3$), 21.20 (CH(**C**H$_3)_2$), 20.42 (**C**H$_3$), 20.37 (**C**H$_3$), 17.14 (**C**H$_3$). IR: υ (cm^{-1}): 2969 (w, CH$_{p\text{-}cym}$), 1603 (s, C=O), 1259 (s, CF_3). UV-visible: (1.0×10^{-5} M, CH_3CN, 298 K): λ_{max} 298 nm (ε = 158 700 $M^{-1} \cdot cm^{-1}$), 398 nm (ε = 214 560 $M^{-1} \cdot cm^{-1}$), 509 nm (ε = 67 460 $M^{-1} \cdot cm^{-1}$). ESI-MS: 882.8 $[M + 4CH_3CN - 4CF_3SO_3]^{4+}$, 1227.1 $[M + 2CH_3CN - 3CF_3SO_3]^{3+}$. Elemental Analysis (%): Calc. for $C_{168}H_{160}F_{18}N_{12}O_{30}Ru_6S_6 \cdot 7\ CH_2Cl_2$: C, 46.07; H, 3.84; N, 3.68. Found: C, 46.12; H, 4.01; N, 3.69.

*Synthesis of Host Guest System of the General Formula [porphin⊂(p-cymene)$_6$Ru$_6$(μ-tpt)$_2$(μ-L)$_3$]$^{6+}$ ([**22d**]$^{6+}$-[**22f**]$^{6+}$)*.

A mixture of 3 equiv (0.16 mmol) of dinuclear metalla-clip (**20d-20f**) of the general formula [(*p*-cymene)$_2$Ru$_2$Cl$_2$(μ-L)], 6 equiv of $AgCF_3SO_3$ (0.32 mmol) and 1 equiv of guest molecule (porphin, 0.053 mmol), in MeOH/ CH_2Cl_2, (1/1, 30 mL) was stirred at reflux for 24 h and then filtered. The solvent was removed, and the dark residue was dissolved in CH_2Cl_2 (3 mL), before slowly adding diethyl ether to precipitate a red solid. The solid was filtered, washed with diethyl ether, and dried under vacuum.

[22d][CF$_3$SO$_3$]$_6$: Red solid, Yield: 128 mg, 0.033 mmol (62%). ^{1}H NMR (400 MHz, CD_2Cl_2): δ (ppm), 9.03 (s, 4H, C**H**$_{po}$), 8.39 – 7.99 (m, 32H, 12H C**H**$_{tpt}$ + 8H C**H**$_{po}$ + 12H C**H**$_{ar}$), 7.88 – 7.79 (m, 3H, C**H**$_{ar}$), 6.93 – 6.90 (m, 3H, C**H**$_{dobq}$), 6.36 (d, 12H, $^3J_{H\text{-}H}$ = 5.8 Hz, C**H**$_{tpt}$), 5.90 – 5.87 (m, 6H, C**H**$_{p\text{-}cym}$), 5.82 – 5.80 (m, 6H, C**H**$_{p\text{-}cym}$), 5.72 – 5.70 (m, 6H, C**H**$_{p\text{-}cym}$), 5.64 – 5.61 (m, 6H, C**H**$_{p\text{-}cym}$), 5.97 – 5.48 (m, 12H, C**H**$_{p\text{-}cym}$), 2.89 – 2.84 (m, 6H, C**H**(CH$_3$)$_2$), 2.16 – 2.14 (m, 18H, C**H**$_3$), 1.40 – 1.38 (m, 36H, CH(C**H**$_3$)$_2$), -6.37 (2H, N**H**po). ^{13}C{^{1}H} NMR (100 MHz, CD_2Cl_2): δ (ppm), 184.89 (**C**=O), 184.85 (**C**=O), 182.14 (**C**=O), 164.43 (**C**=O), 164.40 (**C**=O), 153.43 (**C**$_{tpt}$), 153.37 (**C**$_{tpt}$), 153.35 (**C**H$_{tpt}$), 153.32 (**C**H$_{tpt}$), 131.15 (**C**H$_{po}$), 129.57 (**C**H$_{ar}$), 123.80 (**C**H$_{ar}$), 123.77 (**C**H$_{ar}$), 123.12 (**C**H$_{ar}$), 119.93 (**C**H$_{po}$), 105.10 (**C**$_{p\text{-}cym}$), 105.09 (**C**$_{p\text{-}cym}$), 104.32 (**C**$_{p\text{-}cym}$), 104.29 (**C**$_{p\text{-}cym}$), 99.51 (**C**H$_{dobq}$), 99.48 (**C**H$_{dobq}$), 84.40 (**C**H$_{p\text{-}cym}$), 84.37 (**C**H$_{p\text{-}cym}$), 84.00 (**C**H$_{p\text{-}cym}$), 83.98 (**C**H$_{p\text{-}cym}$), 83.95 (**C**H$_{p\text{-}cym}$), 83.21 (**C**H$_{p\text{-}cym}$), 82.83 (**C**H$_{p\text{-}cym}$), 82.75 (**C**H$_{p\text{-}cym}$), 32.02 (**C**H(CH$_3$)$_2$), 22.72 (CH(**C**H$_3$)$_2$), 22.59 (CH(**C**H$_3$)$_2$), 18.49 (**C**H$_3$). IR: υ (cm^{-1}): 3067.7 (w, CH$_{p\text{-}cym}$), 1606.9 (s, C=O), 1258.4 (s, CF$_3$). UV-visible: (1.0 × 10^{-5} M, CH_3CN, 298 K): λ_{max} 298 nm (ε = 112 010 M^{-1} · cm^{-1}), 398 nm (ε = 211 320 M^{-1} · cm^{-1}), 501 nm (ε = 68 380 M^{-1} · cm^{-1}). ESI-MS: 1793.6 [M – 2CF_3SO_3]$^{2+}$, 1146.1 [M – 3CF_3SO_3]$^{3+}$. Elemental Analysis (%): Calc. for $C_{158}H_{140}F_{18}N_{16}O_{30}Ru_6S_6$ · 6 CH_2Cl_2: C, 44.84; H, 3.49; N, 5.10. Found: C, 44.93; H, 3.57; N, 5.16.

[22e][CF$_3$SO$_3$]$_6$: Red solid, Yield: 151 mg, 0.037 mmol (69%). ^{1}H NMR (400 MHz, CD_2Cl_2): δ (ppm), 8.95 (s, 4H, C**H**$_{po}$), 8.23 – 8.21 (m, 12H, C**H**$_{ar}$), 8.19 (s, 8H, C**H**$_{po}$), 8.16 – 8.13 (m, 24H, C**H**$_{ar}$ + C**H**$_{tpt}$), 7.91 (t, 6H, $^3J_{H\text{-}H}$ = 7.3 Hz, C**H**$_{ar}$), 6.37 (d, 12H, $^3J_{H\text{-}H}$ = 5.3, C**H**$_{tpt}$), 5.81 (d, 12H, $^3J_{H\text{-}H}$ = 5.7 Hz, C**H**$_{p\text{-}cym}$), 5.66 (d, 12H, $^3J_{H\text{-}H}$ = 5.8 Hz, C**H**$_{p\text{-}cym}$), 2.88 – 2.78 (m, 6H, C**H**(CH$_3$)$_2$), 2.20 (s, 18H, C**H**$_3$), 1.39 (d, 36H, $^3J_{H\text{-}H}$ = 6.9 Hz, CH(C**H**$_3$)$_2$), -6.40 (s, 2H, N**H**$_{po}$). ^{13}C{^{1}H} NMR (100 MHz, CD_2Cl_2): δ (ppm), 181.85 (**C**=O), 164.41 (**C**=O), 153.31 (**C**$_{tpt}$),

140.97, 131.21 (**C**H_{ar}), 129.64 (**C**H_{ar}), 129.64 (**C**H_{ar}), 123.92 (**C**H_{ar}), 116.83 (**C**H_{po}), 104.73 (**C**$_{p\text{-}cym}$), 84.53 (**C**$H_{p\text{-}cym}$), 83.20 (**C**$H_{p\text{-}cym}$), 32.11 (**C**$H(CH_3)_2$), 22.71 ($CH(\mathbf{C}H_3)_2$), 18.60 (**C**H_3). IR: υ (cm^{-1}): 3067.7 (w, $CH_{p\text{-}cym}$), 1628 (s, C=O), 1259 (s, CF_3). UV-visible: (1.0×10^{-5} M, CH_3CN, 298 K): λ_{max} 292 nm ($\varepsilon = 174\,260\ M^{-1} \cdot cm^{-1}$), 401 nm ($\varepsilon = 226\,020\ M^{-1} \cdot cm^{-1}$), 506 nm ($\varepsilon = 80\,460\ M^{-1} \cdot cm^{-1}$). ESI-MS: 1907.2 $[M - 2CF_3SO_3]^{2+}$, 1221.2 $[M - 3CF_3SO_3]^{3+}$, 879 $[M - 4CF_3SO_3]^{4+}$. Elemental Analysis (%): Calc. for $C_{176}H_{152}F_{18}N_{16}O_{30}Ru_6S_6 \cdot 2\ CH_2Cl_2$: C, 49.93; H, 3.67; N, 5.23. Found: C, 49.81; H, 4.01; N, 5.21.

[22f][CF_3SO_3]$_6$: Red solid, Yield: 148 mg, 0.035 mmol (65%). ^{1}H NMR (400 MHz, CD_2Cl_2): δ (ppm), 8.94 – 8.71 (m, 4H, C**H**$_{po}$), 8.17 – 8.12 (m, 23H, C**H**$_{tpt}$ + C**H**$_{po}$ + C**H**$_{ar}$), 7.97 – 7.96 (m, 6H, C**H**$_{ar}$), 7.80 (br, 6H, C**H**$_{ar}$), 7.57 – 7.56 (m, 3H, C**H**$_{ar}$), 6.36 – 6.30 (m, 12H, C**H**$_{tpt}$), 5.84 – 5.80 (br, 12H, C**H**$_{p\text{-}cym}$), 5.73 – 5.68 (m, 12H, C**H**$_{p\text{-}cym}$), 3.05 – 3.03 (m, 18H, C**H**$_3$), 2.93 – 2.92 (m, 18H, C**H**$_3$), 2.86 – 2.83 (m, 6H, C**H**$(CH_3)_2$), 2.31 – 2.28 (s, 18H, C**H**$_3$), 1.43 (d, 36H, $^3J_{H\text{-}H}$ = 6.9 Hz, $CH(C\mathbf{H}_3)_2$), -6.43 (2H, N**H**po). ^{13}C{^{1}H} NMR (100 MHz, CD_2Cl_2): δ (ppm), 181.86 (**C**=O), 181.79 (**C**=O), 181.75 (**C**=O), 181.69 (**C**=O), 153.33 (**C**H_{tpt}),139.33 (**C**$_{ar}$), 138.88 (**C**$_{ar}$), 138.85 (**C**$_{ar}$), 130.84 (**C**H_{ar}), 130.74 (**C**H_{ar}), 128.84 (**C**H_{ar}), 123.77 (**C**H_{tpt}), 104.10 (**C**H_{po}), 103.97 (**C**H_{po}), 99.90 (**C**$_{p\text{-}cym}$), 85.10 (**C**$H_{p\text{-}cym}$), 85.05 (**C**$H_{p\text{-}cym}$), 83.13 (**C**$H_{p\text{-}cym}$), 83.07 (**C**$H_{p\text{-}cym}$), 32.09 (**C**$H(CH_3)_2$), 25.11 (**C**H_3), 25.04 (**C**H_3), 22.43 (**C**H_3), 22.40 ($CH(\mathbf{C}H_3)_2$), 18.68 (**C**H_3), 18.66 (**C**H_3), 18.62 (**C**H_3). IR: υ (cm^{-1}): 2969 (w, $CH_{p\text{-}cym}$), 1603 (s, C=O), 1259 (s, CF_3). UV-visible: (1.0×10^{-5} M, CH_3CN, 298 K): λ_{max} 298 nm ($\varepsilon = 197\,300\ M^{-1} \cdot cm^{-1}$), 398 nm ($\varepsilon = 232\,940\ M^{-1} \cdot cm^{-1}$), 511 nm ($\varepsilon = 84\,550\ M^{-1} \cdot cm^{-1}$). ESI-MS: 1329.5 $[M + 2CH_3OH - 3CF_3SO_3]^{3+}$. Elemental Analysis (%): Calc. for $C_{188}H_{176}F_{18}N_{16}O_{30}Ru_6S_6 \cdot 7\ CH_2Cl_2$: C, 48.04; H, 3.93; N, 4.60. Found: C, 48.08; H, 3.98; N, 4.75.

Crystal Data and Structure Refinement for Compounds [trans-4](CF$_3$SO$_3$)$_2$ and [trans-7](CF$_3$SO$_3$)$_2$:

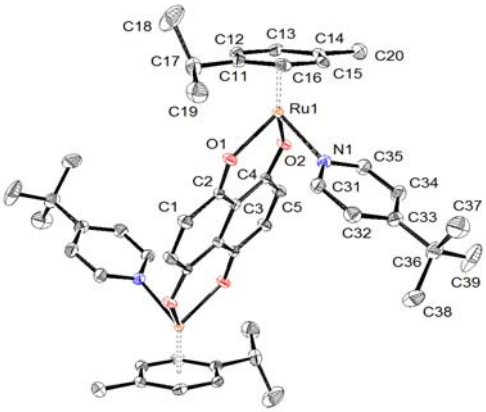

[trans-4](CF$_3$SO$_3$)$_2$

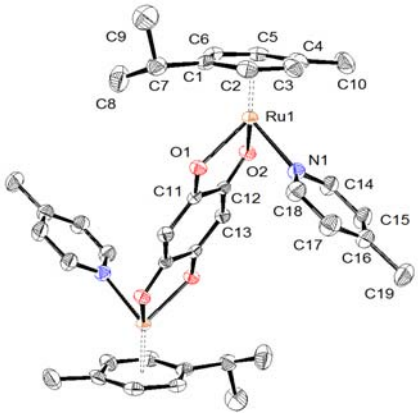

[trans-7](CF$_3$SO$_3$)$_2$:

Table 10. Crystallographic data and structure refinement parameters for compounds [trans 4](CF$_3$SO$_3$)$_2$ · 2 (CH$_3$)$_2$CO and [trans-7](CF$_3$SO$_3$)$_2$.

	[*trans*-**4**](CF$_3$SO$_3$)$_2$	[*trans*-**7**](CF$_3$SO$_3$)$_2$
chemical formula	$C_{56}H_{70}F_6N_2O_{12}Ru_2S_2$	$C_{40}H_{44}F_6N_2O_{10}Ru_2S_2$
formula weight	1343.40	1093.03
crystal system	triclinic	monoclinic
space group	*P* -1	*P* 2$_1$/*c*
crystal size (mm^3)	0.25 × 0.24 × 0.19	0.22 × 0.21 × 0.18
crystal color and shape	green block	green block
a (Å)	11.4339(6)	10.1102(6)
b (Å)	15.2550(8)	9.7424(4)
c (Å)	17.1872(9)	22.0972(14)
α (°)	82.734(4)	90
β (°)	83.408(4)	91.082(5)
γ (°)	80.881(4)	90
cell volume (Å^3)	2922.4(3)	2176.1(2)
T (K)	173(2)	173(2)
Z	2	2
scan range (°)	1.71 < θ < 29.22	1.84 < θ < 29.21
ρ_{calcd} (g cm^{-3})	1.527	1.668
μ (mm^{-1})	0.669	0.874
unique reflections	15804	5893
reflections used [$I > 2\sigma(I)$]	11073	4174
R_{int}	0.0795	0.0632
final *R* indices [$I > 2\sigma(I)$][a]	0.0385, wR_2 0.0873	0.0273, wR_2 0.0509
R indices (all data)[b]	0.0593, wR_2 0.0911	0.0512, wR_2 0.0536
GOF[c]	0.893	0.840
max, min $\Delta\rho/e$ (Å^{-3})	1.927, -1.127	0.620, -0.524

[a] $R_1 = \Sigma||F_o| - |F_c||/\Sigma|F_o|$. [b] $wR_2 = \{\Sigma[w(F_o^2 - F_c^2)^2]/\Sigma[w(F_o^2)^2]\}^{1/2}$. [c] GOF = $\{\Sigma[w(F_o^2 - F_c^2)^2]/(n - p)\}^{1/2}$, where *n* is the number of reflections and *p* is the total number of parameters refined.

Crystal Data and Structure Refinement for Complexes 14a and 14c *(the synthesis of these two complexes and the crystals growing was performed by the Arion group at Vienna University)*

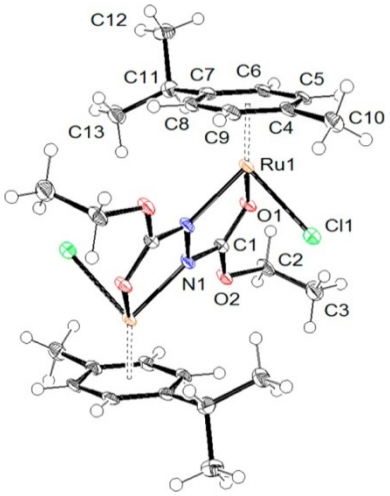

14a

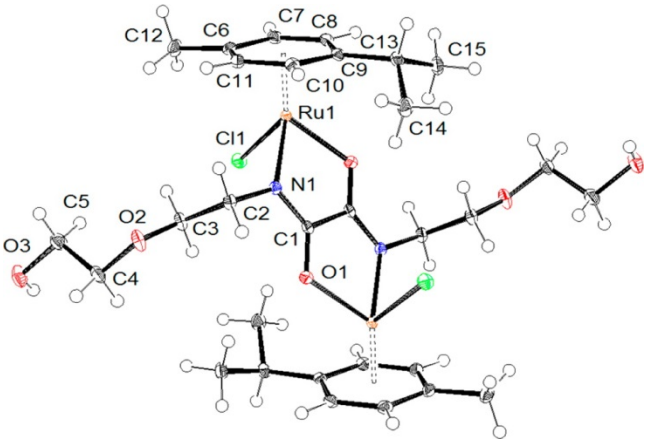

41c

Table 11. Crystallographic data and structure refinement parameters for complexes ***14a*** *and* ***41c****.*

	14a	**14c**
chemical formula	$C_{26}H_{38}Cl_2N_2O_4Ru_2$	$C_{30}H_{46}Cl_2N_2O_6Ru_2$
formula weight	715.62	803.73
space group	*P* -1	*P* -1
a (Å)	8.5335(5)	9.0000(5)
b (Å)	9.4426(5)	9.1532(5)
c (Å)	10.4007(6)	9.3851(6)
α (°)	71.004(3)	96.056(3)
β (°)	70.609(3)	65.188(3)
γ (°)	65.188(3)	95.327(8)
Crystal size (mm^3)	0.18 × 0.15 × 0.10	0.15 × 0.12 × 0.10
T (K)	100(2)	100(2)
Z	1	1
λ (A°)	0.71073	0.71073
ρ_{calcd} ($g\ cm^{-3}$)	1.697	1.747
μ (mm^{-1})	1.303	1.210
R_1[a]	0.0341	0.0224
wR_2[b]	0.0891	0.0622
GOF[c]	1.092	1.032

[a] $R_1 = \Sigma||F_o| - |F_c||/\Sigma|F_o|$. [b] $wR_2 = \{\Sigma[w(F_o^2 - F_c^2)^2]/\Sigma[w(F_o^2)^2]\}^{1/2}$. [c] GOF $= \{\Sigma[w(F_o^2 - F_c^2)^2]/(n - p)\}^{1/2}$, where *n* is the number of reflections and *p* is the total number of parameters refined.

Crystal Data and Structure Refinement for Complexes 20d

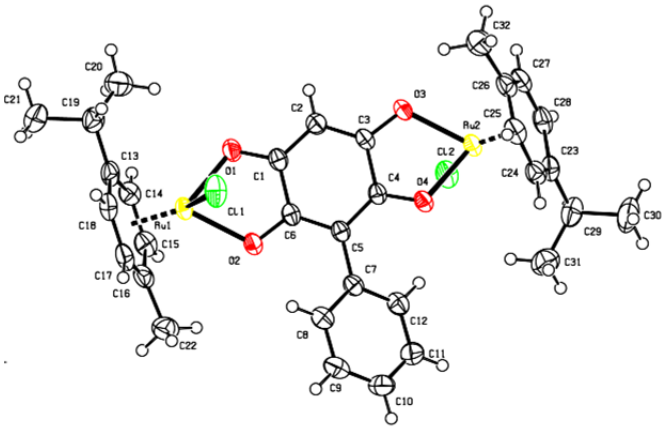

Table 12. *Crystallographic data and structure refinement parameters for complex* ***20d***.

	20d
chemical formula	$C_{32}H_{34}Cl_2O_4Ru_2$
formula weight	755.63
crystal system	orthorhombic
space group	*P na21*
crystal color and shape	Red rod
a (Å)	14.6663(4)
b (Å)	b=11.2056(3)
c (Å)	c=18.1049(7)
α (°)	90
β (°)	90
γ (°)	90
cell volume (Å^3)	2975.44(16)
T (K)	173 K
Z	4
scan range (°)	$1.93 < \theta < 29.220$
ρ_{calcd} (g cm^{-3})	1.687
μ (mm^{-1})	1.231
R_1[a]	0.0271
wR_2[b]	0.0632
GOF[c]	0.969

[a] $R_1 = \Sigma||F_o| - |F_c||/\Sigma|F_o|$. [b] $wR_2 = \{\Sigma[w(F_o^2 - F_c^2)^2]/\Sigma[w(F_o^2)^2]\}^{1/2}$.
[c] GOF = $\{\Sigma[w(F_o^2 - F_c^2)^2]/(n-p)\}^{1/2}$, where *n* is the number of reflections and *p* is the total number of parameters refined.

8

References

1 J. M. Lehn, *Science* **1993**, *260*, 1762-1763.

2 J. M. Lehn, *Angew. Chem. Int. Ed.* **1990**, *29*, 1304-1319.

3 J.-P. Sauvage, M. W. Hosseini, *Comprehensive Supramolecular Chemistry, Volume 9: Templating, Self-Assembly, and Self-Organization*, Pergamon, **1996**.

4 J. M. Lehn, *Supramolecular Chemistry: Concepts and Perspectives*, VCH, **1995**.

5 J. S. Lindsey, *New. J. Chem.* **1991**, *15*, 153-180.

6 B. J. Holliday, C. A. Mirkin, *Angew. Chem. Int. Edit.* **2001**, *40*, 2022-2043.

7 J. M. Lehn, *Angew. Chem. Int. Ed.* **1988**, *27*, 89-112.

8 R. Chakrabarty, P. S. Mukherjee, P. J. Stang, *Chem. Rev.* **2011**, *111*, 6810-6918.

9 A. Werner, *Z. Anorg. Allg. Chem.* **1893**, *3*, 267-330.

10 http://ak-powell.chemie.uni-karlsruhe.de/teaching/Supramolecular%20Chemistry.pdf

11 E. Fischer, *Berichte der deutschen chemischen Gesellschaft* **1894**, *27*, 2985-2993.

12 P. Ehrlich, *Collected studies on immunity*, Wiley, **1906**.

13 J. R. Moran, S. Karbach, D. J. Cram, *J. Am. Chem. Soc.* **1982**, *104*, 5826-5828.

14 C. J. Pedersen, *J. Am. Chem. Soc.* **1967**, *89*, 7017-7036.

15 (a) J. W. Steed, *Chem. Soc. Rev.* **2009**, *38*, 506-519; (b) C. B. Aakeroy, A. Rajbanshi, J. Desper, *Chem. Commun.* **2011**, *47*, 11411-11413; (c) J. Chen, J. Rebek, *Org. Lett.* **2002**, *4*, 327-329.

16 N. Kishi, M. Akita, M. Kamiya, S. Hayashi, H.-F. Hsu, M. Yoshizawa, *J. Am. Chem. Soc.* **2013**, *135*, 12976-12979.

17 G. M. Whitesides, M. Boncheva, *P. Natl. Acad. Sci. USA.* **2002**, *99*, 4769-4774.

18 D. S. Lawrence, T. Jiang, M. Levett, *Chem. Rev.* **1995**, *95*, 2229-2260.

19 (a) D. J. Cram, J. M. Cram, *Acc. Chem. Res.* **1978**, *11*, 8-14; (b) M. Fujita, M. Yoshizawa, in *Modern Supramolecular Chemistry*, Wiley-VCH Verlag GmbH & Co. KGaA, **2008**, pp. 277-313.

20 (a) T. Weilandt, R. W. Troff, H. Saxell, K. Rissanen, C. A. Schalley, *Inorg. Chem.* **2008**, *47*, 7588-7598; (b) D. Zhao, J. S. Moore, *Chem. Commun.* **2003**, 807-818; (c) M. M. Conn, J. Rebek, *Chem. Rev.* **1997**, *97*, 1647-1668.

21 (a) B. H. Northrop, Y. R. Zheng, K. W. Chi, P. J. Stang, *Acc. Chem. Res.* **2009**, *42*, 1554-1563; (b) Y.-R. Zheng, H.-B. Yang, B. H. Northrop, K. Ghosh, P. J. Stang, *Inorg. Chem.* **2008**, *47*, 4706-4711.

22 P. J. Stang, D. H. Cao, S. Saito, A. M. Arif, *J. Am. Chem. Soc.* **1995**, *117*, 6273-6283.

23 P. J. Stang, B. Olenyuk, *Acc. Chem. Res.* **1997**, *30*, 502-518.

24 K. Kobayashi, M. Yamanaka, *Chem. Soc. Rev.* **2015**, *44*, 449-466.

25 D. P. Funeriu, J.-M. Lehn, K. M. Fromm, D. Fenske, *Chem. Eur. J.* **2000**, *6*, 2103-2111.

26 M. Yoneya, S. Tsuzuki, T. Yamaguchi, S. Sato, M. Fujita, *ACS Nano* **2014**, *8*, 1290-1296.

27 M. Fujita, F. Ibukuro, H. Seki, O. Kamo, M. Imanari, K. Ogura, *J. Am. Chem. Soc.* **1996**, *118*, 899-900.

28 B. Kilbas, S. Mirtschin, R. Scopelliti, K. Severin, *Chem. Sci.* **2012**, *3*, 701-704.

29 P. J. Lusby, P. Müller, S. J. Pike, A. M. Z. Slawin, *J. Am. Chem. Soc.* **2009**, *131*, 16398-16400.

30 (a) C. Browne, T. K. Ronson, J. R. Nitschke, *Angew. Chem. Int. Ed.* **2014**, *53*, 10701-10705; (b) I. A. Riddell, M. M. J. Smulders, J. K. Clegg, Y. R. Hristova, B. Breiner, J. D. Thoburn, J. R. Nitschke, *Nat. Chem.* **2012**, *4*, 751-756.

31 J. D. Watson, F. H. C. Crick, *Nature* **1953**, *171*, 737-738.

32 S. Denzinger, *Adv. Mater* **1996**, *8*, 367-367.

33 J.-M. Lehn, *P. Natl. Acad. Sci. USA.* **2002**, *99*, 4763-4768.

34 T. Iwasawa, E. Mann, J. Rebek, *J. Am. Chem. Soc.* **2006**, *128*, 9308-9309.

35 D. Ajami, H. Dube, J. Rebek, *J. Am. Chem. Soc.* **2011**, *133*, 9689-9691.

36 K. Kobayashi, T. Shirasaka, E. Horn, N. Furukawa, *Tetrahedron Lett.* **1999**, *40*, 8883-8886.

37 T. Sawada, A. Matsumoto, M. Fujita, *Angew. Chem. Int. Ed.* **2014**, *53*, 7228-7232.

38 M. R. Jones, N. C. Seeman, C. A. Mirkin, *Science* **2015**, *347*.

39 F. A. Aldaye, A. L. Palmer, H. F. Sleiman, *Science* **2008**, *321*, 1795-1799.

40 F. A. Aldaye, H. F. Sleiman, *J. Am. Chem. Soc.* **2007**, *129*, 10070-+.

41 (a) T. R. Cook, Y. R. Zheng, P. J. Stang, *Chem. Rev.* **2013**, *113*, 734-777; (b) S. Leininger, B. Olenyuk, P. J. Stang, *Chem. Rev.* **2000**, *100*, 853-907.

42 A. Ciesielski, M. El Garah, S. Haar, P. Kovaricek, J. M. Lehn, P. Samori, *Nat. Chem.* **2014**, *6*, 1017-1023.

43 M. Fujita, M. Tominaga, A. Hori, B. Therrien, *Acc. Chem. Res.* **2005**, *38*, 369-378.

44 J. W. Steed, J. L. Atwood, Editors, *Supramolecular Chemistry, Second Edition*, John Wiley & Sons, Ltd., **2009**.

45 M. Fujita, J. Yazaki, K. Ogura, *J. Am. Chem. Soc.* **1990**, *112*, 5645-5647.

46 S. R. Seidel, P. J. Stang, *Acc. Chem. Res.* **2002**, *35*, 972-983.

47 S. Derossi, M. Casanova, E. Iengo, E. Zangrando, M. Stener, E. Alessio, *Inorg. Chem.* **2007**, *46*, 11243-11253.

48 A.-M. Stadler, C. Burg, J. Ramirez, J.-M. Lehn, *Chem. Commun.* **2013**, *49*, 5733-5735.

49 S. Ghosh, S. R. Batten, D. R. Turner, P. S. Mukherjee, *Organometallics* **2007**, *26*, 3252-3255.

50 M. Vázquez, M. R. Bermejo, M. Licchelli, A. M. González-Noya, R. M. Pedrido, C. Sangregorio, L. Sorace, A. M. García-Deibe, J. Sanmartín, *Eur. J. Inorg. Chem.* **2005**, *2005*, 3479-3490.

51 M. Yoshizawa, J. K. Klosterman, M. Fujita, *Angew. Chem. Int. Ed.* **2009**, *48*, 3418-3438.

52 J. Reedijk, *Platin. Met. Rev.* **2008**, *52*, 2-11.

53 J. W. Steed, D. R. Turner, K. J. Wallace, Editors, *Core Concepts in Supramolecular Chemistry and Nanochemistry*, John Wiley & Sons Ltd., **2007**.

54 R. G. Pearson, *J. Am. Chem. Soc.* **1963**, *85*, 3533-3539.

55 R. Singh, *Inorganic Chemistry*, Mittal pubications, **2002**.

56 coordination compound. (2015). In Encyclopædia Britannica. Retrieved from http://www.britannica.com/EBchecked/topic/136410/coordination-compound.

57 H. Taube, *Chem. Rev.* **1952**, *50*, 69-126.

58 H. E. Bryndza, W. Tam, *Chem. Rev.* **1988**, *88*, 1163-1188.

59 M. S. Davies, S. J. Berners-Price, T. W. Hambley, *Inorg. Chem.* **2000**, *39*, 5603-5613.

60 K. Uehara, K. Kasai, N. Mizuno, *Inorg. Chem.* **2010**, *49*, 2008-2015.

61 M. Yoneya, T. Yamaguchi, S. Sato, M. Fujita, *J. Am. Chem. Soc.* **2012**, *134*, 14401-14407.

62 S. Leininger, B. Olenyuk, P. J. Stang, *Chem. Rev.* **2000**, *100*, 853-908.

63 (a) N. C. Gianneschi, M. S. Masar, C. A. Mirkin, *Acc. Chem. Res.* **2005**, *38*, 825-837; (b) J. R. Farrell, C. A. Mirkin, I. A. Guzei, L. M. Liable-Sands, A. L. Rheingold, *Angew. Chem. Int. Ed.* **1998**, *37*, 465-467.

64 J. R. Farrell, C. A. Mirkin, L. M. Liable-Sands, A. L. Rheingold, *J. Am. Chem. Soc.* **1998**, *120*, 11834-11835.

65 R. P. John, K. Lee, B. J. Kim, B. J. Suh, H. Rhee, M. S. Lah, *Inorg. Chem.* **2005**, *44*, 7109-7121.

66 (a) M. J. Wiester, C. A. Mirkin, *Inorg. Chem.* **2009**, *48*, 8054-8056; (b) M. S. Khoshbin, M. V. Ovchinnikov, C. A. Mirkin, L. N. Zakharov, A. L. Rheingold, *Inorg. Chem.* **2005**, *44*, 496-501.

67 C. G. Oliveri, P. A. Ulmann, M. J. Wiester, C. A. Mirkin, *Acc. Chem. Res.* **2008**, *41*, 1618-1629.

68 Y.-M. Jeon, D. Kim, C. A. Mirkin, J. A. Golen, A. L. Rheingold, *Tetrahedron* **2008**, *64*, 8428-8434.

69 J. R. Farrell, A. H. Eisenberg, C. A. Mirkin, I. A. Guzei, L. M. Liable-Sands, C. D. Incarvito, A. L. Rheingold, C. L. Stern, *Organometallics* **1999**, *18*, 4856-4868.

70 A. W. Maverick, F. E. Klavetter, *Inorg. Chem.* **1984**, *23*, 4129-4130.

71 A. W. Maverick, S. C. Buckingham, Q. Yao, J. R. Bradbury, G. G. Stanley, *J. Am. Chem. Soc.* **1986**, *108*, 7430-7431.

72 R. W. Saalfrank, A. Stark, M. Bremer, H.-U. Hummel, *Angew. Chem. Int. Ed.* **1990**, *29*, 311-314.

73 P. Baxter, J.-M. Lehn, A. DeCian, J. Fischer, *Angew. Chem. Int. Ed.* **1993**, *32*, 69-72.

74 C. Brückner, R. E. Powers, K. N. Raymond, *Angew. Chem. Int. Ed.* **1998**, *37*, 1837-1839.

75 (a) S. M. Biros, R. M. Yeh, K. N. Raymond, *Angew. Chem. Int. Ed.* **2008**, *47*, 6062-6064; (b) R. M. Yeh, J. Xu, G. Seeber, K. N. Raymond, *Inorg. Chem.* **2005**, *44*, 6228-6239.

76 (a) K. Mahata, P. D. Frischmann, F. Würthner, *J. Am. Chem. Soc.* **2013**, *135*, 15656-15661; (b) P. D. Frischmann, V. Kunz, V. Stepanenko, F. Würthner, *Chem. Eur. J.* **2015**, *21*, 2766-2769; (c) C. R. K. Glasson, G. V. Meehan, J. K. Clegg, L. F. Lindoy, P. Turner, M. B. Duriska, R. Willis, *Chem. Commun.* **2008**, 1190-1192.

77 A. V. Davis, K. N. Raymond, *J. Am. Chem. Soc.* **2005**, *127*, 7912-7919.

78 D. Fiedler, D. H. Leung, R. G. Bergman, K. N. Raymond, *Acc. Chem. Res.* **2004**, *38*, 349-358.

79 A. G. L. Olive, K. Parkan, C. Givelet, J. Michl, *J. Am. Chem. Soc.* **2011**, *133*, 20108-20111.

80 (a) P. J. Stang, D. H. Cao, *J. Am. Chem. Soc.* **1994**, *116*, 4981-4982; (b) P. J. Stang, V. V. Zhdankin, *J. Am. Chem. Soc.* **1993**, *115*, 9808-9809.

81 K. Severin, *Coord. Chem. Rev.* **2003**, *245*, 3-10.

82 M. Tominaga, K. Suzuki, M. Kawano, T. Kusukawa, T. Ozeki, S. Sakamoto, K. Yamaguchi, M. Fujita, *Angew. Chem. Int. Ed.* **2004**, *43*, 5621-5625.

83 Q.-F. Sun, J. Iwasa, D. Ogawa, Y. Ishido, S. Sato, T. Ozeki, Y. Sei, K. Yamaguchi, M. Fujita, *Science* **2010**, *328*, 1144-1147.

84 Sébastien Bivaud. Cages auto-assemblees riches en electrons : synthese, caracterisation et propriétés d'inclusion. Organic chemistry. Université d'Angers, 2012. French. <tel-00995375>

85 M. Fujita, J. Yazaki, K. Ogura, *Tetrahedron Lett.* **1991**, *32*, 5589-5592.

86 (a) M. Fujita, O. Sasaki, T. Mitsuhashi, T. Fujita, J. Yazaki, K. Yamaguchi, K. Ogura, *Chem Commun* **1996**, 1535-1536; (b) M. Ferrer, A. Gutiérrez, M. Mounir, O. Rossell, E. Ruiz, A. Rang, M. Engeser, *Inorg. Chem.* **2007**, *46*, 3395-3406.

87 (a) X. Lu, X. Li, K. Guo, T.-Z. Xie, C. N. Moorefield, C. Wesdemiotis, G. R. Newkome, *J. Am. Chem. Soc.* **2014**, *136*, 18149-18155; (b) Y.-F. Han, L. Zhang, L.-H. Weng, G.-X. Jin, *J. Am. Chem. Soc.* **2014**, *136*, 14608-14615.

88 S. Neogi, G. Schnakenburg, Y. Lorenz, M. Engeser, M. Schmittel, *Inorg. Chem.* **2012**, *51*, 10832-10841.

89 S. Neogi, Y. Lorenz, M. Engeser, D. Samanta, M. Schmittel, *Inorg. Chem.* **2013**, *52*, 6975-6984.

90 (a) T. R. Cook, V. Vajpayee, M. H. Lee, P. J. Stang, K.-W. Chi, *Acc. Chem. Res.* **2013**, *46*, 2464-2474; (b) A. K. Singh, D. S. Pandey, Q. Xu, P. Braunstein, *Coord. Chem. Rev.* **2014**, *270–271*, 31-56.

91 T. Shibasaki, N. Komine, M. Hirano, S. Komiya, *Organometallics* **2005**, *25*, 523-527.

92 D. D. Pathak, A. T. Hutton, J. Hyde, A. Walkden, C. White, *J. Organomet. Chem.* **2000**, *606*, 188-196.

93 M. I. Bruce, in *Comprehensive Organometallic Chemistry II* (Ed.: E. W. A. G. A. S. Wilkinson), Elsevier, Oxford, **1995**, pp. 291-298.

94 C. Bruneau, P. H. Dixneuf, *Angew. Chem. Int. Ed.* **2006**, *45*, 2176-2203.

95 P. J. Dyson, G. Sava, *Dalton Trans.* **2006**, 1929-1933.

96 C. S. Allardyce, A. Dorcier, C. Scolaro, P. J. Dyson, *Appl. Organomet. Chem.* **2005**, *19*, 1-10.

97 G. Süss-Fink, *Dalton Trans.* **2010**, *39*, 1673-1688.

98 A. Bergamo, G. Sava, *Dalton Trans.* **2011**, *40*, 7817-7823.

99 B. Therrien, *Coord. Chem. Rev.* **2009**, *253*, 493-519.

100 B. Therrien, *Eur. J. Inorg. Chem.* **2009**, *2009*, 2445-2453.

101 G. Winkhaus, H. Singer, *J. Organomet. Chem.* **1967**, *7*, 487-491.

102 M. A. Bennett, A. K. Smith, *J. Chem. Soc., Dalton Trans.* **1974**, 233-241.

103 J. Canivet, B. Therrien, G. Süss-Fink, *Acta Crystallogr. Sect. E.-Struct Rep. Online* **2005**, *61*, m1090-m1091.

104 E. L. Muetterties, J. R. Bleeke, A. C. Sievert, *J. Organomet. Chem.* **1979**, *178*, 197-216.

105 M. A. Bennett, L. Y. Goh, I. J. McMahon, T. R. B. Mitchell, G. B. Robertson, T. W. Turney, A. Wickramasinghe Wasantha, *Organometallics* **1992**, *11*, 3069-3085.

106 W. H. Ang, E. Daldini, L. Juillerat-Jeanneret, P. J. Dyson, *Inorg. Chem.* **2007**, *46*, 9048-9050.

107 P. S. Engel, R. L. Allgren, W.-K. Chae, R. A. Leckonby, N. A. Marron, *J. Org. Chem.* **1979**, *44*, 4233-4239.

108 B. Therrien, G. Süss-Fink, *Inorg. Chim. Acta.* **2006**, *359*, 4350-4354.

109 J. Soleimannejad, C. White, *Organometallics* **2005**, *24*, 2538-2541.

110 R. A. Zelonka, M. C. Baird, *Can. J. Chem.* **1972**, *50*, 3063-3072.

111 M. Stebler-Roethlisberger, W. Hummel, P. A. Pittet, H. B. Buergi, A. Ludi, A. E. Merbach, *Inorg. Chem.* **1988**, *27*, 1358-1363.

112 G. Süss-Fink, *J. Organomet. Chem.* **2014**, *751*, 2-19.

113 (a) J. Mattson, P. Govindaswamy, A. K. Renfrew, P. J. Dyson, P. Stepnicka, G. Süss-Fink, B. Therrien, *Organometallics* **2009**, *28*, 4350-4357; (b) A.-F. Ibao, M. Gras, B. Therrien, G. Süss-Fink, O. Zava, P. J. Dyson, *Eur. J. Inorg. Chem.* **2012**, *2012*, 1531-1535.

114 (a) F. Giannini, M. Bartoloni, L. E. H. Paul, G. Suss-Fink, J.-L. Reymond, J. Furrer, *MedChemComm* **2015**, *6*, 347-350; (b) F. Giannini, J. Furrer, A.-F. Ibao, G. Suss-Fink, B. Therrien, O. Zava, M. Baquie, P. J. Dyson, P. Stepnicka, *J. Biol. Inorg. Chem.* **2012**, *17*, 951-960; (c) F. Giannini, J. Furrer, G. Suss-Fink, C. M. Clavel, P. J. Dyson, *J. Organomet. Chem.* **2013**, *744*, 41-48.

115 (a) F. Giannini, G. Süss-Fink, J. Furrer, *Inorg. Chem.* **2011**, *50*, 10552-10554; (b) F. Giannini, J. Furrer, A.-F. Ibao, G. Süss-Fink, B. Therrien, O. Zava, M. Baquie, P. J. Dyson, P. Stepnicka, *JBIC, J. Biol. Inorg. Chem.* **2012**, *17*, 951-960; (c) F. Giannini, G. Süss-Fink, J. Furrer, *Inorg. Chem.* **2011**, *50*, 10552-10554; (d) F. Giannini, G. Süss-Fink, J. Furrer, *Inorg. Chem.* **2011**, *50*, 10552-10554.

116 H. Yan, G. Süss-Fink, A. Neels, H. Stoeckli-Evans, *J. Chem. Soc., Dalton Trans.* **1997**, 4345-4350.

117 K. Severin, *Chem. Commun.* **2006**, 3859-3867.

118 W.-B. Yu, Q.-Y. He, H.-T. Shi, G. Yuan, X. Wei, *Chem. Asian J.* **2015**, *10*, 239-246.

119 (a) B. Therrien, *Top. Curr. Chem.* **2012**, *319*, 35-56; (b) B. Therrien, J. Furrer, *Advances in Chemistry* **2014**, *2014*, 20.

120 T. Brasey, R. Scopelliti, K. Severin, *Chem. Commun.* **2006**, 3308-3310.

121 K. Yamanari, S. Yamamoto, R. Ito, Y. Kushi, A. Fuyuhiro, N. Kubota, T. Fukuo, R. Arakawa, *Angew. Chem. Int. Ed.* **2001**, *40*, 2268-2271.

122 H. Piotrowski, K. Polborn, G. Hilt, K. Severin, *J. Am. Chem. Soc.* **2001**, *123*, 2699-2700.

123 C. J. Kuehl, C. L. Mayne, A. M. Arif, P. J. Stang, *Org. Lett.* **2000**, *2*, 3727-3729.

124 R. V. Slone, K. D. Benkstein, S. Bélanger, J. T. Hupp, I. A. Guzei, A. L. Rheingold, *Coord. Chem. Rev.* **1998**, *171*, 221-243.

125 M. A. Furrer, A. Garci, E. Denoyelle-Di-Muro, P. Trouillas, F. Giannini, J. Furrer, C. M. Clavel, P. J. Dyson, G. Süss-Fink, B. Therrien, *Chem. Eur. J.* **2013**, *19*, 3198-3203.

126 L. E. H. Paul, B. Therrien, J. Furrer, *Inorg. Chem.* **2011**, *51*, 1057-1067.

127 B. Therrien, G. Süss-Fink, P. Govindaswamy, A. K. Renfrew, P. J. Dyson, *Angew. Chem. Int. Ed.* **2008**, *47*, 3773-3776.

128 M. Wang, V. Vajpayee, S. Shanmugaraju, Y.-R. Zheng, Z. Zhao, H. Kim, P. S. Mukherjee, K.-W. Chi, P. J. Stang, *Inorg. Chem.* **2011**, *50*, 1506-1512.

129 G. Gupta, J. Mahesh Kumar, A. Garci, N. Rangaraj, N. Nagesh, B. Therrien, *ChemPlusChem* **2014**, *79*, 610-618.

130 H. Maeda, J. Wu, T. Sawa, Y. Matsumura, K. Hori, *J. Control. Release* **2000**, *65*, 271-284.

131 (a) M. A. Furrer, J. Furrer, B. Therrien, *Organometallics* **2012**, *31*, 3149-3154; (b) Y.-F. Han, W.-G. Jia, W.-B. Yu, G.-X. Jin, *Chem. Soc.Rev.* **2009**, *38*, 3419-3434.

132 O. Zava, J. Mattsson, B. Therrien, P. J. Dyson, *Chem. Eur. J.* **2010**, *16*, 1428-1431.

133 J. W. Yi, N. P. E. Barry, M. A. Furrer, O. Zava, P. J. Dyson, B. Therrien, B. H. Kim, *Bioconjugate Chem.* **2012**, *23*, 461-471.

134 (a) N. P. E. Barry, J. Furrer, B. Therrien, *Helv. Chim. Acta* **2010**, *93*, 1313-1328; (b) N. P. E. Barry, O. Zava, P. J. Dyson, B. Therrien, *Chem. Eur. J.* **2011**, *17*, 9669-9677.

135 (a) F. Schmitt, J. Freudenreich, N. P. E. Barry, L. Juillerat-Jeanneret, G. Suss-Fink, B. Therrien, *J. Am. Chem. Soc.* **2012**, *134*, 754-757; (b) J. Freudenreich, J. Furrer, G. Süss-Fink, B. Therrien, *Organometallics* **2011**, *30*, 942-951.

136 B. Therrien, *Chem. Eur. J.* **2013**, *19*, 8378-8386.

137 F. Schmitt, J. Freudenreich, N. P. E. Barry, L. Juillerat-Jeanneret, G. Süss-Fink, B. Therrien, *J. Am Chem. Soc.* **2012**, *134*, 754-757.

138 Y.-R. Zheng, P. J. Stang, *J. Am. Chem. Soc.* **2009**, *131*, 3487-3489.

139 M. Fujita, N. Fujita, K. Ogura, K. Yamaguchi, *Nature* **1999**, *400*, 52-55.

140 (a) M. D. Levin, P. J. Stang, *J. Am. Chem. Soc.* **2000**, *122*, 7428-7429; (b) A. Hori, A. Akasaka, K. Biradha, S. Sakamoto, K. Yamaguchi, M. Fujita, *Angew. Chem. Int. Ed.* **2002**, *41*, 3269-3272; (c) Y. Tsujimoto, T. Kojima, S. Hiraoka, *Chem. Sci.* **2014**, *5*, 4167-4172.

141 J. R. Li, H. C. Zhou, *Nat. Chem.* **2010**, *2*, 893-898.

142 S. Hiraoka, Y. Sakata, M. Shionoya, *J. Am. Chem. Soc.* **2008**, *130*, 10058-10059.

143 N. P. E. Barry, J. Furrer, J. Freudenreich, G. Suss-Fink, B. Therrien, *Eur. J. Inorg. Chem.* **2010**, 725-728.

144 (a) T. Rajendran, B. Manimaran, F.-Y. Lee, G.-H. Lee, S.-M. Peng, C. M. Wang, K.-L. Lu, *Inorg. Chem.* **2000**, *39*, 2016-2017; (b) R. Lin, J. H. K. Yip, K. Zhang, L. L. Koh, K.-Y. Wong, K. P. Ho, *J .Am. Chem. Soc.* **2004**, *126*, 15852-15869; (c) P. H. Dinolfo, J. T. Hupp, *J. Am. Chem. Soc.* **2004**, *126*, 16814-16819; (d) S. Ghosh, R. Chakrabarty, P. S. Mukherjee, *Inorg. Chem.* **2009**, *48*, 549-556; (e) G. Marinescu, G. Marin, A. M. Madalan, A. Vezeanu, C. Tiseanu, M. Andruh, *Cryst. Growth Des.* **2010**, *10*, 2096-2103; (f) N. P. E. Barry, F. Edafe, P. J. Dyson, B. Therrien, *Dalton Trans.* **2010**, *39*, 2816-2820; (g) M. Schmidtendorf, T. Pape, F. E. Hahn, *Dalton*

Trans. **2013**, *42*, 16128-16141; hT. Wu, Y.-J. Lin, G.-X. Jin, *Dalton Trans.* **2013**, *42*, 82-88.

145 A. Pitto-Barry, N. P. E. Barry, O. Zava, R. Deschenaux, B. Therrien, *Chem. Asian J.* **2011**, *6*, 1595-1603.

146 J. Mattsson, P. Govindaswamy, A. K. Renfrew, P. J. Dyson, P. Štěpnička, G. Süss-Fink, B. Therrien, *Organometallics* **2009**, *28*, 4350-4357.

147 P. Govindaswamy, D. Linder, J. Lacour, G. Süss-Fink, B. Therrien, *Chem. Commun.* **2006**, 4691-4693.

148 T. R. Ward, O. Schafer, C. Daul, P. Hofmann, *Organometallics* **1997**, *16*, 3207-3215.

149 (a) M. R. Ringenberg, M. J. Nilges, T. B. Rauchfuss, S. R. Wilson, *Organometallics* **2010**, *29*, 1956-1965; (b) M. Bubrin, D. Schweinfurth, F. Ehret, S. Záliš, H. Kvapilová, J. Fiedler, Q. Zeng, F. Hartl, W. Kaim, *Organometallics* **2014**, *33*, 4973-4985.

150 N. P. E. Barry, B. Therrien, *Inorg. Chem. Commun.* **2009**, *12*, 465-468.

151 G. K. Kole, R. Medishetty, L. L. Koh, J. J. Vittal, *Chem. Commun.* **2013**, *49*, 6298-6300.

152 C. Karunakaran, K. R. J. Thomas, A. Shunmugasundaram, R. Murugesan, *J. Mol. Struct.* **2000**, *523*, 213-221.

153 A. Garci, S. Marti, S. Schurch, B. Therrien, *R. Soc. Chem. Adv.* **2014**, *4*, 8597-8604.

154 M. Yokoyama, *J. Artif. Organs.* **2005**, *8*, 77-84.

155 R. Siegel, D. Naishadham, A. Jemal, *CA-Cancer J. Clin.* **2013**, *63*, 11-30.

156 N. C. Lloyd, H. W. Morgan, B. K. Nicholson, R. S. Ronimus, *Angew. Chem. Int. Ed.* **2005**, *44*, 941-944.

157 (a) B. Rosenberg, *Cancer* **1985**, *55*, 2303-2316; (b) B. Rosenberg, L. Van Camp, T. Krigas, *Nature* **1965**, *205*, 698-699.

158 S. M. Cohen, S. J. Lippard, in *Progress in Nucleic Acid Research and Molecular Biology, Vol. Volume 67*, Academic Press, **2001**, pp. 93-130.

159 E. Wong, C. M. Giandomenico, *Chem. Rev.* **1999**, *99*, 2451-2466.

160 N. P. E. Barry, P. J. Sadler, *Chem. Commun.* **2013**, *49*, 5106-5131.

161 E. Antonarakis, A. Emadi, *Cancer Chemother. Pharmacol.* **2010**, *66*, 1-9.

162 J. R. Durig, J. Danneman, W. D. Behnke, E. E. Mercer, *Chem. Biol. Interact.* **1976**, *13*, 287-294.

163 M. Clarke, in *Ruthenium and Other Non-Platinum Metal Complexes in Cancer Chemotherapy, Vol. 10* (Eds.: E. Baulieu, D. Forman, M. Ingelman-Sundberg, L.

Jaenicke, J. Kellen, Y. Nagai, G. Springer, L. Träger, L. Will-Shahab, J. Wittliff), Springer Berlin Heidelberg, **1989**, pp. 25-39.

164 M. J. Clarke, F. Zhu, D. R. Frasca, *Chem. Rev.* **1999**, *99*, 2511-2534.

165 A. Bergamo, L. Messori, F. Piccioli, M. Cocchietto, G. Sava, *Invest. New. Drugs* **2003**, *21*, 401-411.

166 S. Kapitza, M. Pongratz, M. A. Jakupec, P. Heffeter, W. Berger, L. Lackinger, B. K. Keppler, B. Marian, *J. Cancer Res. Clin. Oncol.* **2005**, *131*, 101-110.

167 J. M. Rademaker-Lakhai, D. van den Bongard, D. Pluim, J. H. Beijnen, J. H. M. Schellens, *Clin. Cancer Res.* **2004**, *10*, 3717-3727.

168 F. Lentz, A. Drescher, A. Lindauer, M. Henke, R. A. Hilger, C. G. Hartinger, M. E. Scheulen, C. Dittrich, B. K. Keppler, U. Jaehde, i. c. w. C. E. S. f. A. D. Research-EWIV, *Anti-Cancer Drugs* **2009**, *20*, 97-103.

169 A. L. Noffke, A. Habtemariam, A. M. Pizarro, P. J. Sadler, *Chem. Commun.* **2012**, *48*, 5219-5246.

170 aC. S. Allardyce, P. J. Dyson, D. J. Ellis, S. L. Heath, *Chem. Commun.* **2001**, 1396-1397; bA. Dorcier, P. J. Dyson, C. Gossens, U. Rothlisberger, R. Scopelliti, I. Tavernelli, *Organometallics* **2005**, *24*, 2114-2123.

171 R. E. Aird, J. Cummings, A. A. Ritchie, M. Muir, R. E. Morris, H. Chen, P. J. Sadler, D. I. Jodrell, *Br. J. Cancer* **2002**, *86*, 1652-1657.

172 W. Han Ang, P. J. Dyson, *Eur. J. Inorg. Chem.* **2006**, *2006*, 4003-4018.

173 (a) W. H. Ang, A. Casini, G. Sava, P. J. Dyson, *J. Organomet. Chem.* **2011**, *696*, 989-998; (b) G. S. Smith, B. Therrien, *Dalton Trans.* **2011**, *40*, 10793-10800; (c) S. K. Singh, D. S. Pandey, *R. Soc. Chem. Adv.* **2014**, *4*, 1819-1840; (d) A. A. Nazarov, C. G. Hartinger, P. J. Dyson, *J. Organomet. Chem.* **2014**, *751*, 251-260.

174 (a) A. Mishra, S. C. Kang, K.-W. Chi, *Eur. J. Inorg. Chem.* **2013**, *2013*, 5222-5232; (b) B. Therrien, *CrystEngComm* **2015**, *17*, 484-491.

175 (a) F. Linares, E. Q. Procopio, M. A. Galindo, M. A. Romero, J. A. R. Navarro, E. Barea, *CrystEngComm* **2010**, *12*, 2343-2346; (b) J. Mattsson, P. Govindaswamy, J. Furrer, Y. Sei, K. Yamaguchi, G. Süss-Fink, B. Therrien, *Organometallics* **2008**, *27*, 4346-4356; (c) F. Kühlwein, K. Polborn, W. Beck, *Z. Anorg. Allg. Chem.* **1997**, *623*, 1931-1944.

176 (a) S. W. Magennis, A. Habtemariam, O. Novakova, J. B. Henry, S. Meier, S. Parsons, I. D. H. Oswald, V. Brabec, P. J. Sadler, *Inorg. Chem.* **2007**, *46*, 5059-5068; (b) B. Therrien, G. Süss-Fink, P. Govindaswamy, C. Saïd-Mohamed, *Polyhedron* **2007**, *26*,

4065-4072; (c) P. Govindaswamy, J. Canivet, B. Therrien, G. Süss-Fink, P. Štěpnička, J. Ludvík, *J. Organomet. Chem.* **2007**, *692*, 3664-3675; (d) V. Vajpayee, S. m. Lee, J. W. Park, A. Dubey, H. Kim, T. R. Cook, P. J. Stang, K.-W. Chi, *Organometallics* **2013**, *32*, 1563-1566.

177 (a) M. Yuan, F. Weisser, B. Sarkar, A. Garci, P. Braunstein, L. Routaboul, B. Therrien, *Organometallics* **2014**, *33*, 5043-5045; (b) F. Linares, M. A. Galindo, S. Galli, M. A. Romero, J. A. R. Navarro, E. Barea, *Inorg. Chem.* **2009**, *48*, 7413-7420; (c) W.-Z. Zhang, Y.-F. Han, Y.-J. Lin, G.-X. Jin, *Dalton Trans.* **2009**, 8426-8431.

178 (a) M. Stasiuk, A. Kozubek, *Global Journal of Biochemistry* **2011**, *2*, 262-270 (b) Z. Nikolovska-Coleska, L. Xu, Z. Hu, Y. Tomita, P. Li, P. P. Roller, R. Wang, X. Fang, R. Guo, M. Zhang, M. E. Lippman, D. Yang, S. Wang, *J. Med. Chem.* **2004**, *47*, 2430-2440.

179 W.-Z. Zhang, Y.-F. Han, Y.-J. Lin, G.-X. Jin, *Organometallics* **2010**, *29*, 2842-2849.

180 (a) P. Govindaswamy, D. Linder, J. Lacour, G. Suss-Fink, B. Therrien, *Dalton Trans.* **2007**, 4457-4463; (b) P. Govindaswamy, D. Linder, J. Lacour, G. Suss-Fink, B. Therrien, *Chem. Commun.* **2006**, 4691-4693.

181 (a) B. Therrien, G. Süss-Fink, *Chimia* **2008**, *62*, 514-518; (b) C. A. Murray, C. J. Cardin, B. W. Greenland, A. Swift, H. M. Colquhoun, *Inorg. Chem.* **2013**, *52*, 10424-10430; (c) M. Albrecht, E. Isaak, V. Moha, G. Raabe, R. Fröhlich, *Chem. Eur. J.* **2014**, *20*, 6650-6658; (d) A. M. Castilla, W. J. Ramsay, J. R. Nitschke, *Acc. Chem. Res.* **2014**, *47*, 2063-2073.

182 T. Mosmann, *J. Immunol. Methods* **1983**, *65*, 55-63.

183 (a) P. Govender, B. Therrien, G. S. Smith, *Eur. J. Inorg. Chem.* **2012**, *2012*, 2853-2862; (b) J. Mattsson, O. Zava, A. K. Renfrew, Y. Sei, K. Yamaguchi, P. J. Dyson, B. Therrien, *Dalton Trans.* **2010**, *39*, 8248-8255; (c) A. L. Harris, X. Yang, A. Hegmans, L. Povirk, J. J. Ryan, L. Kelland, N. P. Farrell, *Inorg. Chem.* **2005**, *44*, 9598-9600.

184 J. Freudenreich, C. Dalvit, G. Süss-Fink, B. Therrien, *Organometallics* **2013**, *32*, 3018-3033.

185 (a) M. Brasch, A. de la Escosura, Y. Ma, C. Uetrecht, A. J. R. Heck, T. Torres, J. J. L. M. Cornelissen, *J. Am. Chem. Soc.* **2011**, *133*, 6878-6881; (b) S. Vedachalam, B.-H. Choi, K. K. Pasunooti, K. M. Ching, K. Lee, H. S. Yoon, X.-W. Liu, *MedChemComm* **2011**, *2*, 371-377.

186 (a) N. C. Zeitouni, A. R. Oseroff, S. Shieh, *Mol. Immunol.* **2003**, *39*, 1133-1136; (b) D. K. Chatterjee, L. S. Fong, Y. Zhang, *Adv. Drug Deliv. Rev.* **2008**, *60*, 1627-1637;

(c) W. M. Sharman, C. M. Allen, J. E. van Lier, *Drug Discov. Today* **1999**, *4*, 507-517; (d) R. Bonnett, *Chem. Soc. Rev.* **1995**, *24*, 19-33; (e) F. Schmitt, L. Juillerat-Jeanneret, *Anticancer Agents Med. Chem.* **2012**, *12*, 500-525.

187 R. R. Allison, G. H. Downie, R. Cuenca, X.-H. Hu, C. J. H. Childs, C. H. Sibata, *Photodiagnosis Photodyn. Ther.* **2004**, *1*, 27-42.

188 C. Hopper, C. Niziol, M. Sidhu, *Oral Oncol.* **2004**, *40*, 372-382.

189 M. Ethirajan, Y. Chen, P. Joshi, R. K. Pandey, *Chem. Soc. Rev.* **2011**, *40*, 340-362.

190 (a) D. E. J. G. J. Dolmans, D. Fukumura, R. K. Jain, *Nat. Rev. Cancer* **2003**, *3*, 380-387; (b) R. D. Almeida, B. J. Manadas, A. P. Carvalho, C. B. Duarte, *Biochim. Biophys. Acta.* **2004**, *1704*, 59-86; (c) E. Buytaert, M. Dewaele, P. Agostinis, *Biochim. Biophys. Acta.* **2007**, *1776*, 86-107.

191 J. P. Celli, B. Q. Spring, I. Rizvi, C. L. Evans, K. S. Samkoe, S. Verma, B. W. Pogue, T. Hasan, *Chem. Rev.* **2010**, *110*, 2795-2838.

192 B. Kosharskyy, N. Solban, S. K. Chang, I. Rizvi, Y. Chang, T. Hasan, *Cancer Res.* **2006**, *66*, 10953-10958.

193 S. Verma, G. M. Watt, Z. Mai, T. Hasan, *Photochem. Photobiol.* **2007**, *83*, 996-1005.

194 Y. Choi, J. R. McCarthy, R. Weissleder, C.-H. Tung, *ChemMedChem* **2006**, *1*, 458-463.

195 N. S. Soukos, M. R. Hamblin, S. Keel, R. L. Fabian, T. F. Deutsch, T. Hasan, *Cancer Res.* **2001**, *61*, 4490-4496.

196 S. Dixit, T. Novak, K. Miller, Y. Zhu, M. E. Kenney, A.-M. Broome, *Nanoscale* **2015**, *7*, 1782-1790.

197 (a) D. Bechet, P. Couleaud, C. Frochot, M.-L. Viriot, F. Guillemin, M. Barberi-Heyob, *Trends Biotechnol.* **2008**, *26*, 612-621; (b) A. S. L. Derycke, P. A. M. de Witte, *Adv. Drug Deliv. Rev.* **2004**, *56*, 17-30.

198 N. P. E. Barry, J. Furrer, B. Therrien, *Helv. Chim. Acta.* **2010**, *93*, 1313-1328.

199 N. P. E. Barry, O. Zava, P. J. Dyson, B. Therrien, *Chem. Eur. J.* **2011**, *17*, 9669-9677.

200 G. Viault, D. Grée, S. Das, J. S. Yadav, R. Grée, *Eur. J. Org. Chem.* **2011**, *2011*, 1233-1241.

201 (a) C. M. Clavel, E. Paunescu, P. Nowak-Sliwinska, P. J. Dyson, *Chem. Sci.* **2014**, *5*, 1097-1101; (b) C. M. Clavel, P. Nowak-Sliwinska, E. Paunescu, A. W. Griffioen, P. J. Dyson, *Chem. Sci.* **2015**.

202 J. Li, S. Q. Yap, C. F. Chin, Q. Tian, S. L. Yoong, G. Pastorin, W. H. Ang, *Chem. Sci.* **2012**, *3*, 2083-2087.

203 T. Yogo, Y. Urano, Y. Ishitsuka, F. Maniwa, T. Nagano, *J. Am. Chem. Soc.* **2005**, *127*, 12162-12163.

204 H. L. Anderson, S. Anderson, J. K. M. Sanders, *J. Chem. Soc., Perkin Trans. 1* **1995**, 2231-2245.

205 A. J. Amoroso, A. M. W. C. Thompson, J. P. Maher, J. A. McCleverty, M. D. Ward, *Inorg. Chem.* **1995**, *34*, 4828-4835.

206 M. A. Bennett, T. N. Huang, T. W. Matheson, A. K. Smith, S. Ittel, W. Nickerson, in *Inorganic Syntheses*, John Wiley & Sons, Inc., **2007**, pp. 74-78.

207 N. P. E. Barry, B. Therrien, *Eur. J. Inorg. Chem.* **2009**, *2009*, 4695-4700.

208 T. L. Hwang, A. J. Shaka, *J. Am. Chem. Soc.* **1992**, *114*, 3157-3159.

209 G. Sheldrick, *Acta Crystallogr. Sect. A* **2008**, *64*, 112-122.

Abbreviations

ethylenediamine: en

cyclooctene: COT

isopropyl group: Pr^i

porphin: po

p-Cymene: *p*-cym

oxalato: ox

2,5-dioxydo-1,4-benzoquinonato: : dobq

5,8-dioxydo-1,4-naphthoquinonato: donq

2,5-dichlorido-1,4-benzoquinonato: dClobq

4,4′-bipyridine-D_8 : bpy-D_8

4,4′-bipyridine : bpy

1,2-bis(4-pyridyl)ethylene : bpe

4,4′-azopyridine: bpa

4-phenylpyridine: L^1

4-styrylpyridine: L^2,

4-methylpyridine: L^3

4-*tert*-butylpyridine: L^4

2,4,6-tris(4-pyridyl)-1,3,5-triazine: tpt

1,3,5-tris{2-(4-pyridyl)vinyl}benzene: tpv

acetylacetonato: acac

cis-diamminedichloroplatinum(II): cisplatin

imidazolium-trans-dimethylsulfoxide-imidazole-tetrachlororuthenate: NAMI-A

imidazolium-*trans*-bis(1H-indazole)-tetrachlororuthenate: KP1019

1,3,5-triaza-7-phosphaadamantane: pta

pentamethylcyclopentadienyl: Cp*

metal-to-ligand charge transfer: MLCT

drug concentration necessary for 50% inhibition of cell viability: IC50

enhanced permeability and retention: EPR

electrospray mass spectrometry: ESI-MS

diffusion ordered spectroscopy: DOSY

rotating frame nuclear Overhauser effect spectroscopy: ROESY

selectivity coefficient: ^{a}SC

photodynamic therapy: PDT

List of Structures

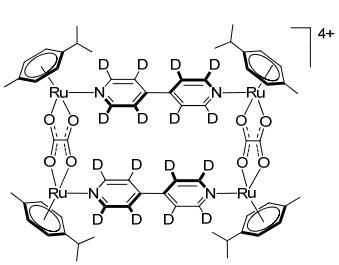

R-ox-homo-D_{16}

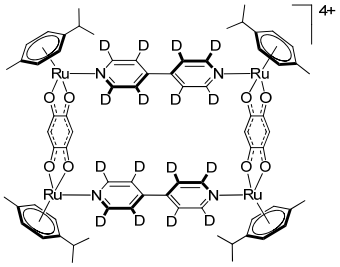

R-dobq-homo-D_{16}

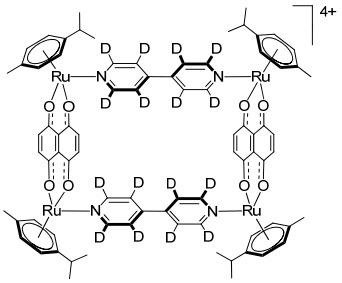

R-donq-homo-D_{16}

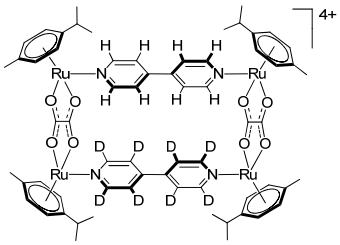

R-ox-hetero H_8-D_8 *(not isolated)*

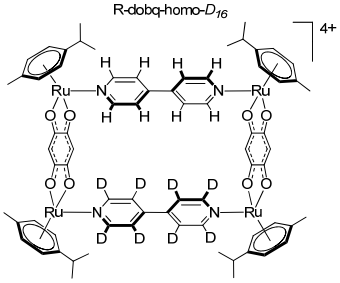

R-dobq-hetero H_8-D_8 *(not isolated)*

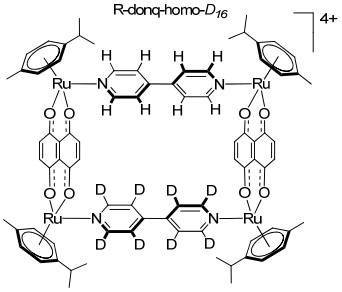

R-donq-hetero H_8-D_8 *(not isolated)*

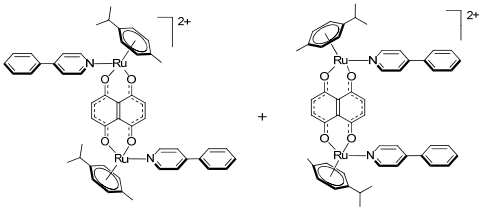

[*trans*-**1**]$^{2+}$ [*cis*-**1**]$^{2+}$

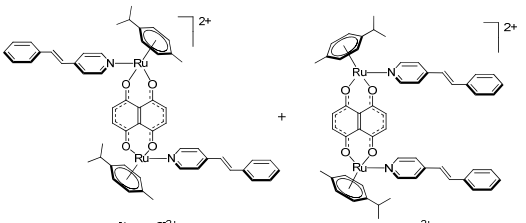

[*trans*-**2**]$^{2+}$ [*cis*-**2**]$^{2+}$

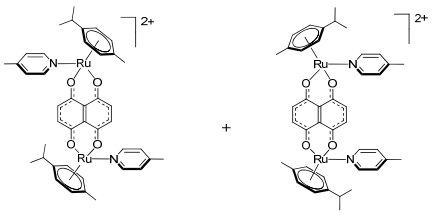

[*trans*-**3**]$^{2+}$ [*cis*-**3**]$^{2+}$

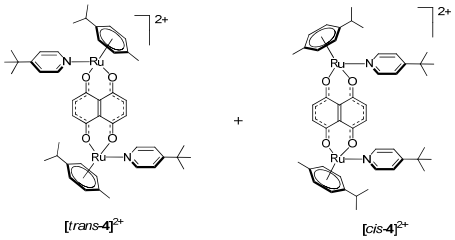

[*trans*-**4**]$^{2+}$ [*cis*-**4**]$^{2+}$

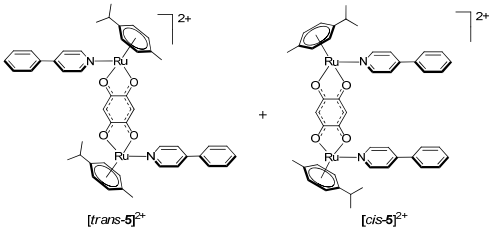

[*trans*-**5**]$^{2+}$ [*cis*-**5**]$^{2+}$

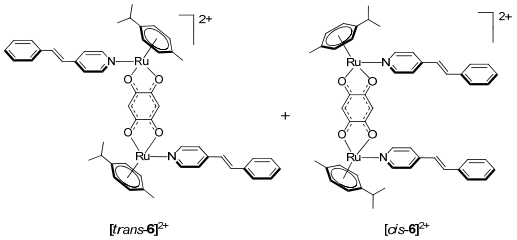

[*trans*-**6**]$^{2+}$ [*cis*-**6**]$^{2+}$

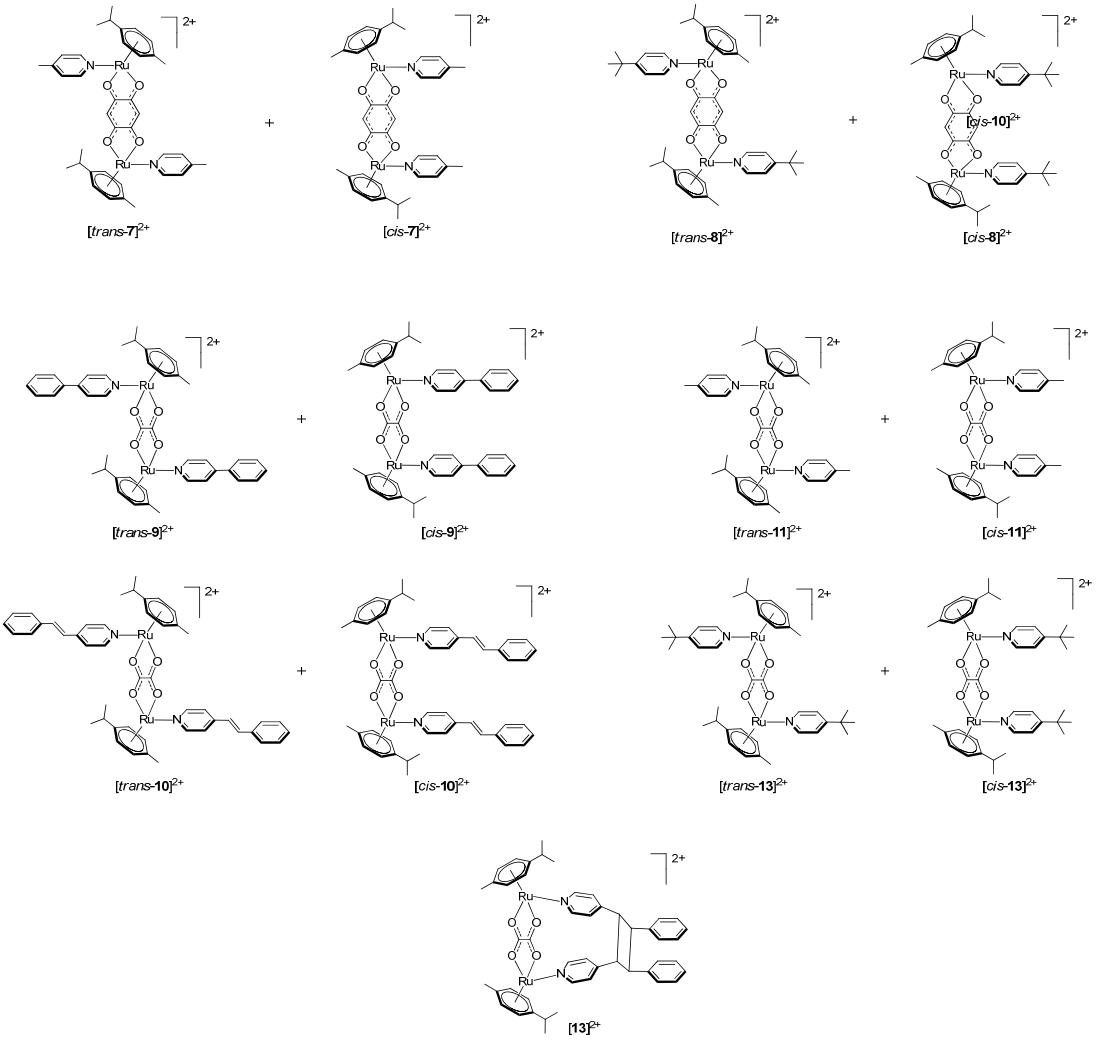
[trans-7]2+
[cis-7]2+
[trans-8]2+
[cis-8]2+
[trans-9]2+
[cis-9]2+
[trans-11]2+
[cis-11]2+
[trans-10]2+
[cis-10]2+
[trans-13]2+
[cis-13]2+
[13]2+

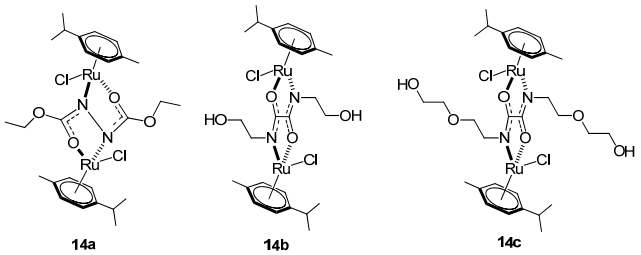

14a **14b** **14c**

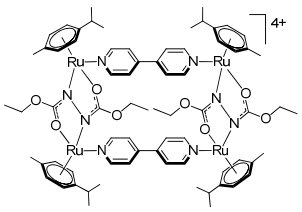

[15a]$^{4+}$

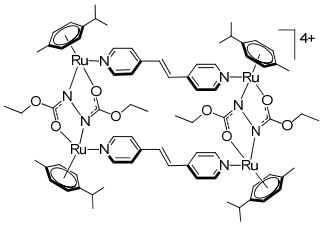

[16a]$^{4+}$

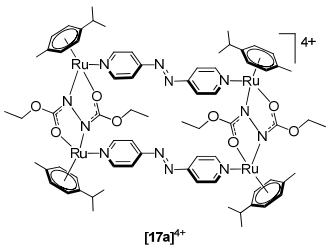

[17a]$^{4+}$

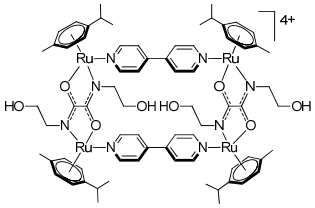

[15b]$^{4+}$

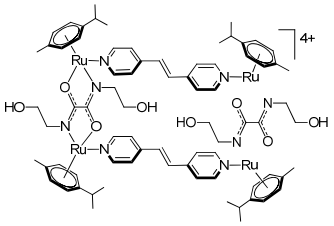

[16b]$^{4+}$

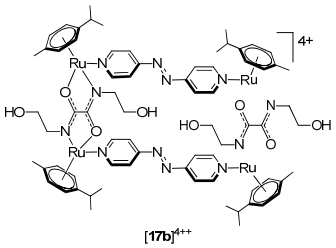

[17b]$^{4+}$

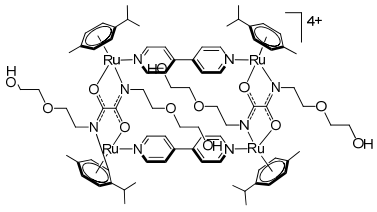

[15c]$^{4+}$

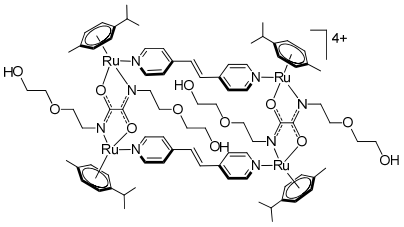

[16c]$^{4+}$

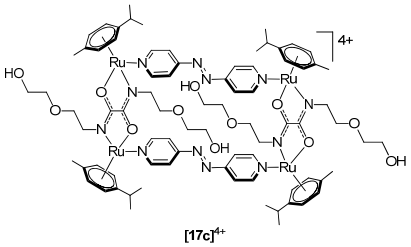

[17c]$^{4+}$

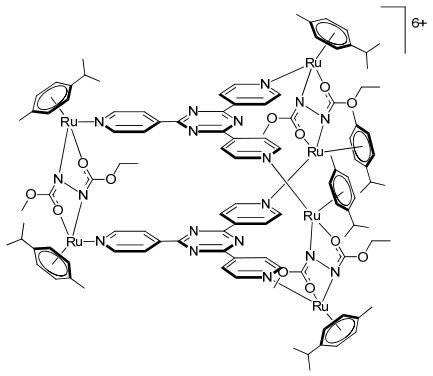

[**18a**]$^{6+}$

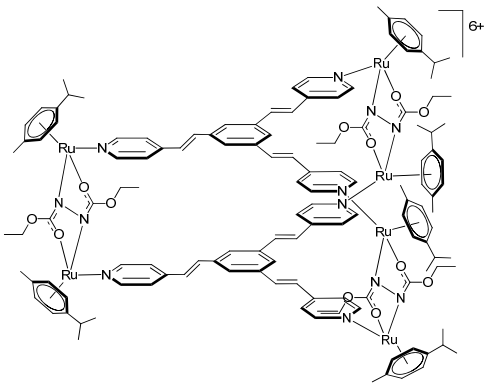

[**19a**]$^{6+}$

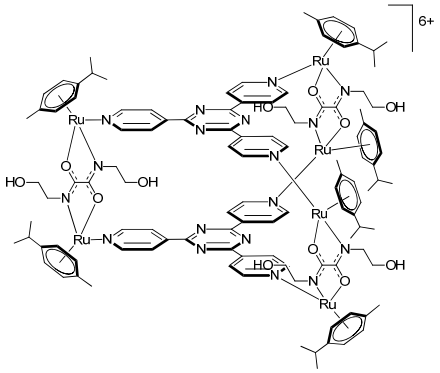

[**18b**]$^{6+}$

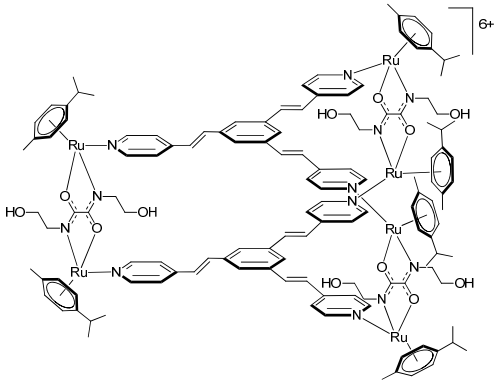

[**19b**]$^{6+}$

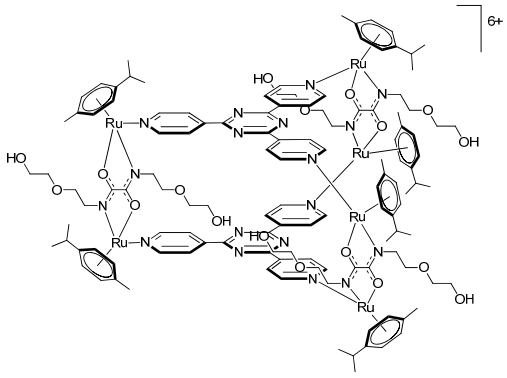

[**18c**]$^{6+}$

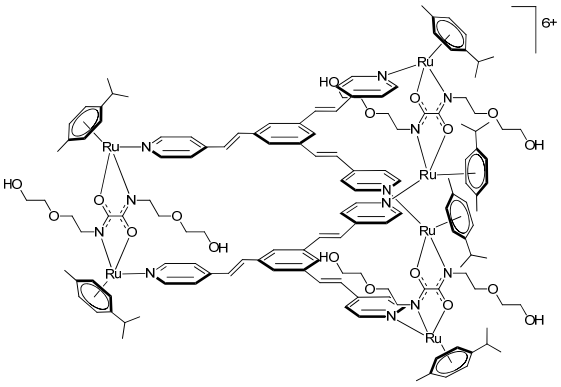

[**19c**]$^{6+}$

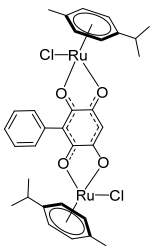

20d

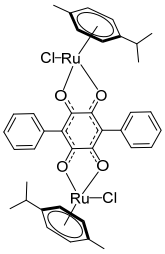

20e

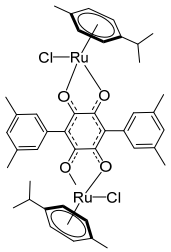

20f

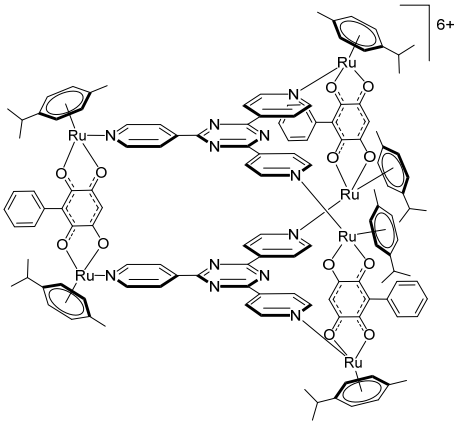

[21d]$^{6+}$

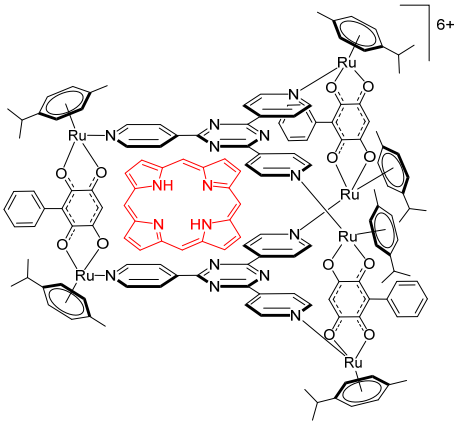

[22d]$^{6+}$

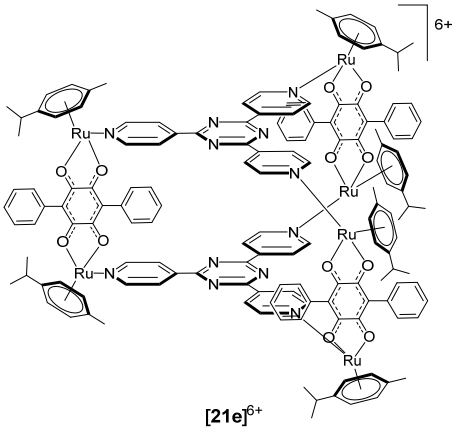

[21e]$^{6+}$

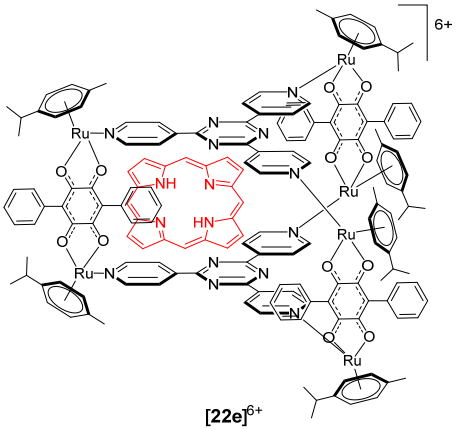

[22e]$^{6+}$

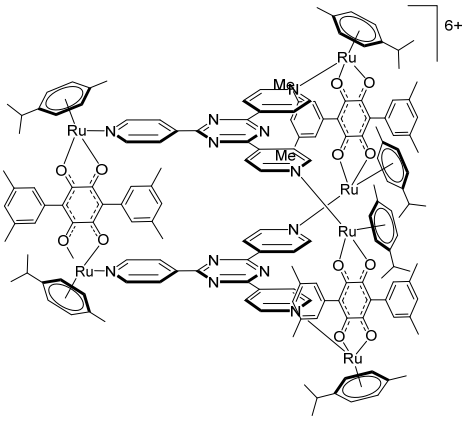

[21f]$^{6+}$

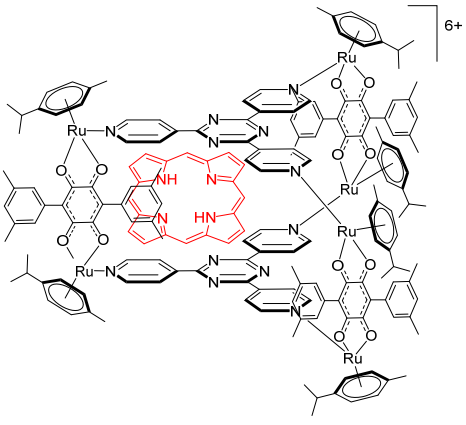

[22f]$^{6+}$

List of Publications

1. Dichlorido(furfurylmine-κN)(η^6-hexamethylbenzene)ruthenium(II), A. Garci, T. T. Thai, G. Süss-Fink, B. Therrien, *Acta Crystallogr. Sect. E* **2011**, *67*, 1592.

2. Synthesis, characterisation and in vitro anticancer activity of hexanuclear thiolato-bridged arene ruthenium metalla-prisms, M. A. Furrer, A. Garci, E. D. Di-Muro, P. Trouillas, F. Giannini, J. Furrer, C. M. Clavel, P. J. Dyson, G. Süss-Fink, B. Therrien, *Chem. Eur. J.* **2013**, *19*, 3198.

3. Synthesis, molecular structure, computational study and *in vitro* anticancer activity of dinuclear thiolato-bridged pentamethylcyclopentadienyl Rh(III) and Ir(III) complexes, G. Gupta, A. Garci, B. S. Murray, P. J. Dyson, G. Fabre, P. Trouillas,; F. Giannini, J. Furrer, G. Süss-Fink, B. Therrien, *Dalton Trans.* **2013**, *42*, 15457.

4. Insight into the dynamic ligand exchange process involved in bipyridyl linked arene ruthenium metalla-rectangles, A. Garci, S. Marti, S. Schürch, B. Therrien, *RSC Adv.* **2014**, *4*, 8597.

5. Anticancer activity of half-sandwich Rh(III) and Ir(III) metalla-prisms containing lipophilic side chains, G. Gupta, J. M. Kumar, A. Garci, N. Rangaraj, N. Nagesh, B. Therrien, *ChemPlusChem* **2014**, *79*, 610.

6. Electron-rich arene-ruthenium metalla-architectures incorporating tetrapyridyl-tetrathiafulvene donor moieties, V. Vajpayee, S. Bivaud, S. Goeb, V. Croue, M. Allain, B. V. Popp, A. Garci, B. Therrien, M. Salle, *Organometallics* **2014**, *33*, 1651.

7. Exploiting natural products to build metalla-assemblies: the anticancer activity of embelin-derived Rh(III) and Ir(III) metalla-rectangles, G. Gupta, J. M. Kumar, A. Garci, N. Nagesh, B. Therrien, *Molecules* **2014**, *19*, 6031.

8. Synthesis and Electrochemical Behavior of a Zwitterion-Bridged Metalla-Cage, M. Yuan, F. Weisser, B. Sarkar, A. Garci, P. Braunstein, L. Routaboul, B. Therrien, *Organometallics* **2014**, *33*, 5043.

9. Strategy to optimize the biological activity of arene ruthenium metalla-assemblies, A. Garci, A. A. Dobrov, T. Riedel, E. Orhan, P. J. Dyson, V. B. Arion, B. Therrien, *Organometallics* **2014**, *33*, 3813.

10. 2,5-Dibromo-3,6-dimethoxycyclohexa-2,5-diene-1,4-dione, E. Orhan, A. Garci, B. Therrien, *Acta Crystallogr. Sect. E* **2014**, *70*, 715.

11. Investigating the formation mechanism of arene ruthenium metallacycles by NMR spectroscopy, A. Garci, G. Gupta, C. Dalvit, B. Therrien, *Eur. J. Inorg. Chem.* **2014**, *33*, 5626.

12. Tunable arene ruthenium metalla-prisms to transport, shield and release porphin in cancer cells, A. Garci, J. P. Mbakidib, S. Leroy-Lhez, V. Sol, B. Therrien, In preparation.

The self-assembly process is a natural phenomenon with the ability to organize biological systems. Its development by chemists as a synthetic process allowed the formation of esthetical structures as well as highly complex supramolecular systems with remarkable biological functions. Since 1990, metal directed self-assembly strategy has largely contributed to the design and synthesis of discrete architectures. The formation of these specific architectures needs some control over the different factors ruling the coordination self-assembly process.

The aim of this thesis was to offer an insight into the rules dictating the formation of arene ruthenium metalla-assemblies built from stable dinuclear metalla-clips and polypyridyl linkers. The characterization of the dynamic ligand exchanges using the $^{1}H/^{2}D$ isotope labeling strategy showed relative stability and inertness of the final structure. In addition, the study of the intermediate species involved during the assembly of metalla-cycles by NMR experiments highlighted the dynamic nature of the Ru-N bond in solution before the final closure of the metalla-cycles. This helped us to describe a plausible thermodynamic germination pathway together with the specific reactivity of such metalla-assemblies.

The promising anticancer-activities of the mononuclear arene ruthenium complexes along with the preferential accumulation of macromolecular species in the cancer cells led to more interest in the anti-proliferative potential of arene ruthenium metalla-cages. Our strategies in order to optimize the biological activity of arene ruthenium metalla-prisms were: Functionalization of the bridging linkers resulted in selectivity improvements of the active compounds towards target cancer cells; and the modification of the portal's size of metalla-cages to control the release of a hydrophobic photosensitizer on the human colon cancer cell line HT-29.